The Antiproliferative Effect of Palm Oil Gamma-Tocotrienol on Isoprenoid Pathway of Hepatoma Cell Line

Article *in* European Journal of Scientific Research · October 2007

CITATIONS
4

READS
2,048

4 authors, including:

Zakiah Jubri
Universiti Kebangsaan Malaysia
33 PUBLICATIONS **253** CITATIONS

SEE PROFILE

European Journal of Scientific Research

ISSN: 1450-216X **Volume 18, No 4 October, 2007**

As of 2005, European Journal of Scientific Research is indexed in ULRICH, DOAJ and CABELL academic listings.

European Journal of Scientific Research

http://www.eurojournals.com/ejsr.htm

Editorial Policies:

1) European Journal of Scientific Research is an international official journal publishing high quality research papers, reviews, and short communications in the fields of biology, chemistry, physics, environmental sciences, mathematics, geology, engineering, computer science, social sciences, medicine, industrial, and all other applied and theoretical sciences. The journal welcomes submission of articles through ejsr@eurojournals.com.

2) The journal realizes the meaning of fast publication to researchers, particularly to those working in competitive & dynamic fields. Hence, it offers an exceptionally fast publication schedule including prompt peer-review by the experts in the field and immediate publication upon acceptance. It is the major editorial policy to review the submitted articles as fast as possible and promptly include them in the forthcoming issues should they pass the evaluation process.

3) All research and reviews published in the journal have been fully peer-reviewed by two, and in some cases, three internal or external reviewers. Unless they are out of scope for the journal, or are of an unacceptably low standard of presentation, submitted articles will be sent to peer reviewers. They will generally be reviewed by two experts with the aim of reaching a first decision within a three day period. Reviewers have to sign their reports and are asked to declare any competing interests. Any suggested external peer reviewers should not have published with any of the authors of the manuscript within the past five years and should not be members of the same research institution. Suggested reviewers will be considered alongside potential reviewers identified by their publication record or recommended by Editorial Board members. Reviewers are asked whether the manuscript is scientifically sound and coherent, how interesting it is and whether the quality of the writing is acceptable. Where possible, the final decision is made on the basis that the peer reviewers are in accordance with one another, or that at least there is no strong dissenting view.

4) In cases where there is strong disagreement either among peer reviewers or between the authors and peer reviewers, advice is sought from a member of the journal's Editorial Board. The journal allows a maximum of two revisions of any manuscripts. The ultimate responsibility for any decision lies with the Editor-in-Chief. Reviewers are also asked to indicate which articles they consider to be especially interesting or significant. These articles may be given greater prominence and greater external publicity.

5) Any manuscript submitted to the journals must not already have been published in another journal or be under consideration by any other journal, although it may have been deposited on a preprint server. Manuscripts that are derived from papers presented at conferences can be submitted even if they have been published as part of the conference proceedings in a peer reviewed journal. Authors are required to ensure that no material submitted as part of a manuscript infringes existing copyrights, or the rights of a third party. Contributing authors retain copyright to their work.

6) Submission of a manuscript to EuroJournals, Inc. implies that all authors have read and agreed to its content, and that any experimental research that is reported in the manuscript has been performed with the approval of an appropriate ethics committee. Research carried out on humans must be in compliance with the Helsinki Declaration, and any experimental research on animals should follow internationally recognized guidelines. A statement to this effect must appear in the Methods section of the manuscript, including the name of the body which gave approval, with a reference number where

appropriate. Manuscripts may be rejected if the editorial office considers that the research has not been carried out within an ethical framework, e.g. if the severity of the experimental procedure is not justified by the value of the knowledge gained. Generic drug names should generally be used where appropriate. When proprietary brands are used in research, include the brand names in parentheses in the Methods section.

7) Manuscripts must be submitted by one of the authors of the manuscript, and should not be submitted by anyone on their behalf. The submitting author takes responsibility for the article during submission and peer review. To facilitate rapid publication and to minimize administrative costs, the journal accepts only online submissions through ejsr@eurojournals.com. E-mails should clearly state the name of the article as well as full names and e-mail addresses of all the contributing authors.

8) The journal makes all published original research immediately accessible through www.EuroJournals.com without subscription charges or registration barriers. European Journal of Scientific Research indexed in ULRICH, DOAJ and CABELL academic listings. Through its open access policy, the Journal is committed permanently to maintaining this policy. All research published in the. Journal is fully peer reviewed. This process is streamlined thanks to a user-friendly, web-based system for submission and for referees to view manuscripts and return their reviews. The journal does not have page charges, color figure charges or submission fees. However, there is an article-processing and publication charge.

Further information is available at: http://www.eurojournals.com/ejsr.htm

European Journal of Scientific Research

Volume 18, No 4 October, 2007

Contents

European Journal of Scientific Research
ISSN 1450-216X Vol.18 No.4 (2007), pp.568-575

http://www.eurojournals.com/ejsr.htm

Coinfection of Cowpea (*Vigna Unguiculata* (L.) Walp) with the Root-Knot Nematode *Meloidogyne Javanica* (Treub) Chitwood and the Fungus *Fusarium Oxysporum (Schlecht.)* Synder and Hansen and Effect on *Plant* Growth

C. C. Iheukwumere
Department of Biological Sciences
University of Agriculture, Makurdi, Benue State Nigeria
E-mail: ceceiheukwumere@yahoo.com

Z. Uvashir
Department of Biological Sciences
Benue State University, Makurdi, Benue State, Nigeria

C. I. Iheukwumere
Department of Food Science and Technology
University of Agriculture Makurdi, Benue State, Nigeria

Abstract

The effect of single and co-infection of cowpea *Vigna unguiculata* L. Walp with 2,500 juveniles of *Meloidogyne javanica* (Treub) Chitwood and 5gms of *Fusarium oxysporum* (Schlecht.) Synder and Hansen on growth and yield components of the crop was investigated. Results showed that single infection with either pathogen or simultaneous inoculation with both, generally reduced growth and yield components of the cowpea when compared to the uninoculated healthy controls. Similarly, simultaneous infection with both pathogens caused the highest reductions in the growth and yield parameters although, some of these reductions were not statistically different from the effects of single and successive infection of the plant. Plants with combined infection exhibited more severe symptoms that included wilting, foliage drooping and mild chlorosis than those infected with either of the pathogens alone. The severity of gall formation in mixed infection was reduced more than in single infection with the nematode. Co-infection in which fungus inoculation preceded that with the nematode by 7 days (F+n) was the most significantly reduced. The implication of this finding, is that mixed infection of this cowpea by these pathogens, as is frequently observed in our farms may in future constitute a serious threat to food security in Nigeria and should therefore, attract attention more than it is presently.

Keywords: Single and coinfection, *Meloidogyne javanica, Fusarium oxysporum,* growth and yield components, cowpea.

Introduction

Cowpea (*Vigna unguiculata* (L.) Walp) is an important and relatively cheap source of protein in Nigeria where it is made into a variety of local dishes (Katung *et al.,* 1993; Alabi and Emechebe, 2006). The cowpea's fodder is also used for animal feed (Alabi and Emechebe, 2006). Although, Nigeria is the leading producer of the cowpea in the world (Katung *et al.,* 1993; Mukhtar and Alhassan, 2006), yields have remained low at 150 – 250kg/ha (Katung *et al.,* 1993).

Most of the cowpea is produced in the rural areas with 80% of it grown in Northern Nigeria (Katung *et al.,* 1993; Alabi and Emechebe, 2006). Some of the major constraints to its production, include the attack by fungal diseases (Alabi and Emechebe, 2006) and phytoparasitic nematodes (Adesiyan *et al.,* 1990). This will continue to be so, because most (if not all) of the available varieties have not been bred for resistance to these pests. And because fungi and nematode pathogens occur wherever susceptible crops are grown, cases of mixed infection by both pathogens in cowpea fields are high. Although, there are reports of mixed infection of the root-knot nematodes – *Meloidogyne* spp and such fungal pathogens as *Pythium* spp, *Fusarium* spp, *Phytopthora* spp, *Rhizoctonia* spp, etc (Adesiyan *et al.,* 1990) in other parts of the world, there is little or no information on mixed infection of cowpea by both *Fusarium* and the root-knot nematode in Nigeria. Previous reports of pathogenicity of these pathogens on cowpea in Nigeria, addressed single infection by either of the pathogens (Oyekan, 1977; Caveness and Ogunfowora, 1985; Emechebe and Shoyinka, 1985; Adesiyan *et al.,* 1990) and not both; hence the need for this study.

This study is therefore, an attempt to evaluate the effect of single and mixed infection of cowpea by *Meloidogyne javanica* and *Fusarium oxysporum* both of which has frequently been observed on cowpea fields in Benue State, for which information is presently lacking.

Materials and Methods

Healthy seeds of cowpea var. MN150 obtained from Akperan Orshi College of Agriculture Yandev, a substation of National Cereals Research Institute (NCRI); were surface sterilized according to the methods of Koenning and McClure (1981) and Iheukwumere (2006) by dipping them for 5mins in 1.05% sodium hypochlorite and rinsing for 5mins in 6 changes of sterile distilled water before sowing. Five seeds were sown per 18-cm – diameter plastic pots containing 2kgs of autoclaved sandy – loam soil (Chaudraguru and Rajarajan, 1990; Iheukwumere, 2002). Seven days after germination, seedlings were thinned to a stand per pot ensuring that they were all of uniform growth and vigour.

Source of Nematode and its Extraction

Galled roots of 8 week-old tomato plants (*Lycopersicum esculentum* Mill) on which M. *javanica* that was previously identified by perineal pattern morphology according to the method of Eisenback *et al*. (1981) was multiplied, were carefully collected and cut into fragments of 1-2cm. The cut pieces of the galled roots, were placed in a Pie-Pan modification of Baermann funnel according to the methods of Whitehead and Hemming (1965) and Iheukwumere (2006) for the extraction of juveniles of the nematode after 48 hours (Noe, 1986) at the laboratory room temperature of 27±2ºC. An aliquot of 1 milliliter extract of the juveniles obtained after 48 hours, was placed in a 40ml round plastic counting dish (Hooper, 1990) and a few drops of water added to evenly spread the juveniles over the entire surface of the dish, to enhance counting. The dish was placed under a stereoscopic microscope and the number of juveniles therein, counted at a magnification of x40 (Iheukwumere, 2005). The suspension of the juveniles was diluted with water to 500 larvae per milliliter (Koenning and McClure, 1981). Five mls of the homogenous extract of the juveniles, was pipetted into test tubes to deliver 2,500 larvae of *M. Javanica* that were subsequently used to inoculate test plants.

Fungus Isolation and Culture

The *Fusarium oxysporum* used for this study was isolated from a diseased tomato stem. Diseased tissues of the infected stem were cut into 1-2mm diameter fragments and sterilized in 0.1% mercuric chloride for 2 minutes. They were rinsed in three changes of sterile distilled water and thereafter plated out on water agar. The plates were incubated at room temperature 27±2ºC for 3 days before sub-culturing on Potato Dextrose Agar (PDA) plates (Chiejina, 2006). The PDA plates were incubated for 5-7 days and sub-cultured repeatedly on clean PDA plates until pure cultures of the isolate were obtained. At the end of the incubation period, the fungus was identified using a stereobinocular microscope (6-50x) based on the fungus habit characteristics (Ataga and Ota-ibe, 2006). Identification was made following fungal descriptions by Barnett and Hunter (1999) and Alexopoulos *et al.* (2002).

Discs cut from 7-day-old cultures of the fungus with 0.5-cm-diameter sterile cork borer (Ataga and Ota-ibe, 2006) were repeatedly transferred onto a sterilized Whatman No. 1 filter paper placed on a Triple Beam Balance until 5gm weight of the fungus was obtained. The 5gm weight of the *F. oxysporum* served as the inoculum for the fungus.

Inoculation of Test Plants

Plants were not watered the day preceding that for inoculation. The 7 day-old seedlings, were inoculated with 2,500 juveniles of the nematode using the trench method of Iheukwumere *et al.* (1995). Seedlings were also infected with the fungus multiplied on PDA by introducing 5gm of the fungus into shallow holes made in the root rhizoshpere of the plants.

Treatment given to the 7-day-old seedlings included:

(i) Uninoculated control plants (C)
(ii) Plants inoculated with 5gm of *F. oxysporum* only (F),
(iii) Plants inoculated with 2,500 juveniles of nematode only (N),
(iv) Plants simultaneously inoculated with 2,500 juveniles of the nematode and 5gm of the fungus (N+F),
(v) Plants inoculated with 5gm of the fungus at 7^{th} day after planting followed by inoculation with 2,500 juveniles of the nematode 7 days later (F+n) and
(vi) Plants inoculated with 2,500 nematode juveniles at 7^{th} day after planting followed by inoculation with 5gm of the fungus 7 days later (N+f).

Treatments were arranged in a completely randomized design with 5 replications per treatment on a cemented platform behind the Botany laboratory of Benue State University Makurdi at 28±3ºC. Plants were watered as was necessary and inspected for symptoms weekly.

The experiment was terminated eight weeks after inoculation and the following growth and yield parameters assessed:-

Shoot fresh and dry weights, shoot and root lengths, root fresh and dry weights, podfresh and dry weights. Data obtained were subjected to ANOVA and means separated by LSD at P=0.05 (Table 1). The severity of root galling was determined by use of 0-5 scale according to the methods of Iheukwumere *et al.* (1995) and Iheukwumere (2006). The number of second stage juveniles present in thoroughly mixed 200ml of each pot soil, was extracted using the Pie-pan modification of Baermann funnel method (Whitehead and Hemming, 1965; Iheukwumere, 2006). Data obtained from gall rating and number of juveniles extracted, were square root transformed before being statistically analyzed (Table 1).

Results

For shoot length, no significant differences were recorded among treatments C, F, F+n and N+f but each of them was significantly higher than those of N and N+F (Table 1). For shoot fresh weight, no

significant differences were detected among treatments N, F, N+F, N+f and F+n but each of them was significantly lower than that for C (Table 1). The shoot dry weight data, indicated that there were no significant differences among C, N, F, N+f and F+n; however, each of them was significantly higher than N+F (Table 1). Data on root length showed that control plants had significantly longer lengths than all the other treatments. These other treatments did not differ significantly amongst their root lengths (Table 1). Root fresh weights of C, N, F and N+f did not differ significantly but were however, significantly higher than those of N+F and F+n (Table 1). The root dry weights of the control plants were significantly higher than those of other treatments. The latter, did not differ significantly among their root dry weights (Table 1). Pod fresh weight data followed same trend as reported for the root dry weight.

For pod dry weight, there was no significant difference between treatments N and N+F each of which was significantly lower than the rest of the other treatments (Table 1). Data on severity of galling, showed that there were no significant differences among treatments N, N+f and N+F although, the severity of the galling decreased slightly in that order of descending magnitude. The least gall rating was noted in treatment F+n which was significantly lower than each of the rest (Table 1).

Discussion

It was observed that single or combined infection generally caused significant reductions in the growth and yield of this cowpea variety as compared to the uninoculated control plants. This is probably so because, the presence of these pathogens in the plant would certainly have impaired the physiological activities in the plant thereby adversely impacting on its growth and yield components. The physiological impairment of this cowpea, could be the result of damage to vascular tissues with the resultant disruption of water and nutrient uptake including the upward translocation by the root system (Hussey, 1985).

Since the two pathogens attacked the roots of the plants, there is no doubt that nutrient and water absorption would have been disrupted to the detriment of the plant. This can also account for the deleterious effects of the infection on the growth and yield components so affected. The effect of the pathogens might also have caused a reduction in photosynthesis with the concurrent increase in respiration which could also be inimical to the growth of the infected plants. (Hussey, 1985; Iheukwumere, 2006).

Although, there were no significant differences between the effects of single and mixed infections by both pathogens in the plant, inoculation in which the fungi and the nematodes were introduced simultaneously caused the highest reduction in most of the growth and yield components considered. The probable reason for this may be that, concomitant introduction of both pathogens gave room for intense competition for the roots and the available nutrients which consequently reduced the growth and development of the plants more than in single infection with either of the pathogens and in cases where the infection of one was made to precede the other by 7 days. The parasitory effects of both pathogens on the roots of the plants would no doubt have impacted more negatively on the plant than infection with each pathogen alone. This may be the reason why the combined infection affected the plant more, hence higher reduction in the growth and yield components of the crop than those by single infections

The above finding, agrees with the observation of Zahid *et al.* (2002) who showed that combined inoculation of *Meloidogyne* spp and *F. oxysporum* simultaneously caused the greatest reduction in shoot and root lengths of clover (*Trifolium repens*) and their corresponding dry weights together with damage on the root system. The infection complex of pathogens in the cowpea elicited such symptoms as wilting and foliage drooping especially during high day temperatures even though soil moisture was adequate. Mild chlorosis was noted on the leaves of the plants with mixed infections which was absent on those of single infection with either pathogen. Similar symptom expression was also observed in multi-pathogen infection of a soybean (Nakajima and Charchar, 1996). Furthermore,

successive infection (i.e. N+f or F+n), where the infection with either of the pathogens was made to precede the other by 7 days could not exert as much damage as was the case with simultaneous inoculation probably because, the introduction of one pathogen into the plant first, might have elicited some kind of tolerance or resistance against the introduction of a subsequent one in the same plant.

The above phenomenon is possible, because it has been established that the infection of a plant may confer to that plant partial or total protection from secondary infection with another pathogen (Mahmood *et al.,* 1974; Husain *et al.,* 1985; Wood, 1992; Iheukwumere *et al.,* 2005). This may explain why successive infection was not as damaging as that by simultaneous infection even though their effects in most cases were not statistically different from that by concomitant infection.

Apart from shoot fresh weight, root length, root dry weight and pod fresh weight which single or mixed infection significantly reduced in comparison with the control, the other growth and yield parameters were not adversely affected by the said infection. This is probably because, infection does not necessarily produce disease at all times in all parts of an infected plant (Matthews, 1981). Furthermore, growth may be evenly reduced throughout a plant or the stunting confined to specific parts or organs of a plant (Matthews, 1981). These may be responsible for why those growth parameters were not adversely affected. Furthermore, it is also possible that the respective pathogens induced the production of certain hormones which probably interacted in a way that caused the various plant organs or tissues to respond differently to the infection (Hussey, 1985). For instance, it is known that the disruption of the regulatory processes of growth hormones by infection, influences the growth and yield components of the plant so affected (Wallace, 1987). In addition, the parasitism of infected plant roots by soil-borne pathogens causes water stress that induces physiological responses that can lead to the partitioning of carbohydrates among plant organs, reduction of photosynthesis and decreased efficiency of carbon fixation (Wilcox-Lee and Loria, 1987), thus leading to different physiological effects on the physiological processes that are associated with the various organs and tissues of this plant. This phenomenon was similarly observed in a soybean that was infected with the same pathogens (Iheukwumere and Okpeh, unpublished).

Of the gall indices, F+n was the most significantly reduced, may be because the introduction of the fungi first, enabled it to establish and destroy the roots thereby reducing the amount of roots that should have been available for nematode growth and development (Muktar and Khan, 1989). It is also possible that the fungus released some nematotoxic antimetabolites that could have hampered nematode development (Morgan-Jones *et al.,* 1984). In addition, it is also an established fact that *F. oxysporum* is known to parasitize the eggs and females of the root-knot nematode including the host giant cells that are necessary for nematode development (Koenning and McClure, 1981; Morgan-Jones *et al.,* 1984).

The foregoing phenomena, may not be the case when both were simultaneously introduced (N+F) or when the nematode was introduced before fungus (N+f) in which cases the fungus would not have the competitive advantage as was the case in F+n since there probably won't be time for it to establish sufficiently enough, to interfere with the nematode development. This might, account for why there was no significant difference between the gall index of N+f and N+F treatments. Although, there was no significant difference between N+F and N+f gall indices, the gall index of N+F was reduced more than that of N+f. This could be the result of some antagonism by the fungus against the nematode in the course of competing for nutrients in the plant. This is likely to be so because, when the nematode was introduced some days (7 days) before that of fungus (N+f), the gall index was slightly higher (than that of N+F); apparently showing that the nematode had some time to adjust and establish infection before the introduction of the fungus. In addition, reduction in gall index was highest in F+n treatments as earlier observed. These phenomenon have similarly been demonstrated in mixed infection involving a root-knot nematode and different viruses in other plant hosts by other workers (Koenning and McClure, 1981; Alam *et al.,* 1990) and in soybean that was mix infected with *M. javanica* and *F. oxysporum* (Iheukwumere and Okpeh, unpublished).

The number of juveniles extracted, followed same trend as reported for the gall indices and may also be due to the reasons adduced for the observations made on the gall indices.

The gall index for N was the highest apparently because there was no competition with any organism and as such, the nematode had all the necessary space and nutrients to its self for growth and development, hence it has the highest gall rating.

The fact that single infection of this cowpea by the fungus or the nematode, can lead to growth and yield reductions of this crop and worse still when both infect simultaneously, stresses the need for preventing infection by both pathogens in the field. This will no doubt, aid the attainment of food sufficiency particularly, plant protein nutrition in this country. Furthermore, more research should be geared towards evaluating multi-infection of our crops rather than dwelling on mono-infection studies as is presently the case. This is essentially because, in the field, the crops are open to a number of biotic factors that can adversely affect their productivity as has been demonstrated in this study.

Acknowledgement

The authors express their gratitude to Mr. Wayas and Mrs. Shiriki both of the Department of Biological Sciences of the Benue State University for their technical assistance.

References

[1] Adesiyan, S. O., Caveness, F. E., Adeniji, M. O. and Fawole, B. (1990). *Nematode Pests of Tropical Crops*. Heinemann Educational Books (Nigeria) Limited, 114pp.

[2] Alabi, O. and Emechebe, A. M. (2006). Evaluation of cowdung extract for the management of scab induced by *Elsihoe phaseoli* in cowpea at Samaru, Northern Nigeria. *Nigerian Journal of Botany* 19 (1): 169-175.

[3] Alam, M. M., Samad, A and Anver, S. (1990). Interaction between tomato masaic virus and *Meloidogyne incognita. Nematologia Mediteranea*, 17:121-122.

[4] Alexopoulos, C. J., Mims, C. W. and Blackwell, M. (2002). *Introductory Mycology*, 4th edition. John Wiley & Sons Inc. Singapore, 869 pp.

[5] Ataga, A. E. and Ota-ibe, G. (2006). Seed-borne fungi of the wild mango (ogbono) *Irvingia gabonensis* (Aubry-Le conte Ex O' Rorke) Bail and their effects on food composition. *Nigerian Journal of Botany* 19(1):54-60.

[6] Barnett, H. L. and Hunter, B. B (1999). *Illustrated Genera of Imperfect Fungi*, 4th edition. The American Phytopathological Society, St. Paul, Minnesota, USA, 218pp.

[7] Caveness, F. E. and Ogunfowora, A. O. (1985), Nematological studies world wide. In: *Cowpea Research, Production and Utilization* (eds. Singh, S. R. and Rachie, K. O.). John Wiley & Sons Ltd. Pp 273-285

[8] Changraguru, T. and Rajarajan, P. A. (1990). Screening of some greengram cultivars/breeding lines against the root-knot nematode *Meloidogyne incognita. International Nematology Network Newsletter* 7(2): 22-23.

[9] Chiejina, N. V. (2006). Potentials of the leaf extracts of *Azadirachta indica* A. Juss and *Ocimum gratissimum* L. for the control of some potato (*Solanum tuberosum* L.) fungal diseases. *Nigerian Journal of Botany* 19(1): 68-73.

[10] Eisenback, J. D., Hirschmann, H., Sasser, J. N. and Triantaphyllou, A. C. (1981). *A Guide to the Four Most Common Species of Root-knot Nematodes* (*Meloidogyne* spp) *With a Pictorial Key*. North Carolina University Graphics, Raleigh, N. C. 48pp.

[11] Emechebe, A. M and Shoyinka, S. A. (1985). Fungal and bacterial diseases of cowpeas in Africa. In: *Cowpea Research*, *Production and Utilization*. (eds. Singh, S. R. and Rachie, K. O.) John Wiley & Sons Ltd. Pp. 173-192.

[12] Hooper, D. J. (1990). Extraction and processing of plant and soil nematodes. In: *Plant Parasitic Nematodes in Subtropical and Tropical Agriculture* (eds. LUC M., Sikora, R. A. and Bridge, J.). C.A.B International Institute of Parasitology, C.A.B. International Wallingforal Oxon OX10 88E UK. Pp. 45-65.

[13] Husain, S. I., Khan, T. A. and Jabri, M. R. A (1985). Studies on root-knot and pea mosaic virus complex of *Pisum sativum. Nematologia Mediterranea* 15:103-109.

[14] Hussey, R. S. (1985). Host-parasite relationships and associated physiological changes. In: *An Advanced Treatise on Meloidogyne Volume 1 Biology and Control* (eds. Sasser, J. N. and Carter, C. C.), International *Meloidogyne* project. North Carolina State University Graphics, Box 7226, Raleigh, North Carolina 27695-7226. pp 144-153.

[15] Iheukwumere, C. C., Atiri, G. L., Fawole, B. and Dashiell, K. E. (1995). Evaluation of some commonly grown soybean cultivars for resistance to the root-knot nematode and soybean mosaic virus in Nigeria. *Fitopatologia Brasileira* 20:190-193.

[16] Iheukwumere, C. C. (2002) Mechanical and biological transmissibility of cowpea aphid-borne mosaic virus (CAbMV) on soybean (*Glycine Max* L. Merrill). *Nigerian Journal of Botany* 15:92-96.

[17] Iheukwumere, C. C. (2005). Effects of single and mixed inoculation of soybean mosaic potyvirus and *Meloidogyne incognita* on the pathogen multiplication, pathogenicity and growth of a susceptible soybean, *Glycine max* (L.) Merrill, variety. *Nigerian Journal of Plant Protection* 22:1-12.

[18] Iheukwumere, C. C. (2006). Interaction of soybean mosaic potyvirus and root-knot nematode (*Meloidogyne incognita* Kofoid and White) Chitwood infection in soybean: Effects on pathogen multiplication, infectivity and growth of the soybean (*Glycine max* (L.) Merrill) var Malayan. *Nigerian Journal of Botany* 19 (1):44-53.

[19] Katung, P. D., Chiezey, U. F. and Shebayan, J. A. Y. (1993) Response of two cowpea (*Vigna unguiculata* (L.) Walp) varieties to different levels of nitrogen and phosphorus fertilizers in a Northern Guinea Savanna Environment. *Journal of Agricultural Science and Technology* 3 (1):21-23.

[20] Koenning, S. R. and McClure, M. A. (1981). Interaction of two potyviruses and *Meloidogyne incognita* in Chili pepper. *Phytopathology* 71:404-408.

[21] Mahmood, K., Akram, M., Nagiv, S. O. A. and Alam, M. M. (1974). Studies on the interaction between bottle-guard mosaic virus and powdery mildew fungus, *Sphaerotheca fuliginea. Indian Phytopathology*. 27:627-629.

[22] Matthews, R. E. F. (1981). *Plant Virology*, 2nd edition. Academic Press Inc. III Fifth Avenue, New York, 877pp.

[23] Morgan-Jones, G., White, J. F. and Rodriguez-Kabana, R. (1984).Fungal parasites of *Meloidogyne incognita* in an Alabama soybean field soil. *Nematropica* 14:93-96.

[24] Mukhtar, F. B and Alhassan, S. (2006). Effect of seed weight and coat on water imbibition and germination of cowpea *Vigna unguiculata* (L.) Walp. *Nigerian Journal of Botany* 19(1): 147-155.

[25] Mukhtar, J. and Khan, A. A. (1989). Disease complex in chickenpea involving *Meloidogyne javanica* and *Sclerotium rolfsi. International Nematology Network Newsletter 6 (4):31-32.*

[26] Nakajima, T. and Charchar, M. J. D. (1996). First occurrence of sudden death syndrome of soybean in Brazil. *Japan Agricultural Research Quarterly* 30:31-40.

[27] Noe, J. P (1986). Cropping systems analysis for limiting losses due to plant-parasitic nematodes: *Guide to Research Methodology*. North Carolina State University Graphics Raleigh, 18pp.

[28] Oyekan, P. O. (1977). Reaction of some cowpea varieties to *Fusarium oxysporum* f.sp. *tracheiphilum* in Nigeria. *Tropical Grain Legume Bulletin* 8, 47-49.

[29] Wallace, H. R. (1987). Effects of nematode parasites on photosynthesis. In: *Vistas on Nematology* (eds. Veech, J. A. and Dickson, D. W), Society of Nematologists Inc. Hyattsville, Maryland. pp 253-259.

[30] Whitehead, A. G. and Hemming, J. R. (1965). A comparison of some quantitative methods of extracting small vermiform nematodes from soil. *Annals of Applied Biology*. 55:25-38.

[31] Wilcox-Lee, D. and Loria, R. (1987). Effects of nematode parasitism on plant-water relationship. In: *Vistas on Nematology* (eds. Veech. J. A and Dickson, D. W), Society of Nematologists Inc. Hyattsville, Maryland. pp 260-266.

[32] Wood, R. K. S. (1992). Induction of disease resistance, In: Interactions plantes microorganisma (ed. Wood, R. K. S.), Foundation Internationale Pour la Science, Senegal February, 1992 ifs, pp 246-252.

[33] Zahid, B. M., Furr, G. M., Nikadrow, A., Hadda, M., Fulkerson, W. J. and Nicol, H. L. (2002). Effects of root and stolon infecting fungi on root colonizing nematodes of white clover. *Plant Pathology* 51:242-250.

European Journal of Scientific Research
ISSN 1450-216X Vol.18 No.4 (2007), pp.576-583

http://www.eurojournals.com/ejsr.htm

The Antiproliferative Effect of Palm Oil Gamma-Tocotrienol on Isoprenoid Pathway of Hepatoma Cell Line

Aida Juliana AJ
Department of Biochemistry, University Kebangsaan Malaysia
Kuala Lumpur

Zakiah J
Department of Biochemistry, University Kebangsaan, Faculty of Medicine
Jalan Raja Muda Abdul Aziz, 50300 Kuala Lumpur, Malaysia
E-mail: zakiah@medic.ukm.my
Tel: +603-40405291; Fax: +603-26938037

Abdul Gapor MT
Chemistry Division, Malaysian Palm Oil Board, Bangi, Selangor, Malaysia

Wan Ngah W.Z
Department of Biochemistry, University Kebangsaan Malaysia
Kuala Lumpur

Abstract

Objectives: Study was conducted to determine the mechanism of antiproliferative activity of gamma-tocotrienol in signal transduction of isoprenoid pathway and Ras protein expression in HepG2 cell line.
Design and Methods: HepG2 and WRL-68 were cultured and exposed with different concentration of GTT to determine the IC50 and their antiproliferative effect by using MTS assay. The GTT uptake was determined by HPLC. The effect of prenylated side chain of GTT was determined by co-incubation of GTT with farnesol and assayed by using BrdU. The Ras protein expression was analyzed using Western blotting.
Results: Results showed that the IC_{50} GTT for HepG2 was 170 μM and WRL-68 was 500 μM within 48 h and its uptake was 12 μM and 40 μM respectively. Co-incubation of GTT with *trans, trans*-farnesol increases cell proliferation and Ras protein expression. While treatment of GTT or farnesol alone reduce cell proliferation and Ras protein expression.
Conclusions: GTT was toxic against HepG2 at a lower concentration. Its antiproliferative activity against HepG2 might be due to the action of its prenylated side chain that induce the conversion of FPP to farnesol and downregulates HMGCoA reductase activity. Reducation of FPP might reduced Ras protein prenylation.

Keywords: Isoprenoid pathway, farnesol, γ-tocotrienols, Ras protein

Introduction

Cell proliferation, differentiation and survival are regulated by a number of extracellular hormones, growth factors and cytokines in complex organisms. These molecules served as ligand for cellular receptors and communicate with the nucleus of cell through a network of intracellular signaling pathway (1). Post-translational addition of isoprenoid lipids via a process termed prenylation is an important event for the biological activity of many proteins that play critical roles in signal transduction and cell growth regulation. Recent observations established a direct connection between the isoprenoid pathway and Ras-induced transformation. In fact, it has been demonstrated that farnesol, an isoprenoid-derived metabolite, is required for the modification that leads to the activation of the Ras oncogene product, $p21^{ras}$. The linkage of a farnesyl group to $p21^{ras}$, catalyzed by the farnesyltransferase (FPtase), initiates a set of additional post-translational modifications, that promote the anchorage of the Ras protein to the cell membrane, thus leading to the functional activation of this oncogene-encoded protein. Ras proteins are generally considered as molecular switches in signal transduction pathways leading to cell proliferation. Dysregulated cell signaling and proliferation may occur in cancer cells through over expression or mutation of proto-oncogenes such as Ras, which functioning as a molecular switches in a large network of signaling mainly in differentiation and proliferation of cells. The involvement of Ras in uncontrolled growth is fundamental, since an increased expression of normal or mutated Ras, has been found in about 30% of all human cancers making this G protein an important target for the development of anti-cancer drugs.

Cell culture studies indicate clearly that tocotrienols influence cholesterol synthesis by directly regulating expression of 3-hydroxy-3-methylglutaryl-coenzyme A reductase (HMG CoA reductase), principally through a postransciptional process involving accelerated degradation of the reductase protein (2). The notion of tocotrienol being an effective as chemopreventive agent has also been enhanced due to its anti-tumor property. A number of studies have shown growth inhibition of tumor cell lines and was more pronounced when exposed to GTT. The effect of tocotrienols on cell proliferation represent a potentially important physiological role in the prevention of cancer. The precise mechanism for the antiproliferative property of tocotrienols is uncertain, but may lie in its prenylated side chain involved in the production of isoprenoid intermediates (farnesol) from the mevalonate biosynthetic pathway (3). These intermediates are thought to be involved in the prenylation of several signal transduction proteins including Ras protein, essential for normal cell growth (4).

Materials and Methods

Materials

Cell hepatoma HepG2 and WRL-68 were purchased from American Type Culture Collection (ATCC), USA; γ-tocotrienol (GTT) was supplied by Malaysian Palm Oil Board (MPOB); Fetal Calf Serum (FCS) purchased from PAA Austria; *trans, trans*-farnesol was from Sigma Chemical USA; CellTiter 96® AQ_{ueous} One Solution Cell Proliferation MTS assay was from Promega, Winconsin USA; BrdU Cell Proliferation ELISA kit was from Roche Diagnostic, Mannheim, Germany; Monoclonal Ras (Clone Ras 10) antibody (from mouse) was from Chemicon Int. USA; Horseradish Peroxidase linked secondary antibody from mouse and polyvinylidine difluoride (PVDF) membrane were from Amersham and Enhanced Chemiluminescent Detection (ECL) was from Perkin Elmer, USA.

Cell Culture

Stock solutions of GTT (0.5 M) were freshly prepared in 100% ethanol and preserved at -20ºC for not more than 1 month. Immediately before use, 0.5 M GTT was prepared from the stock solution by adding fetal calf serum (FCS) and incubated for an overnight (37ºC). Then culture medium and 100% ethanol were added to give the final concentration of 750 μM. HepG2 and WRL-68 cell line were

grown in Eagle minimum essential medium (EMEM) supplemented with 10% FCS in 75 cm^2 flask. Upon reaching confluency, cells were trypsinized, centrifuged and were counted by using a haemocytometer. The cell suspension was adjusted to a concentration of 2 x 10^6 cell/ml for BrdU Cell Proliferation assay and Western Blot Analysis. The cell cultures were divided into four groups; control, cell treated with GTT in the presence of farnesol, GTT without farnesol and farnesol alone. The cell cultures were treated with GTT and farnesol at IC_{50} value of 170µM and 4 µM respectively. Untreated control contains only cell in EMEM and 10% FCS (CCM).

Cell Viability Assay

Cell viability studies were performed by using MTS assay. Serial dilutions of GTT were made (10, 100, 300, 500 and 750 µM) in 50% ethanol. *Trans, trans*-farnesol was freshly prepared from stock and a serial dilution was also made (2, 5, 10, 20, 30 and 35 µM) by diluting with 0.1 % methanol. Briefly cells were cultured in 96 well plates and incubated for 24 hours at 37ºC in 5 % CO_2 incubator. Then, the cultures were treated with a serial dilution of GTT and farnesol. After incubation for another 48 hours, cells were centrifuged to replace the media and MTS was added. Cells were incubated for a further 4 hours. Absorbance was measured at 490 nm. The percentage viability was calculated by comparing the absorbance of cells treated with GTT to the untreated control cells (corresponding to 100% viable cells).

Extraction and HPLC Analysis

GTT uptake was determined by using High Performance Liquid Chromatography (HPLC) analysis. HPLC analysis was carried out as a modification of Meydani et. al. (5). Prior to GTT extraction treated and untreated cells HepG2 and WRL-68 (2x10^6 cells/well) were collected and counted. Then 100µL ice cold PBS and 50 µL butylated hydroxytoluene (BHT) (50 mg/ml) were added and incubated for 10 min at room temperature. Then, 500µL ice cold 95% ethanol was added and vortexed for 1 min, continued by sonication for 40 sec to deproteinized cells. Thereafter, 500µL ice cold HPLC hexane added and the lysate were vortex for 1min, centrifuged at 3000 g for 7 min. After second spin, 450 µL of the top supernatant layer were collected and dried using Heto vacum at 4ºC for 40 min. The residue was kept in -20ºC before run HPLC analysis.

Cell Proliferation

Cell proliferation was done using BrdU Cell Proliferation kit according to the manufacturer's protocol. Cell cultures were set up in 96-well flat bottom plates at 2 × 10^6 cells/well in 100 µL media plus treatments and incubated 24 hours in 5% CO_2 at 37°C. At the end of the treatment time, cell proliferation rate was measured based on the measurement of BrdU incorporation during DNA synthesis. Briefly, BrdU labeling solution (10 µL/well) was added and incubated for 2 hours at 37ºC. Thereafter, FixDenat (200 µL/well) was added and incubated for 30 min at room temperature. Subsequently, anti-BrdU-POD (peroxidase-conjugated anti-BrdU antibody) solution (100 µL/well) was added for 90 min at room temperature. At the end of the assay, 100 µL peroxidase substrate (5-bromo-2′-deoxyuridine labeling) was filled into each well. After 5 min of incubation at room temperature, the reaction was stopped with 25 µL 1 M H_2SO_4 and absorbance of the samples was assessed. Results were expressed as mean absorbance of the samples in an ELISA plate reader at 450 nm with a reference wavelength of 690 nm.

Western Blot Analysis

Cell cultures were grown in 96-well flat bottom plates at 2 × 10^6 cells/well in 100 µL CCM plus treatments and incubated for 24 hours in 5% CO_2 at 37°C. The cells were washed and scraped into PBS, spin 600 rpm for 10 min. The pellet was washed again with PBS cold, incubated for 10 min and transfer to eppendorf tube and spin at maximum speed (13,200rpm) for 10 s. The isolated membrane

fraction (pellet) was put in ice container (4ºC) to prevent denaturation. To extract the protein 200µl lysis buffer (5.26 µl Aprotinin, 10 µl PMSF, 0.1 µl Na_3VO4, 4 µl Leupeptin, 10 µl EDTA, 1 µl DTT and 969.64 µl RIPA buffer) added to each tube and incubated for 30 min (ice). Spin again at max speed (13,200 rpm) for 30 min in cold room. The protein concentration (50 µg) from the supernatant was measured using Bradford assay. Aliquots of protein (50 µg) were subjected to electrophoresis on 12% SDS-PAGE, transferred onto polyvinylidine difluoride (PVDF) membrane at 140 V and 2 h RT to immunoblotted with specific antibodies. Ras antibody from Chemicon diluted 1:1000. Horseradish Peroxidase linked secondary antibody were obtained from Chemicon Int. The Ras protein was detected by ECL detection system. Western blot analysis of Ras protein were analysed using total lab software. Result are presented as mean values ± standard error (S.E) for 3-4 separate experiments each assayed in triplicate.

Statistical Analysis

Statistical data analyses were performed using t-test for independent samples parametric data distribution and considered significant when $p<0.05$. Data analysis was performed using SPSS 12.0.

Result

Effects of GTT on Cell Viability

As shown in Figure 1, GTT was added in various concentrations (10-750 µM) to the culture medium for 48 hours decreased cell proliferation. It showed the effect of GTT on antiproliferative activity of cancer cell HepG2 at IC_{50} of 170 µM compared to normal cell, WRL-68 at 500 µM. As a consequence, concentrations of 170 µM of GTT were used in the following experiments.

Figure 1: HepG2 and WRL-68 viability with GTT treatment. Cells were treated with increasing doses of GTT (ranging from 0-750 µM). Results are expressed as the percentage of viable cells for each dose of GTT. Results represent the mean and SEM of triplicate samples. (*) is significant compared to control ($p<0.05$).

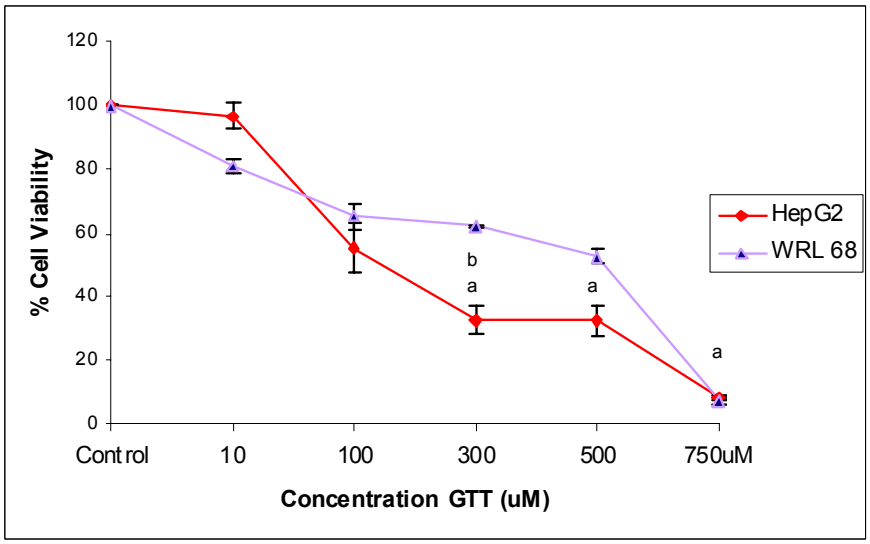

GTT uptake

The amount of GTT uptake was represents in Figure 2. The amount of GTT uptake was increased depends with the dose given to the cells. The uptake was dose dependent manner. At IC_{50} GTT of HepG2, the GTT uptake was 12 µM while at IC_{50} GTT of WRL-68 the GTT uptake was 40 µM.

Figure 2: GTT uptake by HepG2 and WRL-68. Results represent the mean and SEM of triplicate samples. (*) is significant compared to control ($p<0.05$).

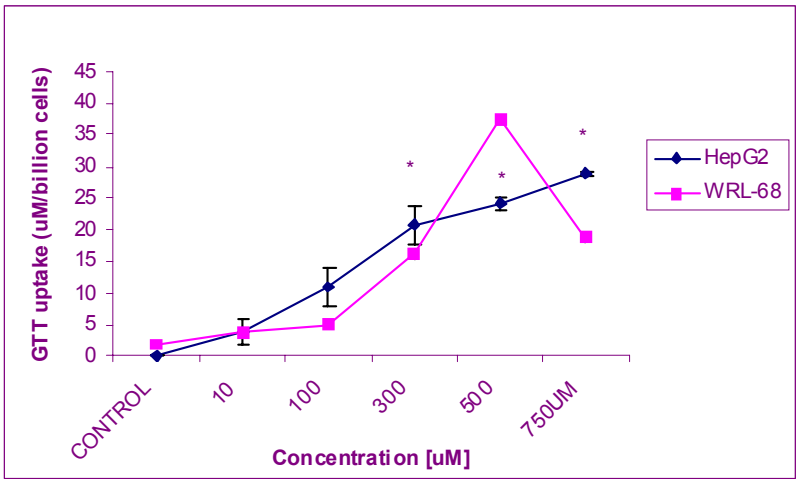

Protein Prenylation

As depicted in Figure 3, treatment either farnesol or GTT suppressed the growth of HepG2 cells as compared to control and WRL-68 treated with GTT ($p<0.05$). The combination treatment of GTT and farnesol reverse the antiproliferative effect of GTT. No changes of cell proliferation were observed in WRL-68 treated with the combination of GTT and farnesol as compared to control or WRL-68 treated with GTT.

Figure 3: GTT effect on protein prenylation. Cells HepG2 and WRL-68 were treated with GTT and co-incubation with farnesol. Results are expressed as the percentage of viable cells. Results represent the mean and SEM of triplicate samples. (a) is significant compared to control (b) is significant compared to WRL-68 treated with GTT ($p<0.05$).

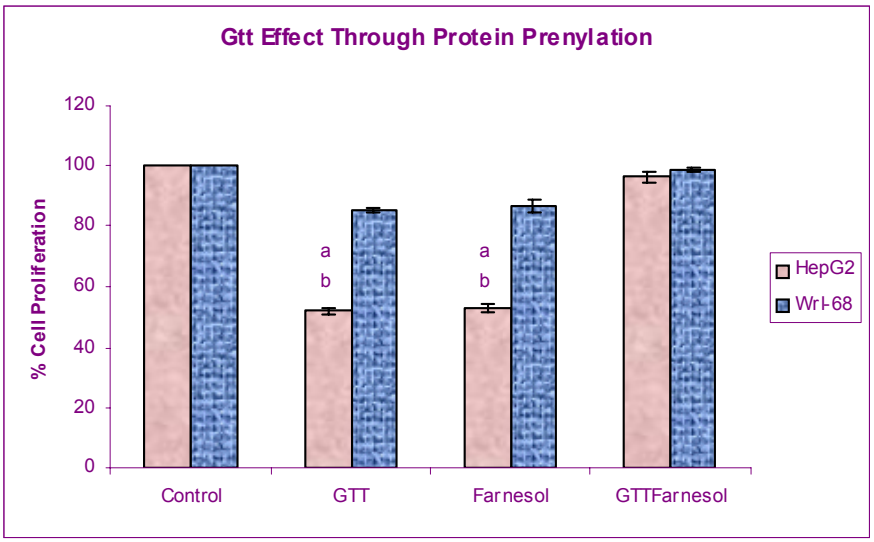

Ras protein Expression

Treatment of HepG2 cells with either GTT or farnesol decreased significantly Ras protein expression as compared to control and WRL-68 treated with GTT ($p<0.05$) (Fig 4). Ras protein expression was increased after co-incubation of GTT with farnesol as compared to HepG2 treated with GTT or farnesol. Treatment of GTT or farnesol or combination of both to WRL-68 showed no changes in Ras protein expression compared to control.

Figure 4: Ras protein expression in cancer cell HepG2 and WRL-68. Ras protein expression was measured by quantitative Western blotting. Results represent the mean and SEM of triplicate samples. (a) is significant compared to control (b) is significant compared to WRL-68 treated with GTT (c) is significant compared to WRL-68 treated with farnesol ($p<0.05$).

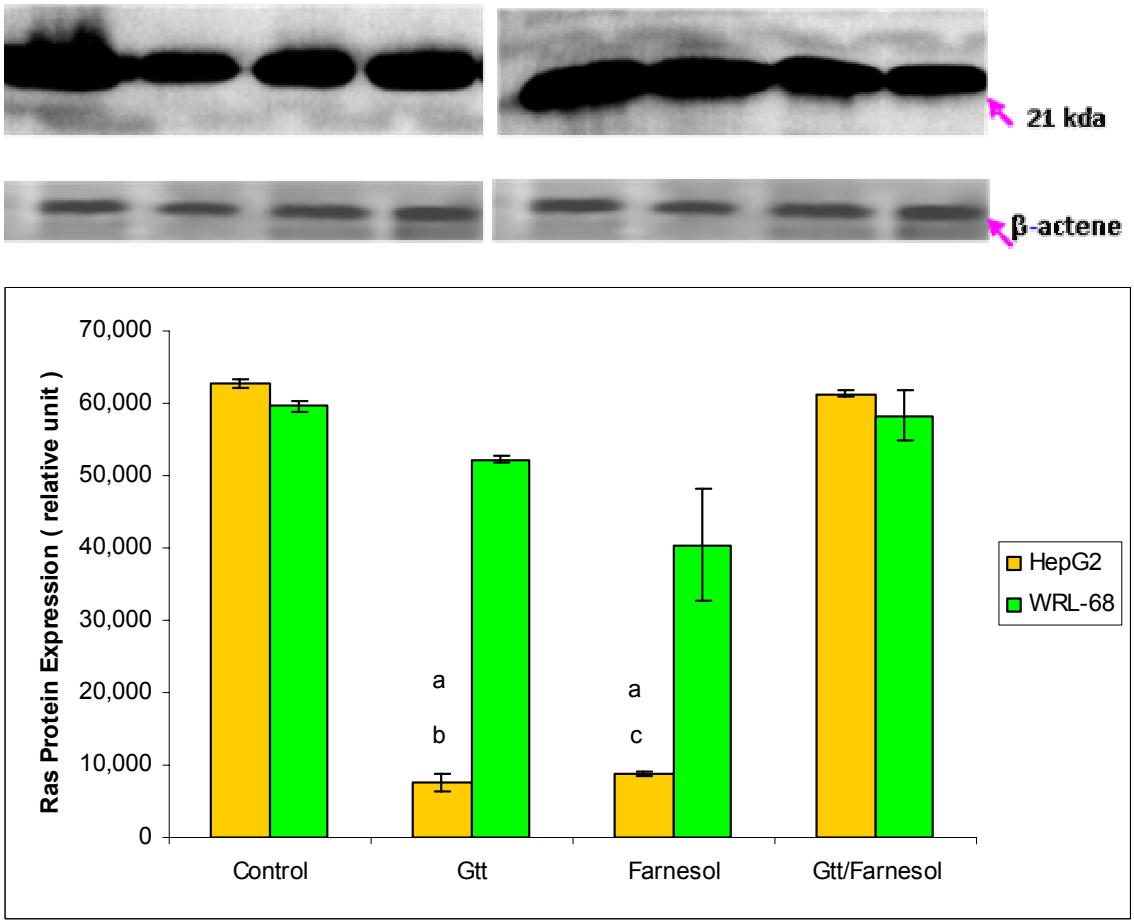

Discussion

Vitamin E is the most important lipid-soluble antioxidant. Antioxidant activity of tocotrienol is higher than tocopherol. It might be caused by the rapid penetration of tocotrienol through skin and efficiently combat oxidative stress and also cholesterol-lowering effect by down-regulating HMG CoA reductase activity (6).

The purpose of the study was to examine the effects of GTT on viability and cell proliferation of HepG2 and WRL-68 at the relevant physiological GTT concentrations. As shown in Figure 1, GTT was effectively inhibits cell viability at IC_{50} of 170 µM for hepatoma cell, HepG2 and 500 µM for normal cell, WRL-68. At lower concentration, GTT give toxic effect to HepG2 cells but did not exhibit cytotoxic effect on normal cell. GTT also decreased the proliferation rate of HepG2 as compared to

WRL-68. GTT was showed the antiproliferative effect against the cancer cells. These results are consistent with the study by Packer et al. (6) who showed that tocotrienol inhibited the proliferation of human breast cancer cell line and also suppressed the growth of murine B16 melanomas *in vitro* and *in vivo*. GTT uptake by the cells was measured and it was dose dependent manner. At IC_{50} 170 μM, the uptake of GTT was 12μM while for IC_{50} WRL-68 were 40μM. It showed that the GTT was taken up by the cells and it was toxic at low dose to cancer cells compared to normal cells.

It was suggested by Theriault et al. (7) that the antiproliferative effect of GTT against HepG2 might be through its prenylated side chain. Its prenylated side chain might induced farnesyl pyrophosphate pyrophosphatase (FPPase) that catalyze the change of farnesyl with the concomitant increase cellular farnesol. In several *in vitro* studies, farnesol is an isoprenoid from mevalonate pathway, has also shown an antiproliferative effects in cultured tumor cells (2). While GTT in the presence of farnesol, reverse its inhibitory effect on cell proliferation. This effect was more pronounce in HepG2 than WRL-68. This result was supported by Theriault et al. (4) who reported that α-tocotrienol in the presence of farnesol can reverse the inhibitory effect of α-tocotrienol on monocyte adhesion in human umbilical vein endothelial cells (HUVECS). It might be due to the inhibition of enzyme FPPase by farnesol or reversible reaction occurs which it will cause the formation of FPP. FPP is the intermediate product in mevalonate pathway. It will undergo other reaction termed protein prenylation. FPP play as important role as substrate for protein prenylation reactions (8).

Protein prenylation is a post-translational event that regulates G proteins such as Ras and Rho by modifying its structure with farnesyl (7). Ras protein is implicated in the signal transduction of growth factors. It is the important protein in signaling and proliferation. Prenylation prevention precludes membrane attachments and abolishes the malignant transforming ability of oncogenic Ras. Thus, inhibition of Ras protein prenylation represents an important strategy for the treatment of cancer (9). To determine the relationship between effect and the regulatory significance in signal transduction, we evaluate the Ras protein expression in cancer and normal cell by Western blotting method. Figure 5 shows comparison of Ras protein expression from HepG2 and WRL68 cell treated with either farnesol or GTT and the combination of both. Results showed a significant decreased of Ras protein expression in HepG2 treated with either GTT or farnesol as compared to control and WRL-68 treated either GTT or farnesol. Further analysis showed that no significant decreased in normal cell WRL-68 treated either GTT or farnesol or combination of both as compared to its control. It suggested that antiproliferative effect of GTT might be through its prenylated side chain, which increased the farnesol levels. Farnesol will inhibit HMG CoA reductase activity. Then FPP formation is reduced and Ras protein expression also reduced

Acknowledgement

This studied was supported by IRPA grants from Ministry of Science, Technology and Environment, Malaysia; 06-02-02-10035EAR, Department of Biochemistry, Faculty of Medicine, UKMKL

References

[1] Adjei AA.: Blocking Oncogenic Ras signaling for cancer therapy. Journal of The National Cancer Institute 2001; 93(14):1062-1074.

[2] Parker RA, Pearce BC, Clark RW, Goron DA, Wright JJ.: Tocotrienols regulate cholestrol production in mamalian cells by post-transciptional suppression of 3-hydroxy-3-methylglutaryl-coenzyme A reductase 1993;25: 268(15):11230-11238.

[3] Crowell PL, Chang RR, Ren ZB, Elson CE, Gould MN.: Selective inhibition of isoprenylation of 21-26kda proteins by the anticarcinogen d-limonene and its metabolites. J Biol Chem 1991;266:17679-17685.

[4] Theriault A, Tzuchao J, Wang Q, Abdul Gapor.: Tocotrienol is the most effective vitamin E for reducing endothelial expression of adhesion molecules and adhesion to monocytes. Atherosclerosis 2002;160:21-30.

[5] Meydani SM, Shapiro AC, Meydani M, Macauley JB, Blumberg JB.: Effect of age and dietary fat (fish, corn and coconut oils) on tocopherol status of C57BL/Nia mice. Lipid 1987;22:345-350.

[6] Packer L, Weber SU, Rimbach G.: Molecular aspects of α-tocotrienol. Antioxidant action and cell signaling. J Nutr 2001;131:369S-373S.

[7] Theriault A, Tzuchao J, Wang Q, Abdul Gapor, Khosrow Adeli.: Tocotrienol; A review of its therapeutic potential. Clin Biochem 1999;32(5):309-319.

[8] Tong H, Holstein SA, Hohl RJ.: Simultaneous determination of farnesyl and geranylgeranyl pyrophosphate levels in cultured cells. Analytical Biochemistry 2005;336(1):51-59.

[9] Oliff A. Farnesyltransferase inhibitors: targeting the molecular basis of cancer. Biochimica et Biophysica Acta 1999;1423:C19-C30.

European Journal of Scientific Research
ISSN 1450-216X Vol.18 No.4 (2007), pp.584-595

http://www.eurojournals.com/ejsr.htm

Contribution to the Survey of the Contamination of the Market Products by the Residues of Pesticides

Traore Karim Sory
UFR des Sciences et Gestion de l'Environnement
Université d'Abobo-Adjamé 02 B.P 801 Abidjan 02 (Côte d'Ivoire)
E-mail: trasory@hotmail.com
Tel: 06 03 61 67

Ehouman Ano Guy Serge
UFR des Sciences et Technologie des aliments
Université d'Abobo-Adjamé 02 B.P 801 Abidjan 02 (Côte d'Ivoire)

Mamadou Koné
UFR des Sciences et Gestion de l'Environnement
Université d'Abobo-Adjamé 02 B.P 801 Abidjan 02 (Côte d'Ivoire)

Dembele Ardjouma
Laboratoire Central d'Agrochimie et d'Ecotoxicologie
Lanada 04 bp 612 Abidjan 04 (Côte d'Ivoire)

Mazellier Patrick
Laboratoire de Chimie de l'Eau et de l'Environnement, Poitiers (France)

Legube Bernard
Laboratoire de Chimie de l'Eau et de l'Environnement, Poitiers (France)

Kamenan Alphonse
UFR des Sciences et Technologie des aliments
Université d'Abobo-Adjamé 02 B.P 801 Abidjan 02 (Côte d'Ivoire)

Houenou Pascal
UFR des Sciences et Gestion de l'Environnement
Université d'Abobo-Adjamé 02 B.P 801 Abidjan 02 (Côte d'Ivoire)

Abstract

La présente étude vise à déterminer les teneurs des résidus de pesticides dans les légumes destinés à la consommation humaine. Ainsi, 450 échantillons dont 90 échantillons de carottes, 90 de tomates, 120 d'aubergines, 60 de concombres et 45 de choux, ont été collectés auprès des maraîchers des régions de Buyo, Grand-lahou et Yamoussoukro. Les résultats d'analyses menées par différentes méthodes chromatographiques ont relevé la présence de nombreux résidus de pesticides (13 insecticides, 5 fongicides). Ces pesticides appartiennent aux familles d'Organochlorés (Endosulfane, Dieldrine, Lindane), d'organophosphorés (Diazinon, Profenofos, Phorate, Parathionethyl, Triazophos,

Chlorpyriphos), de carbamates (Diméthoate, Dithiocarbamate, Manèbe, Carbaryl, Mancozèbe), de pyrethroïdes (Cypermethrine). Au total 55% des légumes analysés sont contaminés. Les résultats ont mis en évidence des teneurs maximales généralement bien au-delà de la norme en vigueur de quatre à six résidus de pesticides en moyenne par échantillon. Il ressort également que les légumes ne concentrent ni ne sont tous contaminés de la même manière. Les légumes-feuilles et les légumes-racines sont les plus contaminés avec plus de 60% des échantillons. Les légumes pourraient donc constituer des vecteurs alimentaires de pesticides non négligeables étant donné leur fréquence de consommation.

Keywords: Environment, residues of pesticides, market products, contamination, health.

1. Introduction

L'agriculture ivoirienne, grande consommatrice de produits phytosanitaires est souvent désignée comme principale responsable dans les problématiques de santé et d'environnement. La mauvaise ou la sur utilisation des pesticides dues à la méconnaissance technique ou à la négligence ont souvent engendré la contamination des différents compartiments environnementaux avec pour conséquence la présence de résidus de pesticides dans les denrées alimentaires (Traoré et al., 2003). Ainsi, ces produits potentiellement dangereux entrent en contact avec l'homme ; et les dangers engendrés par l'exposition à ces résidus ne sont pas tous connus mais on soupçonne des effets neurologiques, tératogènes, clastogènes pour certaines substances (Pardo et Maranon, 1997; Krauthacker et al., 2001 ; Sheridan et Meola, 1999; Traoré et al., 2002). Aussi la production des denrées alimentaires de qualité représente – t – elle un enjeu majeur de santé publique : la consommation de certains aliments, en prévention de différentes maladies et cancers est conseillée alors que, paradoxalement, ces mêmes aliments peuvent être des vecteurs alimentaires de pesticides non négligeables étant donné la fréquence de consommation. Il importe donc de connaître l'état de contamination des denrées alimentaires pour mieux appréhender le risque qu'engendre l'exposition de la population aux pesticides.

L'objectif de cette étude consiste en l'identification des résidus de pesticides, en la détermination de leur concentration dans ces denrées alimentaires destinées à la consommation humaine.

2. Matériel et Méthodes

Notre activité s'est donc concentrée sur les aliments les plus consommés par la population des zones d'étude. Il s'est agit des tomates (*Lycopersicon esculentum P.Mill*), des aubergines (*Solanum integrifolium*), des concombres (*Momordica Charantia L.*), des carottes (*Daucus carota*)] et des choux (*Brassica oleracea* L.).

Les analyses ont porté sur 405 échantillons de légumes dont 60 échantillons de tomates, 60 d'aubergines, 30 de concombres, 20 de carottes et de choux, tous prélevés en accord avec la directive du *Codex Alimentarius* 1993, auprès des maraîchers des régions de Buyo, Grand-Lahou et Yamoussoukro. Ces échantillons ont été analysés à la recherche de 22 résidus de différents pesticides (insecticides et fongicides) en utilisant des méthodes d'analyse de pesticides normalisées à l'échelon européen et nord américain : norme EN 12393-1 à 3:1998-10, norme EN 12396-2:1998-10 et norme DFG-S19 (*Codex Alimentarius, décembre 2005* ; DFG, 1992).

Une prise de 50 grammes prélevée dans un broyat homogène de chaque légume est mixée avec 100 ml de 0,02 N HCL/MeOH (80 :20) pendant 5 min, le mélange obtenu est centrifugé à 4000 tours pendant 15 min puis filtré sous vide sur un filtre en fibre de verre.

Un aliquote (20 ml) de cette solution est ramené à pH 7,5 avec de la soude diluée et est passé sur une colonne Extrelut-20 de marques Merck. Après 20 min d'adsorption, l'élution est avec 100 ml d'un mélange d'hexane et de dichlorométhane dans les proportion 4/5 :1/5. L'éluât est évaporé à sec au rotavapor à une température de 45°C.

Les résidus sont finalement récupérés avec du méthanol (2 ml). Vingt microlitres de cette solution méthanoïque sont injectés dans le chromatographe liquide haute performance (LCHP). Les résidus issus d'un deuxième aliquote (20 ml) traité selon le même mode opératoire sont cette fois-ci, récupérés avec 4 mL d'hexane et trois microlitres sont injectés dans le chromatographe à gaz (CG).

L'identification et la quantification ont été faite par chromatographie en phase gazeuse utilisant une détection par ECD « Electron Capture detector » ou NPD « nitrogen phosphorus detector ». Le détecteur à capture d'électrons 63Ni (ECD) a été utilisé pour la détection des résidus organochlorés, pyréthroïdes. La colonne capillaire (SPB^{TM}608): 30 m x 0,32mm i.d.et 0,25 µm d'épaisseur de film. Température 90°C à 210/250°C en programme ; gaz vecteur:azote haute pureté (99,9%) à 2 bars ; injecteur en mode splitless à 220°C ; détecteur à 300°C. Les pics identifiés ont été confirmés avec une autre colonne de phase et de polarité différente (PTE^{TM}5 ou SPB^{TM}1)

Le détecteur azote phosphore (NPD) a été utilisé pour la détection des résidus de pesticides organophosphorés et les carbamates. La colonne capillaire (PTE^{TM}5): 30 m x 0,32mm i.d.et 0,25 µm d'épaisseur de film ; Température 80°C à 200/230/250°C en programme ; un gaz vecteur : azote haute pureté (99,9%) à 1ml/min ; un injecteur à 200°C et un détecteur à 300°C. le confirmation a été faite avec une colonne capillaire (HP^{TM}1): 30 m x 0,32mm i.d.et 0,25 µm d'épaisseur de film.

Pour les résidus de la famille des imidazoles et benzimidazoles, nous avons utilisé un chromatographe Liquide à Haute Performance (LCHP), couplé d'un détecteur UV à longueur d'onde variable. La colonne de séparation est une colonne Interchim de type Kromasil C18 250 x 4,6 mm (5 µm) munie d'une pré-colonne contenant la même phase. Le débit est de 1 mL.min-1 et l'éluant composé d'un mélange eau-méthanol (V/V) variable en fonction de la molécule recherchée. Le volume injecté est de 20 µl.

La limite de détection est de 0,001 mg/kg pour les organochlorés et de 0,01 à 0,05 mg/kg pour les organophosphorés, les carbamates, les pyréthroides et fongicides étudiés. Les standarts utilisés dont la pureté des résidus varie entre 97,6 et 99,9%, sont fournis par Fluka-Riedel De Häens, Sigma Aldrich et par le Dr Ehretorfer. La validité ainsi que la productivité de la méthode ont été vérifiées par l'analyse d'étalons certifiés provenant du même fournisseur.

Le pourcentage de récupération des insecticides de type organochloré, lors d'essais (n = 3), par cette procédure d'extraction varie de 70 à 120 %.La limite de quantification était de 0,01 mg/kg pour la plupart des pesticides analysés. Pour chaque série d'échantillons, une solution témoin (blanc) préparée avec de l'eau ultra-pure et un échantillon de contrôle de la qualité (matériau de référence, duplicata) sont introduits et traités de la même façon que les échantillons.

3. Résultats et Discussions

3.1. Résultats

Il s'agit des résultats d'analyse des échantillons de produits maraîchers étudiés à savoir la carotte (90 échantillons), la tomate (90), le chou (45), l'aubergine (120) et le concombre (60) : Soit un total de 405 échantillons de légumes frais.

3.1.1. Contamination d'une légume-racine : la carotte

Les échantillons de carottes présentent sept principaux résidus de pesticides qui sont par ordre décroissant de concentration mesurée en µg/Kg **(Figure 1)**: le Diméthoate (64,81), l'Endosulfane (35,70), le Manèbe (34,16), le Parathion-éthyl (33,12), le Lindane (32,31), le Carbaryl (16,48) et le Profenophos (3,15). Les Organochlorés sont les plus présents avec le Lindane et l'endosulfane avec respectivement une fréquence de 67% et 22%, suivis par les Carbamates (carbaryl 31 %, Diméthoate

25 % et manèbe 7%) et enfin les Organophosphorés (Parathionethyl 27% et Profenofos 43%). Ces résultats **(Figure 2)** font ressortir deux types d'anomalies : présence des organochlorés (Lindane, endosulfane, etc.) qui ne sont pas autorisés sur les plantes racines et des dépassements de la LMR occasionnés par l'utilisation du Parathion éthyle et du Diméthoate.

Figure 1: Résidus de pesticides détectés dans les échantillons de carottes - residues of pesticides detected in the samples of carrots

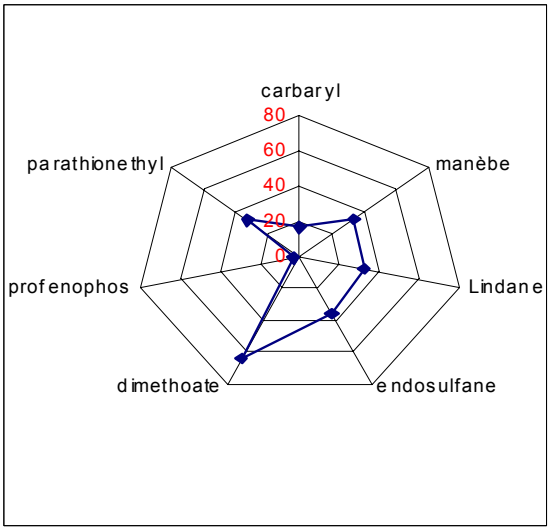

Figure 2: Fréquence de détections et de dépassement de normes dans les échantillons de carottes - frequency of detections and overtaking of norms in the samples of carrots

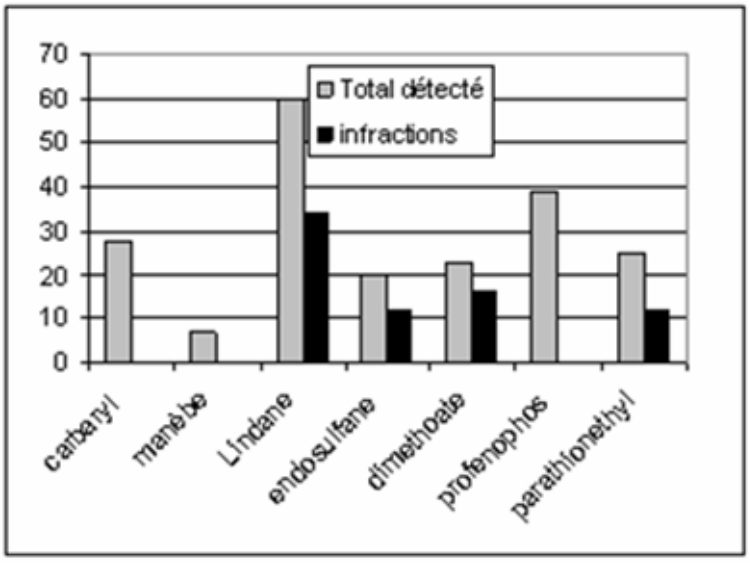

3.1.2 Contamination des légumes-fruits : la tomate, l'aubergine et le concombre

L'analyse des légumes-fruits que sont la tomate, l'aubergine et le concombre indique en plus des familles de pesticides identifiées dans la carotte, celles des Benzimidazoles, des Pyréthrinoïdes. Les Organophosphorés et les Carbamates sont les plus utilisés sur les cultures maraîchères **(figure 3)**. Les plus grandes proportions sont trouvées dans les échantillons d'aubergines.

Figure 3: Concentrations moyennes des familles de pesticides présentes dans les échantillons d'aubergines, tomates et concombres- Middle concentrations of the present pesticide families in the samples of eggplants, tomatoes and cucumbers

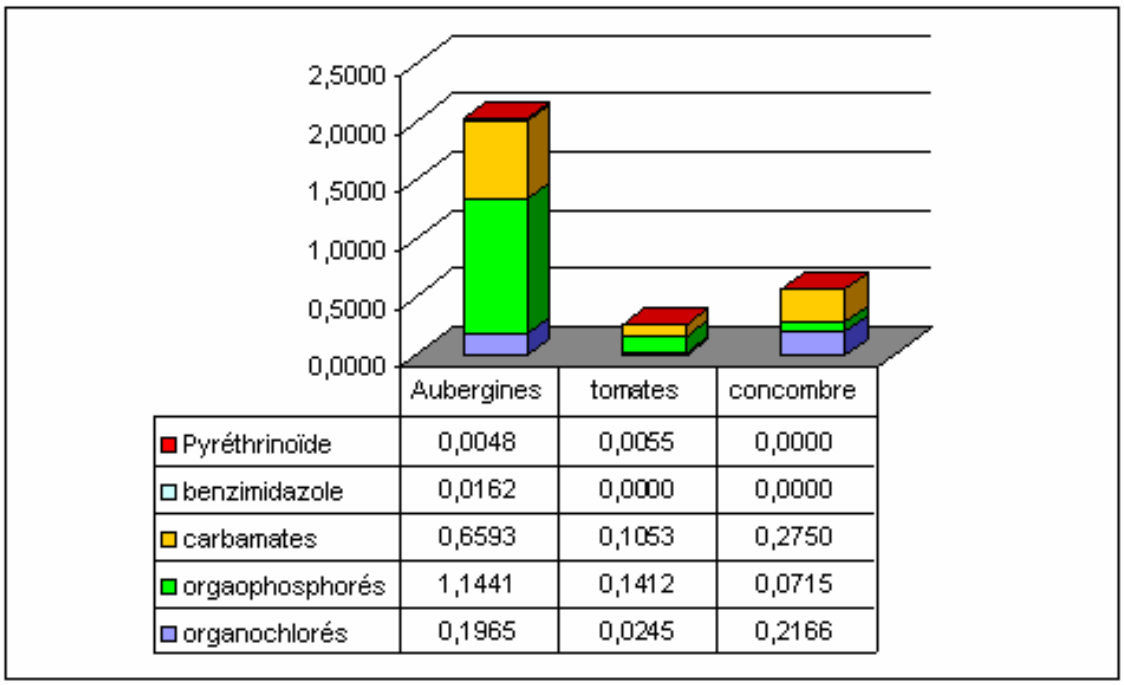

	Aubergines	tomates	concombre
Pyréthrinoïde	0,0048	0,0055	0,0000
benzimidazole	0,0162	0,0000	0,0000
carbamates	0,6593	0,1053	0,2750
orgaophosphorés	1,1441	0,1412	0,0715
organochlorés	0,1965	0,0245	0,2166

Au total 15 molécules différentes de pesticides ont été identifiées dans l'ensemble des légumes-fruits **(figure 4)**. Certaines sont communes à tous les légumes, d'autres par contre semblent être spécifiques à certains légumes. C'est le cas du Diazinon et du Chlorothalonil uniquement détectés dans les échantillons de concombre d'une part, et d'autre part le Thiabendazole, le Triazophos, le Mancozèbe, le Fénitrothion et le Phorate identifiées dans les échantillons d'aubergines.

Les aubergines présentent une contamination plus accentuée en nombre de résidus détectés 12 que les deux autres : sept pour le concombre et six pour la tomate. Les résidus identifiés dans les aubergines ont en général les niveaux les plus élevés avec des maxima de 650,22 µg/kg pour le Diméthoate, 522,21 µg/kg pour le Fénitrothion et 227,54 µg/kg pour le Parathionethyl.

Les concentrations maximales identifiées respectivement dans la tomate et le concombre sont de 125,32µg/kg pour le chlorpyrifos et de 300,21 µg/kg pour le Chlorothalonil.

Les infractions détectées sont soit la présence de pesticides interdits dans les légumes, soit des dépassements des normes. Ces « anomalies » sont présentées sur la **figure 5**.

Figure 4: Concentrations moyennes des résidus de pesticides dans les différents produits maraîchers (concombres, tomates, aubergine) étudiés- Middle concentrations of the residues of pesticides in the different market products (cucumbers, tomatoes, eggplant) studied

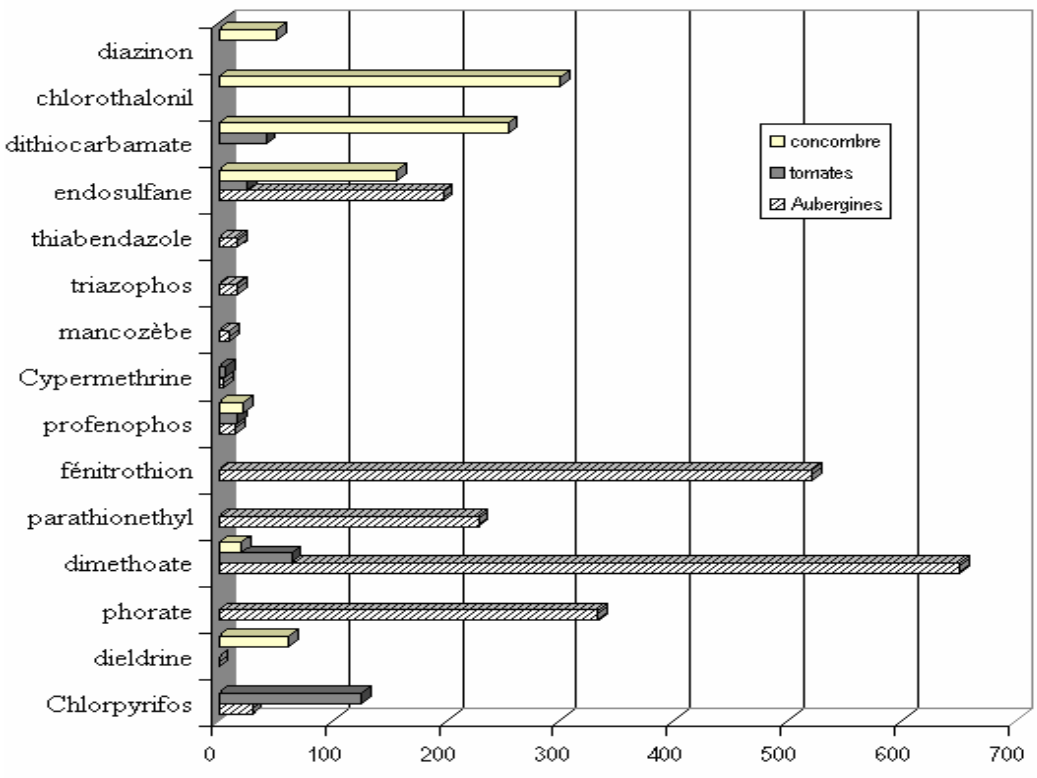

Dans les aubergines on note la présence d'insecticides Organochlorés interdits (l'Endosulfane et la Dieldrine) et le dépassement d'autres composés comme :

- Les insecticides : le Diméthoate (plus de quatre fois au-dessus de la limite de tolérance de 0,05mg/kg), le Triazophos, le Parathionethyl, le Phorate et le Profenofos;
- les fongicides utilisés après récolte comme le Thiabendazole;

Figure 5: Infractions dans les échantillons d'aubergines, tomates et concombres – Infractions in the samples of eggplants, tomatoes and cucumbers.

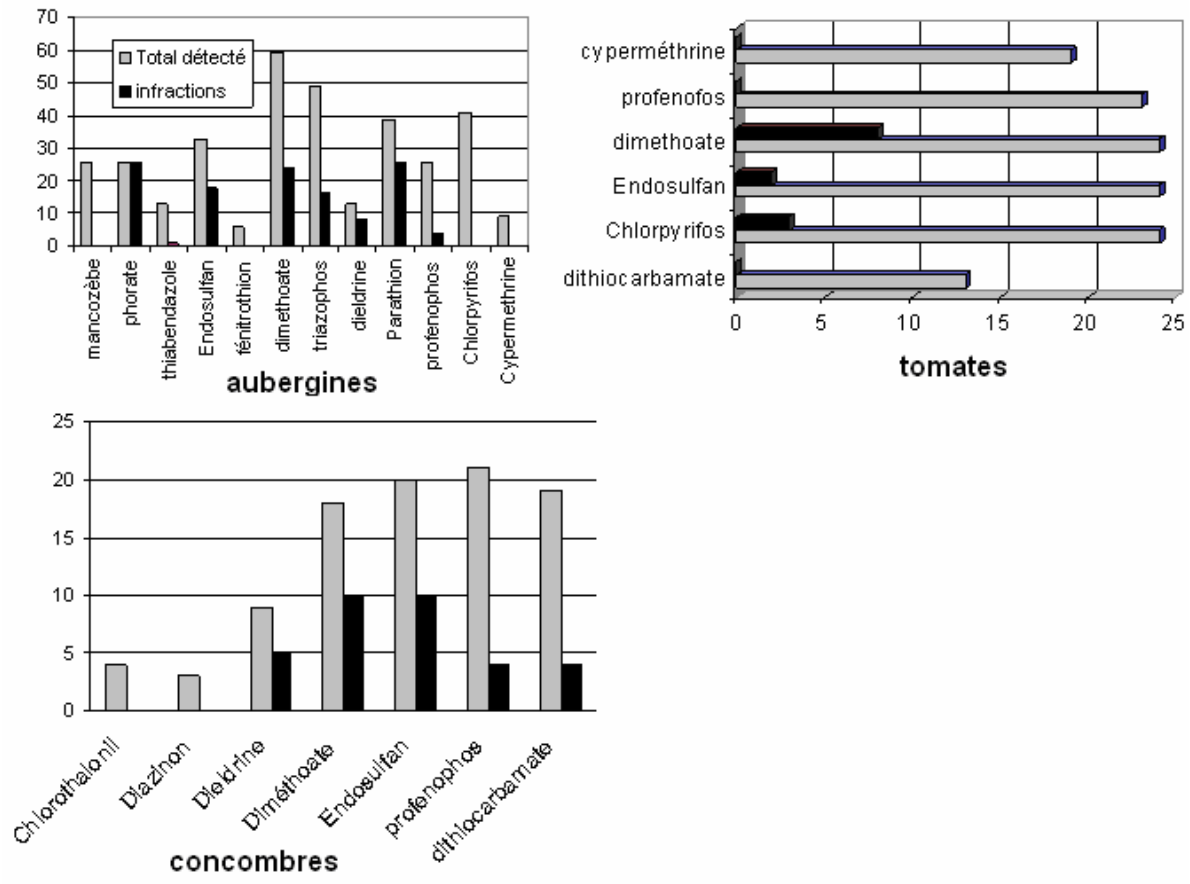

Pour les tomates, les principaux dépassements de la LMR pour certains échantillons sont dus au Diméthoate, au Chlorpyrifos et à l'Endosulfane. Les moyennes de contamination sont respectivement de 0,639 ppm et de 0,125 ppm.

Au niveau du concombre, le Dithiocarbamate et le Chlorotalonil présentent les concentrations moyennes les plus élevées en résidus de pesticides. Soient respectivement 0,300mg/kg et 0,255 mg/kg. Mais Certains échantillons on des concentrations qui dépassent la LMR ; c'est le cas du Diméthoate, l'Endosulfane, le Profenofos et le Dithiocarbamate. On y détecte également des organochlorés : endosulfane et dieldrine.

3.1.3. Contamination d'une légume-feuille : le choux

La **figure 6** présente les quatre principaux résidus détectés dans les échantillons de choux : l'Endosulfane, le Dithiocarbamate, le Diazinon et le Profenofos.

La présence de l'Endosulfane constitue la seule infraction car aucun cas de dépassement de la LMR n'a été constaté. Toutefois la concentration cumulée de tous les pesticides mesurés peut être très élevée.

Figure 6: fréquence de détections et de dépassement de normes dans les échantillons de choux – frequency of detections and overtaking of norms in the samples of cabbages

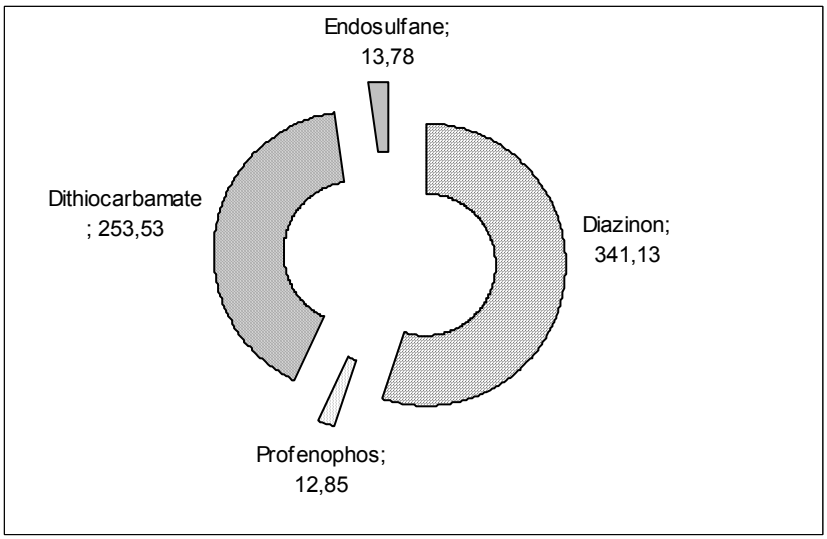

Par exemple, nous avons pu mesurer dans un échantillon moyen les résidus suivants : l'Endosulfane (0,014 mg/kg), le Dithiocarbamate (0,253 mg/kg), le Diazinon (0,341 mg/kg) et le Profenofos (0,013 mg/kg). La somme de tous ces résidus arrive à un total de 0,621 mg/kg de résidus mais cet échantillon doit être considéré comme conforme.

3.2. Discussion

La côte d'Ivoire est située dans la zone intertropicale où les conditions climatiques sont très favorables à la pullulation des ravageurs et maladies des plantes cultivées (Chegaray, Le Cornec, 1982). Les cultures des légumes se font dans les marais ou dans les bas-fonds. Elles sont de ce fait soumises à une plus forte pression parasitaire (Declert, 1990 ; Reckhaus, 1997). et la lutte antiparasitaire est donc presque systématique sur les périmètres maraîchers échantillonnés.

En conséquence, sur 405 échantillons de légumes prélevés dans ces différentes zones d'études, il a été trouvé des résidus de pesticides dans 55% des échantillons, même s'ils étaient en majorité au-dessous des LMR. Il ressort également que les légumes-feuilles et les légumes-racines sont les plus contaminés avec plus de 60% des échantillons **(figure 7)** pour chaque type de légume.

Figure 7: Répartition des résidus de pesticides dans les échantillons de légumes - Distribution of the residues of pesticides in the samples of vegetables

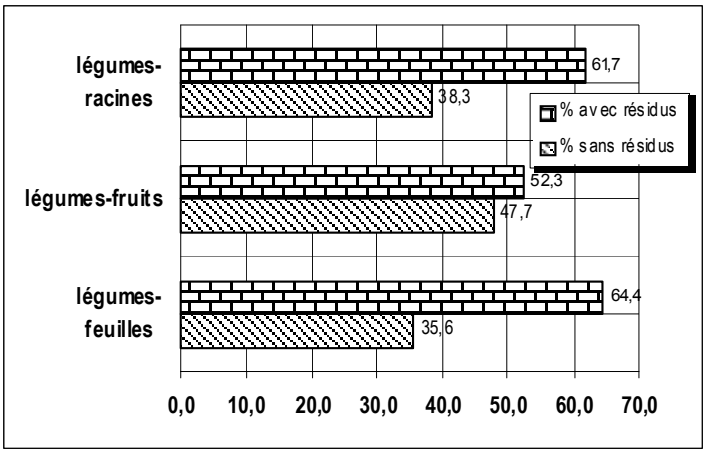

Le problème de contamination devient encore plus crucial en ce sens que les paysans sont en majorité analphabètes ; ils ne respectent pas les doses recommandées et utilisent parfois des produits inappropriés voir interdits sur les légumes (N'Da, 2001 ; .Traoré et al., 2002). Soit par manque de formation, d'informations et/ou de sensibilisation (Barberis et al, 1994 ; Minagra, 1997). Trois mauvaises utilisations de pesticides ont été identifiées : l'application d'une quantité plus importante de pesticides que celle recommandée, l'application trop proche de la date de récolte et l'application d'un pesticide sur une culture pour laquelle il n'est pas approuvé.

Aussi assiste-t on à la présence d'une diversité des résidus trouvés à des concentrations parfois très élevées sur les légumes. Au total, ce n'est pas moins de 18 substances différentes qui ont pu être identifiées sur les échantillons analysés. Les teneurs maximales mesurées sont généralement bien au-delà de la norme en vigueur ; et de surcroît une moyenne de quatre à six résidus de pesticides différents par échantillon (avec dans des cas extrêmes, jusqu'à 13 résidus) a pu être observée.

La présence des résidus de pesticides interdits dans les légumes concerne une quantité non négligeable de légumes contaminées : 10% des échantillons contaminés contiennent de la Dieldrine, 27% du Lindane et 49% de l'Endosulfane. La résurgence de l'Endosulfane et du lindane tous deux jadis interdits, sur le marché ivoiriens des pesticides, serait liée au fait que l'Endosulfane a été réintroduit de façon exceptionnelle ces dernières années au niveau de la culture du cotonnier pour venir à bout de *Helicoverpa armigera* qui a développé une résistance aux insecticides habituellement utilisés (Declert, 1990 ; Cheyda, 1991) alors que le lindane serait autorisés pour le traitement des sols et des semences.

La contamination des légumes par ces polluants interdits peuvent provenir également d'une utilisation frauduleuse (Aboua, 1996), elle peut être aussi le fait de ruissellements d'eau consécutif aux pluies entraînant les polluants d'autres zones traités vers les bas-fonds de culture (Kaba, 1987 ; Aboua, 1996 ;Bah et al, 1999). Ces polluants finissent par s'accumuler dans les sols (Ramade, 1992) et sont absorbés par les végétaux. Ceci montre que les plantes participent à la dissipation des pesticides dans l'environnement. Dissipation qui procède d'un transfert biologique des pesticides du sol ou de la surface de la plante vers l'intérieur de la plante (Fernandez et al., 1998). Elles correspondent aux phénomènes d'absorption et d'exsudation des pesticides par les plantes elles mêmes à travers les feuilles, les tiges ou les racines (CAPCO,2004). En effet lors de l'application foliaire, les produits sont retenus sur les feuilles, c'est le cas des Aryolacides (**2,4 D, dichlorprophos**) qui sont absorbés par le feuillage, puis véhiculés dans la sève des plantes. Les produits lipophiles comme les Organochlorés (Kylin et al., 1996) pénètrent les cuticules des feuilles et demeurent difficilement mobilisables même en cas de pluie. Les pesticides systémiques (Urées substituées, Triazoles, Triazines…) quant à eux pénètrent par la racine et sont également véhiculées par la sève.

Ces pesticides présents dans la plante vont ainsi se repartir dans toutes les parties comestibles de la plante (feuilles, fruits et tubercules). Mais cette contamination des légumes varie selon le type de légumes comme l'atteste le **tableau 1** : dans tous les légumes analysés, le taux de d'échantillons avec résidus est en moyenne de 60% à l'exception des tomates (29%).

Table 1: Bilan des analyses, distribution des échantillons positifs (avec résidus) - Balance of the analyses, positive sample distribution (with residues)

Légumes	Nombres d'échantillons	sans résidus	avec résidus
concombres	90	36 (40%)	54 (60%)
carottes	60	23 (38,3%)	37 (61,6%)
aubergines	120	43 (35,8%)	77 (64,1%)
tomates	90	64 (71,1%)	26 (28,8%)
choux	45	16 (35,5%)	29 (64,4%)

Nous retiendrons que les légumes ne sont pas toutes contaminées de la même manière ; tout d'abord l'apport de produits agrochimiques (en qualité et en quantité) est différent suivants les cultures

considérées, ensuite les légumes ne concentrent pas les résidus toxiques de la même manière (existence de végétaux « concentrateurs »).

Le **tableau 2** qui présente les substances les plus fréquemment retrouvées, précise la concentration maximale mesurée, le nombre d'échantillons positifs, la famille et l'action de pesticides (Insecticides (I), Fongicides (F)).

Table 2: Natures et concentrations maximales des pesticides identifiés dans les légumes- *Natures and maximal concentrations of the pesticides identified in the vegetables*

Pesticides	Action	famille	% positif	Teneur Max (mg/kg)	Norme (mg/kg)
Carbaryl	I	Carb	28	0,025	0,05
Chlorothalonil	F	OC	4	0,724	0.01
Chlorpyriphos	I	OP	65	0,057	0,05
Cypermethrine	I	Pyré	28	0,019	0,05
Diazinon	I	OP	17	0,521	0.02
Dieldrine	I	OC	22	0,105	0,01
Diméthoate	I	Carb	124	1,521	0,02
Dithiocarbamate	F	Carb	56	0,871	2
Endosulfan	I	OC	110	0,347	0,05
Fénitrothion	I	OP	6	0,988	0,01
Lindane	I	OC	60	0,055	0,01
Mancozèbe	F	Carb	26	0,056	2
Manèbe	F	carb	7	0,043	0,2
Parathionethyl	I	OP	64	1,27	0,02
Phorate	I	OP	26	0,385	0,05
Profenofos	I	OP	115	0,082	0,05
Thiabendazole	F	Bz	13	0,036	0,05
Triazophos	I	OP	49	0,075	0.02

Action: I: insecticides ; F: fongicides,
Familles: OC: organochloré ; OP: organophosphoré ; Carb : carbamate ; Pyré : pyréthroïde ; Bz : benzimidazole

La quasi-totalité de ces produits sont des insecticides (13 matières actives) et le reste correspond aux fongicides (cinq matières actives). Les premiers ont pour but d'éliminer les insectes nuisibles et les seconds de limiter les principales maladies des légumes. Ces pesticides utilisés se regroupent au sein de Cinq grandes familles : les Organochlorés (OC), les Organophosphorés (OP), les Carbamates (Carb), les Pyréthroïdes (Pyré) et les Benzimidazoles (Bz). Les pesticides autorisés sur les légumes appartiennent aux trois dernières familles. Cependant les Organochlorés interdits d'utilisation dans les produits agricoles sont encore omniprésents sur les espaces maraîchers. Ces usages inappropriés des pesticides dans la lutte antiparasitaire sur les légumes sont à l'origine d'une bioaccumulation au sein des organes des végétaux (FAO, 1995 ; Fleischer et al., 1998). La consommation des produits issus de ces plantes peut provoquer à long terme une toxicité chronique chez les consommateurs (Eric, 1994).

4. Conclusion

L'utilisation des pesticides dans les zones d'étude génère des résidus dans les légumes. La contamination des légumes apparaît plus diversifiée et complexe. Elle met en jeu de nombreux pesticides dont la nature et les quantités varient suivant les légumes. L'étude a permis d'identifier quantitativement et qualitativement les pesticides les plus impliqués dans l'exposition des populations considérées via consommation des légumes. Au regard de la dangerosité et des quantités trouvées de résidus de pesticides on peut conclure à l'existence probable d'un risque pesticide lié à la consommation des légumes. Il existe ainsi des légumes plus « à risque » soit parce qu'elles sont plus contaminées, soit parce qu'elles sont plus concentrateurs des toxiques.

Le choix des produits phytosanitaires combiné à des pratiques inadaptées (traitement systématique, dosage inapproprié, fréquence des traitements, matériels non adaptés), sont autant de facteur qui contribuent à favoriser la contamination des légumes. On est donc dans une situation où les contraintes de productivité agricole priment souvent au détriment de la qualité des produits.

Cette étude met aussi en évidence la responsabilité, et l'obligation aux termes de la législation ivoirienne qu'ont les structures d'encadrement de mieux contrôler la présence de résidus de pesticides de manière à donner aux consommateurs les plus grandes garanties concernant la sécurité des produits alimentaires.

Remerciement

Nous remercions les membres du *Laboratoire Central d'Agrochimie et d'Ecotoxicologie (LANADA)* et ceux du *Laboratoire de Chimie de l'Eau et de l'Environnement, Poitiers (France)* pour leur étroite.

References

[1] **AbouaK**. *Etude de la contamination par les résidus organochlorés de trois biotopes aquatiques de la région de Buyo à travers les matrices de poissons (Tilapia sp) et sédiments*. Mémoire d'études approfondies en Sciences de l'Environnement, Abidjan : université d'Abobo-Adjamé 1996.

[2] **BahB, RakotomavoH, MAWAP.** *Etude de l'influence des produits agrochimiques sur la qualité de l'eau du barrage de Natio-Kobadara (en vue de son utilisation pour l'alimentation de la ville de Korhogo).* 1999

[3] **BarberisG, Chariada-BousquetJP.** *Législation sur l'homologation des pesticides.* Rome : Service droit et développement, bureau juridique, FAO. 1994. **CAPCO.** Connaissances fondamentales requises pour la formation sur les pesticides Numéro de catalogue : H50-4/14-1995F ISBN : 0-662-99600-3 Ottawa (Ontario) K1A 0K9, 2004. 75p.

[4] **ChegarayJ, Le CornecJ.** La ville d'Abidjan. SEDI, France, Europe Traduction, 1982. 153p.

[5] **CheydaJM.** *Pratiques paysannes et la place des produits phytosanitaires dans la filière coton en Côte d'Ivoire.* - Centre National d'Etude Agronomique des Régions Chaudes, Montpellier. 1991.

[6] **Codex Alimentarius.** *Programme mixte FAO/OMS sur les normes alimentaires* Rome, Italie : CL 2005/52 - PR Viale delle Terme di Caracalla, 00100, 2005.

[7] **DeclertC.** *Manuel de phytopathologie maraîchère tropicale – cultures de Côte d'Ivoire.* Paris : Edition ORSTOM, 1990.

[8] **DFG.** *Manual of pesticide residues analysis thiers and Zeumer, Weinheim, New York* 1992.

[9] **ÉricD, AyotteP, JacquesB.** L'exposition aux composés organochlorés estrogéniques et le cancer du sein. *Bul. Info. santé environnementale-Québec,* 1994 ; (5) : 1-4.

[10] **FAO.** Utilisation efficiente et sans risques des pesticides en Afrique. Rôme : UNDP / FAO, 1995.

[11] **FernandezAR, AlbaA , TejedorA, AgüeraM, ContrerasJ**. Determination of imidacloprid and benzimidazole residues in fruits and vegetables by liquid chromatography-mass spectrometry after ethyl acetate multiresidue extraction. *J AOAC Int ,*1998; (83): 748-55

[12] **FleischerG, AndoliV, CoulibalyM, RandolphT.** *Analyse socio-économique de* la *filière des pesticides en Côte d'Ivoire*. Série de publication N° 06 F du projet de politique des pesticides, Hannovre / Abidjan, 112 p. 1998.

[13] **KabaN.** *Etude synthétique de la pollution par les pesticides et les PCB dans les environnements marins et lagunaires: cas de la Côte d'Ivoire.* CRO, Abidjan, 1987. 40 p.

[14] **KrauthackerB, RomanicaSH, ReinerE.** Polychlorinated biphenyls and organochlorine pesticides in vegetation samples collected in Croatia. Bulletin of Environmental Contamination and Toxicology 66, 2001. 334–341.

[15] **KylinH, NordstrandE, SjödinA, JensenS.** *Airborne lipophilic pollutants in pine needles. - Environmental Science and Pollution.* Research 3(2). 1996.

[16] **Minagra.** *Plan directeur du développement agricole (1992-2015)*.Côte d'Ivoire : MINAGRA, 1997.

[17] **N'daL.** *Monitoring des résidus de pesticides dans les denrées alimentaires de la région des savanes.* Mémoire d'études approfondies en Sciences de l'Environnement, Abidjan : université d'Abobo-Adjamé 2001.

[18] **PardoF, MaranonE.** Contaminacio´n ocea´nica de las plantas. Conatminacio´n e ingenierı´a ambiental. In: Bueno, J.L., Sastre, H., Lavin, S.G. (Eds.), *F.I.C.Y.T. Oviedo.* Spain: 19- 42, 1997.

[19] **RamadeF.** *Précis d'Eco toxicologie.Masson*, Paris, Barcelone, Bonn : 1992. **ReckhausP**. *Maladie et ravageurs des cultures maraîchères à l'exemple de Madagascar*. GTZ. Margraf Verlaf , 1997.

[20] **SheridanRS, MeolaJR.** Analysis of pesticide residues in fruits, vegetables, and milk by gas chromatography/ tandem mass spectrometry. *Journal of AOAC Int* 1999 ; 82 (4): 982–990.

[21] **TraoreKS, MamadouK, DembeleA**. Contamination des peuplements de poissons du lac de BUYO. *J.Soc. Ouest – Afr. Chim*., 2003 ; (16) :137-152

[22] **TraoreKS, MamadouK, DembeleA, LafranceP, BantonO, HouenouP.** Résidus de pesticides organochlorés dans le lait humain d'une zone agricole de Côte d'Ivoire. *J.Soc. Ouest – Afr. Chim*, 2002 ; (13) : 99-109.

European Journal of Scientific Research
ISSN 1450-216X Vol.18 No.4 (2007), pp.596-620

http://www.eurojournals.com/ejsr.htm

Dynamic Mode of Miller Integrator

H. Mechergui
ESSTT (Associated Professor) E.S.S.T of Tunis, 5 AV Taha-Hassein Tunis Tunisia, Laboratory & Research groups: C.3.S
E-mail: hafidmecher@yahoo.com

I. Stantchev
U.T.S: (Professor) Technical University of Sofia, Bulgaria
E-mail: rds@tu-sofia.bg

Abstract

In this study we make a detailed analysis of the Miller integrator in dynamic mode. Indeed, we respectively treat the behaviour of the integrator in the case of low and high frequencies. Thus, the exact formulas of the dynamic errors for the small and the great intervals of time are determined in the case of symmetrical trapezoidal input signal. By using the Duhamel integral we determine the dynamic errors for each interval of time.

The theoretical relations obtained are used to implement a precision analogue converter covering a frequency range of $20\,Hz \div 20000\,Hz$. The found results give an exact estimate of the errors which accompany the miller integrator converter. This study is theoretical, but with a practical orientation. Indeed, the determined formulas are extended to evaluate the metrological parameters of the Miller integrator. The obtained results give an optimal and qualitative solution.

Keywords: Miller Integrator frequencies behaviours, ideal integrator, real integrator, static errors, transient mode, dynamic errors, metrological parameters estimation .

1. Introduction

The measurement of non-sinusoidal signals in dynamic mode is an operation which cannot be carried out by measuring apparatus such as voltmeters of RMS, average or maximum value. Generally, we use visual measuring apparatus, like the oscilloscopes. Unfortunately the error is 3% to 5% [1]. We make recourse to the modern techniques of simulation by software or analytical studies [1,3,9,10].

Indeed, the analytical studies are preferable especially if the formulas obtained make it possible to evaluate the parameters of the system and to have a best solution.

If we study the measuring apparatus in non sinusoidal dynamic mode, the best way of conceiving them is to make an experimental study in order to obtain qualitative solution.

In this study we are interested in the behaviour of the Miller integrator in dynamic mode. This analysis makes it possible to determine the errors which accompany the integrator operation.

It is pointed out that the Miller integrator constitutes a converter which is largely used in the field of the electronics. That's why a detailed study analysis operation of this last is necessary.

Thus we look for the exact formulas and we evaluate the dynamic errors in the field of low and high frequencies in the case of an ideal and real operation.

The study will be made using the Duhamel integral [2,4,5,17]. Indeed, we apply a symmetrical rectangular signal, then we seek the theoretical relations to design a precision electronic converter.

2. Basic Principle of Miller integrator

The most used electronic design of Miller integrator is that represented by the figure.1. If the amplifier is supposed to be ideal, then the conversion function of the integrator is:

$$u_S(t) = \frac{1}{C}\int_0^t i.dt = \frac{1}{C}\int_0^t \frac{u_i(t)dt}{R} = \frac{1}{\tau}\int_0^t u_i(t)dt \tag{1}$$

In sinusoidal mode we have:

$$\dot{U}_S = -\frac{Z_2}{Z_1}\dot{U}_i = \frac{e^{j\frac{\pi}{2}}}{\omega CR}\dot{U}_i \tag{2}$$

Figure 1: Basic structure of an ideal Miller integrator and its phasor diagram.

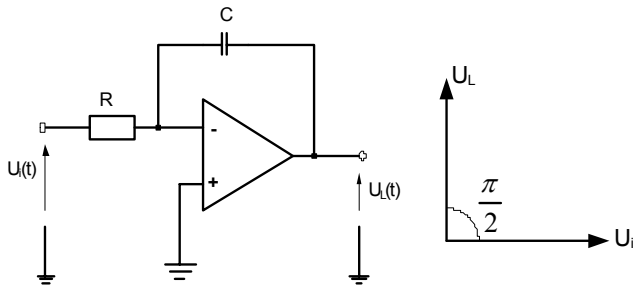

If the amplifier is not ideal, then according to [1] the structure of figure.1 can be replaced by that of the figure.2.

Figure 2: Real structure of a Miller integrator

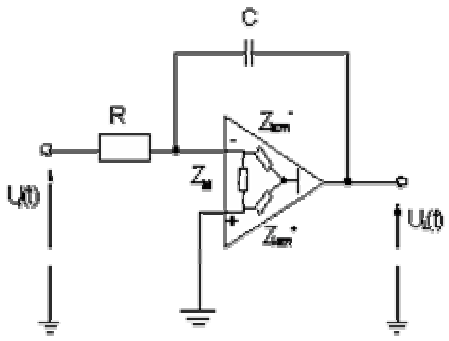

The amplifier uses a negative feedback loop. The conversion function of the Miller integrator is:

$$\overline{K}_F = \frac{\overline{A}}{1 + j\omega C R + \frac{R}{R_i}(1 + j\omega C_i R_i)} \tag{3}$$

with $R_i = R_{id} // R_{im}$, $C_i = C_{id} + C_{im}$ and A the amplifier gain.

Holding account of these considerations and according to [1] the transfer function of the Miller integrator can be given by the expression (4):

$$\dot{K}_F = \frac{\dot{K}}{1+\dot{\beta}\dot{K}} = -\frac{K_0}{ax^2+bx+c} \tag{4}$$

With: $K_0 = \frac{A_0}{1+\frac{R}{R_i}}$: effective loop gain of the amplifier and $\dot{\beta} = j\omega CR = j\frac{f}{f_\beta}$ is the complex feedback factor.

After some algebraic manipulations, the expression (4) can be put in the following form:

$$\dot{K}_F = -\frac{K_0}{(1+j\frac{f}{f_l})(1+j\frac{f}{f_h})} \tag{5}$$

where

$$f_l \approx \frac{f_\beta}{1+K_0} = \frac{1}{2\pi.RC.(1+K_0)} \tag{6}$$

which represents one pole in low frequency. And

$$f_h \approx f_\beta + f_1(1+K_0) \approx f_{(A=1)} \tag{7}$$

where f_h is one pole in high frequency.

The expression (5) represents the first equation form representing the conversion coefficient of a real Miller integrator. After transformation and by using the approximate value of the pole f_l and the relation: $K_0 + 1 \approx K_0$, we lead to:

$$\dot{K}_F = -\frac{f_l}{jf}\frac{K_0}{(1-j\frac{f_l}{f})(1+j\frac{f}{f_h})} \approx \frac{e^{j\frac{\pi}{2}}}{2\pi RC}\frac{1}{(1-j\frac{f_l}{f})(1+j\frac{f}{f_h})} \tag{8}$$

It is noticed that expression (8) represents a mathematical description of an ideal integrator with an aperiodic low frequency block and another block which represents the behaviour in high frequency. This writing form makes it possible to simplify the equation (5) in the used range for the working frequency. Consequently we can determine the dynamic errors associated with the Miller integrator.

3. Principle and Influence of the Miller Integrator Dynamic Error

3.1 Calculation of the Dynamic Errors in the Miller Integrator Transient State

The measurement analogue electronic converters have two operating modes: a static and a dynamic one.

In the first case, the input and output parameters are not depending on time.

For the dynamic mode, the converter is described by differential equations which are based on the physical laws. Indeed, the transient state reflects the behaviour of the system for an input X_i.

This mode depends on the properties of the converters and the topological structure of the assembly as well as the form of $X_i(t)$. The dynamic error is defined by the instantaneous difference between the output signal $Y(p)$ brought back to the input using the conversion static coefficient K_H of the ideal converter and the real signal $X(p)$ at the input i.e. $\Delta X_d(p) = \frac{Y(p)}{K_H} - X(P) = (\frac{K(p)}{K_H} - 1)X(p)$:

The dynamic error is defined as follows:

$$\delta_d(p) = \frac{\Delta X(p)}{X(p)} = \frac{K(p)}{K_H} - 1 \tag{9}$$

This dynamic error depends on the time.

The equation (5) shows that the integrator analysis can be divided into two zones: one in low frequencies and the other in high frequencies.

In the case of the low frequencies, the pole f_h can be neglected and the equation (5) is reduced to:

$$\dot{K}_{Fl} = \frac{e^{j\frac{\pi}{2}}}{2\pi RC}\frac{1}{(1-j\frac{f_l}{f})} = \frac{\dot{K}_{F\infty}}{(1-j\frac{f_l}{f})} \tag{10}$$

The magnitude and the phase function can be expressed as:

$K_{Fl} = \frac{1}{2\pi RCf}\frac{1}{\sqrt{(1+\frac{f_l}{f})^2}}$ and $\varphi_{Fl} = \frac{\pi}{2} + arctg\frac{f_l}{f} = \frac{\pi}{2} + \Delta\varphi_l$

The phasor diagram of figure.3 represents the behaviour of the Miller integrators.

In the low frequency field the transfer function of Miller integrator is given as:

$$K_{Fl}(j\omega) = -\frac{K_0}{(1+j\frac{\omega}{\omega_l})} \tag{11}$$

The Miller integrator transitory function, in Laplace transform, is:

$$H(p) = \frac{K_{Fl}(p)}{P} = -\frac{\omega_l . K_0}{(\omega_l + P).P} \tag{12}$$

From [2,5], we obtain, the transitory function in time domain:

$$H(t) = -K_0(1-e^{-\omega_l t}) \tag{13}$$

The term $\omega_b t << 1$ then expression (13) is reduced to

$$H(t) = -\frac{t}{RC}(1-\frac{t}{2RC(K_0+1)}) \tag{14}$$

Under linear operation, the integrator has a conversion function:

$$u_s(t) = -\frac{t}{RC}.u_i \tag{15}$$

If we apply a step signal of low frequency, the output will contain a non-linearity error of :

$$\delta_l = -\frac{\omega_l . t}{2} = -\frac{t}{2RC(K_0+1)} \tag{16}$$

In high frequency, we neglect f_l and the expression (5) is changed into:

$$\dot{K}_{Fh} = -\frac{e^{j\frac{\pi}{2}}}{2\pi RC}\frac{1}{(1-j\frac{f}{f_h})} \tag{17}$$

The magnitude and the phase function can be expressed as:

$M_{Fh} = \frac{1}{\sqrt{1+(\frac{f}{f_h})^2}}$ and $\varphi_{Fh} = \frac{\pi}{2} - arctg\frac{f}{f_h} = \frac{\pi}{2} - \Delta\varphi_h$

The figure 3.a and the figure.3.b represent respectively the behaviour of miller integrator in low and high frequencies.

Figure 3: Phasor diagram of the Miller integrator

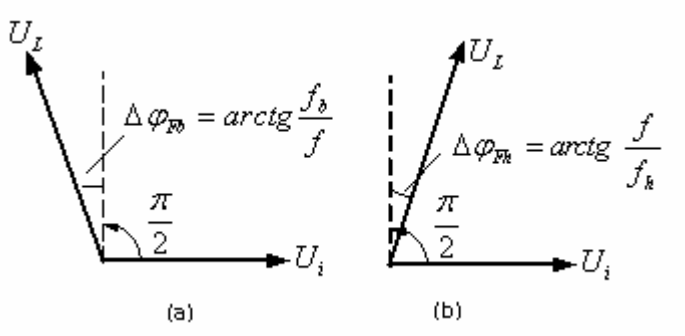

If we replace the operator $P = j\omega$ in the equation (17), then we obtain the transfer function in the temporal field at high frequencies:

$$K_{Fh}(P) = -\frac{1}{RCP(1+\frac{P}{\omega_h})} = \frac{\omega_h}{RCP(\omega_h + P)} \tag{18}$$

For an integrator, the operational transfer function, which gives the transient state, is:

$$H(p) = \frac{K_{Fh}(p)}{P} = -\frac{\omega_h}{RCP^2(\omega_h + P)} \tag{19}$$

If we apply a step signal, at high frequency, to the input of the integrator we can find the original function , in time domain, of the expression (19):

$$H(t) = \frac{t}{RC}[1 + \frac{1}{\omega_h.t}(e^{-\omega_h.t} - 1)] \tag{20}$$

While examining (1.29,20), we notice that for high frequencies the Miller integrator contains a dynamic error:

$$\delta_h = \frac{1}{\omega_h.t}(e^{-\omega_h.t} - 1) \tag{21}$$

Generally, the condition $\omega_h.t >> 1$ is satisfied and in this case we have: $e^{-\omega_h.t} << 1$.

By taking into account this approximation, the expression (21) can be reduced to:

$$\delta_h = -\frac{1}{\omega_h.t} = -\frac{1}{2.\pi.f_h.t} = \frac{1}{2\pi f_1.(K_0 + 1)} \tag{22}$$

where $t \neq 0$ and f_1 is the frequency for which the amplifier gain is $K(f_1) = 1$.

This analysis illustrates well the frequency behaviour of the Miller integrator.

We exploit the details of these results to design measuring converters such as: generators, electronic integrators, analogue modulators and simulators.

3.2. Miller Integrator Dynamic Errors Calculation using a Symmetrical Rectangular Input Signal

3.2.1. Miller integrator in the dynamic mode

In this study, we are interested in the behaviour of the Miller integrator in dynamic mode when applying a rectangular signal input. This analysis makes it possible to determine the errors which are associated with the integrator operation. The study will be made using the Duhamel integral [2]. Indeed, the Duhamel integral method utilizes the Laplace transform .

It has the advantage of the analytically studying for calculating the transitory processes in the linear electric circuits for unspecified input signals.

Thus the exact formulas are determined and we evaluate the dynamic errors in the range of low and high frequencies in the case of an ideal and real operation. Using the theoretical relations obtained, we make a design of a measurement integrator converter.

The voltage $u_i(t)$ applied at the input of the integrator is replaced by a function in staircase with rectangular increases having elementary values Δu_i (figure.4).

Figure 4:

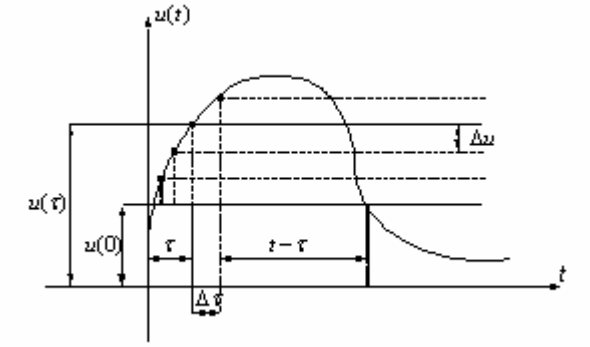

In addition, using the following equation [2]: $\Delta u.H_u(t-\tau) = u'(\tau).\Delta\tau.H_u(t-\tau)$, and if we add all the increases in the voltage signal which act during the interval of time from $t = 0$ to T where $\Delta\tau \to 0$, we obtain, according to [2,4], the following expression:

$$u(t) = u(0).H_u(t) + \int_0^t u'(\tau).\Delta\tau.H_u(t-\tau)d\tau \qquad (23)$$

The equation (23) takes into account the $u(0)$ value for the first increase. This formula represents the first writing form of the Duhamel integral. In addition, the expression (23) is used to determine the dynamic error of the Miller integrator.

3.2.2. Application of a rectangular signal at the input of the Miller integrator

In the general case, a periodic rectangular signal can be represented by the trapezoidal approximation signal like that of figure.5. This approximation is very much used in practice.

Figure 5: Symmetric trapezoidal signal

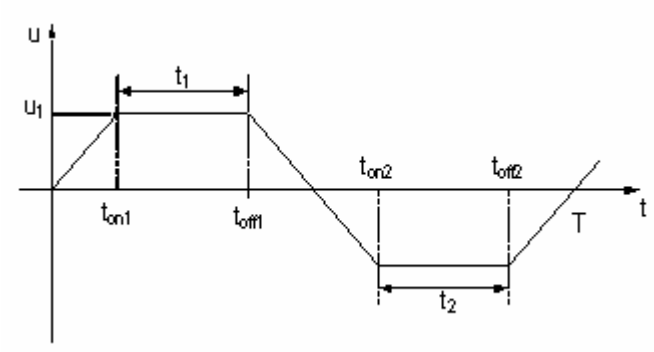

To simplify the solution in dynamic mode we accept some conditions which are close to those of the generator's real signal.

It is supposed that the signal is symmetrical with: $U_1 = -U_2 = U$, and $t_{on1} = t_{off1} = t_{on2} = t_{off2} = \tau$.

To obtain a symmetrical signal output, for null initial conditions, we accept that the study starts in the medium of the one of two halves period for the input signal. Indeed, it is supposed that we have central symmetry compared to the X-coordinate with $t_1 = t_2 = t$.

This assumption gives symmetrical solutions in the time interval of $-\infty$ *to* $+\infty$. To determine the solution using Duhamel integral, we replace the time intervals τ with ξ what gives in this case an input signal having the form of the figure.6.

Figure 6: Symmetric shift signal

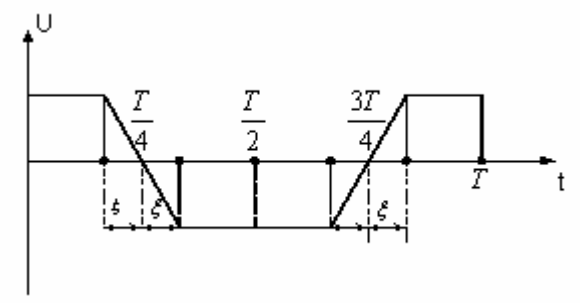

Since we use the Duhamel integral, the period of the input signal is divided into ΔT intervals, where in each interval the signal is described analytically by a mathematical function. According to the expression of (13) we will determine the output response of the system for each interval of time while taking account of the preceding effect outputs.

The transitory function of the ideal Miller integrator is:

$$H(t) = -\frac{t}{RC} \tag{24}$$

- **For the time interval:** $0 \le t \le \frac{T}{4} - \xi$, the voltage signal at the output is:

$$u_S(t) = U(0).H(t) \tag{25}$$

From (24) and (25), we determine the signal output of the integrator as:

$$u_S(t) = -\frac{U}{RC}.t \tag{26}$$

- **For the following interval:** $\frac{T}{4} - \xi \le t \le \frac{T}{4} + \xi$, the signal input is given by:

$$u_i(t) = -\frac{U}{\xi}(t - \frac{T}{4}) \tag{27}$$

and a derivative: $u_i^{'}(t) = -\frac{U}{\xi}$.

According to [2,4], the response output of the invariant system is given by:

$$u_s(t) = U(0).H(t) + \int_0^{\frac{T}{4}-\xi} u_i^{'}(\tau)H(t-\tau).d\tau + \int_{\frac{T}{4}-\xi}^{t} u_i^{'}(\tau)H(t-\xi)d\tau \tag{28}$$

The second term of (28) will always have a zero value, because in the interval of : $0 \le t \le \frac{T}{4} - \xi$ the signal has a derivative: $u_i^{'}(t) = 0$. After some calculations, we obtain:

$$u_S(t) = -\frac{U}{RC}t + \frac{U}{\xi RC}\int_{\frac{T}{4}-\xi}^{t}(t-\tau)d\tau \tag{29}$$

The resolution of (28) gives:

$$u_S(t) = -\frac{U}{RC}\left(\frac{T}{4} - \frac{\xi}{2}\right) + \frac{U}{2\xi RC}\left(t - \frac{T}{4}\right)^2 \tag{30}$$

- **For the interval:** $\frac{T}{4} + \xi \le t \le \frac{3T}{4} - \xi$, the signal is:

$$u_i(t) = -U \tag{31}$$

and the derivative of $u_i(t)$ is $u_i'(t) = 0$. The output signal of the integrator is given by the following expression:

$$u_s(t) = u_i(0).H(t) + \int_0^{\frac{T}{4}-\xi} u_i'(\tau)H(\tau - \tau)d\tau + \int_{\frac{T}{4}+\xi}^{t} u_i'(\tau)H(t-\tau)d\tau + \int_{\frac{T}{4}-\xi}^{\frac{T}{4}+\xi} u_i'(\tau)H(t-\tau)d\tau \tag{32}$$

After algebraic calculations we obtain:

$$u_S(t) = \frac{U}{RC}\left(t - \frac{T}{2}\right) \tag{33}$$

- **For the time interval:** $\frac{3T}{4} - \xi \le t \le \frac{3T}{4} + \xi$, we have

$$u_i(t) = \frac{U}{\xi}\left(t - \frac{3T}{4}\right) \tag{34}$$

and a derivative of $u_i'(t) = \frac{U}{\xi}$. The output signal is then:

$$u_s(t) = \frac{U}{RC}\left(\frac{T}{4} - \frac{\xi}{2}\right) - \frac{U}{2\xi RC}\left(t - \frac{3T}{4}\right)^2 \tag{35}$$

- **For the last time interval of the period:** $\frac{3T}{4} + \xi \le t \le T$, the input signal is constant. Then $u_i(t) = -U$ and the derivative is $u_i'(t) = 0$, therefore the output signal is:

$$u_s(t) = u_i(0).H(t) + \int_{\frac{T}{4}-\xi}^{\frac{T}{4}+\xi} u_i'(\tau)H(t-\tau)d\tau + \int_{\frac{3T}{4}-\xi}^{\frac{3T}{4}+\xi} u_i'(\tau)H(t-\tau)d\tau \tag{36}.$$

After simplification we find:

$$u_s(t) = \frac{U}{RC}(T - t) \tag{37}$$

At the end of the first period and for $t \ge T$, the behavior of the output to the first step input signal is:

$$u_s(t) = U(0).H(t) + \int_{\frac{T}{4}-\xi}^{\frac{T}{4}+\xi} u'(\tau)H(t-\tau)d\tau) + \int_{\frac{3T}{4}-\xi}^{\frac{3T}{4}+\xi} u'(\tau)H(t-\tau)d\tau - U.H(t-\tau) \tag{38}$$

After calculation s the equation (38) becomes:

$$u_s(t) = \frac{U}{RC}(T - t) + \frac{U}{RC}(t - T) = 0 \tag{39}$$

We see that at the end of the first period the ideal integrator returns in its initial state. We determine the responses of the output for $(n+1)$ period of the input voltage i.e. for $nT \le t \le (n+1)T$.

For an ideal integrator, we find the equation (39), and we notice that there is no remnant reaction for the previous periods. By analogy, the reactions of the output will be similar to those of first period but moved in time with $n.T$.

- **For the time interval:** $nT \le t \le nT + \frac{T}{4} - \xi$, we have:

$$u_S(t) = -\frac{U}{RC}(t - nT) \tag{40}$$

If we put $t' = t - nT$, where t' is the starting time from the beginning of $(n+1)$ period, the equation (2.20,40) changes into:

$$u_S(t) = -\frac{U}{RC}.t' \text{ where } 0 \le t' \le \frac{T}{4} - \xi \tag{41}$$

where $0 \le t' \le \frac{T}{4} - \xi$.

- **For the interval:** $nT + \frac{T}{4} - \xi \le t \le nT + \frac{T}{4} + \xi$, we obtain:

$$u_S(t) = -\frac{U}{RC}(\frac{T}{4} - \frac{\xi}{2}) + \frac{U}{2.\xi.R.C}(t - nT - \frac{T}{4})^2 \tag{42}$$

It is supposed that: $t = nT + \frac{T}{4} - \xi + t''$; with $0 \le t'' \le 2\xi$.

Taking into account this consideration, the equation (42) becomes:

$$u_s(t'') = -\frac{U}{RC}(\frac{T}{4} - \frac{\xi}{2}) + \frac{U}{2\xi RC}(t''-\xi)^2 = \frac{U}{RC}(t''^2 - t'' + \xi - \frac{T}{4}) \tag{43}$$

- **In the same way for the interval:** $nT + \frac{T}{4} + \xi \le t \le nT + \frac{3T}{4} - \xi$, we have:

$$u_s(t''') = \frac{U}{RC}(t''' + \xi - \frac{T}{4}) \tag{44}$$

with: $0 \le t''' \le \frac{T}{2} - 2\xi$.

- **For:** $nT + \frac{3T}{4} - \xi \le t \le nT + \frac{3T}{4} + \xi$, we find:

$$u_L(t'') = -\frac{U}{RC}(\frac{t''^2}{2\xi} - t'' + \frac{\xi}{4} - \frac{T}{4}) \tag{45}$$

with: $0 \le t'' \le 2\xi$.

- **For the last interval:** $nT + \frac{3T}{4} + \xi \le t \le nT + T$, the output signal is:

$$u_s(t') = -\frac{U}{RC}(t' - \frac{T}{4} + \xi) \tag{46}$$

Where $0 \le t' \le \frac{T}{4} - \xi$.

Thus we determine the response of the ideal Miller integrator, for the various intervals of the signal input $u_i(t)$.

4. Behaviour of a Real Miller Integrator for an Input Signal Having Great Intervals of Time (Low Frequencies Fields)

4.1. Determination of the analytical expressions

We use the same method described into 3.2. Indeed, the general form of the output response will be the same one, as for the ideal integrator, we replace the transitory function of the Miller integrator by the expression (13). We present the results without going into the details of calculation.

- **For the first interval:** $0 \le t \le \frac{T}{4} - \xi$, and while using (24) and (25), we obtain the final expression:

$$u_s(t) = U.K_0.(e^{-\omega_l t} - 1) \tag{47}$$

where the coefficient of performance K_0 and the angular velocity for the poles at low frequencies take part.

- **For the interval:** $\frac{T}{4}-\xi \le t \le \frac{T}{4}+\xi$, and using (13) and (47) we arrive at:

$$u_s(t) = -U.K_0(1-e^{-\omega_l t}) + \frac{K_0 U}{\xi}\int_{\frac{T}{4}-\xi}^{t}(1-e^{-\omega_l(t-\tau)})dt \tag{48}$$

Once calculation done, we obtain:

$$e^{-\omega_l t}\left(1+\frac{e^{\omega_l(\frac{T}{4}-\xi)}}{\omega_l \xi}\right) u_s(t) = -U.K_0\,(\frac{t-\frac{T}{4}}{\xi}-\frac{1}{\omega_l \xi}+) \tag{49}$$

- **For the interval:** $\frac{T}{4}+\xi \le t \le \frac{3T}{4}-\xi$, using the general expression (32) and after transformation we arrive at:

$$u_s(t) = -U.K_0\left\{1+e^{-\omega_l t}\left[1-\frac{e^{\omega_l \frac{T}{4}}}{\xi\,\omega_l}(e^{\omega_l \xi}-e^{-\omega_l \xi})\right]\right\} \tag{50}$$

- **For:** $\frac{3T}{4}-\xi \le t \le \frac{3T}{4}+\xi$, we find:

$$u_S(t) = U.K_0.[\frac{1}{\omega l \xi}-\frac{t-\frac{T}{4}}{\xi}+e^{-\omega l t}[1-\frac{e^{\omega l \frac{T}{4}}}{\omega l \xi}(e^{\omega l \xi}-e^{-\omega l \xi})\times\times(e^{\omega_l \frac{3T}{4}}-e^{\omega_l \frac{T}{4}})] \tag{51}$$

- **For the last interval, the substitution of (13) in (36), yields:**

$$u_S(t) = U.K_0.[(-1+e^{-\omega l.t}\times[\times(1+\frac{e^{\omega_l \xi}-e^{-\omega_l.\xi}}{\omega_l.\xi}(e^{\omega_l \frac{3.T}{4}}-e^{-\omega_l \frac{T}{4}})] \tag{52}$$

After the end of the first period, for $t \ge T$, and according to(13) and 38 we arrive at:

$$u_s(t) = U.K_0.[-1+e^{-\omega_l.t}\times(1+\frac{e^{\omega_l \xi}-e^{-\omega_l.\xi}}{\omega_l.\xi}(e^{\omega_l \frac{3.T}{4}}-e^{-\omega_l \frac{T}{4}})] + U.K_0\left[1-e^{-\omega_l(t-T)}\right] \tag{53}$$

Taking everything into account, we obtain:

$$u_s(t) = U.K_0.e^{\omega_l t}.C \tag{54}$$

with:

$$C = (e^{\omega_l \frac{T}{2}}-1).(\frac{e^{\omega_l \xi}-e^{-\omega_l \xi}}{\xi \omega}.e^{\omega_l \frac{T}{4}}-1-e^{\omega_l \frac{T}{2}}) \tag{55}$$

The expression (55) has a magnitude independent on time.

To determine the stationary regime, we consider the output response after n periods of the input signal from where:

$$u_s(t) = U.K_0.C.(e^{-\omega_l t}+e^{-\omega_l(t-T)}++e^{-\omega_l(t-2T)}+...+e^{-\omega_l(t-(n-1)T)}) \tag{56}$$

Equation (56) shows that its term depend on the respective period of the input signal (the first term depends on the first period, the second term depends on the second period and so on). By using the formula of the geometrical series sum:

$$S_n = a_1\frac{q^n-1}{q-1} \tag{57}$$

we arrive at the final solution:

$$u_s(t) = U.K_0.C.e^{-\omega_l t}\left(\frac{e^{\omega_l nT}-1}{e^{\omega_l T}-1}\right) \tag{58}$$

- **For the first interval of** $(n+1)$ period, that means for $nT \le t \le nT + \frac{T}{4} - \xi$, the output response is equal to the sum of the preceding reaction of the first n periods and the reaction of the first under interval, moved with $t = nT$ in time i.e.:

$$u_s(t) = U.K_0.C.e^{-\omega_l t}\left(\frac{e^{\omega_l nT} - 1}{e^{\omega_l T} - 1}\right) + K_0 U\left(e^{-\omega_l (t - nT)} - 1\right) \tag{59}$$

After substitution of $t = nt + t'$ in (59), with $0 \le t' \le \frac{T}{4} - \xi$, we obtain:

$$u_s(t) = U.K_0.C.\left(\frac{e^{-\omega_l .t'} - e^{-\omega_l .t'}.e^{-\omega_l nT}}{e^{\omega_l T} - 1}\right) + + K_0.U.\left(e^{-\omega_l t'} - 1\right) \tag{60}$$

To determine the stationary regime we seek the limit while making $n \to \infty$ which gives:

$$u_s(t') = U.K_0.C\frac{e^{-\omega_l t'}}{e^{\omega_l T} - 1} + K_0.U.\left(e^{-\omega_l t'} - 1\right) \tag{61}$$

While developing (61) we lead to:

$$u_s(t') = -U.K_0.\left[1 - \frac{e^{\omega_l \xi} - e^{-\omega_l \xi}}{\omega_l \xi}.\frac{e^{\omega_l \frac{T}{4}}}{1 + e^{\omega_l \frac{T}{2}}}.e^{-\omega_l .t'}\right] \tag{62}$$

- **For the second interval:** $n.T + \frac{T}{4} - \varsigma \le t \le n.T + \frac{T}{4} + \varsigma$, the output signal is the sum of the preceding reaction and that of the interval corresponding to the first period with an argument $t - n.T$:

$$u_s(t) = U.K_0.C.e^{-\omega_l .t}.(\frac{e^{\omega_l nT} - 1}{e^{\omega_l T} - 1}). + K_0.U.[\frac{t - nT - \frac{T}{4}}{\varsigma} + -\frac{1}{\omega_l .\xi} + .e^{-\omega_l (t - nT)}.(1 + \frac{e^{\omega_l \frac{T}{4}}}{\omega_l \xi}.e^{-\omega_l .\xi}] \tag{63}$$

After replacing of $t = nT + \frac{T}{4} - \xi + t''$ with $0 \le t'' \le 2\xi$ and while making $n \to \infty$, we obtain:

$$u_s(t'') = K_0.U.[-1 + \frac{t''}{\xi} - \frac{1}{\omega_l .\xi} + e^{-\omega_b .t''}.\frac{(e^{2\omega_l \xi} + e^{\omega_l \frac{T}{2}})}{(e^{\omega_l \frac{T}{2}} + 1)\omega_l \xi}] \tag{64}$$

- **For the interval:** $nT + \frac{T}{4} + \xi \le t \le nT + \frac{3T}{4} - \xi$, the expression of the stationary regime is obtained while adding (50) and (58) in the interval of time $t - nT$. After transformation we lead to $u_S(t''') = K_0.U.\times$:

$$\times[1 - \frac{1 - e^{-2\omega_l \xi}}{\omega_l .\xi}.\frac{e^{\omega_l \frac{T}{2}}}{(e^{\omega_l \frac{T}{2}} + 1)}.e^{-\omega_l .t'''}] \tag{65}$$

This relation is obtained for: $0 \le t''' \le \frac{T}{2} - 2\xi$.

- **For the time interval:** $nT + \frac{3T}{4} - \xi \le t \le nT + \frac{3T}{4} + \xi$, we obtain:

$$u_S(t'') = -K_0.U.[(-1 + \frac{t''}{\xi} - \frac{1}{\omega_l \xi} + e^{-\omega_l t''}) \times \frac{e^{2\omega_l \frac{T}{2}\xi} + e^{\omega_l \frac{T}{2}}}{(e^{\omega_l \frac{T}{2}} + 1)\omega_l \xi}.e^{-\omega_l .t'''}] \tag{66}$$

- **Finally for the last interval** $(n+1)$ **of periods:**

$nT + \frac{3T}{4} + \xi \le t \le nT + T$, and while using (52) and (58) for the time interval of $t - nT$, we obtain finally (2.47,67):

$$u_s(t')=-K_0.U.[1-\frac{1-e^{-2\omega_l\xi}}{\omega_l.\xi}.\frac{e^{\omega_l\frac{T}{2}}}{(e^{\omega_l\frac{T}{2}}+1)}.e^{-\omega_b t'}] \quad (67)$$

After this calculations and knowing the transitory function of the ideal Miller integrator we can easily calculate the dynamic errors caused by the electronic converter when working in the field of low frequencies.

4.2. Calculation of the dynamic error for the great intervals of time (case of low frequency)

To facilitate the analysis in stationary regime we made a reference translation for the coordinate. Thus when $n \to \infty$, the origin coincides with the beginning of the n^{th} period.

To determine the maximum dynamic error, we look for the errors in the various intervals of time by using the following expression:

$$\varepsilon(t)=\frac{U_S(t)-U_{SN}(t)}{U_{SN}(t)}=\frac{U_S(t)}{U_{SN}(t)}-1 \quad (68)$$

Where $U_{SN}(t)$ and $U_S(t)$ are respectively the signal response of the Miller integrator in case of an ideal et a real one .

- **For the first interval:** $0 \le t \le \frac{T}{4}-\xi$ and by taking account of (41) and (62) and according to (68) we obtain the following relation:

$$\varepsilon(t')=\frac{K_0}{t'}\frac{R.C}{}\times(1-\frac{e^{\omega_l.\xi}-e^{-\omega_l.\xi}}{\omega_l.\xi}.\frac{e^{\omega_l.\frac{T}{4}}}{e^{\omega_l.\frac{T}{2}}+1}e^{-\omega_l t'})-1 \quad (69)$$

If we replace $K_0 \approx \frac{1}{\omega_l.R.C}$ (70), which is deduced from (7), then the expression (69) changes into:

$$\varepsilon(t')=\frac{1}{\omega_l t'}\times(1-\frac{e^{\omega_l.\xi}-e^{-\omega_l.\xi}}{\omega_l.\xi}.\frac{e^{\omega_l.\frac{T}{4}}}{e^{\omega_l.\frac{T}{2}}-1}e^{-\omega_l t'})-1 \quad (71)$$

- **For** $\varepsilon(t')=\frac{1}{\omega_l t'}\times(1-\frac{e^{\omega_l.\xi}-e^{-\omega_l.\xi}}{\omega_l.\xi}.\frac{e^{\omega_l.\frac{T}{4}}}{e^{\omega_l.\frac{T}{2}}-1}e^{-\omega_l t'})-1$, the final value of the dynamic error, for the low frequencies, is given as follows:

$$\varepsilon_l=\frac{1}{\omega_l.(\frac{T}{4}-\xi)}(1-\frac{e^{2.\omega_l.\xi}-1}{\omega_l.\xi}.\frac{1}{e^{\omega_l\frac{T}{4}}+1})-1 \quad (72)$$

Since $\omega_l\frac{T}{2}<<1$, then $e^{2\omega_l.\xi}$ and $e^{\omega_l.\frac{T}{2}}$ can be broken up into factorial series which is limited to the second term i.e.:

$$e^{2.\omega_l.\xi}\approx 1+\frac{2.\omega_l.\xi}{1!} \text{ and } e^{\omega_l.\frac{T}{2}}\approx 1+\frac{\omega_l.\frac{T}{2}}{1!}$$

Taking account of these expressions we have:

$$\varepsilon_{br} \approx \frac{1}{\omega_l(\frac{T}{4}-\xi)}[1-\frac{2\omega_l.\xi}{\omega_b.\xi(2+\omega_l.\frac{T}{2})}]-1 = \frac{1}{(\frac{T}{4}-\xi)}[\frac{\frac{T}{2}}{(2+\omega_l.\frac{T}{2})}]-1 \quad (73)$$

If we put this expression under a common denominator and we neglect the term $\omega_l \frac{T}{2}$, because it is small compared to 2, then the expression (73) is reduced to:

$$\varepsilon_{lr} \approx \frac{\xi}{(\frac{T}{4}-\xi)} - \frac{\omega_l.\frac{T}{2}(\frac{T}{4}-\xi)}{2(\frac{T}{2}-\xi)}] = \frac{4.\xi}{T-4.\xi} - \frac{\omega_l.T}{4} \quad (74)$$

- **For the second interval:** $\frac{T}{4}-\xi \le t \le \frac{T}{4}+\xi$, and using the same way of calculation, for the dynamic error analysis, as that of the interval: $0 \le t \le \frac{T}{4}-\xi$, we obtain:

$$\varepsilon_l(t'') = \frac{1}{\omega_l(\frac{t''^2}{2\xi}-t''-\frac{T}{4}+\xi)}[-1+\frac{t''}{\xi}-\frac{1}{\omega_l.\xi} + e^{-\omega_l t''}.(\frac{e^{2\omega_l\xi}+e^{\omega_l\frac{T}{2}}}{(e^{\omega_l\frac{T}{2}}+1).\omega_l.\xi})]-1 \quad (75)$$

Since $0 \le t'' \le 2.\xi$, then the expression (75) is reduced to:

$$\delta_{lrp} = -\frac{1}{\omega_l(\frac{T}{4}-\xi)}(1-\frac{1-e^{-2\omega_l\xi}}{\omega_l\xi}.\frac{e^{\omega_l\frac{T}{2}}}{e^{\omega_l\frac{T}{2}}+1})-1 \quad (76)$$

The approximate expression of the dynamic error is:

$$\varepsilon_{lrp} = -\frac{4.\xi}{T-4\xi} - \frac{\omega_l.T}{4} \quad (77)$$

- **For the interval :** $\frac{T}{4}+\xi \le t \le \frac{3T}{4}-\xi$,the expression of the dynamic error will have the following form:

$$\varepsilon_{lrp}(t''') = \frac{1}{\omega_l(t'''+\xi-\frac{T}{4})} \times (1-\frac{1-e^{-2\omega_l\frac{T}{2}}}{\omega_l\xi}.\frac{e^{\omega_l\frac{T}{2}}}{e^{\omega_l\frac{T}{2}}+1}.e^{-\omega_l t'''})-1 \quad (78)$$

with $0 \le t''' \le \frac{T}{2}-2.\xi$.

The limiting value of the error will be obtained for $t = \frac{3T}{4}-\xi$ which corresponds to: $t''' = \frac{T}{2}-2\xi$

Indeed, the expression (2.58,78) is reduced to:

$$\varepsilon_{lrp} = -\frac{1}{\omega_l(\frac{T}{4}-\xi)}(1-\frac{1-e^{2\omega_l\xi}-1}{4.\omega_l\xi}.\frac{1}{e^{\omega_l\frac{T}{2}}+1})-1 \quad (79)$$

After comparison of the expressions (72) and (79), we notice that the final value of the errors, for $t = \frac{T}{4}-\xi$ and $t = \frac{3T}{4}-\xi$, are the same ones. This is due to the symmetry of the both halves of the periods.

- **For the interval of time:** $\frac{3T}{4}-\xi \le t \le \frac{3T}{4}+\xi$, we find for the dynamic error an expression similar to that of (75):

$$\varepsilon_l(t') = \frac{1}{\omega_l(t' + \xi - \frac{T}{4})} \times (1 - \frac{1 - e^{-2\omega_l \xi}}{\omega_l \xi} \cdot \frac{e^{\omega_l \frac{T}{2}}}{e^{\omega_l \frac{T}{2}} + 1} \cdot e^{-\omega_l t'}) - 1 \quad (80)$$

This expression is valid for: $0 \le t' \le \frac{T}{4} - \xi$.

5. Determination of the Miller Integrator Function Response in Case of the Small Intervals of Time (Field of the High Frequencies)

5.1. Determination of the analytical expressions

In this study we use the same procedure as that of the low frequencies. Indeed, the transitory function (20) is put in the form of:

$$H(t) = \frac{1}{RC}(\frac{1}{\omega_h} - \frac{e^{-\omega_h . t}}{\omega_h} - t) \quad (81)$$

The study of the transient state of the function (81), in the interval of $0 \le t \le \frac{T}{2} - \xi$, takes account of the expressions (25) and (27). After calculation we obtain:

$$U_L = \frac{U}{R.C}(\frac{1}{\omega_h} - \frac{e^{-\omega_h t}}{\omega_h} - t) \quad (82)$$

- **For the interval of time:** $\frac{T}{4} - \delta \le t \le \frac{T}{4} + \delta$, and using (28) and (81) we arrive at:

$$U_S(t) = \frac{U}{R.C}(\frac{1}{\omega_h} - \frac{e^{-\omega_h t}}{\omega_h} - t) + - \int_{\frac{T}{4} - \xi}^{t} \frac{U}{\xi} \cdot \frac{1}{RC}[\frac{1}{\omega_h} - \frac{e^{-\omega_h (t-\tau)}}{\omega_h} - (t - \tau)]d\tau \quad (83)$$

By developing the expression (83) we lead to:

$$U_S(t) = \frac{U}{RC}[\frac{\xi}{2} - \frac{T}{4} + \frac{1}{\omega_h^2} + \frac{(t - \frac{T}{4})^2}{2.\xi} + . - \frac{t - \frac{T}{4}}{\omega_h \xi} - \frac{e^{-\omega_h t}}{\omega_h}(1 + \frac{e^{\omega_h \frac{T}{4}} . e^{-\omega_h \xi}}{\omega_h \xi})]. \quad (84)$$

- **For the interval:** $\frac{T}{4} + \xi \le t \le \frac{3.T}{4} - \xi$, we use the general equation (32). While replacing $H(t)$ with its equation (81) and taking account of (31) and after substitution, we find:

$$U_s(t) = \frac{U}{RC}[-\frac{1}{\omega_h} - \frac{T}{2} + t + - \frac{e^{-\omega_h . t}}{\omega_h^2 . \xi}(1 - \frac{e^{\omega_h . \xi} - e^{-\omega_h . \xi}}{\omega_h} . e^{\omega_h . \frac{T}{4}})]. \quad (85)$$

- **For the interval:** $\frac{3T}{4} - \xi \le t \le \frac{3T}{4} + \xi$, we obtain:

$$U_s(t) = \frac{U}{RC}[-\frac{\xi}{2} + \frac{T}{4} - \frac{1}{\omega_h^2 . \xi} - \frac{(t - \frac{3T}{4})^2}{2.\xi} + \frac{t - \frac{3T}{4}}{\omega_h . \xi} + - \frac{e^{-\omega_h t}}{\omega_h}(1 - \frac{e^{\omega_h \frac{3T}{4}} . e^{-\omega_h . \xi}}{\omega_h \xi} - \frac{e^{\omega_h . \delta} - e^{-\omega_h . \xi}}{\omega_h \xi} . e^{\omega_h . \frac{T}{4}})] \quad (86)$$

- **For the last interval:** $\frac{3T}{4} + \xi \le t \le T$ and after having replaced (81) into (36), we arrive at:

$$U_S(t) = \{ \; T - t + \frac{1}{\omega_h} - \frac{e^{-\omega_h . t}}{\omega_h} \times \; [1 + \frac{e^{\omega_h . \xi} - e^{-\omega_h \xi}}{\omega_h \xi}(e^{\omega_h \frac{3T}{4}} - e^{\omega_h \frac{T}{4}})] \; \} \quad (87)$$

At the end of the first period $(t \ge T)$, while using (38) and after transformation, we lead to: (88):

$$U_s(t)=\frac{U}{R.C.\omega_h}e^{-\omega_h.t}\left(\frac{e^{\omega_h.\xi}-e^{-\omega_h.\xi}}{\omega_h.\xi}\xi.e^{\omega_h.\frac{T}{2}}+\ -e^{\omega h.t}-1).(e^{\omega h.t}-1)\right)=-\frac{U}{R.C}.e^{-\omega_h.t}.B \tag{88}$$

We put:

$$B=\frac{1}{.\omega_h}\left(\frac{e^{\omega_h.\xi}-e^{-\omega_h.\xi}}{\omega_h.\xi}\times .e^{\omega_h.\frac{T}{4}}-e^{\omega_h.\frac{T}{2}}-1)\times(e^{\omega_h.\frac{T}{2}}-1\right) \tag{89}$$

According to the used procedure, we obtain the output response after n periods of the input signal, i.e.:

$$U_S(t)=-\frac{U}{RC}.B.(e^{-\omega_h.t}+e^{-\omega_h(t-T)}+e^{-\omega_h(t-2.T)}+...+e^{-\omega_h[t-(n-1).T]})=-\frac{U}{R.C}.B.e^{-\omega_h.t}.\frac{e^{\omega_h.nT}-1}{e^{\omega_h.T}-1} \tag{90}$$

After that we determine the output response for the intervals of the period $(n+1)T$.

- **For** $nT\le t\le nT+\frac{T}{4}-\xi$ and by making recourse to (82) and (90) we obtain:

$$U_S(t)=-\frac{U}{R.C}.B.e^{-\omega_h t}.\frac{e^{\omega_h nT}-1}{e^{\omega_h T}-1}+\frac{U}{R.C}[\frac{1}{\omega_h}-\frac{e^{-\omega_h(t-nT)}}{\omega_h}-(t-nT)]. \tag{91}$$

While replacing $t=nT+t'$ and if $n\to\infty$, then for $0\le t'\le\frac{T}{4}-\xi$, we obtain, after a transformation, for the stationary regime:

$$U_S(t')=\frac{U}{R.C.\omega_h}(1-\omega_h t'+\ -\frac{e^{\omega_h\xi}-e^{-\omega_h\delta}}{\omega_h.\xi}\xi.\frac{e^{\omega_h\frac{T}{4}}}{e^{\omega_h\frac{T}{2}+1}}.e^{-\omega_h t'}) \tag{92}$$

- **For the interval:** $nT+\frac{T}{4}-\xi\le t'\le nT+\frac{T}{4}+\xi$, we have:

$$U_S(t'')=\frac{U}{R.C.\omega_h}(1+\omega_h\xi-\omega_h\frac{T}{4}+\frac{\omega_h t''^2}{2.\xi}.+\ -((\omega_h+\frac{1}{\xi}).t''+\frac{1}{\omega_h\xi}-\frac{e^{-\omega_h t''}}{e^{\omega_h\frac{T}{2}+1}}.\frac{e^{2\omega_h\xi}+e^{\omega_h\frac{T}{2}}}{\omega_h\xi}) \tag{93}$$

with $0\le t''\le 2\xi$.

- For $nT+\frac{T}{4}+\xi\le t\le nT+\frac{3T}{4}-\xi$ we find:

$$U_S(t''')=-\frac{U}{R.C\omega_h}[1-\omega_h(t'''-\frac{T}{4}+\xi)+\ -\frac{1-e^{-2\omega_h\xi}}{\omega_h\xi}.\frac{e^{\omega_h\frac{T}{2}}}{e^{\omega_h\frac{T}{2}+1}}.e^{-\omega_h t'''}] \tag{94}$$

with: $0\le t'''\le\frac{T}{2}-2\xi$

- **For the interval:** $nT+\frac{3T}{4}-\xi\le t\le nT+\frac{3T}{4}+\xi$ we have:

$$U_S(t'')=-\frac{U}{R.C.\omega_h}[1+\omega_h\xi-\omega_h\frac{T}{4}+\frac{\omega_h t''^2}{2.\xi}+\ -(\omega_h+\frac{1}{\xi}).t''+\frac{1}{\omega_h\xi}-\frac{e^{-\omega_h t''}}{e^{\omega_h\frac{T}{2}+1}}.\frac{e^{\omega_h\frac{T}{2}}+e^{2\omega_h\xi}}{\omega_h\xi}] \tag{95}$$

- **For** $nT+\frac{3T}{4}+\xi\le t\le nT+T$, we lead to:

$$U_s(t')=\frac{U}{R.C\omega_h}[1-\omega_h(t'-\frac{T}{4}+\xi)+\ -\frac{1-e^{-2\omega_h\xi}}{\omega_h\xi}.\frac{e^{\omega_h\frac{T}{2}}}{e^{\omega_h\frac{T}{2}+1}}.e^{-\omega_h t'}] \tag{96}$$

After having determined the conversion function on the output of the Miller integrator for each interval of time, we seek the dynamic error in the case of an operation in high frequency.

5.2. Dynamic error analysis in the case of the small intervals of time (field of the high frequencies)

To determine the dynamic error of the integrator we proceed in the same manner as the preceding study. Thus, the dynamic error in the interval of $0 \le t \le \frac{T}{4} - \delta$ is:

$$\varepsilon_h(t) = \frac{1}{\omega_h t'}\left(\frac{e^{\omega_h \xi} - e^{-\omega_h \xi}}{\omega_h \xi} \cdot \frac{e^{\omega_h \frac{T}{4}}}{e^{\omega_h \frac{T}{2}} + 1} e^{-\omega_h t'} - 1\right) \tag{97}$$

After transformation we obtain:

$$\varepsilon_h(t') = \frac{1}{\omega_h t'}\left(\frac{1 - e^{-2\omega_h \delta}}{\omega_h \delta} \cdot \frac{e^{-\omega_h (t' + \frac{T}{4} - \delta)}}{e^{\omega_h \frac{T}{2}} + 1} - 1\right) \tag{98}$$

with $0 \le t' \le \frac{T}{4} - \xi$.

The final value of the dynamic error for $t' = \frac{T}{4} - \xi$, is:

$$\varepsilon_h rp = \frac{4}{\omega_h (T - 4\xi)}\left(\frac{1 - e^{-2\omega_h \xi}}{\omega_h \xi} \cdot \frac{e^{-\omega_h (\frac{T}{4} - \xi)}}{e^{\omega_h \frac{T}{2}} + 1} - 1\right) \tag{99}$$

Usually the following conditions are satisfied: $\omega_h \frac{T}{2} >> 1$ $\omega_h \xi >> 1$, $\omega_h (\frac{T}{2} - 2\xi) >> 1$ and $e^{-\omega_h \frac{T}{2}} \approx 0$.

If we take account of these approximations then (99) is reduced to:

$$\varepsilon_{hrp} = -\frac{4}{\omega_h (T - 4\xi)} \tag{100}$$

- **For the error analysis in the interval:** $\frac{T}{4} - \xi \le t \le \frac{T}{4} + \xi$, the equation (93) will change into

$$U_s(t'') = \frac{U}{R.C}\left[\left(\frac{t''^2}{2.\xi} - t'' - \frac{T}{4} + \xi\right)\left[1 + \frac{1}{\omega_h (\frac{t''^2}{2.\xi} - t'' - \frac{T}{4} + \xi)} \times \left(1 - \frac{t''}{\xi} + \frac{1}{\omega_h . \xi} - \frac{e^{-\omega_h t''}}{e^{\omega_h \frac{T}{2}} + 1} \cdot \frac{e^{2\omega_h . \xi} + e^{\omega_h . \frac{T}{2}}}{\omega_h . \xi}\right)\right]\right]. \tag{101}$$

While replacing (43) and (101) in (68) we obtain:

$$\varepsilon_h(t'') = \frac{1}{\omega_h (\frac{t''^2}{2.\xi} - t'' - \frac{T}{4} + \xi)} \times \times \left(1 - \frac{t''}{\xi} + \frac{1}{\omega_h \cdot \xi} - \frac{e^{-\omega_h (\frac{T}{2} - 2.\xi)} + 1}{\omega_h . \xi (1 + e^{-\omega_h \frac{T}{2}})} \cdot e^{-\omega_h . t''}\right) \tag{102}$$

with $0 \le t'' \le 2\xi$.

The final value of the dynamic error for: $t = \frac{T}{4} + \xi$, with $t'' = 2\xi$, is:

$$\varepsilon_{hrp} = \frac{4}{\omega_h (T-4\xi)} \left(1 - \frac{1-e^{-2\omega_h 2}}{\omega_h \delta (1+e^{-\omega_h \frac{T}{2}})}\right) \tag{103}$$

The approximate value of this error is:

$$\varepsilon_{hrp} \approx \frac{4}{\omega_h (T-4\xi)} \left(1 - \frac{1}{\omega_h \xi}\right) \tag{104}$$

- **For the interval:** $\frac{T}{4}+\xi \le t \le \frac{3T}{4}-\xi$, the dynamic error is:

$$\varepsilon_h(t''') = \frac{1}{\omega_h (t''' - \frac{T}{4}+\xi)} \times \times \left(\frac{1-e^{-2\omega_h \xi}}{\omega_h . \delta} . \frac{e^{-\omega_h t'''}}{1+e^{-\omega_h \frac{T}{2}}} - 1\right) \tag{105}$$

The limiting value of this error is:

$$\varepsilon_{hrp} = \frac{4}{\omega_h (T-4\xi)} \left(\frac{1-e^{-2\omega_h . \xi}}{\omega_h \xi} \xi . \frac{e^{-\omega(\frac{T}{2}-2\varepsilon)}}{1+e^{-\omega_h \frac{T}{2}}} - 1\right) \tag{106}$$

Form expression (106), we find the approximate value of the error such as :

$$\varepsilon_{hrp} \approx -\frac{4}{\omega_h (T-4\xi)} \tag{107}$$

- **For the interval:** $\frac{3T}{4}-\xi \le t \frac{3T}{4}+\xi$, the dynamic error is:

$$\varepsilon_h(t'') = \frac{1}{\omega_h (\frac{t''^2}{2.\xi} - t'' - \frac{T}{4}+\xi)} . \left(1 - \frac{t''}{\xi} + \frac{1}{\omega_h \xi} + - \frac{e^{-\omega_h (\frac{T}{2}-2.\xi)}+1}{\omega_h \xi . (1+e^{-\omega_h \frac{T}{2}})} . e^{-\omega_h t''}\right) \tag{108}$$

with: $0 \le t'' \le 2\xi$.

- **For the interval:** $\frac{3T}{4}+\xi \le t \le T$, we have:

$$\varepsilon_h(t') = \frac{1}{\omega_h (t' - \frac{T}{4}+\xi)} . \left(\frac{1-e^{-2\omega_h \xi}}{\omega_h . \xi} . \frac{e^{-\omega_h t'}}{1+e^{-\omega_h \frac{T}{2}}} - 1\right) \tag{109}$$

The expressions (108) and (109) give the dynamic error as a function of time. The maximum value of the dynamic error will be calculated for the limit values of time and this is repeated for in the different intervals.

5.3. Presentation of a particular case: symmetrical rectangular signal

The study of a square signal shows that last has almost a null positive going time and a small negative going transition. This case is illustrated by the figure.7.

Taking account of these assumptions, the dynamic error will be given when $\xi \to 0$.

We make the analysis for: $\frac{T}{4}-\xi \le t \le \frac{T}{4}+\xi$, and $\frac{3T}{4}-\xi \le t \le 3\frac{T}{4}+\xi$

Figure 7: Rectangular signal input

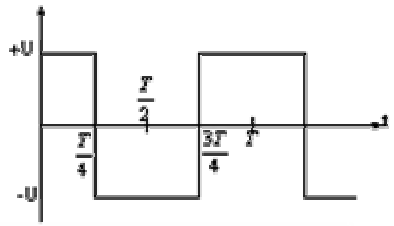

The study, in the great intervals of time (i.e. low frequency) gives:

- **For the time interval:** $0 \le t \le \frac{T}{4}$, we suppose $\xi \to 0$ in we the expression (71). Since $\xi \to 0$, we need to look for the derivative of:

$$\frac{e^{\omega_l \xi} - e^{-\omega_l \xi}}{\omega_l \xi} \tag{110}$$

which give:

$\frac{e^{\omega_l \xi} - e^{-\omega_l \xi}}{\omega_l}$. When $\xi \to 0$ the derivative of (110) is equal to 2 and the dynamic error is:

$$\varepsilon_l(t') = \frac{1}{\omega_b t'}\left(1 - \frac{2.e^{\omega_b (t' + \frac{T}{4})}}{1 + e^{-\omega_b \frac{T}{2}}}\right) - 1 \tag{111}$$

The limiting value becomes:

$$\varepsilon_{lrp} = \frac{4}{\omega_b T}\left(\frac{1 - e^{-\omega_b \frac{T}{2}}}{1 + e^{-\omega_b \frac{T}{2}}}\right) - 1 \tag{112}$$

This value can be approximated by:

$$\varepsilon_{lrp} = -\frac{\omega_b T}{4} \tag{113}$$

- **For the interval of time:** $\frac{T}{4} \le t \le \frac{3T}{4}$ and supposing $\xi \to 0$ we obtain:

$$\varepsilon_l(t'') = \frac{1}{\omega_l (t' - \frac{T}{4})}\left(1 - \frac{2.e^{\omega_b t''}}{1 + e^{-\omega_b \frac{T}{2}}}\right) - 1 \tag{114}$$

- **For** $0 \le t'' \le \frac{T}{2}$, the expression (114) can be reduced to

$$\varepsilon_{lrp} = \frac{4}{\omega_l T}\left(\frac{1 - e^{-\omega_l \frac{T}{2}}}{1 + e^{-\omega_l \frac{T}{2}}}\right) - 1 \tag{115}$$

It is seen that expression (115) is the same one as that of (112) because the rectangular signal is symmetrical.

- For the time interval $\frac{3T}{4} \le t \le T$ and while making $\xi \to 0$, we obtain:

$$\varepsilon_l(t') = \frac{1}{\omega_l (t' - \frac{T}{4})}\left(1 - \frac{2.e^{\omega_l t'}}{1 + e^{-\omega_l \frac{T}{2}}}\right) - 1 \tag{116}$$

with $0 \le t'' \le \frac{T}{2}$.

For the small intervals of time (case of the high frequencies) the error, for $0 \le t \le \frac{T}{4}$, is:

$$\varepsilon_l(t') = \frac{1}{\omega_l t'}\left(\frac{2.e^{-\omega_l(t'+\frac{T}{4})}}{1+e^{-\omega_l\frac{T}{2}}} - 1\right) \tag{117}$$

with $0 \le t' \le \frac{T}{4}$.

The limit value of the error is:

$$\varepsilon_{hrp} = -\frac{4}{\omega_h T}\left(\frac{1-e^{-\omega_h\frac{T}{2}}}{1+e^{-\omega h\frac{T}{2}}}\right) \tag{118}$$

After approximations, we obtain the final value of the error:

$$\varepsilon_{lrp} \approx -\frac{4}{\omega_l T} \tag{119}$$

- **For the time interval:** $\frac{T}{4} \le t \le \frac{3T}{4}$, the corresponding expression is:

$$\varepsilon_h(t'') = \frac{1}{\omega_l(t'' - \frac{T}{4})} \times \left(\frac{2.e^{-\omega_h t''}}{1+e^{-\omega_h\frac{T}{2}}} - 1\right) \tag{120}$$

with $0 \le t'' \le \frac{T}{2}$.

The approximate error will be:

$$\varepsilon_{hrp} = -\frac{4}{\omega_h T}\left(\frac{1-e^{-\omega_h\frac{T}{2}}}{1+e^{-\omega h\frac{T}{2}}}\right) \tag{121}$$

- **For time interval:** $\frac{3T}{4} \le t \le T$, we have:

$$\varepsilon_h(t') = \frac{1}{\omega_b(t'' - \frac{T}{4})}\left(\frac{2.e^{-\omega_h t''}}{1+e^{-\omega_b\frac{T}{2}}} - 1\right) \tag{122}$$

6. Results Analysis

The comparison of the results obtained for the dynamic errors which are caused by the application of a step signal or a rectangular signal at the input of the Miller integrator gives the following conclusions:

For the small intervals of time (case of the high frequencies) the dynamic error for a rectangular signal (98) is different from (115) that of an input signal level as given by (21) and there is existence in front of the expression $e^{-\omega_h t}$ a multiplication factor of $\frac{2e^{-\omega_h\frac{T}{4}}}{1+e^{-\omega_h\frac{T}{2}}}$ which becomes null for $\omega_h \frac{T}{4} >> 1$.

From here we conclude that until a certain frequency, the formula of the dynamic error obtained by application of a step signal at the input can be, also, used for the integration

of the periodic rectangular signals having a fast positive going transition while replacing t by $\frac{T}{4}$ in the expression (22).

In addition, while comparing (16) and (113), we notice that with certain approximations the formula of the error for the great time intervals, which is determined by the transient state function, can be used to calculate the dynamic error in the case of an input rectangular periodic signal and this while replacing t by $\frac{T}{2}$ in the expression (16). For precise results we advise to use the complete formula (112).

7. Application: Design and Determination of the Miller Integrator Metrological Parameters

7.1. Introduction

The expressions of the dynamic errors show that for the design and realization of the measurement integrators it is necessary to use an operational amplifier with high quality. In [2] we show that an operational amplifier must have the following parameters: an open gain $A_0 \geq 10^5$, an input resistance $R_i = 10^{10}\Omega$, a dissymmetry current I_{i0} of some pA and a temperature drift U_{i0} below than $(5 \div 10)\mu V / °C.$

Taking account of these parameters and the operating conditions of the Miller integrator which has a frequency range up to $(5 \div 10)\mu V / °C.$, for the case of this study, we choose an operational amplifier of type TLO81 (Texas Instruments USA). It has a JFET input and built-in standard frequency compensation.

7.2. Analytical Calculations

According to the parameters imposed in this work we design a Miller integrator covering a frequency range of $0 \div 20\,kHz$ for an input amplitude signal of $U_{im} = 1V$. The imposed maximum dynamic error is of $\varepsilon_h \leq 1\%$.

In practice, the normal operation of Miller integrator which converts a rectangular voltage signal into a triangular one, has a limited low frequency of $20\,Hz$.

From the conversion function (1) of the ideal integrator we can determine the value of the output signal

$$U_{sm} = \frac{1}{\tau} \cdot \frac{T}{4} . U_{im} \tag{123}$$

With respectively T and U_{im} the period and the amplitude of the input signal and τ is the integrator time-constant. The period of the input signal, $T = \frac{1}{f}$, varies from $T = \frac{1}{20} = 0.05\,s$ until $T = \frac{1}{20000} = 5.10^{-5}\,s$.

Consequently, for the same time-constant, the integrator amplitude output, for a frequency of $20\,kHz$, will be reduced by 1000 compared to that of $20\,Hz$.

This result gives a very low output .

To avoid this disadvantage, we divide the interval of frequency into three intervals. Indeed, we selected for each interval a time-constant.

Generally, we have choosing the following ranges: $20Hz \div 200\,Hz$; $200Hz \div 2000Hz$ and $2000Hz \div 20000Hz$

To minimize the error due to the dissymmetry of the input and the drift in temperature of the operational amplifier, we must have an input constant resistance about $(5 \div 10)k\Omega$, thus we selected a decade capacitor for the three intervals. The design of the studied Miller integrator is given by the figure.8.

For the first interval $20Hz \div 200\,Hz$ the period varies from $0.05\,s$ *to* $0.005\,s$.

To obtain an output voltage of $150\,mV$ *to* $200\,mV$ for the higher limit of under interval we determine the time constant τ according to the formula given in (123) such as: $\tau = \frac{T}{4}.\frac{U_{im}}{U_{sm}} = \frac{0.005}{4}.\frac{1}{(0.15 \div 0.2)} \approx (0.006 \div 0.008)\,s.$

The components R and C must be variable. The capacitor is chosen $C = (0.01 \div 1)\,\mu F$ which satisfies the conditions of precision, stability and $C >> C_i$.

The resistance R must take account of the integrator

input impedance. If we accept for C_1 a standard value of $C_1 = 1\,\mu F$ and according to the condition (123) we obtain: $R = (6000 \div 8000)\,\Omega$.

Figure 8: Circuit diagram of three ranges Miller integrator

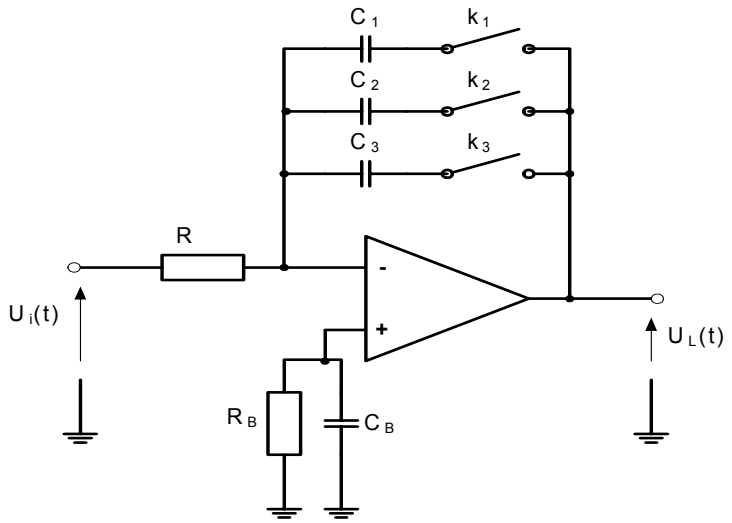

To have a conversion coefficient equal to 1 for the first signal harmonic with a frequency $f = 20\,Hz$, the following condition should be satisfied: $R = \frac{1}{\omega C_1} = \frac{1}{2.\pi.f.C_1} = 7957\Omega.$

We selected a standard value of $R = 7960\,\Omega$.

For a given value of the components R and C, we obtain the following amplitudes:

- **For** $f = 20\,Hz$, the output amplitude is:

  $U_{Lm} = \frac{1}{7960.1.10^{-6}} \times \frac{0.05}{4} \times 1 = 1.57\,V$.

- For $f = 200\,Hz$, we have

  $U_{Lm} = \frac{1}{7960.1.10^{-6}}.\frac{0.005}{4}.1 = 0.157\,V$

  .

- For the second range of the frequency: ($200 \div 2000)\,Hz$ it is seen that the limits are 10 times larger.

To fulfil the same conditions that the preceding range it is necessary to decrease the value of τ with 10, so we accept $C_2 = 0.1\,\mu F$.

For the third selected range: $(2000 \div 20000)\,Hz$, we have chosen $C_3 = 0.01\,\mu F$. It is noticed that the errors of dissymmetry at the AO input are minimal if we connect a resistance $R_B = R = 7960\Omega$ to the

non-inverting input [2]. Generally, we add in parallel to R_B a capacitor which eliminates the noise due to resistance R_B.

We select a capacitor having weak dielectric losses, a negligible inductance with dielectric coefficient absorption near to 1.

According to these considerations we choose a ceramic capacitor of $C_B = 3.9\,\mu F$.

7.3. Determination of the dynamic error for the great intervals of time (case of low frequency)

It is supposed that the conditions for the rectangular signal are not imposed thus we can determine its parameters. To determine the dynamic error in the case of the great intervals, we must find the pole for the low frequency f_l and this according to the formula given by (1.17), where $K_0 \approx A_0$.

For the low frequency of operation, $f = 20\,Hz$ and $C = 1\,\mu F$ we have, for the Miller integrator, a frequency pole :

$$f_l = \frac{1}{2\pi.7960.1.10^{-6}(1+200.10^3)} =$$

$$= 9.997.10^{-5}\ Hz \approx 1.10^{-4}\ Hz.$$

with: $(1+K_0) = \dfrac{1}{2\pi\, f_l .R.C}$

So we can calculate the additional term: $\omega_l .T$:

$$\omega_l .T = 2.\pi.1.10^{-4}.\frac{1}{20} = \pi 10^{-5}.$$

Using the expression (2.92) we obtain the dynamic error as follows:

$$\varepsilon_{lrp} = [\frac{4}{\pi.10^{-5}}.(\frac{e^{\pi\frac{10^{-5}}{2}}-1}{e^{\pi\frac{10^{-5}}{2}}})-1].100\% = -4.23.10^{-5}\%$$

According to the approximate expression (2.93) we have also: $\varepsilon_{lrp} \approx -\dfrac{\omega_l .T}{4}.100\% = -\dfrac{\pi.10^{-5}}{4}.100\% = -7.854.10^{-4}\%.$

If we apply a step signal in the input and making recourse to expression (2.26) we have: $\varepsilon_{lrp} = -\dfrac{\pi.10^{-5}}{4}.100\% = -7.854.10^{-4}$.

7.4 Determination of the dynamic error for the small intervals of time (case of the high frequency).

According to the formula (8), we determine the pole for the high frequencies of the Miller integrator:

$f_h = f_{(A=1)} = 3.10^{+6}\ Hz$.

For $f = 20\ kHz$, the additional term $\omega_h .T$ is:

$$\omega_h .T = 2\pi.f_h .\frac{1}{f} = \frac{2\pi.3.10^6}{20.10^3} = 300.\pi\ .$$

So $e^{-\omega_h .\frac{T}{2}} = e^{-150\pi} \approx 0$.

The expressions of the dynamic error for the small intervals give the following value of the error:

$$\varepsilon_{hrp} = -\frac{4}{300\pi}.100\% = -0.424\%$$

The analysis of the obtained results shows that the imposed dynamic error covers a frequency interval varying up $f_h = 45\,kHz$ and its limits value is:

$$\varepsilon_{hrp} = -\frac{4.45.10^{-3}}{2.\pi.3.10^{6}}.100.\% = -0.955.\% < 1\% .$$

7.5. Comparative analysis of the obtained results

In table.1 we present the dynamic errors, for the low frequencies, which are given from the exact formulas and the approximate formulas and this for a rectangular signal.

From table.1 we notice that the approximate formula obtained from the transitory function is applicable only for the values of $\omega_l.T$ with the lower part of 1.10^{-5} i.e. for a rather small low frequency pole and relatively short signals.

For the high frequencies, the results of the errors are summarized in table.2

The analysis of the results of table.2 shows that for the high frequencies the formula of the error due to the non linearity for a step signal input can be used to determine the dynamic error of the Miller integrator for a rectangular signal in the interval of time $\frac{T}{4}$.

Table 1: Dynamic Error in case of low frequencies

Formulas of the dynamic error	$\omega_l.T = 1.10^{-6}$	$\omega_l.T = 1.10^{-5}$	$\omega_l.T = 5.10^{-5}$	$\omega_l.T = 1.10^{-4}$
Dynamic error obtained from the exacts formulas	$-2.5.10^{-5}\%$	$-2.5.10^{-4}\%$	$-1.10^{-5}\%$	$-6.2810^{-8}\%$
Dynamic error value calculeted from the approximate formulas	$-2.5.10^{-5}\%$	$-2.5.10^{-4}\%$	$-1.25.10^{-3}\%$	$-2.5.10^{-3}\%$

Table 2: Dynamic Error in case of high frequencies

Formula of the dynamic error	$T = 1.10^{-4}\,s$ $\omega_h.T = 600.\pi$	$T = 1.10^{-5}\,s$ $\omega_h.T = 120.\pi$	$\omega_b.T = 5.10^{-5}$ $\omega_h.T = 60.\pi$	$T = 1.10^{-6}\,s$ $\omega_h.T = 6.\pi$
Exact error using a transitory function	–0.212%	–1.060%	–2.12%	–21.03%
Exact error value for a rectangular signal	–0.212%	–1.06%	–2.12%	–21.217%
Dynamic error value using the approximate formula	–0.212%	–1.06%	–2.12%	–21.220%

For a real rectangular signal, the errors depend on the transitory step signals applied to the input and which can be rather numerous.

In any event to make a conclusion on the influence of the transitory signal input pulses on the dynamic error, we treat respectively the two following cases, one with 1% positive going transition time and the other with 10%.

For first case we have:

$$\xi = 1\%.\frac{T}{2} = 0.01\frac{5.10^{-5}}{2} = 2.5.10^{-7}\,s$$

So we obtain for the dynamic error:

$$\delta_{hrp} = -\frac{4}{\omega_h(T-4.\xi)} = = -\frac{4}{6.\pi.10^{+6}\,(5.10^{-5}-4.25.10^{-7})} = -0.00433 = 0.433\%.$$

For second case we have:

$$\xi = 10\%.\frac{T}{2} = 0.1\frac{5.10^{-5}}{2} = 25.10^{-6}\,s$$

And the dynamic error is $\delta_{hrp} = -\frac{4}{\omega_h(T-4.\xi)} = -\frac{4}{6.\pi.10^{+6}(5.10^{-5}-4.25.10^{-6})} = -0.00530 = -0.53\%.$

We notice that in high frequency the increase of positive going transition time of the signal involves the increase in the dynamic error. In addition the influence of ξ is similar to that of the low frequencies.

8. General Conclusion

According to the study presented in this work we can give the following conclusions:

We have found the theoretical expressions of the dynamic errors for Miller integrator using an input signal having a trapezoidal form.

The relations obtained make it possible to do precise calculations of the integrator dynamic mode during its design. The solution put forward respectively covers the large ones and the small intervals of time (case of low and the high frequency). The analysis made in this study

uses the Duhamel integral which makes it possible to

present analytical solutions in the time domain.

We made a comparison between the exact and

approximate expressions of the dynamic errors in stationary regime with those obtained by the transitory function.

The computation results obtained allowed making the design of a Miller integrator covering frequency range of:

$20\,Hz \div 20000\,Hz$.

It would be also interesting to study the case when the input signal is not regular and having a non symmetrical form.

References

[1] STANTCHEV, 1994) STANTCHEV I., *électroniques analogiques des appareils de mesure,* Université Technique de Sofia, 1994 (ISBN 954-438-094-9).

[2] James.W, Susan A.Ridiel, Electric Circuit Fifth Edition, Addision- 1996 Wesley Puplishing company ISBN 0-201-40100-2.

[3] Measurement Systems, Fourth edition, Application and Design, International edition 1990, Printed in Singapore, ISBN: 0-07-017338-9

[4] Farhi S.L, Methode temporelles d'analyse des processus transitoires dans les circuits électriques linéaires , Sofia 1981, ISBN : 456-536-034-2.

[5] Zeniveki G.V, Jonkin A.V et Outstil S.V Stradov- Les bases des circuits électriques linéaires – Nanka 1990.

[6] François Manneville, Esquieux Jacque Théorie du signal et composants, Dunod, paris 2000, ISBN 2 10 004812 0.

[7] Haddouk Amira, Détecteur synchrone application dans l'instrumentation, Mastere 29-10-05 , ESSTT , Uniersity of Tunis.

[8] Chevalier Raymond , Conte René, Elements de métrologie, Les éditions la liberté InC- Quebec, Erolles Editur, Paris , ISBN : 0-88609-017-X

[9] Malvino N, Electronic principles, International Editions 1993,McGraw- Hill, ISBN : 0-02-800845-6, printed in Singapore.

[10] C.D. McGillen, J.I Aunion, and K.Yu " signals and noise in evoked brain potentials" IEEE trans .BRomed .Eng, vol . BME-32, PP. 1012-1016 Dec .1986.

[11] Jerzy, Kolonko.A, Accurate measurement of power, energy, and true RMS voltage using synchronous counting, IEEE transaction s on instrumentation and measurement, vol. 42, No.3 June 1993. http:// perso.wanado.fr/fr6 crp/elec/index.htm.

[12] TT- Lang" l'électronique dans les techniques de mesures", techniql'ingénieur R430(1984).

[13] G;Ash et Coll. Les capteurs en instrumentation industrielle. Dunod, collection EAA, Paris 1998, 864 pages , 5eme édition ISBN:2100047582.

[14] Hubert Lumbroso, circuits electriques 92 problèmes resoles classes supérieures, Dunod 1995, ISBN:2 10 0027964.

[15] http://www.medicalcybernetics.de/methods/duhamel.html

[16] http://www.proba.jussieu.fr/cours/sightml/node13.html

[17] http://laennec.univlyon1.fr/SCIENTIFIQUES/IFC/IFC/instn/m4c2/m4c2_5htm

[18] http://fr.wikipedia.org/wiki/Produit_de_convolution.

European Journal of Scientific Research
ISSN 1450-216X Vol.18 No.4 (2007), pp.621-627

http://www.eurojournals.com/ejsr.htm

Solution of Non-Linear Volterra Integro-Differential Equations

A. Khani
Mathematics Department, University of Kerman, Kerman, IRAN
E-mail: khani@azaruniv.edu

Mahmoud Mohseni Moghadam
Mahani Mathematical Research Center, University of Kerman, Kerman, IRAN
E-mail: mohseni@math.msu.edu

Sedaghat Shahmorad
Department of Applied Mathematics, University of Tabriz, Tabriz, IRAN
E-mail: shahmorad@tabrizu.ac.ir

Abstract

In this paper we study a new method to find a numerical solution for the general form of Non-linear Volterra Integro-Differential Equations (NVE). To this end, we will present our method based on the matrix form of (NVE). The corresponding unknown coefficients of our method have been determined by using computational aspects of matrices. Finally accuracy of the method has been verified by presenting some numerical computations.

Keywords: Volterra Integro-Differential Equations, Matrix Forms, Numerical Solutions.
American Mathematical Subject Classification (AMSC): 65R20

1. Introduction

In 1981, Ortiz and Samara [1] proposed an operational technique for finding a numerical solution of non-linear ordinary differential equations with some supplementary conditions based on the Tau method [2]. During the last 25 years considerable work has been done both in development of the above technique, its theoretical analysis and numerical applications. Various techniques have been described in a series of papers [3-7] for the case of linear ordinary differential eigenvalue problems. In [8-12] numerical solution of partial differential equations and their related eigenvalue problems has discussed. The Tau method developed in [13] for the iterated solutions of linear operator equations and in [14-16] for the numerical solution of linear Fredholm and Volterra integral and integro-differential equations. The object of this paper is to present a similar operational approach by using the Adomian decomposition method for the general form of non-linear Volterra integro-differential equations of the second kind with initial conditions. This method leads to an algorithm with remarkable simplicity, while retaining the accuracy of results.

2. Non-Linear Volterra integro-Differential Equations

Consider the non-linear Volterra integro-differential equation

$$y^{(m)}(x)+g_1(x)G_1(y,y',\ldots,y^{(m-1)})+\cdots g_r(x)G_r(y,y',\ldots,y^{(m-1)})-$$

$$\int_0^x\left(k_1(x,t)F_1(y(t),y'(t),\ldots,y^{(m)}(t))+\cdots+k_s(x,t)F_s(y(t),y'(t),\ldots,y^{(m)}(t))\right)dt=f(x),\quad x\in[0,a]$$

or the compact form

$$y^{(m)}(x)+\sum_{i=1}^{r}g_i(x)G_i(y,y',\mathrm{K},y^{(m-1)})-\int_0^x\sum_{i=1}^{s}k_i(x,t)F_i(y(t),y'(t),\mathrm{K},y^{(m)}(t))dt=f(x),\quad x\in[0,a] \tag{2.1}$$

with the initial conditions

$$y^{(j)}(0)=d_j,\quad j=0,1,\mathrm{K},m-1. \tag{2.2}$$

Here we assume that $g_i(x)$ for $i=1,2,\ldots,r$, $k_j(x,t)$ for $j=1,2,\ldots,s$ and $f(x)$ are polynomials, otherwise they can be approximated by polynomials to any degree of accuracy (by Taylor series or any other suitable method). Moreover, we suppose that $y_n(x)$ to be a polynomial approximation of degree n for $y(x)$. Then one can write

$$\begin{aligned}
&g_i(x)=\sum_{j=0}^{n}g_{ij}x^j=\underline{g_j}\,\underline{\underline{X}} && i=1,2,\ldots,r\\
&k_l(x,t)=\sum_{i=0}^{n}\sum_{j=0}^{n}k_{ij}^{(l)}x^it^j && l=1,2,\ldots,s\\
&f(x)=\sum_{j=0}^{n}f_jx^j=\underline{f}\,\underline{\underline{X}}\\
&y_n(x)=\sum_{j=0}^{n}a_jx^j=\underline{a_n}\,\underline{\underline{X}}
\end{aligned} \tag{2.3}$$

where $\underline{g_i}=[g_{i0},\ldots,g_{in},0,\ldots]$, $\underline{f}=[f_0,f_1,\ldots,f_n,0,\ldots]$, $\underline{a_n}=[a_0,a_1,\ldots,a_n,0,\ldots]$ and $\underline{\underline{X}}=[1,x,x^2,\ldots,]^T$ are the coefficients vectors of $g_i(x)$, right-hand side of equation (2.1), unknown coefficients vector and the basis vector respectively. Without loss of generality we have taken all polynomials of degree n, because if $g_i(x)$, $k_j(x,t)$, $f(x)$ and $y_n(x)$ are respectively of different degrees n_{gi}, (n_{xl},n_{tl}), n_f and n_y then we can set $n=\max\{n_{g1}\ldots n_{gr}n_{x1}\ldots n_{xs}n_{t1}\ldots n_{ts},n_f,n_y\}$.

3. Converting NVE to a System of Algebraic Equations

The effect of differentiation or shifting on the coefficients $\underline{a_n}=[a_0,a_1,\ldots,a_n,0,\ldots]$ of a polynomial $y_n(x)=\underline{a_n}\,\underline{\underline{X}}$ is the same as that of post-multiplication of $\underline{a_n}$ by either the matrix η or the matrix μ defined by $\mu=\begin{bmatrix}0&1&0&0&\\&0&1&0&\vdots\\&&0&1&\\&\cdots&&&\ddots\end{bmatrix}$ and $\eta=\begin{bmatrix}0&&&&\\1&0&&&\vdots\\0&2&0&&\\&\cdots&&&\ddots\end{bmatrix}$.

Lemma 3.1

If $y_n(x)$ be a polynomial of the form

$$y_n(x)=\sum_{i=0}^{n}a_ix^i=\sum_{i=0}^{\infty}a_ix^i$$

Then

i) $\frac{d^r}{dx^r} y_n(x) = \underline{a_n} \eta^r \underline{\underline{X}}, \quad r = 1,2,\ldots$

ii) $x^r y_n(x) = \underline{a_n \mu^r} \underline{\underline{X}}, \quad r = 1,2,\ldots$

where $\underline{a_n} = [a_0, a_1, \ldots, a_n, 0, \ldots]$.

The proof follows immediately by induction.

Lemma 3.2

Let $p(x) = \underline{p}\underline{\underline{X}}$ and $q(x) = \underline{q}\underline{\underline{X}}$ with $\underline{p} = (p_0, p_1, \ldots)$ and $\underline{q} = (q_0, q_1, \ldots)$, then $p(x)q(x) = \underline{pq}(\mu)\underline{\underline{X}}$.

Proof: See [1].

By using the Adomian decomposition method (See [17]) one can simplify the non-linear terms as follows:

By setting $\hat{G}_i(x) = G_i(y(x), y'(x), \ldots, y^{(m-1)}(x))$, we have

$$\begin{aligned}\hat{G}_i(x) &= G_i\left(\sum_{j=0}^{\infty} a_j x^j, \sum_{j=0}^{\infty} (j+1) a_{j+1} x^j, \mathrm{K}, \sum_{j=0}^{\infty} \frac{(j+m-1)!}{j!} a_{j+m-1} x^j\right) \\ &= \sum_{l=0}^{\infty} A_l^{Gi} x^l \\ &= \underline{A}^{Gi} \underline{\underline{X}}\end{aligned} \tag{3.1}$$

where $\underline{A}^{Gi} = [A_0^{Gi}, A_1^{Gi}, \ldots]$ with

$$A_l^{Gi} = \frac{1}{l!}\left\{\frac{d^l}{dx^l} G_i\left(\sum_{j=0}^{\infty} a_j x^j, \sum_{j=0}^{\infty} (j+1) a_{j+1} x^j, \ldots, \sum_{j=0}^{\infty} \frac{(j+m-1)!}{j!} a_{j+m-1} x^j\right)\right\}_{x=0} = \frac{\hat{G}_i^{(l)}(0)}{l!}$$

which is depend on $a_0, a_1, \ldots, a_{l+m-1}$ for $i = 1,2,\ldots,r$, and $l = 0,1,\ldots$.

By using this method for the non-linear terms under integral sign, we have

$$\begin{aligned}\hat{F}_i(x) &= F_i(y(x), y'(x), \mathrm{K}, y^{(m)}(x)) \\ &= F_i\left(\sum_{j=0}^{\infty} a_j x^j, \sum_{j=0}^{\infty} (j+1) a_{j+1} x^j, \mathrm{K}, \sum_{j=0}^{\infty} \frac{(j+m)!}{j!} a_{j+m} x^j\right) \\ &= \sum_{l=0}^{\infty} A_l^{Fi} x^l \\ &= \underline{A}^{Fi} \underline{\underline{X}}\end{aligned} \tag{3.2}$$

where $\underline{A}^{Fi} = [A_0^{Fi}, A_1^{Fi}, \ldots]$ with

$$A_l^{Fi} = \frac{1}{l!}\left\{\frac{d^l}{dx^l} F_i\left(\sum_{j=0}^{\infty} a_j x^j, \sum_{j=0}^{\infty} (j+1) a_{j+1} x^j, \ldots, \sum_{j=0}^{\infty} \frac{(j+m)!}{j!} a_{j+m} x^j\right)\right\}_{x=0} = \frac{\hat{F}_i^{(l)}(0)}{l!}$$

which is depend on $a_0, a_1, \ldots, a_{l+m}$ for $i = 1,2,\ldots,s$, and $l = 0,1,\ldots$.

Now if we replace $y(x)$ by $y_n(x) = \sum_{i=0}^{n} a_i x^i$, and use lemma 3.2 and relations (3.1) and (3.2) then

$$\sum_{i=1}^{r} g_i(x) G_i(y_n, y_n', \ldots, y_n^{(m-1)}) = \sum_{i=1}^{r} \underline{A}^{Gi} g_i(\mu) \underline{\underline{X}}$$
$$= (\sum_{j=1}^{r} A_0^{Gj} g_{j0}, \sum_{i=0}^{2} \sum_{j=1}^{r} A_i^{Gj} g_{j,2-i}, \sum_{i=0}^{3} \sum_{j=1}^{r} A_i^{Gj} g_{j,3-i}, \ldots) \underline{\underline{X}} \tag{3.3}$$

and

$$\int_0^x k_i(x,t) F_i(y(t), y'(t), \ldots, y^{(m)}(t)) dt = \underline{A}^{Fi} \underline{K}_i \underline{\underline{X}}, \quad i = 1,2,\ldots,s \tag{3.4}$$

Where

$$g_i(\mu) = \begin{bmatrix} g_{i0} & g_{i1} & g_{i2} & g_{i3} & \cdots & g_{i,n} & 0 & 0 & \cdots \\ 0 & g_{i0} & g_{i1} & g_{i2} & \cdots & g_{i,n-1} & g_{i,n} & 0 & \cdots \\ 0 & 0 & g_{i0} & g_{i1} & \cdots & g_{i,n-2} & g_{i,n-1} & g_{i,n} & \cdots \\ & & & \vdots & & & & & \ddots \end{bmatrix}$$

and

$$\underline{K}_i = \begin{bmatrix} 0 & k_{0,0}^{(i)} & k_{1,0}^{(i)} + \frac{1}{2}k_{0,1}^{(i)} & k_{2,0}^{(i)} + \frac{1}{2}k_{1,1}^{(i)} + \frac{1}{3}k_{0,2}^{(i)} & k_{3,0}^{(i)} + \frac{1}{2}k_{2,1}^{(i)} + \frac{1}{3}k_{1,2}^{(i)} + \frac{1}{4}k_{0,3}^{(i)} & \cdots \\ & 0 & \frac{1}{2}k_{0,0}^{(i)} & \frac{1}{2}k_{1,0}^{(i)} + \frac{1}{3}k_{0,1}^{(i)} & \frac{1}{2}k_{2,0}^{(i)} + \frac{1}{3}k_{1,1}^{(i)} + \frac{1}{4}k_{0,2}^{(i)} & \cdots \\ & & 0 & \frac{1}{3}k_{0,0}^{(i)} & \frac{1}{3}k_{1,0}^{(i)} + \frac{1}{4}k_{0,1}^{(i)} & \cdots \\ & & & 0 & \frac{1}{4}k_{0,0}^{(i)} & \cdots \\ & & & \vdots & & \ddots \end{bmatrix}$$

with

$$(\underline{k}_i)_{l,j} = \sum_{q=l-1}^{j-2} \frac{1}{q+1} k_{j-q-2,q-l+1}^{(i)} \qquad i = 1,2,\ldots,s, \quad l = 1,2,\ldots,n, \quad j > l$$

and so, the matrix form of (2.1) can be written as:

$$\underline{a}_n \eta^m \underline{\underline{X}} + \sum_{i=1}^{r} \underline{A}^{Gi} g_i(\mu) \underline{\underline{X}} - \sum_{i=1}^{s} \underline{A}^{Fi} \underline{K}_i \underline{\underline{X}} = \underline{f} \underline{\underline{X}}$$

which yields

$$\underline{a}_n \eta^m + \sum_{i=1}^{r} \underline{A}^{Gi} g_i(\mu) - \sum_{i=1}^{s} \underline{A}^{Fi} \underline{K}_i = \underline{f},$$

since $\underline{\underline{X}}$ is a base vector. Now, we are in a position to determine the unknown coefficients. Note that we use (2.2) to write

$$a_j = \frac{d_j}{j!} \qquad j = 0,1,\ldots,m-1,$$

which determines the unknowns for the index $j = 0,1,\ldots,m-1$.

Other coefficients are determined by using (3.2), (3.3}), (3.4}), equation (2.1) and solving the following system of equations since $\underline{K}_i$ for $i = 1,2,\ldots$ is an upper triangular matrix, the solution of the above system is obtained by:

$$a_{m+j} = \frac{f_j + \sum_{l=1}^{s} \sum_{i=0}^{j-1} A_i^{Fl} (\underline{K}_l)_{i+1,j+1} - \sum_{i=0}^{j} \sum_{l=1}^{r} A_i^{Gl} g_{l,j-i}}{\frac{(m+j)!}{j!}}, \qquad j = 0,1,\ldots,n-m$$

4. Numerical Examples

The following examples are given to clarify accuracy of the presented method.

Example 1:

$$\begin{cases} y^{(3)}(x) + e^{2y(x)y'(x)} + e^{-y''(x)} + \int_0^x (2\cos(2t)e^{2y(t)y'(t)} + \sin(t)e^{y(t)} - y(t))dt = 1 + e \\ y(0) = 1, \quad y'(0) = 0, \quad y''(0) = -1, \quad 0 \le x \le \dfrac{\pi}{2}. \end{cases}$$

The exact solution is given by $y(x) = \cos(x)$. For the numerical results with $n = 5,10,15$ see Table 1.

Example 2:

$$\begin{cases} y''(x) - Ln(y(x)y'(x)) + \int_0^x (2\sin(t)e^{-(x+t)}y(t)y'(t) + 2e^{-x}\cos(t)y'(t) - y(t))dt = 2\sin(x) - 2x + 1 \\ y(0) = 1, \quad y'(0) = 1, \quad 0 \le x \le 1. \end{cases}$$

The exact solution is given by $y(x) = e^x$. For the numerical results with $n = 5,10,15$ see Table 2.

Example 3:

$$y'(x) - \sqrt{y(x)} - \int_0^x 2y'(t)dt = 2 - e^x, \quad y(0) = 1, \quad 0 \le x \le 1.$$

The exact solution is given by $y(x) = e^{2x}$. For the numerical results with $n = 5,10,15$ see Table 3.

Figure 1: A plot of example (1) and example(2).

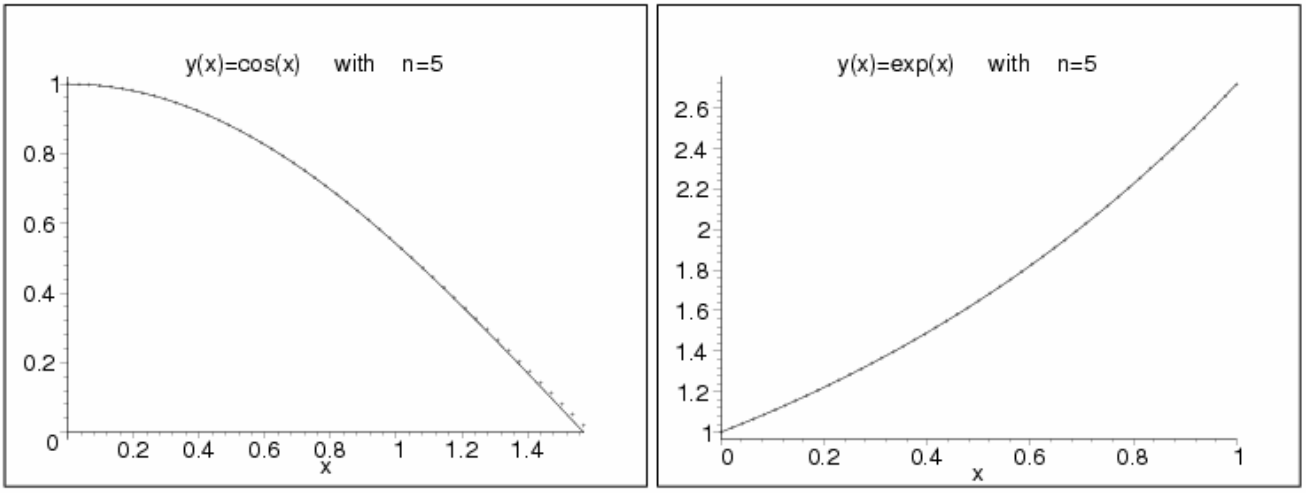

Remark 5.1: Note that, in the following figures, the continued line plots show the exact solution and the dot plots show the approximate solution.

Remark 5.2: Note that in the following tables, the notations Exact, App. and Abs.Err., have been used for exact solution, approximate solution obtained by our method and absolute error of approximate solution respectively.

Table 1: example (1)

		n=5		n=10		n=15	
x	**Exact**	**App.**	**Abs.Er.**	**App.**	**Abs.Err.**	**App.**	**Abs.Err.**
0.00	1.000000	1.000000	0	1.000000	0	1.000000	0
0.31	0.951057	0.951058	1.33E-06	0.951057	1.93E-15	0.951057	4.30E-22
0.63	0.809017	0.809102	8.49E-05	0.809017	7.89E-12	0.809017	2.82E-17
0.94	0.587785	0.588743	9.58E-04	0.587785	1.02E-09	0.587785	1.85E-14
1.26	0.309017	0.314335	5.32E-03	0.309017	3.21E-08	0.309017	1.84E-12
1.57	0.000000	0.019969	2.00E-02	0.000000	4.65E-07	0.000000	6.51E-11

Table 2: example (2)

		n=5		n=10		n=15	
x	**Exact**	**App.**	**Abs.Err.**	**App.**	**Abs.Err.**	**App**	**Abs.Err.**
0.00	1.000000	1.000000	0	1.000000	0.00	1.000000	0
0.20	1.221403	1.221403	9.149350e-08	1.221403	5.217518e-16	1.221403	3.169542e-25
0.40	1.491825	1.491819	6.030975e-06	1.491825	1.086896e-12	1.491825	2.102167e-20
0.60	1.822119	1.822048	7.080039e-05	1.822119	9.565183e-11	1.822119	1.397570e-17
0.80	2.225541	2.225131	4.102618e-04	2.225541	2.304785e-09	2.225541	1.411549e-15
1.00	2.718282	2.716667	1.615162e-03	2.718282	2.731266e-08	2.718282	5.077107e-14

Table 3: example (3)

		n=5		n=10		n=15	
x	**Exact**	**App.**	**Abs.Err.**	**App.**	**Abs.Err.**	**App.**	**Abs.Err.**
0.00	1.000000	1.000000	0	1.000000	0	1.000000	0
0.20	1.491825	1.491819	6.030975e-06	1.491825	1.086896e-12	1.491825	2.102167e-20
0.40	2.225541	2.225131	4.102618e-04	2.225541	2.304785e-09	2.225541	1.411549e-15
0.60	3.320117	3.315136	4.980923e-03	3.320117	2.066314e-07	3.320117	9.504631e-13
0.80	4.953032	4.923115	2.991776e-02	4.953027	5.076410e-06	4.953032	9.726884e-11
1.00	7.389056	7.266667	1.223894e-01	7.388995	6.138994e-05	7.389056	3.546513e-09

References

[1] E.L. Ortiz, H. Samara, An operational approach to the Tau method for the numerical solution of non-linear differential equations, Computing 27, 15 - 25 (1981).

[2] C. Lanczos, Trigonometric interpolation of empirical and analytical functions, J. Math. Phys. 17, 123 - 199 (1938).

[3] K.M Liu, E.L. Ortiz, Eigenvalue problems for singularly perturbed differential equations, in J.J.H. Miller (Ed.), Proceeding of the BAIL II conference, Boole press, Dublin, pp. 324-329 (1982).

[4] K.M. Liu, E.L. Ortiz, Approximation of eigenvalues defined by ordinary differential equations with the Tau method, in B. Ka gestrm, A. Ruhe (Eds). Matrix pencils, Springer, Berlin, pp. 90-102 (1983).

[5] K.M. Liu, E.L. Ortiz, Tau method approximation of differential eigenvalue problems where the spectral parameter enters nonlinearly, J. Comput. Phys. 72, 299-310 (1987).

[6] K.M. Liu, E.L. Ortiz, Numerical solution of ordinary and partial function-differential eigenvalue problems with the Tau method, Computing (wien) 41, 205-217 (1989).

[7] E.L. Ortiz, H. Samara, Numerical solution of differential eigenvalue problems with an operational approach to the Tau method, Computing 31, 95-103 (1983).

[8] K.M. Liu, E.L. Ortiz, Numerical solution of eigenvalue problems for partial differential equations with the Tau-lines method, Comp. Math. Appl. B 12 (5/6) 1153-1168 (1986).

[9] K.M. Liu, E.L. Ortiz, K.S. Pun, Numerical solution of steklov's partial differential equation eigenvalue problem, in J.J.H. Miller (Ed.), Computational and asymptotic methods for boundary and interior layers III, Boole Press, Dublin, pp. 244-249 (1984).

[10] E.L. Ortiz, K.S. Pun, Numerical solution of nonlinear partial differential equations with Tau method, J. Comp. Appl. Math. 12/13, 511-516 (1985).

[11] E.L. Ortiz, K.S. Pun, A bi-dimensional Tau-elements method for the numerical solution of nonlinear partial differential equations with an application to Burgers'equation, Comp. Math. Appl. B 12 (5/6), 1225-1240 (1986).

[12] E.L. Ortiz, H. Samara, Numerical solution of partial differential equations with variable coefficients with an operational approach to the Tau method, Comp. Math. Appl. 10 (1), 5-13 (1984).

[13] M.K. EL-Daou, H.G. Khajah, Iterated solutions of linear operator equations with the Tau method, Math. Comput. 66 (217), 207-213 (1997)

[14] S.M. Hosseini, S. Shahmorad, Numerical solution of a class of integro-differential equations by The Tau method with an error estimation, Appl. Math. Comput 136, 559-570 (2003).

[15] S.M. Hosseini, S. Shahmorad, Tau numerical solution of Fredholm integro- differential equations with arbitrary polynomial bases, Appl. Math. Modelling 27, 145-154 (2003).

[16] S.M. Hosseini, S. Shahmorad, A matrix formulation of the Tau for Fredholm and Volterra linear integro-differential equations, The Korean J. Comput. Appl. Math. Vol. 9, NO.2, 497-507 (2002).

[17] T. Badredine, K. Abbaoui, Y. Cherruault, Convergence of Adomian's method applied to integral equations, Kybernetes, Vol. 28, No. 5, pp. 557-564 (1999).

[18] P. Linz, Analytical and Numerical Methods for Volterra equations, SIAM, Philadelphia, PA, (1985).

[19] J. Abdul Jerri, Introduction to Integral Equations with Applications, John Wiley and Sons, New York, (1999).

European Journal of Scientific Research
ISSN 1450-216X Vol.18 No.4 (2007), pp.628-638

http://www.eurojournals.com/ejsr.htm

Niveaux de Contamination des ETM (Cu, Zn , Fe, Cd et Pb) Dans les Tissus Mous du Gastéropode *Tympanotonus Fuscatus Radula* Collecté Dans La Lagune Ebrié (Côte d'Ivoire)

Mamadou Koné
Laboratoire des Sciences de l'Environnement- Université d'Abobo-Adjamé 02 BP 801 Abidjan 02

Diomande Dramane
Laboratoire Environnement et Biologie Aquatique- Université d'Abobo-Adjamé 02 BP 801 Abidjan 02

Traore Karim Sory
Laboratoire des Sciences de l'Environnement- Université d'Abobo-Adjamé 02 BP 801 Abidjan 02

Dembele Ardjouma
Laboratoire Central d'Agrochimie et d'Ecotoxicologie- LANADA 04 BP 612 Abidjan 04

Houenou Pascal Valentin
Laboratoire des Sciences de l'Environnement- Université d'Abobo-Adjamé 02 BP 801 Abidjan 02

Abstract

The levels of concentrations of the ETM Cu, Pb, Fe, Cd, Zn and Pb have been determined in the soft tissue (edible part) of the gastropod *Tympanotonus fuscatus radula* sampled on seven sampling stations identified through the Ebrié lagoon. The results show a geographical variability of the bioavailability of the ETM dependant on the metal and the level of pollution of the environment. So the metallic contamination index are the most elevated for the toxic elements (Cd and Pb), mainly in the sampling zones under industrial influence (Biétri and Attécoubé). Besides the metallic concentrations in the soft tissue present a good correlation ($p < 0,05$) with the length of the shells for the essential elements (Cu, Fe, Zn). Due to its bioaccumulation capacities, *Tympanotonus fuscatus radula* have the potential of being used as bioindicator to control the metallic pollution of the Ebrié lagoon.

Keywords: Heavy metal, *Tympanotonus*, lagune Ebrié, Côte d'Ivoire, bioaccumulation

Introduction

Le système lagunaire Ebrié s'étend entre 3°40 et 4°50 de longitude Ouest et entre 5°20 et 5°10 de latitude Nord [1]. Selon [2], de nombreuses études ont porté sur la faune benthique de cette lagune ([3], [1] et [4], [5], [6], [7], [8]), la répartition géographique des espèces ainsi que la structure des peuplements et leur évolution.

Par ailleurs la lagune Ebrié jouxtant la ville d'Abidjan dans sa partie urbaine (Fig.1.a), elle reçoit de nombreux déversements constitués des eaux et des déchets qu'elles charrient :

- eaux continentales venant des fleuves et rivières,

- eaux de ruissellement des rues, lixiviats provenant des dépôts d'ordures,
- eaux usées domestiques et des milieux hospitaliers,
- effluents industriels.

Il en résulte diverses formes de pollution auxquelles se sont intéressées de nombreuses recherches visant à les caractériser : pollution chimique (métaux lourds, pesticides, PCB) et organique des eaux lagunaires et des sédiments [9] [10] [11], pollution bactérienne voire organique et bactérienne des eaux [12], [14], [15]. En outre, des études d'impact de ces pollutions sur la faune ont été également entreprises [16], [17], [18]. Des études plus récentes se sont intéressées à la modélisation hydrodynamique des eaux de la lagune Ebrié[19] ou celle de l'évolution de la pollution chimique[20]. Il ressort de ces études que la lagune Ebrié est très polluée dans tous ces compartiments (eaux, sédiments, faune) du fait des déversements d'origine naturelle et anthropique qui s'y opèrent et dont les conséquences sont la perte de certains usages des eaux et la non comestibilité de la plupart de ses ressources.

La présente étude porte sur le gastéropode *T fuscatus radula* que l'on trouve dans les eaux lagunaires le long de la Côte Ouest africaine, du Sénégal au Congo [2]. Selon [3], *T. fuscatus*, typique des eaux saumâtres, est un gastéropode présent en lagune Ebrié. Il peut s'accommoder de fonds pauvres en oxygène et vit sur des sédiments vaseux, qualifiés de « vases fines noir » [7], riches en débris organiques dont il se nourrit en léchant la pellicule de surface [6].

Des études ont montré que **les** mollusques accumulent les éléments-traces dans leurs tissus mous [21] mais également dans leurs coquilles [22]. Ainsi, du fait de leur capacité à accumuler les contaminants, les mollusques ont parfois été utilisés comme bioindicateurs de diverses contaminations dont les éléments traces [23] [24] [25].

Notre recherche vise à évaluer l'aptitude de par *T. fuscatus radula* à accumuler des éléments traces, en vue de son utilisation, à terme, comme bioindicateur de la pollution minérale de la lagune Ebrié en général, et, en particulier dans la surveillance des ETM dans le milieu naturel.

A cet effet, le présent travail se propose de :

1) déterminer le niveau de concentrations métalliques de Cu, Pb, Fe, Cd, Zn et Pb dans les tissus mous des *T fuscatus radula* prélevés dans des zones pollués ;
2) investiguer les corrélations entre les niveaux déterminés et la taille des coquilles ou la masse de tissus mous de *T. fuscatus radula*,
3) vérifier la variabilité géographique de la disponibilité des ETM au gastéropode *T. fuscatus radula*.

Materiel et Methodes

Choix et repérage des stations d'échantillonnage

La position et la localisation exactes des stations d'échantillonnage sont données respectivement à la figure 1 et au tableau 1. Chacune d'elles a été choisie en raison de la présence d'activités socio-économiques importantes :

- zone de Cocody (Fig.1.b) : elle reçoit principalement les rejets domestiques des communes de Cocody, d'Adjamé (Williamsville et 220 logements) et de Treichville. Elle subit également, du fait des courants, l'influence des rejets du Pont Général de Gaulle comprenant, selon [11] des matières de vidange ;
- zone de la baie de Biétri (Fig.1.c) : en aval d'une zone à forte dominante industrielle (alimentaire, pétrochimique, peinture, agrochimique, métallurgique), elle reçoit également les rejets de l'abattoir et des tanneries artisanales.
- zone de la baie du Banco (Fig. 1.d) : zone de circulation maritime, en aval des ateliers de réparation des navires (CARENA), elle reçoit les rejets des ateliers métallurgiques et des huiles

vidanges, les rejets d'origine domestique des communes d'Attécoubé, d'Adjamé et d'une partie de celle de Yopougon.;

Figure 1: Carte des stations d'échantillonnage dans la zone lagunaire Ebrié jouxtant la ville d'Abidjan

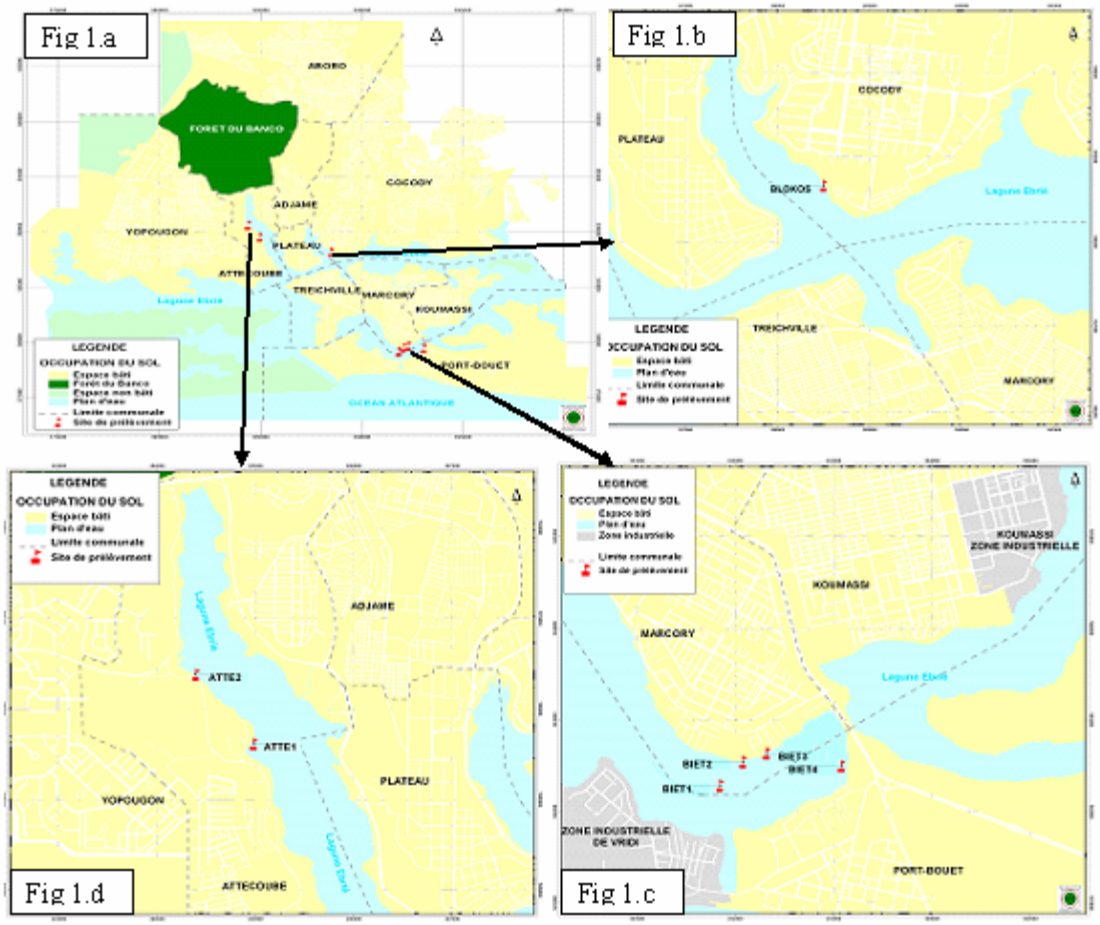

Table 1: Coordonnées GPS des stations d'échantillonnage

zones de prélèvement	Stations d'échantillonnage	Coordonnées GPS	
		Longitude	Lattitude
Attecoube	Atté 1	W :004°02'16.8''	N : 05°20'00.2
	Atté 2	W :004°02'35.9''	N : 05°20'25.0
Bietri	Biétri 1	W :003°58'33.5''	N : 05°16'01.9''
	Biétri 2	W : 003°58'25.9''	N : 05°16'10.3''
	Biétri 3	W : 003°58'18.1''	N : 05°16'13.3''
	Biétri 4	W : 003°57'53.4''	N : 05°16'08.8''
Cocody	Blokos	W :004°00'12.7''	N : 05°19'18.9''

Prélèvement des mollusques et prétraitement des échantillons

Les mollusques vivants ont été collectés manuellement, nettoyés, débarrassés des débris minéraux et acheminés au laboratoire dans des bocaux aérés contenant de l'eau de lagune. L'espèce d'intérêt, *T. fuscatus radula* (Fig. 2) y a été isolée et vidée de son contenu gastrique après un séjour de 48 heures dans l'eau déionisée.

Figure 2: *T. fuscatus radula*

Afin de permettre des comparaisons ultérieurement, les mollusques ont été répartis en cinq classes de tailles (tableau 2). Celles-ci sont définies après la mesure de la longueur de coquille de chaque spécimen (distance séparant les deux pointes extrêmes de la coquille). Une fois les mollusques décoquillés, les tissus mous (chair des mollusques) prélevés ont été regroupés pour faire un homogénat par classe et par station d'échantillonnage puis conservés au congélateur à -20 °C jusqu'à la minéralisation.

Table 2: Constitution de classes de taille des mollusques en fonction de la longueur des coquilles

Longueur des coquilles (cm)	<2	[2 ; 2,5]	[2,5 ; 3]	[3 ; 3,5]	[3,5 ; 4]	≥ 4
Classe de taille	1	2	3	4	5	6

Mise en solution des tissus biologiques (minéralisation)

Tous les réactifs utilisés sont de pureté analytique. Tout le matériel utilisé pour la digestion a été trempé dans de l'acide nitrique à 5% pendant 24 h, rincé à l'eau déminéralisée, séché à l'étuve puis maintenu bouché ou emballé avant utilisation. Le protocole de digestion des tissus mous est celui proposé par le Centre d'Expertise en Analyse Environnementale du Québec [26].

Dosage des ETM dans les tissus mous

Les ETM d'intérêt (Cu, Zn, Fe, Pb, Cd) sont alors dosés, dans les digestats obtenus, à l'aide d'un spectromètre d'absorption atomique de marque Thermoélémental type M6 muni d'un système d'atomisation à flamme et d'un correcteur au deutérium. Les longueurs d'onde de détection des métaux sont respectivement de 248,3nm ; 324,8 nm ; 213,9 nm ; 217,0 nm ; 228,8 nm pour Fe, Cu, Zn, Pb et Cd. Les limites instrumentales de détection pour Fe, Cu, Zn, Pb, Cd sont respectivement de 6 ; 3 ; 1,0 ; 10 ; 1,5 ppb. La courbe d'étalonnage n'est validée que si le coefficient de détermination de la droite r^2 > 0,995. Pour chaque échantillon, la concentration métallique retenue est la moyenne de trois déterminations faites avec un temps de mesure de quatre secondes chacune. Une telle moyenne n'est retenue par le logiciel que si les trois déterminations différent entre elles de moins de 5%. Les taux de recouvrement, compris entre 90 et 110%, ont été déterminés en utilisant des solutions dopées.

Traitement statistique des données

Les traitements statistiques des données et les tracés de graphes ont été faits en utilisant les logiciel STATA Intercooleed dans sa version 8 (STATA CORPORATION) et le tableur EXCEL 2003.

Le test de Kruskal et Wallis suivi de celui de Mann-Whitney (post-hoc) ont été appliqués pour comparer les concentrations :

- entre les différentes classes de taille de *T. fuscatus radula* (capacité d'accumulation) et
- entre les mollusques issus de stations d'échantillonnage différentes (variabilité géographique) ;
- entre les différents ETM dans les tissus mous de T. fuscatus radula (biodisponibilité) ;

3. Resultats et Discusssions

3.1. Teneur en ETM dans la chair du *tympanautonus fuscatus radula*

Les résultats présentés dans le tableau 3, donnent le niveau d'imprégnation moyen des mollusques (exprimés en mg/kg) ainsi que les valeurs maximales et minimales pour chaque ETM, par zone de prélèvement. Les teneurs moyennes en ETM de chacune des classes de taille ont été évaluées avec un intervalle de confiance de 95%.

Table 3: Moyenne, maximum, minimum et écart-type des concentrations en ETM (mg/kg) par zone de prélèvement

Zone		Cu	Fe	Zn	Pb	Cd
Attécoubé	Moy	17,416	107,491	9,293	0,048	0,046
	Min	5,811	16,975	2,046	0,007	0,007
	Max	32,477	308,458	14,612	0,178	0,173
	Sd	10,493	110,128	4,371	0,061	0,055
Biétri	Moy	16,579	74,298	15,023	2,096	0,123
	Min	7,318	23,979	8,933	0,169	0,014
	Max	24,350	223,963	24,691	4,643	0,588
	Sd	5,644	56,383	5,921	1,377	0,162
Cocody	Moy	15,563	77,925	13,583	0,786	0,251
	Min	6,504	54,746	7,257	0,590	0,143
	Max	20,359	99,555	21,537	1,074	0,429
	Sd	6,310	19,277	6,283	0,020	0,125

Les résultats montrent que tous les échantillons analysés sont contaminés par les ETM et que leurs niveaux de contamination varient selon les métaux. On observe que le fer présente les plus fortes concentrations (de 16,975 à 308,458 mg/kg pour la zone 1 et de 23,979 à 223,963 mg/kg pour la zone 2 et de 54,746 à 99,555 pour la zone 3), avec des moyennes respectives de 107,491, 74,298 et 77,925 mg/kg. Les concentrations minimales et maximales pour le cuivre sont respectivement de 5,811 et 32,477 mg/kg pour la zone d'Attécoubé, de 7,318 et 24,350 mg/kg pour la zone de Biétri et de 6,504 et 20,359 mg/kg pour la zone de Cocody. Les autres ETM (Pd, Cd et Zn) sont en concentrations relativement plus faibles mais sont décelés dans tous les échantillons.

La figure 3 présente, pour chaque ETM à l'étude (Fig.3a à 3e), la distribution de sa concentration en fonction de la taille de classe des mollusques.

Figure 3: Distribution des teneurs en ETM dans les tissus mous par classe de taille

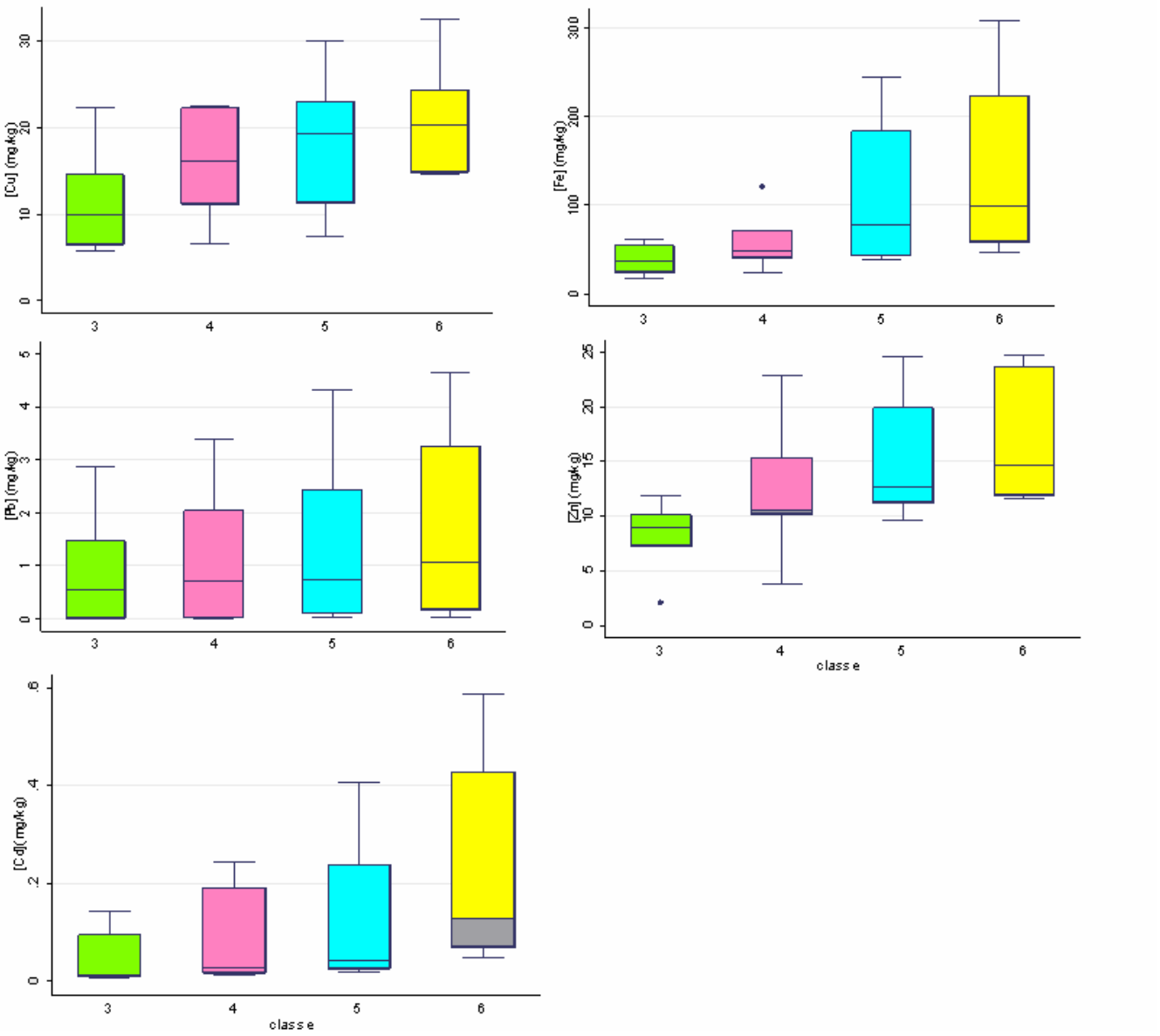

De manière générale, on observe que la concentration moyenne des ETM augmente lorsque la taille des spécimens augmente (l'indice étant fonction de la taille). Le test de la somme des rangs de Kruskal et Wallis montre que les concentrations observées sont significativement différentes d'une classe à l'autre au seuil de 5% ($p< 0,05$), pour tous les ETM sauf pour le plomb. On peut donc conclure à une bioaccumulation des ETM par *T. fuscatus radula*.

Indice de contamination

L'indice de contamination (IC) a été déterminé par zone de prélèvement pour chacun des ETM : $IC_{ETMt} = \frac{concentration \ \max imale}{concentration \ \min imale}$ de l'ETM [27]. Cet indice traduit le rapport de bioaccumulation des ETM entre le plus jeune et le plus âgé de la population échantillonnée, mais pourrait également traduire la biodisponibilité des ETM dans chacune des zones.

La figure 4 qui présente les différents indices de contamination métallique, confirme la bioaccumulation par les mollusques, des ETM à l'étude.

Figure 4 : Indice de contamination métallique des mollusques par zone de prélèvement et par ETM

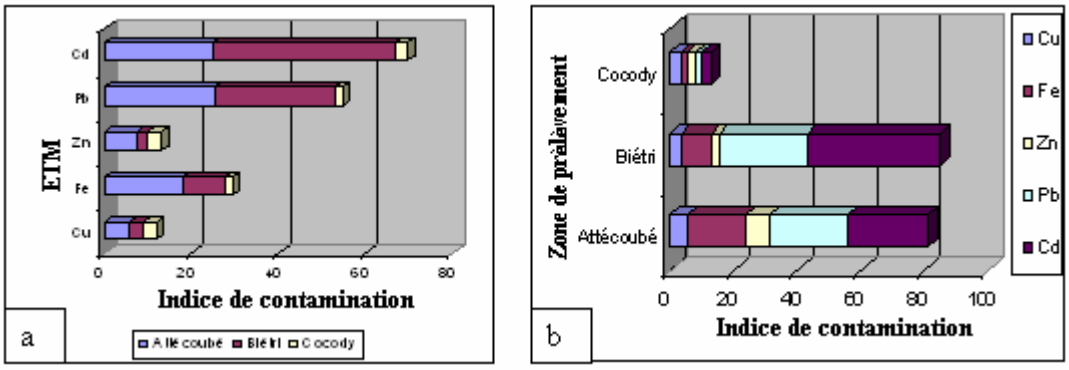

Dans l'ensemble des trois zones (Fig.4a), il ressort une plus grande contamination de *T. fuscatus radula* par les éléments toxiques (Cd puis Pb) que les éléments essentiels (respectivement Fe, Zn, Cu). Les zones de plus grande contamination (Fig. 4b) semblent être Biétri puis Attécoubé. Cocody reste la zone où les indices de contamination sont les plus bas pour tous les métaux. Ce classement des zones reflète bien le niveau de contamination probable de l'environnement lagunaire ; en effet, celui-ci est principalement sous influence industrielle à Biétri, mixte industrie- habitation pour Attécoubé et essentiellement habitation pour Cocody.

3.2. Variabilité géographique des concentrations métalliques des tissus mous de *T. fuscatus radula*

La figure 5a présente les grahes en toile des teneurs moyennes de chaque ETM dans les tissus mous de *T. fuscatus radula* des différentes stations d'échantillonnage.

Il ressort des graphes que les teneurs en ETM des tissus mous de *T. fuscatus radula* varient d'une station à l'autre, ce qui traduit une variabilité spatiale de la contamination du gastéropode par les ETM. Cette observation est confirmée par l'analyse statistique ; en effet analyse de variance (Anova oneway) au seuil de 5 % montre que les différences observées sont significatives($p< 0,05$), voire hautement significatives ($p<0,0001$).

Le diagramme en bâtonnets (Fig. 6b) montre que les éléments essentiels (Fe, Zn, Cu) sont les plus présents dans les tissus mous de *T. fuscatus radula* au contraire des éléments toxiques. Cela est probablement lié aux besoins nutritionnels du gastéropode d'une part et, d'autre part, pour la survie de l'espèce, à la nécessaire détoxification des éléments les plus toxiques nonobstant les quantités présentes dans l'environnement. En effet, d'après [28], selon la stratégie développée par chaque organisme, la concentration des métaux dans les tissus résulte d'un équilibre entre l'accumulation, l'élimination et la dilution due à la croissance corporelle.

Figure 6: Teneurs moyennes et % en ETM des tissus mous de *T. fuscatus radula* par station

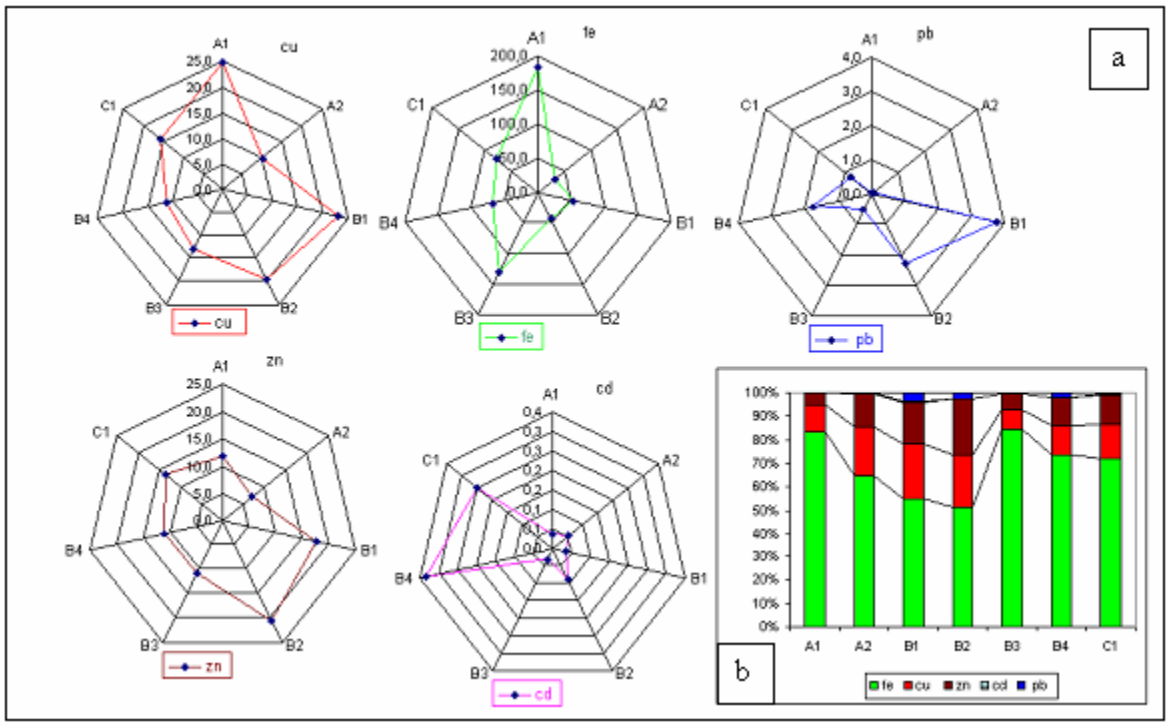

Stations : A1= Atté1; A2= Atté2; B1= Biet1; B2= Biet2; B3=Biet3; B4= Biet4; C1= Blokos

Toutes les observations précédentes suggèrent l'existence de plusieurs situations à travers l'espace d'étude :

- des stations de plus grande disponibilité de certains des ETM ou de plus grande proximité avec des sites de déversement de ceux-ci ; c'est notamment le cas des stations B4 pour le cadmium, B1 pour le plomb, A1 et B1 pour le cuivre, A1 pour le fer et, dans une moindre mesure, B2 pour le zinc ;
- une pollution de sources multiples semble caractériser le plomb pour lequel on observe le plus grand nombre de stations statistiquement différentes à l'analyse des concentrations des tissus mous des mollusques ;
- une origine plutôt naturelle qu'anthropique pour le zinc et le cuivre, pour lesquels la majorité des stations présente peu de différence significative ;
- des stations localisées de contamination ponctuelle pourraient expliquer la grande disponibilité des autres ETM à des stations précises : A1 et B3 pour le fer et A1, B1 et B2 pour le cuivre et enfin B4 et C1 pour le cadmium.

Corrélation entre les concentrations en ETM des tissus mous de *T. fuscatus radula*

Afin d'examiner les corrélations entre les teneurs des différents ETM dans les tissus mous de *T. fuscatus radula*, le test non paramétrique de corrélation de rang de Spearman a été utilisé pour un intervalle de confiance de 95%. Les coefficients de corrélation ainsi que les p-value sont présentés dans le tableau 4 pour tous les paramètres.

Table 4: Matrice de corrélation de rang de Spearman (rho (p-value)) entre les concentrations en ETM, la taille et la masse de tissu mou

	Cu	Fe	Zn	Pb	Cd	Taille	Masse
Cu	1,0000 0,0000						
Fe	0,4663 0,0124*	1,0000 0,0000					
Zn	**0,8270** **0,0000****	0,3985 0,0357*	1,0000 0,0000				
Pb	0,4311 0,0220*	0,0123 0,9504	**0,6673** **0,0001****	1,0000 0,0000			
Cd	0,1762 0,3696	0,3820 0,0448*	0,4176 0,0276*	0,3824 0,0446*	1,0000 0,0000		
Taille	0,5634 0,0018*	0,4973 0,0071*	**0,6270** **0,0004***	0,1861 0,3430	0,2092 0,2853	1,0000 0,0000	
Masse	0,5532 0,0023*	0,3578 0,0616	0,5497 0,0024*	0,1476 0,4536	0,1722 0,3809	**0,8723** **0,0000****	1,0000 0,0000

(*) Corrélation significative au seuil de 5%($p<0,05$) (**) Corrélation significative au seuil de 0,01%($p<0,0001$)

De nombreuses corrélations sont observées. Celle mise en évidence entre la masse de tissu mou et la taille (longueur de la coquille de T. fuscatus radula) semble conforter notre choix de regrouper les mollusques par classe de taille à des fins de comparaison. Cette classification s'avère essentielle car nous avons constaté que la teneur de la majorité des ETM augmente avec la taille. Ainsi, les oligoéléments (Cu, Zn) présentent une corrélation significative ou très faiblement non significative (Fe avec p-value=0,0616) avec la longueur de la coquille de T. fuscatus radula. La grande dispersion des concentrations de Fe dans les tissus mous de T. fuscatus radula pourrait expliquer cette dernière observation. Par contre, les éléments toxiques (Pb et Cd) semblent, à ce niveau de concentration, n'être corrélés ni avec la masse de tissu mou ni avec la longueur de la coquille.

Par ailleurs, des corrélations significatives (Zn-Fe, Zn-Cd, Cu-Fe, Cu-Pb, Fe-Cd et Pb-Cd) ou hautement significatives (Zn-Cu et Zn-Pb) sont observées entre les concentrations d'ETM différents dans les tissus mous de T. fuscatus radula. Selon [29] tous ces métaux, du fait de leur affinité avec le soufre, coexistent aussi bien au travers des liaisons métal-protéines existant dans les organismes vivants que dans les dépôts minéraux.

Conclusion

T. fuscatus radula est présent dans toutes les stations d'échantillonnage ; il est contaminé par les ETM (Fe Cu Zn Pb Cd) qu'il accumule. La teneur en ETM des tissus mous de *T. fuscatus radula* dépend du lieu de son prélèvement et de la taille du mollusque. Ces résultats (large distribution géographique du mollusque ; tendance à la bioaccumulation des ETM ; variabilité géographique de la contamination du mollusque) sont autant d'atouts plaidant pour une utilisation de *T. fuscatus radula* comme bioindicateur de la pollution de la lagune Ebrié par les ETM. Cependant les recherches doivent être poursuivies afin de confirmer ces tendances et de vérifier d'autres critères d'un bon bioindicateur. Ainsi, *T. fuscatus radula* doit être comparé avec d'autres bioindicateurs potentiels afin de confirmer son adaptabilité à la pollution métallique lagunaire quelque soit la station choisie ; en outre, il est nécessaire, par la recherche de corrélations, de montrer que les niveaux des concentrations des ETM dans les tissus mous de *T. fuscatus radula* sont le reflet de ceux du milieu lagunaire.

References

[1] Gomez, M., (1975). Premières données sur la faune benthique de la lagune Ebrié. Rapp DEA, Inst. Univ. Ecol. Abidjan, 36 p.

[2] Zabi S. G.F., et Le Loeuf, P., (1993). Revue des connaissances sur la faune benthique des milieux margino-littoraux d'Afrique de l'Ouest. Deuxième partie : peuplements et biotopes. Rev. Hydrobiol. Trop. 26 (1) : 19-51.

[3] Binder E., (1968). Répartition des mollusques dans la lagune Ebrié (Côte d'Ivoire). Cah. Orstom, sér. Hydrobiol., 2-(3-4) : 3-34.

[4] Gomez, M., (1978). Données biologiques sur deux peuplements benthiques autour de l'Ile Boulay et de l'Ile Leydet. Thèse de Doct. Spécialité, Univ. Nat. Côte d'Ivoire, Abidjan 108 p.

[5] Zabi S. G.F., (1982a). Les peuplements benthiques lagunaires liés à la pollution en zone urbaine 'Abidjan (Côte d'Ivoire).Actes du symposium sur les Lagunes Côtières, SCOR/IABO/UNESCO, Bordeaux, 8-14 Septembre 1981. Oceanol. Acta, suppl. n° 4 : 441-455²c.

[6] Zabi S. G.F., (1982b). Répartition et abondance des espèces de la macrofaune benthique de la lagune Ebrié 'Côte d'Ivoire). Doc. Scient. Centre Rech. Océanogr. Abidjan, 13 (1) : 7 -96.

[7] Zabi S. G.F., (1984). Rôle de la biomasse dans la détermination de l'Importance Value » pour la mise en évidence des unités de peuplement benthique en lagune Ebrié(Côte d'Ivoire). Doc. Scient. Centre Rech. Océanogr. Abidjan, 15 (1-2) : 55 -87.

[8] Sankaré, Y., et Ettien, N. (1991). Analyse des effets de l'ouverture du chenal de Grand-Bassam (estuaire du fleuve Comoé, lagune Ebrié) sur la macrofaune benthique lagunaire. J. Ivoir. Océanol. Limnol., 1 (2) : 81-90

[9] Chantraine, J-M., and Dufour, P. (1983). Réseau national d'observation de la qualité des eaux marines et lagunaires en Côte d'Ivoire. Etude de faisabilité octobre-septembre 1981. Office de la Recherche Scientifique et Technique d'Outre Mer., 400pp.

[10] Durand, J.R., Dufour, P., Guiral, D., Zabi S. G.F., (1994). Environnement et Ressources Aquatiques de Côte d'Ivoire. Tome II- Les Milieux Lagunaires. ORSTOM, Paris, 546 pp.

[11] Marchand, M., Martin, J. L., (1985). Détermination de la pollution chimique (Hydrocarbures, Organochlorés, Métaux) dans la lagune d'Abidjan (Côte d'Ivoire) par l'Etude des Sédiments. Océanogr. Trop. 20 (1), 23-39.

[12] Pages, J., (1975). Etude de la pollution bactérienne en lagune Ebrié. Document Scientifique Centre de Recherche Océanographique Abidjan, 6 : 97-110.

[13] Pages, J., and Citeau, J. (1978). La pollution bactérienne de la lagune et de la mer autour d'Abidjan. Document Scientifique Centre de Recherche Océanographique Abidjan, 9 : 43-50.

[14] Kouassi A. M., Guiral, D., Dosso, M., (1990). Variations saisonnières de la contamination microbienne de la zone urbaine d'une lagune tropicale estuarienne. Cas de la ville d'Abidjan (Côte d'Ivoire). Rev. Hydrol. Trop. 23, 181-194.

[15] Adingra A.A., Arfi, R., (1998).Organic and bacterial pollution in the Ebrié lagoon, Côte d'Ivoire. Mar. Pollut. Bull. 36 (9), 689-695.

[16] Métongo, B.S., Sankaré, Y., (1990). Teneur en métaux lourds des organes chez le crabe comestible (Callinectes amnicola, Decapode, Portunidea) en lagune Ebrié (Côte d'Ivoire). Agron. Afr. 2 (2), 116-125.

[17] Métongo B S, 1991, Concentrations en métaux toxiques chez Crassostrea gasar (huître de Mangrove) en zone urbaine lagunaire d'Abidjan(Côte d'Ivoire). J. Ivoir. Océanol. Limnol.. Abidjan 1(1), 33-45.

[18] Métongo, B.S., Kouamenan K. F., (1991). Concentrations en mercure dans les muscles de thons albacores (Thunnes albacares) du Golfe de Guinée (1987-1988). J. Ivoir. Océanol. Limnol.. Abidjan 1(1), 1-8.

[19] I. Brenon, S. Mondé, N. Pouvreau, J.C. Maurin (2004). Modeling hydrodynamics in the Ebrié lagoon (Côte d'Ivoire). Journal of African Earth Sciences 39 : 535-540.

[20] P. A. G. M. Scheren, C Kroeze, F. J. J. G. Janssen, L. Hordijk, K. J. Ptasinski (2004). Integrated water pollution assessment of the Ebrié Lagoon, Ivory Coast, West Africa. Journal of Marine Systems 44 : 1-7.

[21] A.A. Otitoloju and K.N. Don-pedro, (2004). Integrated laboratory and field assessments of heavy metals accumulated in edible periwinkle, *Tympanotonus fuscatus var radula* (L.)

[22] Davies, O. A., Allison M. E. and Uyi, H. S., (2006). Bioaccumulation of heavy metals in water, sediment and periwinkle (Tympanotonus fuscatus var radula) from the Elechi Creek, Niger Delta. African Journal of Biotechnology Vol. 5(10),pp. 968-973.

[23] Philips D.J.H., (1980). Quantitative aquatic biological indicators. London: Applied Science Publishers.

[24] Rainbow, P.S., (1995). Biomonitoring of heavy metal availability in the marine environment. Mar. Pollut. Bull. 31 (4-12), 183-192.

[25] Seong-Gil Kang, Man-Sok Choi, In-Sook Oh, David A. Wright, Chul-Hwan Koh, (1999); Assesssment of metal pollution in Onsan Bay, Korea using Asian periwinkle *Littorina brevicula* as biomonitor. The Science of the Total Environment 234 : 127-137;

[26] Centre d'expertise en analyse environnementale du Québec (2003). Détermination des métaux dans les tissus animaux : méthode par spectrométrie au plasma d'argon après minéralisation acide, MA. 207 – Mét 1.0, Ministère de l'Environnement du Québec, 19 p.

[27] Mouvet, C., (1984). Métaux lourds et mousses aquatiques, Spéciations physico-chimiques, bioaccumulation et toxicité, Université de Liège, Belgique, 157 pp.

[28] Rainbow, P.S.,(1990). Heavy metal levels in marine invertebrates. In: Furness, R.W., Rainbow, P.S.(Eds), Heavy Metals in the Marine Environment. CRC Press, Florida, pp. 67-80.

[29] V TALBOT et A. CHEGWIDDEN (1982): Cadmium and other Heavy Metal Concentration in selected Biota from Cockburn Sound, Western Australia. Aust. J. MAR. Freshw., 1982 (33) 779-88.

European Journal of Scientific Research
ISSN 1450-216X Vol.18 No.4 (2007), pp.639-644

http://www.eurojournals.com/ejsr.htm

Late Presentation of Appendicitis in a Nigeria Teaching Hospital

Mbanaso.A.U
Department of Surgery, Abia State University Teaching Hospital, Aba
Abia State, Nigeria

Adisa.A.C
Department of Surgery, Abia State University Teaching Hospital, Aba
Abia State, Nigeria

Akunekwe.M.I
Department of Surgery, Abia State University Teaching Hospital, Aba
Abia State, Nigeria

Abstract

Acute appendicitis is a very common cause of acute abdomen in our society. The aim of this study was to identify the pattern of presentation of patients with acute appendicitis in our centre (Abia State University Teaching Hospital) and to determine the proportion of patients that presented with the complications of appendicitis (e.g. appendix mass, appendix abscess and perforated acute appendicitis with a view a view to proffering preventive solutions where appropriate and improving outcome.

We studied the pattern of presentation of cases of acute appendicitis from 1995 to 2004(10 Year period), We corroborated this with a survey among the students and staff of Abia - State University Teaching Hospital, to ascertain how many of them had had appendicectomy and how many presented with the complications of appendicitis.

All patients admitted as surgical emergencies with a clinical diagnosis of Acute Appendicitis, Appendix mass/abscess, gangrenous appendix and perforated acute appendicitis were included in the study. The patient characteristics, clinical diagnosis and findings at operation were recorded on a dedicated proforma.

Out of the 144 cases of appendicitis that presented between 1995 and 2004(10 year period), 64(44.4%) presented with one of the following complications e.g. appendix mass, appendix abscess, gangrenous appendix and perforated acute appendicitis. There were 76 females and 68 males with a Male: Female ratio of 1:1.1, the peak age was 11-20 years. The negative appendectomy rate was 2%.

Over 60% of our patients presented late (more than three days) after the onset of the symptoms.

There was zero mortality but the morbidity was high (40%) had septic complications like wound infections, abdominal abscesses, entero -cutaneous fistulae.

In the survey conducted , of the 540 respondents among the staff and students of Abia State university Teaching Hospital, 110 had had appendicectomy in the past out of which 36(32.7%) presented with its complications. Late presentation to the hospital results in increased morbidity and mortality.

This is the bane of medical practice in our community where **P**overty, **I**gnorance and preventable **D**iseases (the so called social '**PIDs**') abounds.

There is an urgent need to improve on health education for our populace and also the need by the government in developing countries to strive to attain the millennium developmental goal so as to reduce poverty and illiteracy.

Keywords: Appendicitis, PID, Appendix mass

Introduction

The term 'acute appendicitis' was coined by Reginald Fitz (Williams , 1983.) who was the Shattuck Professor of Pathological Anatomy at Harvard University. He read his classic paper to the Association of American Physicians in June 1886: the title was 'Perforating inflammation of the vermiform appendix: with special reference to early diagnosis and treatment'. He analyzed the clinical history and post mortem findings in 257 patients and advised on the need for early diagnosis and treatment to reduce the mortality seen in perforated acute appendicitis (Fitz, 1886).

One hundred and fifteen years after this wonderful advice, it seems as if it is falling on deaf ears in our community as a significant proportion of our patients still present late and often present with the complications of an acute appendicitis.

Appendicitis is said to be more common in urban, industrialized societies and relatively rare in developing countries where a less-refined, high-fiber diet is typically consumed. The decreasing rate of acute appendicitis in the western countries is attributed to a changing trend in the adoption of high fibre diet (Basta et al, 1990; Burkitt, 1971; Walker, 1980)

In sub-Sahara Africa particularly in Aba, Abia State, Nigeria, it is presently a very common cause of acute abdomen (Yeboah, 2005; Mugande et al, 2004; Serengbe et al, 2002). In our environment the food items are varied. Most families consume large quantities of carbohydrate diet with high sugar content, as well as high fibre content (roughage).

Although, the exact cause is unknown. Appendicitis is generally considered to be Sporadic, non - communicable disease process. Its etiological factors have long been debated. There is little or no seasonal variation. Dietary, genetic, and infectious or immunologic explanations for the etiology of appendicitis have been advanced, but it has not proven possible to implicate reliably any cause in a given patient (Koepsell ,1991; Brender, 1985; Barker, 1985).

Appendicitis is primarily a disease of adolescents and young adults with a peak incidence in the second and third decades of life(Ricci, 1991; Primatesta, 1994). It is very uncommon in children younger than 5 years and by age 70, the risk of appendicitis is less than 1 in 100 (Peltokallio, 1981).

Patients and Methods

First, the records of all patients with appendicitis and appendix related cases, were reviewed form 1995 - 2004(10 years).The age, sex, duration of symptoms before presentation, operative findings and pathological analyses were extracted from the patients' folders and theatre records.. Note was made of those who presented with appendix mass and were managed conservatively, until interval appendicectomy was done later. Those who were found with some other conditions of the caecum like carcinoma of the caecum were excluded from the study.

Secondly in this study, a questionnaire was distributed among the students and staff of the Abia State University Teaching Hospital Teaching. This included medical students, student nurses, the nursing staff and other workers in the hospital. The questionnaire was designed to capture the following - age of the subject, age at which appendicectomy was carried out, whether complicated or not, family history of appendicitis and why those with complication reported late to the hospital.

Results

The total number of appendix related problems managed at the ABSUTH between 1995 and 2004(10 yr period) was 144 (Table 1). Of this, 64(44%) patients were admitted (Table 1) with complications like appendix mass, appendix abscess, perforated acute appendicitis or gangrenous appendix.

The age range of these patients was between 10 and 50yrs (Table 2). The largest number was in the second and third decades. (Table 3) Negative appendicectomy rate was 2% and majority of them were adolescent females More females were affected than males (76 females and 68 males) M: F ratio 1:1.1 In the survey carried out among students and staff of ABSUTH, 800 questionnaires were distributed. Those who responded were 540, while 501 completed the questionnaire correctly, (Table4.)

The largest number of respondents was between 21 and 30 years (321) as shown in Table 5. Table 6 shows that the greatest number of our respondents (66) had appendicectomies between 11 and 20 years; majority being in their teens.

Out of the 110 respondents who had appendicectomy at one time or the other as much as 36(32.7%) presented to their Physicians with one form of complication or the other.

The largest being those with appendix abscess 16(44%) followed by perforated acute appendicitis 11 (30.6%)

Discussion

Appendicitis is one of the commonest surgical diseases and a leading cause of acute abdomen in many societies.

Most presentations conform to the classical textbook description of initial central abdominal (peri-umbilical) pain, which later localizes to the right iliac fossa, with tenderness at the Mc Burney's point, anorexia, nausea, vomiting and leucocytosis.

Our findings in Aba, (south east of Nigeria, populated predominantly by the Igbos) showed that despite the fact, that acute appendicitis is a common non-traumatic cause of abdominal pain, as known in most societies, that our own patients report late.

Over 60% of our patients presented more than three days after the onset of symptoms, some even presented a week or more. This accounted for the high rate of appendix mass and appendix abscess and perforation seen in this study (17%, 20% and 7% respectively).

The reasons are not far fetched. Obviously the level of poverty of the people is worse now than previously. This started with the Structural Adjustment Programme, to the abysmal devaluation of our currency. Nigeria is ranked as one of the poorest countries in the world. Many of these patients could not afford the cost of hospital treatment; in fact many of them had gone to Private Hospitals for treatment but were refused surgery as a result of inability to afford the cost of hospital treatment.

The other reason for possible late presentation of patients could also be attributed to quackery and self medication. Patients obtain drugs freely over the counter without prescription from a Physician. Their first point of contact when ill and worse still when they have abdominal pain is to the patent medicine dealer or quacks. They come to the hospitals only when the ill health becomes complicated.

In our community, the people commonly attribute abdominal pain to PID (Pelvic Inflammatory Disease) and menstrual pain especially in females until proved otherwise, in which case treatment will be started in a non orthodox manner, before ever, the Physician is approached.

Also it has been found that the general opinion (though wrong) is that most cases of acute abdominal pain are because of Peptic Ulcer Disease. These patients buy antacids first and self medicate before coming to the Doctor.

The high rate of negative appendectomy in our study(2%) especially in adolescent females underscore the need for more thorough investigations and clinical scoring system like the Alvarado score to exclude other pelvic or gynaecological lesions especially where the clinical signs are equivocal(Alvarado,1991).

Radiological investigations like Ultrasonography and CT scan have been shown to improve the diagnostic accuracy of appendicitis, but the cost effectiveness and the fact that they are not readily available in our community limits the use of these diagnostic tools(Horton et al, 2000; Balthazar et al, 1991; Malone et al, 1993).

We observed that in 80% of those with perforation, operative and pathological findings showed the presence of faecoliths either in the appendix itself or in the peritoneal cavity after being dislodged from the appendix lumen. This probably lends credence to the fact that obstruction of the appendix lumen is a strong factor in the evolution of perforations (Sinanan, 1993; Bennion et al, 1995).

The hallmarks of appendicitis with perforation are increasing intensity of abdominal pain, local or diffuse peritonitis, temperature elevation greater than 38°C, and tachycardia. Nonperforated appendicitis is not commonly associated with temperature elevation over 38°C.

Even though in our series, there was no recorded mortality, the morbidity was high especially in those with complicated appendicitis and these included entero-cutaneous fistula (in 3% of cases), intra-abdominal abscesses (5% cases), wound sepsis (32%), prolonged hospital stay and high medical bills.

The zero mortality was probably because of improved diagnosis and management in a teaching hospital setting, There is an urgent need for public health education of the populace once more, despite the poor socio-economic condition of the people.

We do not also want to lose sight of the fact, that ours is a reference hospital, and therefore, the more difficult or seemingly complicated cases are referred to us.

Acute appendicitis continues to be an important surgical entity in most communities.

Appropriate care demands careful and early diagnosis, prompt fluid management, antibiotic therapy and prompt surgical intervention.

The commonly used term “Simple appendicitis” is an out worn phrase.

Such terms make us neglect this important acute abdominal condition and the patient reports late, and we allow the “sun to set” on such cases of acute abdomen and invariably the patients report with complications like perforation, appendix mass, appendix abscess or gangrene, as found in our series.

There is an urgent need to improve on health education for our populace and also the need by the government in developing countries to strive to attain the millennium developmental goal so as to reduce poverty and illiteracy.

Results

Table 1: Frequency of appendicitis in Aba over a 10 year period 1995 – 2004.

Year	Number of Appendicectomies	Number complicated	Percentage of complication
1995	17	10	58.9
1996	19	6	31.5
1997	13	9	69.2
1998	14	7	50
1999	16	5	31.2
2000	14	7	50
2001	13	4	37.7
2002	11	4	36.3
2003	15	6	40
2004	12	6	50
Total	**144**	**64**	**44.4**

Table 2: Age at Presentation

Age range	Number
1 – 10 years	8
11 – 20 years	54
21 – 30 years	51
31 – 40 years	17
41 – 50 years	10
Above 50 years	4
Total	**144**

Table 3: Complications at Presentation

Type of Complication	Percentage	
Appendix mass	12	19%
Perforation	20	31%
Abscess	28	44%
Gangrenous Appendix	4	6%
Total	**64**	**44.4%**

Table 4: Response to survey

Questionnaire distributed	800
Number of Respondents	540
Number of those who completed the form correctly	501

Table 5: Age Range of Respondents

Age	Number	%
0-10	0	0
11-20	53	10.7
21-30	321	63.9
31-40	70	14.
> 40	57	11.4
Total	501	100

Table 6: Age at which Appendectomy was carried out in those who responded to the survey

Age	Number	%
0-10	10	9.1
11-20	66	60.0
21-30	28	25.5
31-40	5	4.5
>40	1	0.9
Total	110	100

References

[1] Williams GR. Presidential Address (1983): A History of Appendicitis. Ann Surg 197:495-506.

[2] Fitz RH (1886). Perforating inflammation of the vermiform appendix: with special reference to its early diagnosis and treatment. Am J Med Sci 92:321-46.

[3] Basta M, Morton NE, Mulvihill JJ, Radovanovic Z, Radojicic C, Marinkovic D(1990). Inheritance of acute appendicitis: Familial aggregation and evidence of polygenic transmission. Am J Hum Genet 46:377-82.

[4] Burkitt DP. The aetiology of appendicitis. Br J Surg 1971;58:695-9.

[5] Walker ARP, Walker BF. Appendectomy in South African interethnic school pupils. Am J Gastroenterol 1987;82:219-22.

[6] Ohene-Yeboah M (2005). Causes of acute peritonitis in 1188 consecutive adult patients in Ghana. Trop Doct 35:84-5.

[7] Mungadi IA, Jabo BA, Agwu NP (2004).A review of appendicectomy in Sokoto, North-western Nigeria. Niger J Med. 13:240-3.

[8] 8.Serengbe BG, Gaudeuille A, Soumouk A, Gody JC, Yassibanda S, Mandaba JL(2002). Acute abdominal pain in children at the Pediatric Hospital in Bangui (Central African Republic). Epidemiological, clinical, paraclinical, therapeutic and evolutive aspects. Arch Pediatr. 9:136-41

[9] Koepsell TD (1991). In search of the causes of appendicitis. Epidemiology 2:319-21.

[10] Brender JD, Marcuse EK, Weiss NS, Koepsell TD(1985). Is childhood appendicitis familial? Am J Dis Child. 139:338-40.

[11] Barker DJP(1985). Acute appendicitis and dietary fibre: an alternative hypothesis. BMJ. 290:1125-7.

[12] Ricci MA, Trevisani MF, Beck WC (1991). Acute appendicitis: a 5-year review. Am Surg 57:301-5.

[13] Primatesta P, Goldacre MJ (1994). Appendicectomy for acute appendicitis and for other conditions: an epidemiological study. Int J Epidemiol 23:155-60.

[14] Peltokallio P, Tykka H (1981). Evolution of the age distribution and mortality of acute appendicitis. Arch Surg 116:153-6.

[15] Alvarado A (1991). A practical score for the early diagnosis of acute appendicitis. Ann Emerg Med. 20:1048-9

[16] Horton MD, Counter SF, Florence MG, Hart MJ (2000). A prospective trial of computed tomography and ultrasonography for diagnosing appendicitis in the atypical patient. Am J Surg . 179:379–381.

[17] Balthazar EJ, Megibow AJ, Siegel SE, Birnbaum BA(1991). Appendicitis: prospective evaluation with high-resolution CT. Radiology 180:21–24.

[18] Malone AJ Jr,Wolf CR, Malmed AS, Melliere BF(1993). Diagnosis of acute appendicitis: value of unenhanced CT. Am J Roentgenol 160:763–766.

[19] Sinanan M(1993). Acute Abdomen and Appendix. In: Greenfield LJ, Mulholland MW, Oldham KT, Zelenock GB, editors. Surgery: Scientific Principles and Practice. Philadelphia: JB Lippincott. pp 1120-42.

[20] Bennion RS, Thompson JE Jr (1995). Appendicitis. In: Donald E. Fry, editor. Surgical Infections. Boston: Little, Brown. pp 241-50.

European Journal of Scientific Research
ISSN 1450-216X Vol.18 No.4 (2007), pp.645-654

http://www.eurojournals.com/ejsr.htm

Réponses Minérales Chez la Fève (*Vicia faba* L.) au Stress Salin

Rabah Chadli
Département de Biologie Faculté des Sciences Université de Mostaganem Algérie
E-mail: chadlirabah@yahoo.fr

Moulay Belkhodja
Laboratoire de Physiologie Végétale Faculté des Sciences Université d'Oran Algérie
E-mail: belkhod@yahoo.fr

Abstract

Faba bean is one of the crop species cultivated in Algeria because their ecological, alimentary and natural fertilizer interests. The changes observed in the agricultural soils conclude to a salinization of the root zone caused by the important ionic accumulation resulting from the irrigation waters. In this case, the plants release various mechanisms for example the osmotic adjustment under the ionic control for their adaptation to this new ecological state.In the order to understand the salt tolerance mechanism of the plants, this study proposes an analysis of the Na^+, K^+ and Ca^{++} cations in the organs of the young faba bean (*Vicia faba* L.) plants in response to 300 and 400 meq of $NaCl+CaCl_2.l^{-1}$ of nutritious Hoagland solution and seawater stress. Results indicate that Na^+ accumulates significantly in the leaves and the stems while the roots impoverish dramatically when the salinity concentration of the middle increases. So,the leaves grew riched strongly on K^+ under $NaCl+CaCl_2$ and seawater stress; the K^+ amount rises in the roots only for the plants receiving 300 meq of $NaCl+CaCl_2$, then it reduces under high salinity and seawater treatments. In return, Ca^{++} accumulates from the roots to the leaves with the increasing of the salt concentration; the Ca^{++}amounts remain significant in the stems and the leaves with regard to the roots only for the plants stressed with high salinity (400 meq of $NaCl+ CaCl_2$ and seawater) and comparatively to the all organs of control plants. On the other hand, the ratio K^+/Na^+ used as a parameter to appreciate the plant tolerance to the salinity, fluctuates according to the salt treatment and the organ of the plant; the ratio enhances when the salinity of the medium increases while for the stems, it becomes higher until 400 meq of $NaCl+CaCl_2$.

Keywords: Salt stress, $NaCl+CaCl_2$, seawater, cations, adaptation, faba bean.

Introduction

Selon la FAO (2005), 20% des terres irriguées sont affectées par le phénomène de la salinisation dans le monde; l'Algérie fait partie depuis longtemps de ces régions avec 3 millions d'hectares (Szabolcs,1994).Ces changements de l'écosystème, signalés dans les zones du bassin méditerranéen (Levigneron et *al.,* 1995), constituent incontestablement un facteur limitant pour la biodiversité végétale notamment pour les plantes cultivées.Dans ces sols, les plus importantes perturbations sont enregistrées au niveau de la rhizosphère (Binzel et Reuveni,1994) à cause de fortes accumulations de sels dans les eaux d'irrigation (Berthomieu et *al*.,2003).Ces perturbations proviendraient de l'excès de

cations comme le Na^+ (Abdelkader et Saleh,2002;Wahid,2004) créant un déséquilibre ionique affectant la balance nutritionnelle au niveau du sol (Sairam et Tyagi,2004) et de la plante (Belkhodja et al.,2000). Dans ces sols, la salinité devient une menace permanente pour de nombreuses espèces végétales (Gupta et Sharma,1990), affectant la croissance de la plante (Liu et Zhu,1998) notamment pour la plupart des glycophytes (Hamdy *et al*.,2002;Belkhodja et Bidai, 2004) et la production agricole (Pitman et Lauchli, 2002). La salinité joue un rôle important dans l'existence et la distribution des plantes; à la différence des halophytes poussant mieux sur un sol riche en sels (Abdelkader et Saleh, 2002), les glycophytes sont exposées à des modifications de leur comportement physiologique,biochimique,hormonal,moléculaire et minéral selon le degré de salinité dans le milieu (Shabala et *al.,* 2005; Martinez et *al.,2007*).Dans ces conditions, la plante, exposée à la contrainte saline, déclenche des mécanismes de tolérance ou une réaction d'adaptation (Kumar et *al.,* 1994; Flowers, 2003) lui permettant de faire face à cette nouvelle situation du milieu et poursuivre sa croissance (Belkhodja, 2004).Cette réaction d'adaptation se traduit par la mise en place d'un ajustement osmotique interne (Niu et *al.,* 1995; Rehman et *al.,* 2002; Munns, 2005) grâce à la présence d'ions (Parida et Das,2005), contribuant à une réduction des pertes d'eau et au maintien de la turgescence cellulaire (Garg et *al.,2002;* Moinuddin et *al., 2005*). Divers critères sont possibles pour évaluer la réponse des plantes à la salinité dont leur statut ionique. Alem et Amri (2005) notent que le contrôle de l'exportation et de la répartition des ions dans la plante est un critère déterminant de la tolérance au stress salin.Parmi les ions, les Na^+ et K^+ jouent un rôle clef dans le processus d'osmorégulation de la cellule et accompagnent les anions organiques dans leur accumulation et leur migration (Moinuddin et *al.,* 2005). Aux Na^+ et K^+, s'implique le Ca^{++}, en assurant une fonction clef dans le signal de la réponse au stress conduisant à l'adaptation de la plante (Fernandez-Balester et *al.,* 1997; Yokoi et *al.,2002*). Cette adaptation peut être plus liée au caractère de sélectivité ionique du ratio K^+/Na^+ utilisé comme un index de la tolérance à la salinité pour de nombreuses espèces (Shannon et Noble, 1995*;* Asch et *al.,* 2000*;* Quian et *al.,* 2001).

Ce travail s'oriente vers une analyse de l'influence de la salinité sur la réponse minérale de jeunes plantes d'une légumineuse, la fève (*Vicia faba* L.), espèce à divers intérêts aux plans écologiques, alimentaires (Polignano et *al.,* 1991) et comme fertilisant grâce à la fixation symbiotique de l'azote (Dordjevic et *al.,* 1989).

Pour évaluer la variabilité minérale de la fève (*Vicia faba* L.) au stress salin, nous proposons d'abord une analyse des variations ioniques à travers le processus d'accumulation des cations Na^+, K^+ et Ca^{++} dans les organes de jeunes plantes stressées au $NaCl+CaCl_2$ et à l'eau de mer. Ensuite, seront examinés les ratios K^+/Na^+ de chaque organe et les ratios de la teneur ionique foliaire sur la teneur ionique racinaire pour l'évaluation du caractère inclusif et /ou exclusif de la fève.

Matériel et Méthodes

Matériel végétal

Les expérimentations sont menées sur des graines de la fève *Vicia faba* L. fournies par l'IDGC (Institut de Développement des Grandes Cultures) de Sidi bel Abbés (Algérie).Les graines ont séjourné dans un réfrigérateur à 7°C pendant longtemps pour la levée de dormance.

Méthodes

Avant le semis, les graines sont désinfectées dans une solution d'hypochlorite de sodium à 8% durant trois minutes et rincées plusieurs fois à l'eau distillée pour éliminer toutes traces de chlore. Après germination en boîte de Pétri, les plantules sont transférées dans des pots en plastique (15 cm de diamètre,20 cm de hauteur) remplis de 2 kg d'un mélange de sable et de tourbe (2V/V) et déposés en salle de culture à la température ambiante sous une photopériode de 12 h. Les plantules sont arrosées tous les deux jours à la solution nutritive de Hoagland (1938).Au stade 5 feuilles,les plantes témoins

reçoivent la solution nutritive, un lot de plantes est stressé à 300 et 400 meq de NaCl+$CaCl_2$ (V/V) par litre de solution nutritive, un autre lot est arrosé à l'eau de mer. Après 6 semaines,les plantes sont récoltées,les feuilles,tiges et racines sont séparées,pesées,enveloppées dans du papier aluminium puis étuvées durant 48 heures à 80°C. Les échantillons sont broyés puis 1g de poudre de chaque échantillon est incinéré à 450 °C dans un four à moufle durant 4 heures.La cendre est dissoute dans 5 ml d'HCl (2N), chauffée durant 10 mn, filtrée à l'aide d'un filtre sans cendres et le volume est amené à 100 ml.De la solution obtenue, les Na^+ et K^+ sont dosés par photométrie de flamme (Flame Photometer Cornning 400) respectivement à 590 µm et 760 µm. Le Ca^{++} est analysé par spectrophotométrie d'absorption atomique à la longueur d'onde de 422,7 nm.

Les teneurs en Na^+, K^+ et Ca^{++} (µg.mg^{-1}de PS) sont analysées à l'aide du test de Fisher à P = 5%.

Résultats

1. Variations des cations dans les plantes sous stress salin

Teneurs en Na^+ dans les différents organes

La figure 1 montre que le Na^+ migre remarquablement vers le système aérien sous la contrainte salin. Ce cation s'accumule davantage lorsque la concentration du milieu augmente soit sous stress au NaCl+$CaCl_2$ ou à l'eau de mer.En effet, sa teneur passe significativement de 0.52 µg. mg^{-1} de PS dans les feuilles des plantes témoins à 4.33 et 5.52 µg.mg^{-1} respectivement dans celles des plantes stressées à 300 et 400 meq NaCl+ $CaCl_2$; sous le traitement à l'eau de mer, la teneur en Na^+ foliaire représente environ douze fois plus celle des feuilles témoins (6,06 contre 0,52 µg.mg^{-1} de PS). Le Na^+ reste toutefois plus important dans les tiges que dans les feuilles sans différences significatives des teneurs entre les deux organes,teneurs en Na+ examinées à l'aide de l'analyse de la variance grâce au test de Fisher à P= 5% (tableau 1).

En revanche, les racines sont plus appauvries en ce cation même si l'on observe une sensible accumulation sous le traitement salin au NaCl+$CaCl_2$ significative (2,87 et 2,58 µg.mg^{-1} de PS sous 300 et 400 meq de NaCl+$CaCl_2$ par rapport aux racines des plantes témoins (0,67 µg.mg^{-1} de PS).

Figure 1: Teneurs en Na^+ (µg.mg^{-1} de PS) dans les différents organes des plantes de la fève *Vicia faba* L. âgées de 6 semaines sous stress salin au NaCl+$CaCl_2$ et à l'eau de mer.

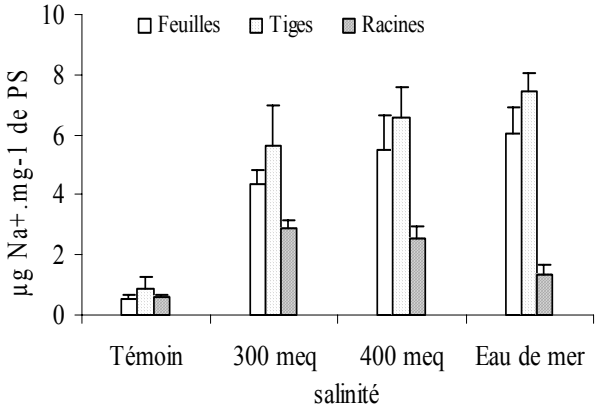

Table 1: Test statistique de signification de Fisher (P=5%) des teneurs en Na^+ (µg.mg^{-1}de PS) des organes de jeunes plantes de la fève *Vicia faba* L.stressées au NaCl+$CaCl_2$ et àl'eau de mer.

	Témoin	300 meq	400 meq	Eau de mer	m ± ó
Feuilles	0.52±0.16	4.33±0.50*	5.52±1.14*	6.06±0.87*	4.10±2.49
Tiges	0.87±0.39*	5.62±1.23* NS	6.59±1.02* NS	7.45±0.61*NS	5.13±2.93
Racines	0.62±0.03 NS	2.87±0.30***	2.58±0.35***	1.31±0.39**NS****	1.85±1.04
m ± ó	0.67±0.18	4.27±1.37	4.89±2.07	4.94±3.21	

* Effet salinité significatif sur les teneurs en Na^+ par rapport aux plantes témoins à au seuil 5%,
** Effet organe sur les teneurs en Na^+ par rapport aux feuilles sous chaque traitement, NS effet non significatif, m ± σ = moyenne statistique associée à l'écart type

Teneurs en K^+ dans les différents organes

Le K^+ s'accumule plus dans les feuilles lorsque la salinité du milieu augmente; la teneur varie pratiquement du simple à cinq à sept fois plus celle du K^+ analysé dans les feuilles des plantes stressées au NaCl+$CaCl_2$ ou à l'eau de mer (fig.2). La charge en ce cation dans les feuilles reste significativement élevée par rapport aux feuilles des plantes témoins. Ce cation fluctue peu dans les tiges si bien que les teneurs chez les plantes témoins et celles exposées à 300 meq de NaCl+$CaCl_2$ et à l'eau de mer sont très voisines (0,79 pour respectivement 0,74 et 0,82µg.mg^{-1} de PS).Par contre, dans les racines, le K^+ s'accumule jusqu'à un maximum de 1,12 µg.mg^{-1} de PS sous le traitement à 300 meq de NaCl+$CaCl_2$ par rapport au témoin; dès que la concentration du milieu augmente, le taux d'accumulation de ce cation atteint 76,78% dans les racines des plantes soumises à 400 meq de NaCl+$CaCl_2$ alors qu'il n'est que de 50% dans les racines nourries à l'eau de mer comparativement à l'effet du traitement au NaCl+$CaCl_2$ à 300 meq (0,86 et 0,56 µg.mg^{-1} contre 1,12 µg.mg^{-1} de PS).

Figure 2: Teneurs en K^+ (µg.mg^{-1} de PS) dans les différents organes des plantes de la fève *Vicia faba* L. âgées de 6 semaines sous stress salin au NaCl+$CaCl_2$ et àl'eau de mer.

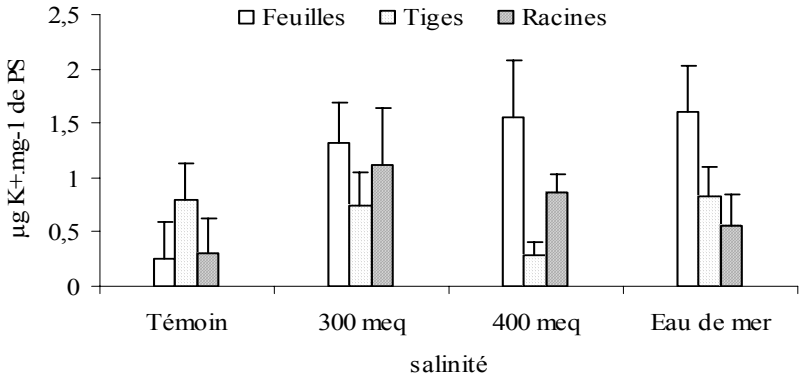

L'analyse statistique (tableau 2) montre que la salinité agit significativement sur l'accumulation du K^+ singulièrement dans les feuilles comparativement aux feuilles des plantes témoins; cette différence dans la richesse en K^+ s'exprime de nouveau en faveur des feuilles par rapport aux tiges et aux racines seulement en présence de 400 meq de NaCl+$CaCl_2$ et à l'eau de mer.

Table 2: Test statistique de signification de Fisher (P = 5%) des teneurs en K^+ (µg.mg^{-1} de PS) des organes de jeunes plantes de la fève *Vicia faba* L. stressées au NaCl +$CaCl_2$ et àl'eau de mer.

	Témoin	300meq	400meq	Eau de mer	m ± ó
Feuilles	0.25 ±0.34	1.31±0.38*	1.56±0.52*	1.61±0.41*	1.18±0.63
Tiges	0.79±0.35*	0.74±0.31 **NS****	0.28±0.12****	0.82±0.28 **NS****	0.65±0.25
Racines	0.30±0.32 NS	1.12±0.52* NS	0.86±0.17***	0.56±0.29 **NS****	0.71±0.35
m± ó	0.44±0.29	1.05±0.29	0.90±0.64	0.99±0.54	

Teneurs en Ca^{++} dans les différents organes

Le Ca^{++} s'accumule rapidement dans les parties aériennes pour y doubler sous l'effet de la salinité à 300 meq de NaCl+$CaCl_2$ (2,38 et 2,50 µg.mg^{-1} PS respectivement dans les feuilles et les tiges contre 1,29 et 1,23 µg.mg^{-1} PS pour le témoin) ; alors que la teneur en ce cation quadruple dans les mêmes organes quand la salinité passe à 400 meq de NaCl+$CaCl_2$ et à l'eau de mer (fig.3). En outre, il convient de remarquer que lorsque les plantes sont arrosées à la solution saline à 300 meq, la charge en Ca^{++} reste sensiblement élevée dans les tiges que dans les feuilles dans µg.mg^{-1} PS. Le phénomène inverse est observé sous l'influence du traitement à 400 meq et à l'eau de mer. Au niveau racinaire,l'accumulation du Ca^{++} est fortement ralentie dans le milieu enrichi à 400 meq de NaCl+$CaCl_2$ et à l'eau de mer; le taux d'accumulation varie autour de 50% sous les deux traitements comparé au témoin et au traitement à 300 meq de NaCl+$CaCl_2$.

Figure 3: Teneurs en Ca^{++} (µg.mg^{-1} de PS) dans les différents organes des plantes de la fève *Vicia faba* L. âgées de 6 semaines sous stress salin au NaCl+$CaCl_2$ et à l'eau de mer.

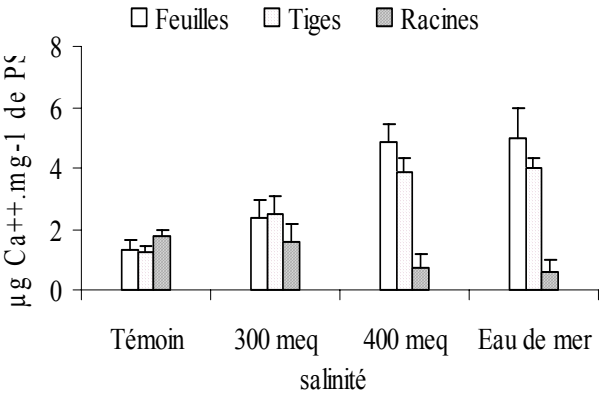

L'analyse statistique (tableau 3) met en évidence une réponse significative de l'effet de la salinité sur l'accumulation du Ca^{++} notamment pour les feuilles et les tiges des plantes recevant la salinité à 400 meq et à l'eau de mer; alors que la salinité à 300 meq de NaCl+$CaCl_2$ ne modifie pas le comportement calcique des plantes dans les différents organes lorsque l'on observe les teneurs en Ca^{++} enregistrées comparées à celles des plantes témoins. Les teneurs en ce cation n'accusent pas de différences significatives entre les feuilles et les tiges quel que soit le traitement.

Table 3: Test statistique de signification de Fisher (P=5%) des teneurs en Ca^{++} (µg.mg^{-1} PS) des organes de jeunes plantes de la fève *Vicia faba* L.stressées au NaCl +$CaCl_2$ et à l'eau de mer.

	Témoin	**300 meq**	**400 meq**	**Eau de mer**	**m ± ó**
Feuilles	1.29±.035	2.38±0.54 **NS**	4.83±0.59 *	4.97±1.03*	3.36±1.82
Tiges	1.23±0.17 NS	2.50±0.33 **NS** NS	3.85±0.63* NS	4.00±0.91* NS	2.89±1.29
Racines	1.78±0.21*	1.57±0.58 **NS****	0.71±0.45****	0.61±0.36****	1.16±0.59
m ± ó	1.43±0.30	2.15±0.50	3.13±2.15	3.19±2.28	

2. Ratio K^+ / Na^+ selon les différents organes

La figure 4 montre que les ratios K^+/Na^+ calculés pour les plantes témoins donnent des valeurs plus élevées pour les tiges (0,90); alors qu'ils s'équilibrent entre les feuilles et les racines (ratio de 0,48 pour chacun des organes). Sous les traitements salins, les tiges sont affectées par les valeurs de ratios les plus basses par rapport au témoin (0,13, 0,04 et 0,11 respectivement sous 300, 400 meq de sels et à l'eau de mer); ces ratios baissent sensiblement pour les feuilles lorsque la salinité augmente de concentration. Pour les racines, les ratios s'atténuent sensiblement sous stress au NaCl+$CaCl_2$ pour augmenter de nouveau sous alimentation des plantes à l'eau de mer (0,42).

Figure 4: Ratios K^+ / Na^+des feuilles, tiges et racines de jeunes plantes de la fève *Vicia faba* L. âgées de 6 semaines stressées au NaCl+$CaCl_2$ et à l'eau de mer.

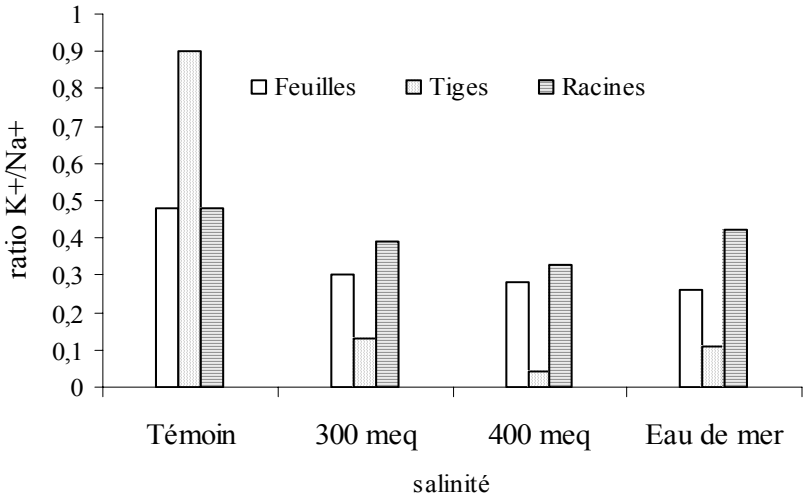

3. Ratios des teneurs cationiques des feuilles/ teneurs cationiques des racines

Les ratios des teneurs cationiques de la partie foliaire et celles de la partie racinaire expriment nettement l'influence de la salinité (fig.5). En effet, pour les plantes témoins les valeurs des ratios calculées pour les cations Na^+, K^+ et Ca^{++} sont très voisines; il faut noter dans ce cas que chacun des ratios montre une tendance vers l'équilibre cationique entre la partie aérienne et la partie racinaire

Figure 5: Ratios Na^+ feuilles/Na^+ racines; K^+feuilles/K^+racines;Ca^{++} feuilles/Ca^{++}racines de jeunes plantes de la fève *Vicia faba* L. stressées au NaCl+$CaCl_2$ et à l'eau de mer.

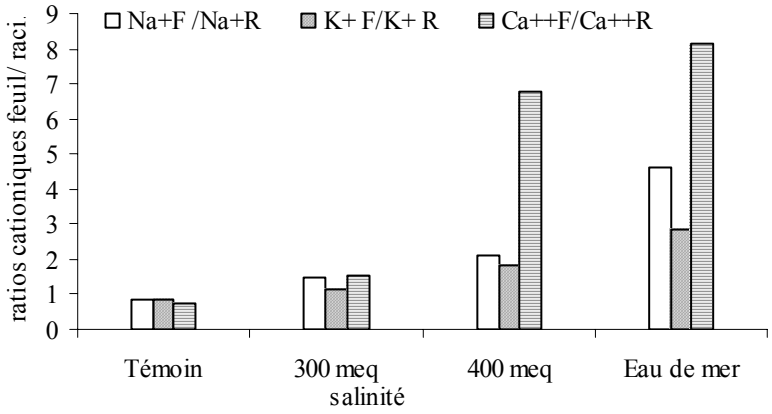

pour chacun des cations. Néanmoins, dès que les plantes sont sous stress salin, les ratios respectifs vont au-delà de l'unité révélant l'expression de la sélectivité beaucoup plus au niveau foliaire que vers le système racinaire. Il faut remarquer que des différences importantes dans l'évolution des ratios quel que soit le cation sont observées avec l'augmentation de la concentration du milieu. Les ratios les plus élevés sont signalés pour le Ca^{++} sur les plantes traitées à 400 meq de NaCl+$CaCl_2$ et à l'eau de mer, soit des valeurs de ratios respectives de 6,80 et 8,14 ce qui représente environ 9 à 11 fois la valeur du ratio calculé pour les plantes témoins (0,72). Pour les ratios Na^+, leurs valeurs, sous les traitements à 400 meq et à l'eau de mer, passent de 2,5 fois à 5,5 fois celles enregistrées pour les plantes témoins (2,13 et 4,62 contre 0,83). Par contre les ratios des teneurs en K^+ foliaire sur les teneurs en K^+ racinaire progressent lentement lorsque le milieu de culture devient de plus en plus salé; les ratios K^+

augmentent environ de 2,5 fois sous la salinité au NaCl+ $CaCl_2$ à 3,5 fois sous le traitement à l'eau de mer.

Table 4: Ratios des teneurs ioniques des feuilles/ teneurs ioniques des racines des plantes de la fève Vicia faba L. selon la salinité du milieu.

Cations $_{Feuilles}$/Cations $_{Racines}$	Témoin	300 meq	400 meq	Eau de mer
Na^+_F / Na^+_R	0.83	1.50	2.13	4.62
K^+_F / K^+_R	0.83	1.16	1.81	2.87
Ca^{++}_F / Ca^{++}_R	0.72	1.51	6.80	8.14

La comparaison entre les ratios (tableau 4) pour chaque traitement montre que pour les plantes non stressées, les valeurs des ratios n'affichent pas de différences importantes puisque les ratios Na^+ et K^+ donnent les mêmes valeurs sinon le ratio baisse pour le Ca^{++}.Sous le traitement à 300 meq de NaCl+$CaCl_2$, les valeurs des ratios entre les cations ne varient pas alors que sous 400 meq de NaCl+$CaCl_2$, le ratio Ca^{++} triple par rapport au ratio Na^+ (6,80 contre 2,13) et augmente de 1,5 fois (8,14 contre 4,62) sous le stress à l'eau de mer.

Discussion et Conclusion

Les résultats que nous venons de décrire sur l'analyse des cations monovalents et bivalents comme les Na^+, K^+ et Ca^{++} suggèrent une variabilité cationique de la réponse de la fève *Vicia faba* L. comme un bon marqueur physiologique au stress salin. En effet, l'apport de la solution saline au NaCl+$CaCl_2$ ou à l'eau de mer provoque une migration du Na^+ dans les parties aériennes avec une forte accumulation dans les tiges des plantes. Dans les racines, le Na^+ atteint son maximum à salinité modérée (300 meq de NaCl+$CaCl_2$), alors que sous stress salin sévère (400 meq et à l'eau de mer), son accumulation ralentit lentement. En revanche, le K^+ se compartimente préférentiellement dans les feuilles à des teneurs significativement élevées lorsque la salinité du milieu augmente; dans les racines, ce cation est au maximum sous stress modéré puis s'atténue à fortes concentrations en sels. Le Ca^{++} s'accumule dans le sens racines tiges feuilles des plantes avec une charge calcique très importante dans les tiges et les feuilles sous stress salin sévère alors qu'il n'est présent qu'à l'état de traces dans les racines. Divers travaux rapportent que le transport du Na^+ et son accumulation dans les feuilles peuvent causer la toxicité chez les plantes glycophytes (Niu et *al.*,1995; Davenport et Tester,2000). Nos résultats montrent que ce cation a tendance à s'accumuler beaucoup plus dans les tiges que dans les feuilles des plantes de la fève; cette forme de séquestration du Na^+ en excès dans les tiges implique une haloprotection foliaire d'une forte charge de ce cation atténuant ainsi l'effet de toxicité (Guillermo et *al.*,2001;Gama et *al.,* 2007). Outre, cette réduction de la toxicité résulte de la présence importante de K^+ signalée dans les feuilles et de l'accumulation du Na^+ dans les tiges. Cette sélectivité du K^+ sur le Na^+ suggère le caractère exclusif du Na^+ observé chez les glycophytes (Tester and Davenport,2003; Caitlin et *al.*,2007) mécanisme conférant la tolérance de la fève à la salinité. Cette tolérance peut se justifier par l'accumulation préférentielle du K^+ dans les feuilles contre les hautes teneurs en Na^+ (Zaman et *al.*,2005), par le rôle du K^+ dans l'ajustement osmotique cellulaire (Rodriguez et Rubio,2006) et dans le maintien d'un ratio K^+/Na^+ élevé nécessaire pour la photosynthèse (Allen et *al.,*1995;Munns et *al.,*2000), ratio clef de la tolérance des plantes à la salinité (Maathuis et Amtmann,1999; Chinnusamy et *al.,*2005), amélioré par la présence du Ca^{++} dans le milieu (Cramer et *al.,*1985). Les résultats indiquent que les ratios K^+/Na^+ sont élevés pour les feuilles et les racines des plantes de la fève sous la contrainte saline quelle que soit la concentration du milieu ce qui conduit à une sélectivité ionique plus importante au niveau des deux organes grâce à un contrôle racinaire probable du transport du Na^+ vers les feuilles (Yeo et *al.,*1999). Le caractère exclusif est confirmé par les ratios des teneurs cationiques foliaires/teneurs cationiques racinaires spécifiquement pour le Ca^{++}; les ratios pour ce cation bivalent augmentent en effet avec la concentration en sel du milieu et restent plus élevés comparativement aux ratios calculés pour le Na^+ et le K^+ quel que soit le traitement salin.

La responsabilité physiologique du Ca^{++} n'est donc pas à exclure; sa forte compartimentation exclusivement dans les tiges et les feuilles de la fève stressée à haute salinité (400 meq de NaCl+ $CaCl_2$ et à l'eau de mer) atténuerait l'effet toxique du Na^+ et participerait au maintien de la sélectivité du K^+ sur le Na^+ au niveau de la membrane plasmique comme le rapportent Zhong et Lauchli (1994) sur le coton. Selon Lauchli (1990), l'addition du Ca^{++} dans le milieu de culture améliore la tolérance à la salinité chez les glycophytes en soutenant le transport du K^+ (Zhu,2001;James et *al.,*2006) via la sélectivité des canaux potassiques (Reid et Smith,2000;Tester et Davenport,2003) et des canaux calciques (Sanders et *al.,*1999), le Ca^{++} agissant comme un second messager de l'ABA contrôlant la fermeture des stomates sous stress abiotiques (Hartung et Jeschke,1999;Schroeder et *al.,* 2001).L'interaction cationique (Ca^{++}) et hormonal (ABA) dans l'appréciation de la tolérance de la fève au stress salin sera l'objectif de notre prochaine recherche.

References

[1] D Z. Abdel-Kader and AAH. Saleh.,2002. Protection induced by external Ca^{++} application on proline accumulation, ion balance, photosynthetic pigments, ABA concentration and protein of mustard seedlings (*Sinapis alba* L.) under salinity stress. Egyptian J.of Biology,4,p.14-22.

[2] C.Alem et A.Amri.,2005. Importance de la stabilité des membranes cellulaires dans la tolerance à la salinité chez l'orge. Reviews in Biology and Biotechnology. Vol.4,1, p.20-31.

[3] GJ. Allen, RG.Wyn Jones and RA.Leigh.,1995.Sodium transport measured in plasma membrane vesicles isolated from wheat genotypes with differing K^+/Na^+ discrimination traits. Plant Cell. Environ 18: 105–115.

[4] F.Asch, M.Dingkuhn, K.Dörffling and K.Miezan.,2000.Leaf K/Na ratio predicts salinity induced yield loss in irrigated rice. Euphytica 113, 109–118.

[5] M.Belkhodja, R.Chadli and Z.Hadj Ziane.,2002.The ionic response of faba bean (*Vicia faba* L.) to the salt stress. Egypt. J. of Applied Sciences, N°15,(12), 422-437.

[6] M.Belkhodja and Y.Bidai.,2004. Réponse de la germination des graines d'*Atriplex halimus* L. sous stress salin. Revue Sécheresse , N°4, vol.15,331-335.

[7] M.Belkhodja.,2004.The physiological response of faba bean (*Vicia faba* L.) to the salinity:a study of the plant transpiration. Egyptian J.of Applied Sci.,vol.5, N°10,8 p.

[8] P. Berthomieu,G. Conéjéro,A.Nublat, WJ.Brackenbury,C.Lambert,C.Savio,N.Uozumi,S.Oiki, K.Yamada and F.Cellier.,2003.Functional analysis of *AtHKT1* in *Arabidopsis* shows that Na^+ recirculation by the phloem is crucial for salt tolerance. EMBO J 22: 2004–2014.

[9] M.L.Binzyl and M. Reuveni.,1994.Cellular mechanisms of salt tolerance in plant cells. Hort.Rev. 16: 33-69.

[10] S.Caitlin Byrt, J. Damien Platten, Wolfgang Spielmeyer, Richard A. James, Evans S. Lagudah, Elizabeth S. Dennis, Mark Tester and Rana Munns.,2007. HKT1;5-Like Cation Transporters Linked to Na^+ Exclusion Loci in Wheat, *Nax2* and *Kna1*. *Plant Physiology* 143:1918-1928

[11] V.Chinnusamy,A.Jagendorf and J.Zhu.,2005.Understanding and Improving Salt Tolerance in plants Symposium genetic and metabolic engineering for value added traits.Crop Sci.,45:437-48.

[12] G.R.Cramer, A.Lauchli, and V.S.Polito.,1985. Displacement of Ca^{+2} by Na^+ from plasmalemma of root cells. A primary response to salt stress? Plant Physiol., 79: 207-211,

[13] RJ.Davenport and M.Tester.,2000.A weakly voltage-dependent, nonselective cation channel mediates toxic sodium influx in wheat.Plant Physiol,122: 823–834.

[14] MA.Dordjevic, AM.Van Lammeren,A.Van Kammen and Bisselin.,1989.The relashionship between nodul gene expression and the rhizobium Nod gene in Vicia faba L. root nodule development. Molecular Plant-Microbe Interactions,2:53-63.

[15] FAO.,2005.Global Network on Integrated Soil Management for Sustainable Use of Saltaffected Soils. Rome, Italy: FAO Land and Plant Nutrition Management Service.

[16] G.Fernandez-Ballester, A.Cerda and V.Martinez.,1997. Role of calcium in short-term responses of bean plants to osmotic or saline shocks. *J. of Plant Physiology,* 151, 741–747.http://jxb.oxfordjournals.org/cgi/external_ref?access_num=000071188800014&link_type=ISI

[17] TJ.Flowers .,2003.Improving crop salt tolerance. J Exp Bot 55: 307–319.

[18] P.B.S Gama, S.Inanaga, K.Tanaka and R.Nakazawa.,2007. Physiological response of common bean (*Phaseolus vulgaris* L.) seedlings to salinity stress.African J.of Biot.Vol. 6 (2), p79-88.

[19] A. K.Garg, JK. Kim,T.G. Owens, A. P. Ranwala,Y.D. Choi,L.V. Kochian and R. J.Wu.,2002. Trehalose accumulationin rice plants confers high tolerance levels to different abiotic stresses. Proc. Natl. Acad. Sci. USA 99: 15898-15903.

[20] E. Guillermo, M.Santa and E.Epstein E., 2001. Potassium/sodium selectivity in wheat and the amphiploid cross, wheatx *Lophopyrum elongatum. Plant Science* 160, 523–534.

[21] SK.Gupta and SK.Sharma.,1990. Response of crops to high exchangeable sodium percentage. Irrig.Sci.,19,p.173-179.

[22] A.Hamdy, N.Katerji, J.W.Van Hoorn and M.Mastrorilli.,2002. Mediterranean crop responses to water and soil salinity, ecophysiological and agronomic analyses.Options Méditerranéennes Série B 36, p.1-3.

[23] W.Hartung and WD.Jeschke.,1999. Abscisic acid: a long-distance stress signal in salt stressed plants. In: Lerner H.R. (ed). *Plant response to environmental stresses, from phytohormones to genome reorganization*. Marcel Dekker Inc., Basel, NY, USA, pp 333-348.

[24] RA,James, RJ.Davenport and R.Munns.,2006. Physiological characterisation of two genes for Na+ exclusion in durum wheat: *Nax1* and *Nax2*. Plant Physiol 142: 1537–1547

[25] S.Kumar, K.M. Naidu, and H.J. Sehtia.,1994. Causes of growth reduction in elongating and expanding leaf tissue of sugarcane under saline conditions.Aust.J.Plant Physiol.21:79-83

[26] A. Läuchli, 1990. In *Calcium in Plant Growth and Development*, vol. 4 of *American Society of Plant Physiologists Symposium Series*, R. T. Leonard and P. K. Hepler, Eds. (American Society of Plant Physiologists, Rockville, MD, , pp. 26-35.

[27] A. Levigneron, F.Lopez, G.Vansuyt,P. Berthomieu,P.Fourcroy, F.Casse-Delbart .,2005.Plants facing salt stress.Cahiers d'Etudes et de Rech. Francophones/Agricultures.Vol.4, p.263-73.

[28] J.Liu and J.K.Zhu.,1998.A Calcium Sensor Homolog Required for Plant Salt Tolerance. *Science*, Vol. 280. no. 5371, pp. 1943 – 1945.

[29] JP.Martinez, H.Silva, JF.Ledent and M.Pinto M., 2007.Effect of drought stress on the osmotic adjustment, cell wall elasticity and cell volume of six cultivars of common beans (*Phaseolus vulgaris* L.) European journal of agronomy. Jan., Vol. 26,1,p. 30-38.

[30] F.J.M.Maathuis and A.Amtmann .,1999.K^+ nutrition and Na^+toxicity: The basis of cellular K+/Na+ ratios.Ann.Bot.84, p.123–133.

[31] M. Mezni, A. Albouchi, E. Bizid et M.Hamza.,2002.Effet de la salinité des eaux d'irrigation sur la nutrition minérale chez trois variétés de luzerne pérenne (*Medicago sativa*).Agro.,22,283–291.

[32] A. Moinuddin, R.A.Fischer,K.D.Sayre and M.P.Reynolds.,2005.Osmotic Adjustment in Wheat in Relation to Grain Yield under Water Deficit Environments.Agro.J.97:1062-1071.

[33] R. Munns.,2005. Genes and salt tolerance: bringing them together. New Phytol .167: 645–663.

[34] X.Niu,RA.Bressan,PM.Hasegawa and J.Pardo.,995.Ion homeostasis in NaCl stress environments .*Plant Physiology* 109, 735–742.

[35] AK.Parida and AB.Das.,2005.Salt tolerance and salinity effects on plants: A.Rev.Ecotoxicol. Environ. Safety,60:324-349.

[36] MG.Pitman, and A. Läuchli.,2002.Global impacts of salinity and agricultural ecosystem. *In* A Läuchli, U Lüttge eds, Salinity: Environment-Plants-Molecules. Kluwer Academic, Dordrecht, The Netherlands, pp 3–20

[37] D.Polignano, R.Splendido and P.Ugenti.,1991. Protein polymorphism among genotypes of faba bean (*Vicia faba* L.) from Ethiopia and Afghanistan.Fabis, p.8-11.

[38] Y.L.Qian, S.J.Wilhelm and K.B. Marcum.,2001.Comparative response of two Kentucky bluegrass cultivars to salinity stress. Crop Sci. 41: 1895-1900.
[39] M.S. Rehman, H.Miyake,and Y.Takeoka.,2002.Effect of exogenous glycinebetaine on growth and ultrastructure of salt stressed rice seedlings (*Oryza sativa* L). Plant Prod.Sci.5:33-44.
[40] RJ. Reid and FA.Smith .,2000. The limits of sodium/calcium interactions in plant growth. Australian Journal of Plant Physiology 27, 709–715.
[41] A.N.Rodríguez and F.Rubio.,2006. High-affinity potassium and sodium transport systems in plants. J.of Exp. Botany 57(5):1149-1160.
[42] R.Sairam and A.Tyagi.,2004.Physiology and molecular biology of salinity stress tolerance plants.Current Science,Vol.36,N°3,p.407-421.
[43] D.Sanders,C. Brown and J.F.Harper,1999.Communicating with calcium.Plant Cell,11:691-7 06.
[44] J.I.Schroeder, G.J. Allen, V. Hugouvieux, J.M. Kwak, and D.Waner.,2001. Guard cell signal transduction. Annu. Rev. Plant Physiol. Plant Mol. Biol. 52:627–658.
[45] S. Shabala, L. Shabala, EV.Volkenburgh and I.Newman., 2005.Effect of divalent cations on ion fluxes and leaf photochemistry in salinized barley leaves.J.of Exp.Bot.,56,415:1369-1378.
[46] MN.Shannon and CL. Noble C.L., 1995.Variation in salt tolerance and ion accumulation among subterranean clover varieties.Crop Sci. 35,788–804.
[47] I.Szabolcs.,1994.Soils and salinisation.*In* Handbook of Plant and Crop Stress.Ed.M Pessarakali. p.3–11. Marcel Dekker, New York.
[48] M. Tester and R.Davenport.,2003. Na^+ tolerance and Na^+ transport in higher plants. Ann Bot (Lond).91: 503–537.
[49] A.Wahid.,2004.Analysis of toxic and osmotic effects of sodium chloride on leaf growth and economic yield of sugarcane.Bot.Bull.Acad.Sin.,45:133-141.
[50] A.R Yeo, S.A.Flowers, G. Rao, K.Welfare, N.Senanayake, and T.J. Flowers.,1999. Silicon reduces sodium uptake in rice (*Oryza sativa* L.) in saline conditions and this is accounted for by a reduction in the transpirational bypass flow. Plant Cell Environ. 22:559–565.
[51] S.Yokoi,RA.Bressan and PM. Hasegawa.,2002.Salt stress tolerance of plants.JIRCAS Working Report,25-33.
[52] B. Zaman, B.H. Niazi, M.Athar and M. Ahmad.,2005.Response of wheat plants to $Na^+$and Ca^{++} on interaction under saline environment.Int..J.of Environ.Sci.and Techno., 2,1,Spring,p.7-12.
[53] JK.Zhu.,2003.Regulation of ion homeostasis under salt stress Current Opinion in Plant Biology, 6: 441–445.
[54] HL. Zhong and A. Lauchli., 1994. Spatial-distribution of solutes, K, Na, Ca and their deposition rates in the growth zone of primary cotton roots: effects of NaCl and $CaCl_2$. *Planta* 194, 34–41.

European Journal of Scientific Research
ISSN 1450-216X Vol.18 No.4 (2007), pp.655-662

http://www.eurojournals.com/ejsr.htm

An Adaptable Recursive Neural-Network Model for Mackey-Glass Time Series Prediction

A.Shahmansoorian
Islamic Azad University, Islamshahr Branch, Islamshahr, Iran
E-mail: A_shahmansoorian@IIAU.AC.IR

A. Mohammadzadeh Fakhr Davoud
Aerospace Research Institute, Tehran Iran
E-mail: A_mohammadzadeh@ARI.AC.IR

Abstract

Artificial Neural Networks in time series prediction generally minimize a symmetric statistical error, such as the sum of squared errors, to learn relationships from the presented data. How ever, using other capabilities such as recursive Neural Networks causes more precision forecasting system. We can use such the systems to prediction of real time series such as weathering, business, traffic and etc. In this study, we will consider a recursive Neural Network to predict the Mackey-Glass time series. The effective parameters will be considered to obtain the best results. The learning method for recursive Neural Network is Back-Propagation and the system will be under learning until the error converges to its limit. This limit is defined by negative exponential behavior of error.

Keywords: Recursive Neural Network, time series, Mackey-Glass- back propagation learning.

1. Introduction

Neural networks have been successfully applied to many different problems such as time series data forecasting, pattern recognition, optimization, classification, and etc.[1-5]. This is due to the versatility of a multilayer feed-forward neural network in approximating an arbitrary static non-linearity and the computational efficiency of the back-propagation learning algorithm. In many of Neural Networks, there are some single feed forward layers, which are connected to each other in a line, and the complexity of system is not enough to predict the high degree systems. Thus we are forced to increase the total layers of Neural Network and the number of internal functions in each layer to increase the complexity of Neural Network. In many cases, this will causes instability of closed loop system. In this study, we use a new recursive Neural Network (**RNN**) with special layers to solve such problems. In this paper we use internal feedback to increase the complexity of Neural Network and we will consider the result of simple Neural Network.

The new RNN has special feed forward and feed back (learning) formula. Thus we will consider the related formula to achieve the complete RNN.

The case study of this paper is Mackey-Glass time series. This time series is a flexible time series which we can determine its complexity with a simple coefficient. We will use proper complexity for this time series to avoid overlaps in the predictions. The results are evaluated and the efficiency of

Neural Network is optimized. In this paper simulations and the plots are provided using MATLAB software.

2. Literature Review

Application of Neural Networks in Prediction of time series, pattern recognition, and optimization is an attractive subject due to its simplicity, and universality. The traffic prediction and modeling of MPEG video sources [1] is done by recursive Neural Networks, which uses the simple Neural Network (non-internal feed back) and uses more complex internal functions to increase the efficiency of system. It uses the Reduced Gradient method for learning the parameters of Neural Network and uses time delayed-desired-output as input vector.

Market clearing price Prediction [3] is done by Multilayer perceptron (MLP) network and has a Back Propagation learning method. It uses the single line Neural Network and increases the complexity by Kalman Filter Method. As it seen, the simple Neural Network has not enough complexity to achieve the normal behavior, thus in any study, we should take a strategy to increase the complexity of Neural Networks.

In [4] the Prediction of geometric activity is done by Neural Networks. The learning method is Back Propagation and uses local holder exponents. In [5] the global modeling by recurrent Neural Network is considered. Using Compensatory Neuron Model (CNM) it achieves the fully recurrent neural network, and using Jordan Recurrent Neural Networks, a complex Neural Network is obtained which is used for prediction of Mackey-Glass time series.

In the references [1-5], a Neural Network does the prediction of a time series. But in each of them, a special method is used to achieve the best results, but all of them are meaning increasing the complexity of Neural Network. In this study, we use the internal feedback and convert the Neural Network to a Recursive Neural Network (RNN) to obtain the best complexity.

3. Mackey-Glass Time Series

We have considered the time series generated by the Mackey-Glass [15] discrete time equation

$$\frac{dx}{dt} = \frac{0.2x(t-\tau)}{1+x^{10}(t-\tau)} - 0.1\times x(t)$$

Time series is generated assuming random initial conditions. For clearance of behavior of time series, for 3 values for time constant, 500 data samples are generated and are shown in Fig. (1). As shown in this figure, according to increasing the time constant, complexity of time series increases and periodic behavior of time series decreases. The first curve shows the minimum time constant (equal 5 seconds) and it has a periodic behavior. The second curve shows the time constant equal 20 seconds, and the periodic behavior is decreases and nonlinear behavior is increases. The third curve has time constant equal to 40 seconds, and the periodic behavior is completely reduced and the system has maximum complexity. Thus, we use time constant equal 40 seconds to obtain more complexity in time series.

Figure 1: Mackey Glass time series behavior

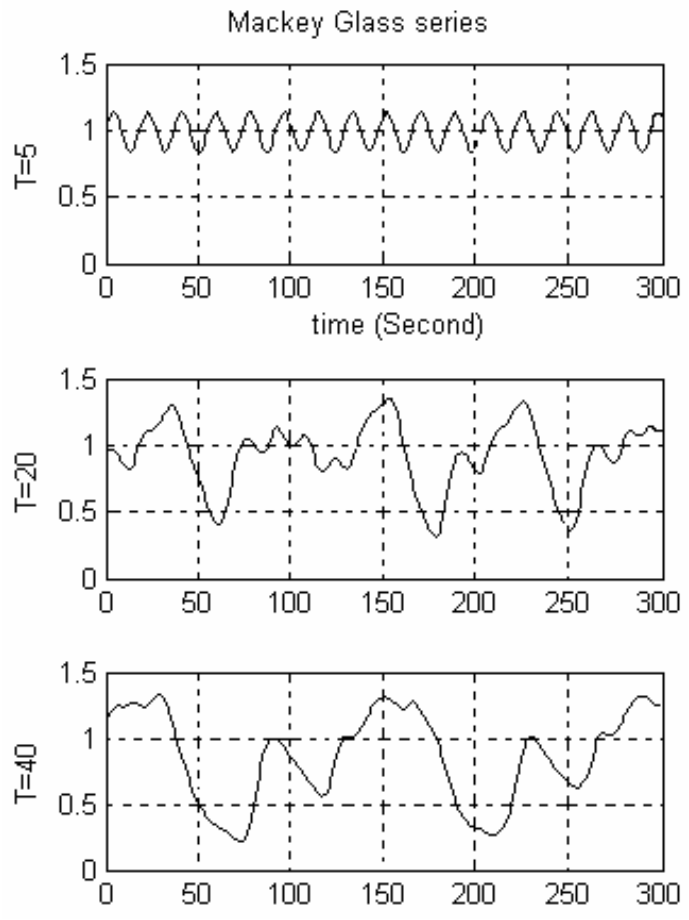

4. Recursive Neural Network

The Recursive Neural Network (RNN) has structure as shown in Fig. (2). We use a RNN with 2 layer and use a feed back layer which increases memory of the system, Because the values of next step affects on the current step. Also the functions used in the feed back layer causes high complexity of RNN. Effects of the number of layers and number of transfer function in each layer will be discussed later. Also the effects of other parameters such as learning factor and etc. will be considered. The transfer function used in the RNN is exponential and has equation as follow.

$$f(X,P)=\frac{1}{1+e^{-\frac{X}{P}}}$$

The learning rule of the RNN is Back Propagation and the structure of learning rule is brought in Fig. (3).

Figure 2: RNN structure

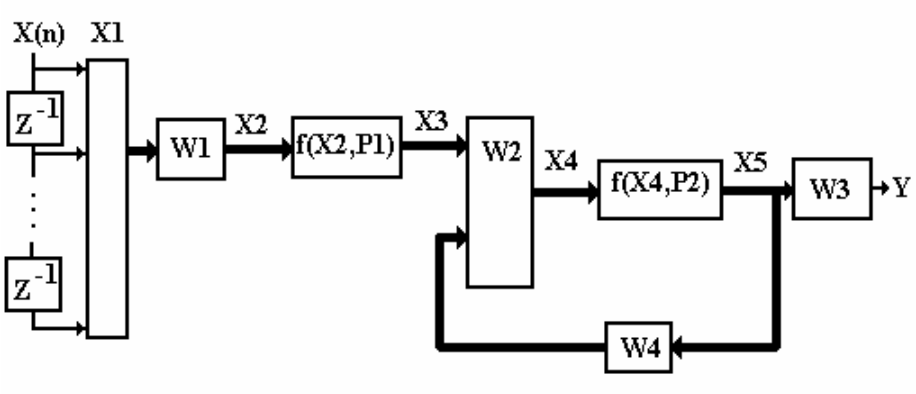

Figure 3: Back Propagation structure.

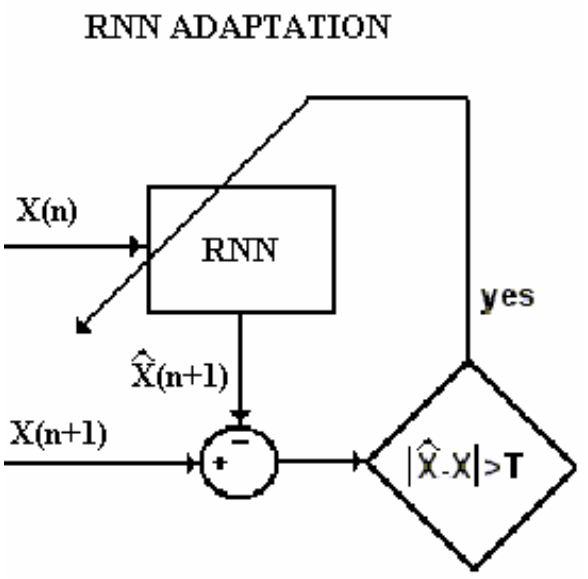

The feed forward equation of RNN is listed and noted according to structure above.

$$X2 = W1.X1,$$

$$X3 = f(X2, P1),$$

$$X4 = W2.(X3 + W4.X5),$$

$$X5 = f(X3, P2),$$

$$Y = \hat{X}(n+1) = W3.X5$$

The Back Propagation learning rules are listed here. Sum of the squared error is used as cost function.

$$e = X(n+1) - \hat{X}(n+1)$$

$$E = \frac{1}{2}\sum e^2,$$

Thus, according to Back Propagation learning rule we have:

$$W3 = W3 - \eta \frac{\partial E}{\partial W3}$$

$$= W3 - \eta . \frac{\partial E}{\partial e} . \frac{\partial e}{\partial Y} . \frac{\partial Y}{\partial W3}$$

$$= W3 - \eta . (e) . (-1) . X5$$

And for other parameters we have:

$$W2 = W2 - \eta . (e) . (-1) . W3 . \frac{\partial f(X4, P2)}{\partial X4} \ldots .$$

$$\ldots (X3 + W4 . X5)$$

$$W1 = W1 - \eta . (e) . (-1) . W3 . \frac{\partial f(X4, P2)}{\partial X4} . W2 \ldots .$$

$$\ldots . \frac{\partial f(X2, P1)}{\partial X2} . X1$$

$$W4 = W4 - \eta . (e) . (-1) . W3 . \frac{\partial f(X4, P2)}{\partial X4} . W2 . X5$$

$$P1 = P1 - \eta . (e) . (-1) . W3 . \frac{\partial f(X4, P2)}{\partial X4} . W2 \ldots .$$

$$\ldots . \frac{\partial f(X2, P1)}{\partial P1}$$

$$P2 = P2 - \eta . (e) . (-1) . W3 . \frac{\partial f(X4, P2)}{\partial P2}$$

As shown here, the RNN has a recursive- high complex structure with internal memory. This structure helps to minimize the error of prediction of high complex systems.

5. Simulation Results

In this case study, we compare the RNN with a simple Neural Network (NN). The simple NN can be obtained by reducing W4 from RNN. At first step, we use 5 input (dimension of X1) and dimension 8 and 6 for layer 1 and 2. We will train the network with 20000 data sample to ensure the RNN will be converges to optimum values of parameters. Because of feedback of RNN, this system has high complexity and thus, it has high sensitivity to the parameters. Therefore an unsuitable value for training factor η may cause the system to be unstable. In table (1) the results of various training factor is shown. We use variance of error to compare the efficiency of RNN. For uniformity of results, we will calculate the last 1000 data samples.

Table 1: effects of η on RNN error

η(p)	0.05	0.05	0.05	0.05	0.1	0.01
η(w)	0.1	0.3	0.4	0.5	0.4	0.4
Error	0.002	2.8e-4	3.5e-4	NAN	NAN	NAN

Table (1) guide us that η(p) (means training factor for P parameters) should be small. Because the sensitivity of P parameter is high and it can make the RNN to be unstable. Thus we will choose it equal 0.05. Also the η(w) (means training factor for W parameters) has less sensitivity and its value may be chosen more larger. It may vary 0.1 to 0.5 to obtain a stable and trained network. Thus we will choose it equal 0.3. In Fig. (4), behavior of RNN is shown. The second figure is simultaneous plot of output and desired value, which have overlap.

Figure 4: behavior of RNN

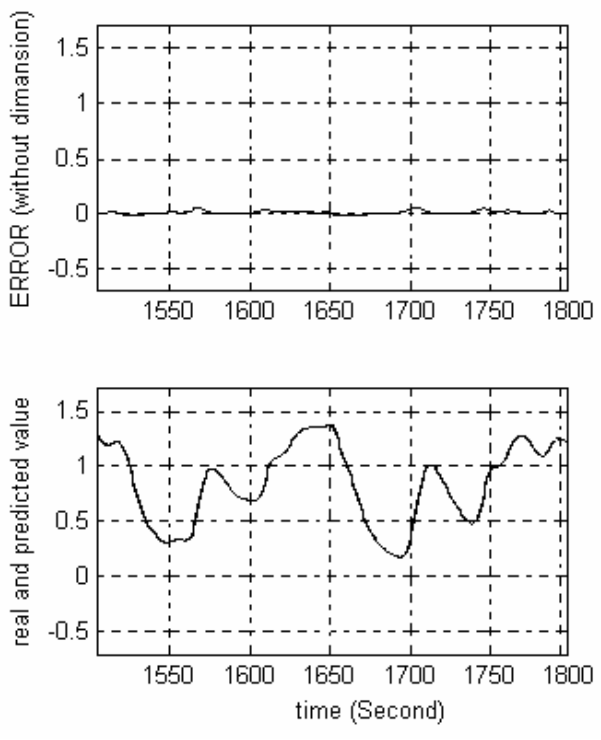

If the feedback W4 reduced from RNN, we will have the simple NN. In this case the complexity of NN will decrease. Table (2) includes the effects of various training factors on the NN error. In Fig. (5), behavior of NN is shown. The structures of two Neural Networks are identical and there is no difference between number of layers and dimension of layers. This will help us to compare two Neural Networks. As shown in table (1), (2) in identical cases, the error of RNN is about 0.1 of NN error and the tracking of desired value in RNN is better than NN.

Table 2: effects of η on NN error

η(p)	0.05	0.05	0.05	0.05	0.1	0.01
η(w)	0.1	0.3	0.4	0.5	0.4	0.4
Error	0.005	0.002	0.003	NAN	NAN	NAN

Figure 5: behavior of NN

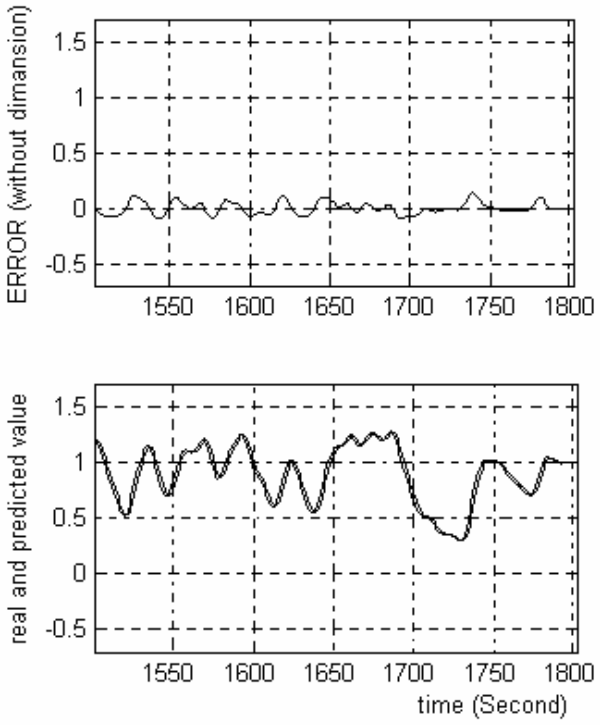

6. Conclusions

Using artificial systems in time series prediction is very usual, because of high performance and simplicity of structure. In this study, two Neural Networks has been considered. The first is RNN, which is obtained by adding an internal feedback to a simple NN to achieve high complexity and the other is a simple NN. Both of the Neural Networks are identical and have similar layers so the efficiency of them has been compared. The case study is a Mackey Glass time series with high complexity (τ = 40 seconds). Tracking of high complex systems, need high complex Neural Network. We can achieve that by either adding some layers to Neural Network, which causes the NN to be unstable, or increase the complexity of NN by internal feedback. RNN is more sensitive and it could be easily unstable rather than simple NN. But by choosing correct values for training factor, if the RNN converges, it would has better result than simple NN. In particular, both of the weights and parameter of transfer functions are trained so that the network output, after the adaptation, is approximately equal to the real value. In this paper we have studied the simple NN and RNN. The RNN has better behavior and the tracking error of RNN was about one tenth of simple NN.

References

[1] Anastasios D. Doulamis, Nicolaos D. Doulamis, Stefanos D. Kolias, "*An Adaptable Neural-Network Modal for Recursive Nonlinear Traffic Prediction,*" IEEE Trans. Neural Network. Vol. 14, January 2003.

[2] D.C. Park, M.A. EL-Sharkawi, R.J. Marks, "*An Adaptively trained Neural Network,*" IEEE Trans. Neural Network. Vol. 2, May 1991.

[3] Li Zhang, Peter B. Luh, "*Neural Network-Based Market Clearing price Prediction and Confidence Interval Estimation With an improved Extended Kalman Filter Method* " IEEE Transactions on Power System, Vol. 20, no. 1, Feb 2005.

[4] Z.voros, D.jankovicova, "*Neural Network Prediction of geometric activity: a method using local holder exponents*", Nonlinear Processes in Geophysics 2002.

[5] R.N.Yadav, P.K.Kalra "*Modeling with recurrent Neural Networks using compensatory neuron Modal* " Neural Information Processing Vol. 6, No.3, March 2005.

[6] Ho Joon Kim, Tae-Wan Ryu, "Time Series Prediction Using an Interval Arithmetic FIR Network" Neural Information Processing, Vol. 8, No.3, September 2005.

[7] P. R. Chang and J. T. Hu, "Optimal Nonlinear Adaptive prediction and modeling of MPEG video in ATM networks using pipelined recurrent neural network" IEEE J. Select, Areas Common., Vol. 15, Aug. 1997

[8] S. Haykin, "Neural Networks: A Comprehensive Foundation" New York: Macmillan, 1994.

[9] J. Connor, D. Martin, and L. Altas, "Recursive neural network and robust time series prediction" IEEE trans. Neural Networks, Vol. 5, pp.240-254, Mar. 1994.

[10] A. Doulamis, N. Doulamis, and S. Kollias, "On line retrainable neural networks: Improving the performance of neural networks in image analysis problems" IEEE Trans. Neural Networks Vol. 11, pp. 134-155, Jan. 2000.

[11] H. White, "Economic Prediction using neural networks- the case of IBM daily stock returns" Foundation of research, MIT Press, Cambridge, MA, 1988.

[12] M.H. Hassoun, "Fundamentals of Artificial neural networks" Prentice Hall of India, 1998.

[13] B.A. Pearlmutter, "Gradiant calculation for dynamic recurrent neural networks: a survay" IEEE Transaction on Neural Networks, 6(5): 1212-1228, 1995.

[14] D. W. Bunn, "Forecasting loads and prices in competitive power markets" Proc. IEEE, Vol. 88, No. 2, pp. 163-169, Feb. 2000.

[15] M.C. Mackey and L. Glass, "Oscillations and chaos in physiological control systems" Science, 197:287-289, 1977.

European Journal of Scientific Research
ISSN 1450-216X Vol.18 No.4 (2007), pp.663-673

http://www.eurojournals.com/ejsr.htm

Fetus-in-Fetu: A Review Article

Ganiyu. A. Rahman
Division of General Surgery, Department of Surgery
University of Ilorin Teaching Hospital, Ilorin, Nigeria
E-mail: garahman1@yahoo.com
Tel: 234803357990; Fax – 031220020

Yisau A. Abdulkadir
Department of Diagnostic Radiology
University of Ilorin Teaching Hospital, Ilorin, Nigeria

Lukman. O. Abdur-Rahman
Division of Pediatric Surgery, Department of Surgery
University of Ilorin Teaching Hospital, Ilorin, Nigeria

Abstract

INTRODUCTION: the inclusion of a malformed parasitic twin (homunculus) in the body of its partner (autosite) is an age long mystery first reported by Meckel in 1800. There has been several postulated embryogenetic mechanisms such as defective twinning, genetic imperfect embryo and the defective implantation that explained the variable locations and the degrees of organ differentiation.
OBJECTIVE: retrospectively review the epidemiology, embryogenesis, pathology, presentations and management of this rare condition to bridge the gap in knowledge of the reported cases to date.
METHODS: electronic search of the abstracts and article of all available reported cases of fetus in fetu was carried out and analysis done.
RESULTS: a total of 160 cases have been reported, majority (25.6%) of which originated from Asia, Europe (16.3%) and North America (16.3%). The age at diagnosis ranges from 16 weeks in utero to the oldest at 47 year. The male to female ratio is 2:1. Nearly all body parts have been identified. Acardiac and anencephaly are features in over 95% of cases. While intra-abdominal is the commonest location. Radiology is paramount to the diagnosis.
CONCLUSION: The advents of modern imaging methods have enhanced the early and improved diagnosis of fetus in fetu and in its differentiation from teratoma. Beaudion et al theory of defective implantation of a twinning and variable impaired mesenchymal induction of the homunculus by the autosite cells indeed explained all observable features of FIF to teratoma.

Keywords: Fetus-in-fetu, Teratoma, monozygotic diamniotic twinning, retroperitoneal

Introduction

Fetus-in-fetu (FIF) was first described by Meckel in 1800 [1, 2]. In FIF, malformed parasitic twin is found inside the body of its partner (autosite), usually in the abdominal cavity in a rare condition[1-5]. Several embryogenetic mechanism have been postulated such as modified or defective twinning, genetically imperfect embryo theory and the defective implantation theory [1, 5, 6.] FIF generally is an aberration of monozygotic diamniotic twinning in which unequal division of the totipotent inner cell mass of the developing blastocyst leads to the inclusion of a smaller cell mass within a maturing sister embryo[1-9]. The clinical presentations are non-specific but rather are dependent on the site and size of the mass involved. The diagnoses are mainly radiological, while histology and cytology are sometime necessary for confirmation. Teratoma and FIF are closely related but malignant transformation of the latter is rare[10]. Thus, excision surgery often is curative in the affected patient.

Various authors since the year 2000 to date have quoted less than 100 reported cases as aftermath of Hoeffel et al[2] extensive review published in 2000, which documented 88 cases. Therefore, this article is meant to retrospectively review the epidemiology, embryogenesis, pathology, presentations and management of this rare condition to bridge the gap in knowledge of the reported cases to date.

Methodology

Thorough search of the Electronic English literature was carried out using Search engines such as Pubmed, medline and google with search words that includes: 'foetus in foetu, 'fetus in fetus', "parasitic twins' fetus in fetus+Nigeria, fetus in fetus +Africa, teratoma. All reports of cases of FIF were identified and retrieved. Data collected include authors name, year of publication and region where the case report emanated. Specific data on characteristic of FIF such as age at diagnosis, sex of patient(autosite), site of homunculus, the identified body parts, presentations and management. Abstract of all the identified cases were evaluated. Data was analysed using SPSS 11.0 for windows.

Results

One hundred and sixty (160) cases of FIF were retrieved during our search (Table 1). The search identified the authors and year of publication in all cases. The papers presented before 1978 were found to either not have abstracts or scanty information on abstracts. However, from 1978 to 2007 the available information on Pubmed was detailed. This constituted about 74.4% of all the cases reviewed. Where available, it sufficiently identified patient age, sex, location of the homunculus and the region where the case was been reported. The ages at diagnosis ranged from 16 weeks in utero to the oldest of 47 years. A total of 15% were diagnosed prenataly from 1806 to year 2007. In 23.1% age at presentation was not stated, the 15% diagnosed prenataly may be part of this (fig.1). There was no prenatal diagnosis before 1978. The male to female ratio was 2:1, though in 36.9% of cases the sex was not known. About 25.6% of the reported cases of FIF emanated from Asia, 16.3% each from North America and Europe respectively. Only three cases (1.9%) have been reported from Africa and they were all from South Africa (Table 2). Intra-abdominal retroperitoneal location is the dominant site of FIF occurring in 53.1% followed by the head and neck with 10% (fig 2). Other rare sites of occurrence in 3.8% of cases are scrotal sac, oral cavity, liver, intrapulmonary, ovary, mediastinum, pelvis, adrenal gland and within an undescended testis. Nearly all the body parts have been identified in various degrees in the included fetus. Fetu masses may show varying degrees of organ system differentiation and deformity. Brain tissue and intestine were detected in half of reported cases. Other uncommon organs reported are thyroid, parathyroid, pancreas, spleen, kidney, adrenal, testis, ovaries, urinary bladder, tongue, salivary glands, lymphnodes, trachea, and teeth. The rarest reported body part was the presence of a functioning heart. FIF was single in 88% while the remaining were multiple. Povysilova (1983) reported a case of encranium containing 21 rudimentary fetuses in a premature boy.

Table 1: Published Cases of Fetus-in-FETU (1806-2007)

S/No.	Study/Case	Age	Sex	Body Location	Region
1	Majhi et al (2007)	8 yrs	F	Abd. retrop.	India
2	Mohan et al (2007)	3 yrs	M	Abd. retroperi.	India
3	Coolen et al (2007)			Abd.	Canada
4	Woodard et al (2006)			Cervical	USA
5	Kajbafzadeh & Baha (2006)	6 mon.	M	Cranium	Iran
6	Basu et al (2006)				India
7	Basu et al (2006)				India
8	Miura et al (2006)		M	Abd. retroperito	Japan
9	Miura et al (2006)		M	Cranium	Japan
10	Buckles et al (2006			Cranio cervical	USA
11	Tiwari et al (2006)				USA
12	Higgins & Coley (2006)		M	Abd.	USA
13	Higgins & Coley (2006)		M	Abd.	USA
14	Weiss et al (2006)	23	F	Abd.	USA
15	Khatami et al (2006)	4 yrs	M	Abd.	Iran
16	Chua et al (2005)		M	Abd. retrop.	Singapore
17	Wada et al (2005)				Japan
18	Neto et al (2005)	12 yrs	F	Pulmonary	Brazil
19	House et al (2005)			Abdominal	Australia
20	Borges et al (2005)			Neck	USA
21	Bozilow et al (2005)	2½yrs	M	Abd. retroperi.	Poland
22	Bozilow et al (2005)	11 days	M	Abd. retroperi.	Poland
23	Lee et al (2005)	39 yrs	M	Abd.	Taiwan
24	Aoki et al (2004)			Mediastinum	Japan
25	Beaudoin et al (2004)			Mediastinum ant.	Paris/France
26	Kapoor et al (2004)			Mouth	USA
27	Brand et al (2004)		M	Abd.	Lisbon/Portugal
28	Sharma et al (2003)				
29	Mohta et al (2003)				
30	Gilbert et al (2003)	1 yr		Abd.	USA
31	Varanell et al (2003)		M	Abd.	USA
32	Sinha et al (2003)	1½ yrs	F	Abd.	India
33	Iyer et al (2003)				USA
34	Sarioglu (2003)			Mouth	Germany
35	Hong et al (2002)	2 days	M	Abd.	Korea
36	Wanger et al (2002)				USA
37	Chadha (2002)				India
38	Chadha (2002)				India
39	Napar et al (2002)	2 yrs	M	Abd.	India
40	Lee et al (2002)				Hong Kong
41	Jones et al (2001)				USA
42	Awasthi et al (2001)			Abd.	India
43	Federici et al (2001)	8 mon.	M	Abd.	Italy
44	Nastanski & Dowey (2001)				USA
45	Mills et al (2001)				USA
46	Lanniruberto et al (2001)		Cranial		Italy
47	Massad et al (2001)	27 yrs	M	Abd.	USA
48	Al-Zaiem & Algarim (2000)		M	Abd. retrop.	Saudi
49	Arenholtz (2000)				USA
50	Hoeffel et al (2000)	19 mon.F	Abd.		France
51	Khadaroo et al (2000)	1 day		Abd.	Canada
52	Patankar et al (2000)				USA
53	Patankar et al (2000)				USA
54	Magnus et al (1999)			Abd.-Liver	South Africa
55	Magnus et al (1999)				South Africa
56	Magnus et al (1999)				South Africa
57	Shrivastara et al (1999)	27 yrs	M	Abd. retrop.	India
58	Kumar et al (1999)	3 mon.	M	Abd. retrop.	India

59	Shin et al (1999)	1 day	M	Scrotal sac	South Korea
60	Thakral et al (1998)	1 day	F	Ovary	Oman
61	Bhat et al (1998)			Abd.	India
62	Khatib et al (1998)			Abd.	Montpellier/France
63	Sequira et al (1998)	16 yrs	M	Abd. retrop.	India
64	Montgomery et al (1998)		Abd.		USA
65	Fowler (1998)	2 days	F	Abd.	USA
66	Moorthy et al (1997)	25 yrs	M	Abd. retrop.	India
67	Hopkins et al (1997)	5 days	M	Abd.	USA
68	Sanal et al (1997)		M	Sacrum	Turkey
69	Hanguinet et al (1997)		Abd.		Switzerland
70	delagansie et al (1997)				France
71	Chen et al (1997)			Abd.	Taiwan
72	Goldstein et al ((1996)		Cranial		Israel
73	Vigal et al (1996)				Asturias
74	Fink et al (1995)	3 mon.	M		Cambridge
75	Kang et al (1994)	3 mon.	F	Abd.	Korea
76	Luzzatto et al (1994)	9 days	M	Abd.	Italy
77	Hung & Lam (1993)	2 mon.	F	Cranial	Taiwan
78	Hing et al (1993)		F	Abd.	Europe
79	Samujh et al (1993)				India
80	Hsiao et al (1993)	5 yrs	F	Abd.	Taiwan
81	Tsai et al (1993)	2 mon.	F	Cranial	Taiwan
82	Kim & Shinn (1993)	6 mon.	M	Abd.	Korea
83	Senyuz et al (1992)		M	Mouth	Turkey
84	al-Baghdadi (1992)	4 mon.	M	Liver	Iraq
85	Yang & Leow (1992)				Taiwan
86	Dagradi et al (1992)	47 yrs	M	Abd.	Italy
87	Carles et al (1991)				France
88	Federici (1991)	3 wks	F	Abd. retrop.	
89	Federici (1991)	1 mon.	F	Abd. retrop.	
90	Federici (1991)	1 mon.	F	Abd. retrop.	
91	Gurses et al (1990)	4 mon.	M		Turkey
92	Bernal-Sprekelsen (1990)	6 wks	F	Abd.	Spain
93	Martinez-Urrutia et al (1990)		F	Abd.	Spain
94	Chitrit et al (1990)		F	Adrenal	France
95	Chateil et al (1990)	5 mon.	M	Abd.	France
96	Eng et al (1989)	9 mon.	F	Abd.	Taiwan
97	Ng & Tan (1989)	3 mon	M	Abd.	
98	Rastogi et al (1988)				
99	Burtner & Conn (1988)	16 mon.M			
100	Heifetz et al (1988)	1 day	M		Canada
101	Sutherland (1988)	1 day	M	Abd. retrop.	
102	Sada et al (1986)		F		
103	Yasuda et al (1985)	5mon.	F	Abd.	
104	Alpers (1985)	1day	M	Abd.	
105	Narasimharo et al (1984)	2days	M		
106	Chi et al (1984)	8wks	M	Abd.	Korea
107	Montupet et al (1984)	3mon.	F	Abd.	
108	Montupet et al (1984)	4wks	F	Abd.	
109	Nicolini et al (1983)		M		
110	Sutthiwan et al (1983)	2mon.	M	Abd.	
111	George et al (1983)	3mon.			
112	Povysilova (1983)			Cranial	
113	Corona-Reyes (1982)			Testicle	
114	Sangvichien & Sull (1982)	2mon.	M		
115	Nocera et al (1982)	9mon.	F	Abd.	Mexico
116	Afshar et al (1982)	2mon.	F	Cranial III ventricle	
117	Kadir (1981)	10yrs	M		
118	Blumberg et al (1980)	4mon.	F	Abd.	
119	Di Lieto et al (1978)				Italy

120	Schmidt & Sperling (1978)		M	Abd.	Germany
121	Derzhavin et al (1976)			Abd.	Russia
122	Knox & Webb (1975)	9yrs	M		
123	Knox & Webb (1975)	3mon.	M		
124	Subbiah et al (1975)				
125	Parker (1974)	6wks	M		
126	Berlov et al (1974)				
127	Du plessis et al (1974)	6 mon.	M		
128	Grosfeld et al (1974)	6 wks	M	Abd.	USA
129	Tadal et al (1974)				
130	Tadal et al (1974)	6 mon.	M		
131	Fiedler & Rose (1974)			Cranial	Germany
132	Kakizoe & Tahara (1972)	13 days	M	Scrotal sac	
133	Lamabadusunya (1972)	20 mon.	F		
134	Lal (1971)		M	Abd.	
135	Numanoglu (1970)	3 mon.	M		
136	Grant et al (1968)	1 day	M	Abd	
137	Lee (1965)	2 mon.	M		
138	Jensen et al (1965)	17 yrs	M	Abd.	
139	Ariga (1965)	5 days	F	Abd.	
140	Broghammer et al (1963)	1 day	F		
141	Ikede (1963)	10 mon.	M	Abd.	
142	Janovskins (1962)	9 yrs	M		
143	Lewish (1961)			Abd. retro.	
144	Tasuda (1960)	18 mon.	M	Abd.	
145	Fujkura (1959)	14 mon.	F	Abd.	
146	Fujikura & Hunter (1959)	14 mon.	F		
147	Tagirovetal (1957)				
148	Gross & Clatworthy (1951)	2 days	F		
149	Junqueiral (1951)				
150	Kimmel et al (1950)	1 day	F	Cranial	
151	Farris (1950)			Abd.	
152	Maxwell (1947)	4 mon.	F	Abd.	
153	Hoeven (1943)	15 mon.	M	Abd.	
154	Brunkow (1942)	14 mon.	F	Abd.	
155	Anderson (1939)	5 wks	F	Abd.	
156	Goto (1927)	12 yrs	M	Abd.	
157	Taylor (1887)	11 mon.	M	Abd.	
158	Klebs (1876)			Abd.	
159	Schoenfeld (1841)		M	Abd.	
160	Highmore (1815)	15 yrs	M	Abd.	
161	Young (1806)	9 mon.	M	Abd.	

Figure 1: Age at presentation of FIF (n=160)

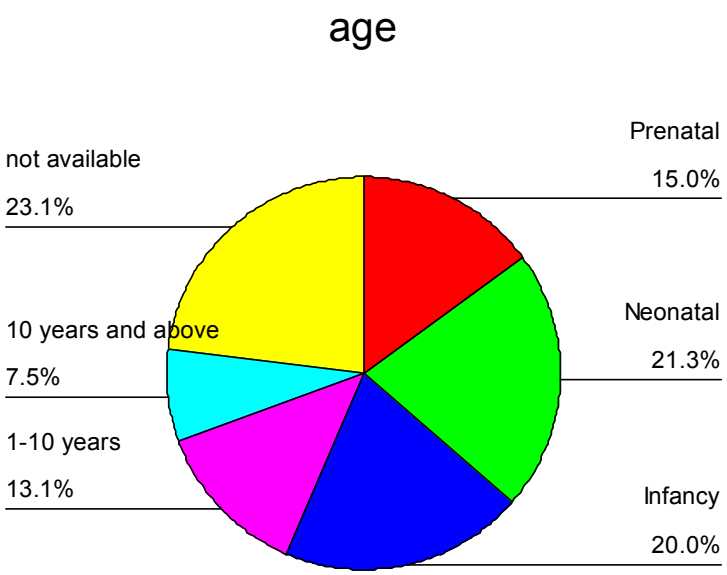

Table 2: Regions of the World where cases of FIF have been reported (1806-2007)

	Frequency	Percent
Africa	3	1.9
Europe	26	16.3
North America	26	16.3
South America	2	1.3
Australia	1	.6
Asia	41	25.6
Not available	61	38.1
Total	160	100.0

Figure 2: Body location of FIF (n=160)

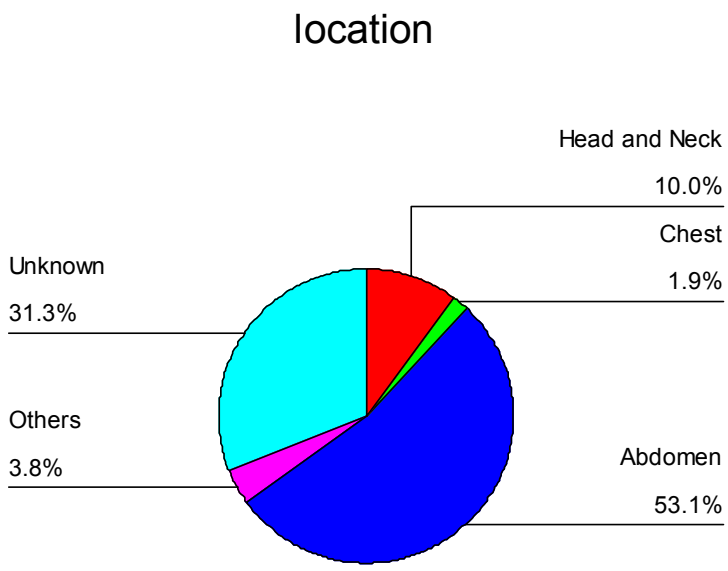

Epidemiology

FIF has an incidence of 1 in 500,000 births [2]. Extensive literature review by Chua et al (2005) [1] and Hoeffel et al (2000) [2] showed that there were less than 100 reported cases worldwide[1]. This present

review shows 160 reported cases world wide in the electronic English literature. The regional distribution of FIF has not been previously documented. However, our report shows that FIF affect predominantly the Caucasians. It is extremely rare in Africa, where only three cases have been reported (all from South Africa) unlike Asia that accounted for 25.6% of the reported cases,. The West African sub region with the largest population of blacks and the largest twinning rate in the world has no documented case reported to the best of our knowledge.

Hoeffel et al [2] review shows that only four of 88 reported cases (4.5%) have been described in patients 10 years of age or older, with the oldest reported case occurring in a 47-year old man[11]. In this review, the earliest diagnosed FIF in utero was at 16-week gestational age, while the oldest patient at diagnosis remains the same with Hoeffel et al [2, 12]. Unlike the Hoeffel et al, twelve 0f the 160 reported cases (7.5%) were described in patients 10years of age and above, 13.1% between 1-10years, 41.3% at neonatal infancy and 15.0% were diagnosed in utero (prenatally).

Thakral et al [3] reported equal male and female predisposition unlike our finding of 2:1 male predominance, which is same as Patankar et al [13] and Federici et al [4]. This is in contrast to teratomas, which has female preponderance. There has not been any report as to the racial incidence. However, majority of the reported cases (58.2%) are from Asian, European and Latin American countries. Fetus in fetus was rarely reported amongst Africans. Further study need to be done to exclude environmental factor as a risk to development of FIF.

Embryogenesis (Aetiopathogenesis)

The aetiopathogenesis of FIF remains controversial but theories abounds. It is thought to be an unequal division of totipotential cells of blastocyst where the result is the inclusion of a mal-cellular mass in the more mature embryo [1]. This is a form of monozygotic diamniotic twin pregnancy, where the parasitic twin installs and grows in the body of its partner [2, 7]. Studies on blood group systems and chromosome cultures from the autosite and the homunculus showed no difference between the two [14]. It has also been shown that when intra-abdominal gonads were found, these corresponded histologically to the sex of the autosite [2, 15].

Some investigators have hypothesized that fetus-in-fetu results from a modified process of twinning, and have traced a progression from normal twins to conjoined symmetrical twins, through parasitic fetuses and fetal inclusion, and finally to teratoma [10].

The main focus of controversy is whether fetus-in-fetu is a distinct entity or represents a highly organized teratoma. Du Plessis et al[16] reported an interesting patient with both a well formed fetus-in-fetu and a malignant teratoma, stating that that was “a potential triplet situation gone awry, resulting in the host, his parasitic twin and a teratoma arising from a third embryo which may have escaped the influence of a primary organizer”.

Willis [17] believes that teratomas originate from the early separation of a focus of multi-potential tissue in the growing embryo that develops in a chaotic way in the host organism. However, Spencer [6] has found out that the association of conjoined twins and their parasites with FIF, acardiacs, and teratomas was more frequent than could be attributed to chance. Therefore, he hypothesized that these anomalous fetuses form a continuum, strongly suggesting that they are all variations of abnormal conjoined twinning, with the site of union and the extent of damage (or defect) of one embryo resulting in (1) an externally attached parasitic twin, (2) an enclosed fetus in fetu, (3) an internal teratoma, or (4) an acardiac connected via the placenta. Common patterns among them are a family history of twinning, the predominance of females, and the frequent presence of a twin or triplet accompanying the malformation.

The several reports on chromosomal abnormality presumed that it is a genetically imperfect embryo that develops into a defective fetus. Of singular importance is the fact that rarely, if ever, is either a functional heart or a competent brain found in any of these abnormal fetuses, suggesting that the etiology of all of them is a primary cardiac malformation with secondary disruption in the development of the brain. Although this Spencer’s theories appear more encompassing, it cannot

explain why southwestern Nigeria with the highest rate of twinning in the world has no documented case of FIF*. Again, a case of FIF with a pulsating single chamber heart has been documented, which negate the primary acardiac theory [19].

Majority of authors who also admit that the origin of FIF is a monozygotic monochorionic diamniotic pregnancy shared the above theories. Some authors of recent believe FIF could derived from dichorionic diamniotic pregnancy in which the anomaly is related to defective implantation rather than an abnormal process of twinning [5, 7, 8]. According to Beaudoin et al [5] during implantation (second week of development) the second embryo (that becomes homunculus) may invade the extra embryonic mesenchyma of the other (the autosite) instead of the uterine wall and one or all of the following could happened. (1) primary gastrulation could occur normally in both leading to two primitive streaks, (2) the homunculus may fail to differentiate its own extra embryonic mesenchyma into cardiogenic zone leading to acardiac, (3) the inductors signal for the parasitic notochord may be disable by those of the surrounding host leading to absent axial skeleton and (4) some of the parasitic cell submitted to impaired induction may develop into teratomas or multiple fetiform structures as reported by some authors. This hypothesis, account for the various location of FIF in the host mesenchymal system and the different organ system differentiation of reported FIF.

Pathology and Presentation

The commonest presentation is an abdominal mass that is typically located in the upper retroperitoneum [2]. This is in contrast to teratomas that usually arise in the lower retroperitoneum. However, fetus-in-fetu has been reported to occur in other more unusual sites, such as within the cranium [20, 21], scrotum [22], oral cavity [23], liver [9], intrapulmonary[24], ovary[19] and mediastinum [5]. Other reported site include pelvis, cervical region, adrenal gland and within an undescended testis [25].

The majority of FIF are single although up to 5 fetuses have been found in the skull of a newborn [20] and Povysilova [21] reported a case of encranium containing [21] rudimentary fetuses in a premature boy.

The size of FIF varies. Cases of reported fetuses-in-fetu weighed between 13 grams [26] and 2000 grams [13]. The size of the fetus is likely to be related to its blood supply. Fetuses with distinct vascular connections to the host are relatively bigger with better developed features [2, 13, 15]. The absence of umblilical vessels and a definite vescular connection leads to growth retardation and arrest in organ system differentiation[1]. However, Kang et al [8] reported a monstrous FIF having a well-developed umbilicus, weighed 380g in a 3-month-old girl. It had four extremities, head, buttock, and vertebral bodies with a meningomyelocele. The thoracic cavity of the included fetus had only a saclike foregut structure, but the abdominal cavity revealed a full length of intestine with a Meckel diverticulum, bilateral ovaries, urinary bladder, and cloaca with external opening. The cephalic end was composed of well-developed tooth germs, tongue and buccopharynx, mandible, maxilla, sphenoid bone, and salivary glands. Thus include fetus is usually incomplete but nearly all body parts have been variably documented in various reported cases [8, 23]. Most are epencephalic and acardiac, which are consistent with both the ‘genetic imperfect embryo theory’ or the ‘defective implantation theory’.

In terms of attachment to the host, the fetus is typically suspended by a pedicle within a complete sac containing fluid or sebaceous material. There is usually no placenta or chorionic villi at the point of attachment to the host, though in one case primitive chorionic villi were seen[8, 19]. Definite vascular connections to the host are rarely described[2, 11, 13]. Heifetz et al [26] reported that the predominant blood supply appears to be derived from the plexus where fetus-in-fetu and the sac are attached to the host’s abdominal wall.

Symptoms of fetus-in-fetu relate mainly to its mass effect and include abdominal distension, feeding difficulty, emesis, jaundice, pressure effect on the renal system and dyspnoea[2,4,11,27]. Occasionally, the anomaly is asymptomatic [28]. de Langausie et al [29] reported signs of maceration with the threat of consumptive coagulopathy in their patient and Chua et al[1] reported the first case of FIF resulting in bilateral undescended testes.

Investigation

Radiological findings is the main stay of preoperative diagnosis of FIF. In reviewing the literature, most case reports up to 1980 showed that the preoperative diagnosis of FIF was made only in 16.7% of cases and in fact up to mid-1990s, fewer than a quarter of the cases were diagnosed prior to surgery[2,4] because Computed Tomographic (CT) and magnetic resonance imaging (MRI) scans were not performed. Both of which, have enhanced the accuracy of preoperative diagnosis[22, 30].

Plain X-rays remain an initial investigative modality of choice, with up to about half of the cases showing the presence of a vertebral column and axial skeleton[2, 17]. If, however, there is insufficient calcification it will be radiolucent on plain radiograph thus accounting for some of the non-demonstration of vertebral column by this modality in some instances [4]. The demonstration of vertebral column in accordance with Willis' theory [17], secures the diagnosis of FIF. However, review of the literature showed that in about 9% of cases of fetus-in-fetu, there was no vertebral column, even on pathological examination. The latter finding has led to another definition of FIF by Gonzalez-Crussi[31]. FIF is applied to any structure in which the fetal form is in a very high development of organogenesis and to the presence of a vertebral axis[31]. Federici et al [4] and Eng et al[15] proposed that in the presence of structures with an advanced grade of fetal organisation such as eyes, parts of the central nervous system, well-developed limb-like processes, skin and colon, the diagnosis of fetus-in-fetu can be applied, even in the absence of a real axial structure.

Ultrasounds, which is relatively cheap, readily available and have no known risk at diagnostic scan has offered some diagnostic potential at identification of FIF in both prenatal and later in life [9, 19-21, 27, 32]. Ultrasound have been used in the he Ex Utero Intrapartum Treatment procedure to secure the fetus's airway in a cervical FIF [27]. Khatib et al [32] made the earliest ultrasonic diagnosis at 16weeks gestational age. However, its operator dependency and the drawback of poor tissue characterization in the presence of fat and gas may limit its diagnostic accuracy.

These drawback of ultrasound are the advantages of CT in the investigation of FIF. Nocera et al[32] initially described the CT appearance of fetus-in-fetu. The CT findings are those of a mass that consisted of a round or tubular collection of fat that surrounded a central bony structure. CT might be of assistance particularly where a spinal column is so vestigial that it cannot be identified with certainty and yet other features of the mass would strongly suggest FIF. CT scans enhance the accuracy of preoperative diagnosis. The increasing use of ultrasound and CT has identified more and more cases [13]. The ability to diagnose fetus-in-fetu prenatal ultrasonography was first reported by Nicolini et al [32] in 1983 and since then has been found useful making appropriate prenatal counseling possible [9, 19, 32].

In recent years, magnetic resonance imaging MRI has been used to diagnose up to four cases of FIF including prenatal diagnosis [2, 30]. MRI allows imaging in the sagittal and coronal planes and does not rely on calcification for demonstrating the vertebrae. This helps in identifying insufficiently calcified vertebrae and vertebral axis [22]. Although there has been limited report on the use of MRI at diagnosing FIF, it seems to be an ideal technique for demonstrating the wide range of tissue within such lesions. With recent advancements in MRI, which have made faster scans possible and ultimately prenatal diagnosis in a moving fetus. Thus, MRI has the potential as imaging modality of choice for the diagnosis of fetus-in-fetu [22].

Differential diagnosis of FIF includes well differentiated teratoma, meconium pseudocyst with linear calcification[34], intraluminal meconium calcification[35] and mesenchymal harmatoma of the chest and abdominal wall[36] among others. According to Willis, the presence of an axial skeleton distinguishes a teratoma from a fetus-in-fetu[17].

Treatment

Complete excision of the surrounding membrane ensures definitive cure[1, 17, 23, 26, 28]. Hopkins et al [28] reported malignant recurrence following resection of a fetus-in-fetu. This was presumably caused by transformation of adherent membranes remaining at the surgical site. As a result of this, early and

frequent postoperative surveillance is recommended, especially if the sac cannot be completely resected. This may be achieved with moderate sensitivity using tumour marker concentration[28].

Prognosis

Majority of reported cases are benign hence FIF has good prognosis.

References

[1] Chua JHY, Chui CH, Sai Prasad TR, Jacobsen AS, Meenakshi A, Hwang WS. Fetus-in-fetu in the pelvis: report of a case and literature review. Ann Acad Med Singapore. 2005; 34: 646-649.

[2] Hoeffel CC, Nguyen KQ, Tran TT, Fornes P. Fetus-in-fetu: a case report and literature review. Pediatrics. 2000; 15: 1335-1344.

[3] Thakral CL, Maji DC, Sajwani MJ. Fetus-in-fetu: a case report and review of the literature. J Pediatr Surg. 1998; 33: 1432-4.

[4] Federici S, Ceccarelli PL, Ferrari M, Galli G, Zanetti G, Domino R. Fetus-in-fetu: report of three cases and review of literature. Pediatr Surg Int. 1991; 6: 60-65.

[5] Beaudoin S, Gouizi G, Mezzine S, Wann AR, Barbet P. Mediastinal fetus in fetu. Case report and embryological discussion. Fetal Diagn Ther. 2004;19:453-5.

[6] Spencer R. Parasitic conjoined twins: external, internal (fetuses in fetu and teratomas), and detached (acardiacs). Clin Anat. 2001;14:428-44.

[7] Gurses N, Gurses N, Bernay F. Twin fetuses in fetu and a review of the literature. Z. Kinderchir. 1990; 45: 319-322.

[8] Kang YK, Suh YL, Kim CW, Chi JG. Fetus in fetu: a case with complete umbilical cord and fetal sac. Pediatr Pathol. 1994;14: 411-9.

[9] Magnus KG, Millar AJ, Sinclair-Smith CC, Rode H. Intrahepatic fetus-in-fetu: A case report and review of the literature. J Pediatr Surg. 1999; 34:1861-4.

[10] Gross RE, Clatworthy HW. Twin Fetuses-in-fetu. J Pediatr. 1951; 38: 502-508.

[11] Dagradi AD, Mangiante GL, Serio GF, Musajo FG, Menestrina FV. Fetus-in-fetu removal in a 47-year-old man. Surgery. 1992; 112: 598-692.

[12] Khatib MO, Deschamps F, Couture A, Giacalone PL, Boulot P. Early prenatal ultrasonographic diagnosis of fetus in fetu J Gynecol Obstet Biol Reprod (Paris). 1998; 27: 438-40.

[13] Patankar T, Fatterpekar GM, Prasad S, Maniyar A, Mukherji SK. Fetus-in-fetu: CT appearance-report of two cases. Radiology. 2000; 214: 735-737.

[14] Boyce MJ, Lockyer JW, Wood CB. Fetus-in-fetu: Serological assessment of monozygotic origin by automated analysis. J Clin Pathol. 1972; 25: 793-798.

[15] Eng HL, Chuang JH, Lee TY, Chen WJ. Fetus-in-fetu: a case report and review of the literature. J Pediatr Surg. 1989; 24: 296-299.

[16] Du Plessis JPG, Winship WS, Kirstein JD. Fetus-in-fetu and teratoma. S Afr Med J. 1974; 48: 2119-2122.

[17] Willis RA. The borderland of embryology and pathology. 2nd ed. Washington DC Butterworths, 1966;2: 422-462.

[18] Brand A, Alves MC, Saraiva C etal. Fetus in fetu-diagnostic criteria and differential diagnosis: A case report and literature review. J Pediatr Surg. 2004; 39: 616-8.

[19] Kimmel DL, Moyer EK, Peale AR, Winborne LW, Gotwalss JE. A cerebral tumour containing five human fetuses: a case of fetus in fetu. Anat Rec. 1950; 106: 141-165.

[20] Povysilova V. Encranius with multiple rudimentary fetus in fetu in a premature boy. Cesk Patol.1983; 19:49-54.

[21] Sinha A, Sarin YK, Sengar M.Magnetic Resonance Imaging (MRI) in the Diagnosis of Fetus-in-fetu. Indian Pediatrics. 2003;40: 63-64.

[22] Senyuz OF, Rizalar R, Celayir S, Oz F. Fetus in fetu or giant epignathus protruding from the mouth. J Pediatr Surg. 1992; 27: 1493-1495.
[23] Neto EB, de Carvalho CM, Belo MT, Vieira AF, de Oliveira TB, Pereira MC, Leal GM, Branco MM. A rare case of intrapulmonary fetus-in-fetu. Rev Port Pneumol. 2005;11:321-5.
[24] Alpers CE, Harrison MR. Fetus in fetu associated with an undescended testis. Pediatr Pathol. 1985;4:37-46.
[25] Heifetz SA, Alrabeeah A, Brown BS, Lau H. Fetus-in-fetu: a fetiform teratoma. Pediatr Pathol. 1988; 8: 215-26.
[26] Woodard TD, Yong S, Hotaling AJ. The Ex Utero Intrapartum Treatment (EXIT) procedure used for airway control in a newborn with cervical fetus in fetu: a rare case. Int J Pediatr Otorhinolaryngol. 2006;70:1989-94
[27] Hopkins KL, Dickson PK, Ball TI, Ricketts RR, O'Shea PA, Abramowsky CR. Fetus-in-fetu with malignant recurrence. J Pediatr Surg. 1997; 32: 1476-9.
[28] de Lagausie P, de Napoli Cocci S, Stempfle N, Truong QD, Vuillard E, Ferkadji L, et al. Highly differentiated teratoma and Fetus-in-fetu: a single pathology? J Pediatr Surg. 1997; 32: 115-116.
[29] Coolen J, Bradshaw B, Bhargava R, Lees G, Demianczuk N. Fetus-in-fetu: confirmation of prenatal diagnosis with MRI. Prenat Diagn. 2007; 27: 73-6.
[30] Gonzalez-Crussi F. Extragonadal teratomas. Atlas of Tumour Pathology. 2nd ser., fasc. 18. Washington, DC: Armed Forces Institute of Pathology. 1982.
[31] Nicolini U, Dell'Agnola CA, Ferrazzi E, Motta G. Ultrasonic prenatal diagnosis of fetus-in-fetu. J Clin Ultrastruct. 1983; 11: 321-2.
[32] Nocera RM, Davis M. Hayden CK. Jr. Schwartz M. Swischuk LE. Fetus in fetu. AJR Am J Roentgenol. 1982; 138: 762-764.
[33] Khadaroo RG, Evans MG, Honore LH, Bhargava R, Phillipos E. Fetus-in-fetu presenting as cystic meconium peritonitis: diagnosis, pathology, and surgical management. J Pediatr Surg. 2000; 35: 721-723.
[34] Duncan AW. Quiz case: multiple calcifications of intraluminal meconium enterolithiasis. Eur J Radiol. 2001; 37: 120-122.
[35] Kim JY, Jung WH, Yoon CS, et al. Messenchymal hamartomas of the chest wall in infancy: radiologic and pathologic correlation. Yonsei Med J. 2000; 41: 615-622.

European Journal of Scientific Research
ISSN 1450-216X Vol.18 No.4 (2007), pp.674-679

http://www.eurojournals.com/ejsr.htm

The Splitting Technique for Resolution of the Transport and Biodegradation Problem in a Saturated Porous Media

S. A. Kammouri
Laboratoire de Calcul Scientifique, Ecole Superieure de Téchnologie, Fès, Maroc

M. El Hatri
Laboratoire de Calcul Scientifique, Ecole Superieure de Téchnologie, Fès, Maroc

Abstract

The present paper describes a numerical model, which allows to compute solute transport and biodegradation in a saturated porous media. Mathematical formulation of such processes leads to a set of non- linear partial differential equations coupled to ordinary differential equations. The transport equation is approximated by a finite volume scheme whereas biodegradation equations are treated separately as a system of ordinary differential equations. Numerical results for biorestoration using Monod kinetics are presented.

1. Introduction

Microbial biodegradation is one of the most promising technique for groundwater decontamination. It is a natural process that can be accelerated by the injection of certain nutrients such as dissolved oxygen, nitrates, and acetate.

Biological decontamination is physically and chemically complex involving transport of substrates, nutrients, microorganisms and interaction of components between the aqueous and the solid phase through adsorption and biodegradation.

In this study, we simulate biorestoration process in an homogeneous medium (a saturated aquifer). The mathematical model is a system of non-linear differential equations [2] that couple unstructured microbial growth kinetics with the transport of bioactive components in groundwater systems.

The numerical method implemented here is based on a splitting technique, which allows as to treat separately the different physical and chemical processes. The approach decouples the transport portion of the equations from the reaction portion, by first solving the transport problem which is approximated by a finite volume scheme. The concentrations obtained from this step are then used as the initial concentrations to solve the reaction equations which are treated as ordinary differential equations and are solved with a second –order, explicit Runge-Kutta method with time steps that are generally much smaller than those used for transport.

2. Mathematical Model

The general transport and biodegradation model for a single phase and incompressible flow is described by coupling non-linear partial differential equations. Here, for a solute undergoing linear instantaneous adsorption, we obtain the following system of equations [4]:

Transport-diffusion- and reaction of substrates:

$$R_i \frac{\partial(\theta_w C_i)}{\partial t} = \nabla(\theta_w D_{ci} \nabla C_i - \theta_w V C_i) + \mu_0 \left[\frac{C_i}{C_i + K_{ci}}\right]\left[\frac{N_i}{N_i + K_{ni}}\right] B \tag{1}$$

$$_i \frac{\partial(\theta_w N_i)}{\partial t} = \nabla(\theta_w D_{ni} \nabla N_i - \theta_w V N_i) + \mu_0 \left[\frac{C_i}{C_i + K_{ci}}\right]\left[\frac{N_i}{N_i + K_{ni}}\right] B \tag{2}$$

Development of bacteries:

$$_i \frac{\partial(\theta_w N_i)}{\partial t} = \nabla(\theta_w D_{ni} \nabla N_i - \theta_w V N_i) + \mu_0 \left[\frac{C_i}{C_i + K_{ci}}\right]\left[\frac{N_i}{N_i + K_{ni}}\right] B \tag{3}$$

Darcy's law:

$$\vec{V} = -\frac{K}{\mu(C)}(\nabla P - \beta(C))\vec{e_z} \tag{4}$$

The continuity equation:

For incompressible flow and if a source is present in the medium:

$$\nabla V = q \tag{5}$$

Where we denote:

C_i= The concentration of various substrates in solution.
N_i= The concentration of nutrients.
B=The concentration of various bacterial species.
K=The permeability tensor of the porous medium.
P=The pressure.
μ= The viscosity of the mixture.
β= The fluid density.
R_i=The retardation factor due to adsorption.
D_{ci}=The diffusion/dispersion tensor of substrates.
D_{ni}=The diffusion/dispersion tensor of nutrients.
μ_0=The maximum substrate utilization rate per unit mass of microorganisms.
K_{ci}=The substrates half saturation constant.
K_{ni}= The nutrients half saturation constant.
K_d=The substrates constant of decay.

In this model, the flow is governed by Darcy's law (4) and the continuity equation (5). A coupled system of parabolic advection-diffusion-reaction (1)-(2) describes adsorption, transport and removal of substrates C (contaminants) and nutrients N. Bacterial transport is neglected, microorganism growth and decay are then simulated by a set of coupled differential equations.

3. Numerical Method

The numerical resolution of the coupled system of equations (1)-(5) is achieved by a splitting procedure [3] which can be described in the following way.

The combination of Darcy's law (4) with the continuity equation (5) gives the following elliptic equation known as the pressure equation:

$$-\nabla\left(\frac{K}{\mu(C)}\left(\nabla P - \beta(C)\overrightarrow{ez}\right)\right) = q \tag{6}$$

So in the first step, knowing C at time t, we compute the pressure P on the center of all cells with the classical finite volume scheme. we consider a rectangular cell (control volume) Ω_{ij} of $\delta x \times \delta y$ size with $\partial\Omega_{ij}=\Gamma_{i+1/2,j}\cup\Gamma_{i-1/2,j}\cup\Gamma_{i,j+1/2}\cup\Gamma_{i,j-1/2}$("*Figure*1.").

Figure 1: Representation of a control volume Ω_{ij}

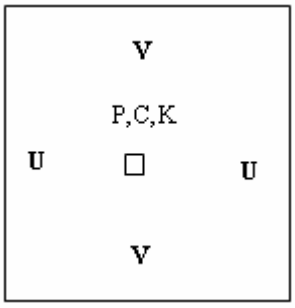

By integrating equation (6) on the cell Ω_{ij} and by green's formula, we get the discretized equation for pressure: (we denoted $\alpha=K/\mu(C)$)

$$\frac{\delta x}{\delta y}(\alpha_{i+1/2,j}(P_{i+1,j}-P_{i,j})-\alpha_{i-1/2,j}(P_{i,j}-P_{i-1,j}))+\frac{\delta x}{\delta y}(\alpha_{i,j+1/2}(P_{i,j+1}-P_{i,j})-\alpha_{i,j-1/2}(P_{i,j}-P_{i,j-1}))$$
$$=-\delta x((\alpha\beta)_{i,j+1/2}-(\alpha\beta)_{i,j-1/2})+\overline{q_{i,j}} \quad (7)$$

Equation (7) with the boundary conditions can be written as a system of equations of the form: AP=L. The resolution of this system enables as to determine the profile of pressure at each time.

Afterwards, Darcy velocities are calculated on the edge of the cells by utilizing equation (4). In a second step, advection-diffusion-reaction equations (1) and (2) are decoupled by time splitting method. A finite volume scheme is used to treat the transport equation. so, by integrating equation (1) without the kinetic term on the cell Ω_{ij}, and by green's formula we can write: (we assume that C is linear on each Γ_k)

$$\int_{\Gamma i+1/2,j} d^{11}\frac{\partial C}{\partial y}dy=\frac{\delta y}{\delta x}d^{11}_{i+1/2,j}(C^{n+1}_{i+1,j}-C^{n+1}_{i,j}) \quad (8)$$

$$\int_{\Gamma i+1/2,j} d^{12}\frac{\partial C}{\partial y}dy=d^{12}_{i+1/2,j+1/2}(C^{n+1}_{i+1/2,j+1/2}-C^{n+1}_{i+1/2,j+1/2})$$
$$+d^{12}_{i+1/2,j-1/2}(C^{n+1}_{i+1/2,j}-C^{n+1}_{i+1/2,j-1/2}) \quad (9)$$

Where d^{ij} are the coefficients of dispersion which are discretized on the control volume as it is shown in ("*Figure 2*.").

Figure 2: Discretization of dispersion coefficients

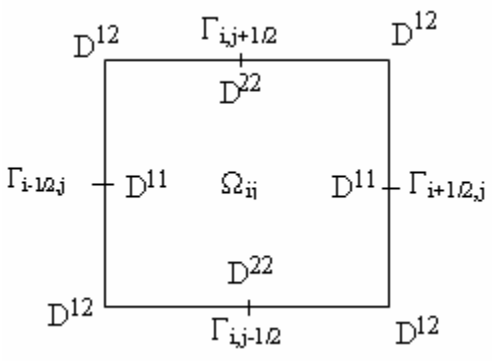

By utilizing the same procedure for the flux $H_{i+1/2,,j}$, $H_{i,j+1/2}$ and $H_{i,j-1/2}$, we get the following numerical scheme:

$$
\begin{aligned}
&C_{i,j}^{n+1} - \frac{\delta}{\delta x^2}\left(a^{11}_{i+1/2,j}\left(C^{n+1}_{i+1,j} - C^{n+1}_{i,j}\right) - a^{11}_{i-1/2,j}\left(C^{n+1}_{i,j} - C^{n+1}_{i-1,j}\right)\right)\\
&+\frac{\delta}{\delta y^2}\left(a^{22}_{i,j+1/2}\left(C^{n+1}_{i,j+1} - C^{n+1}_{i,j}\right) - a^{22}_{i,j-1/2}\left(C^{n+1}_{i,j} - C^{n+1}_{i,j-1}\right)\right)\\
&-\frac{\delta}{2\delta x\delta y}\left(a^{12}_{i+1/2,j+1/2}\left(C^{n+1}_{i+1,j+1} - C^{n+1}_{i,j}\right) - a^{12}_{i-1/2,j-1/2}\left(C^{n+1}_{i,j} - C^{n+1}_{i-1,j-i}\right)\right)\\
&+\frac{\delta}{2\delta x\,\delta y}\left(a^{12}_{i+1/2,j+1/2}\left(C^{n+1}_{i+1,j-1} - C^{n+1}_{i,j}\right) - a^{12}_{i-1/2,j+1/2}\left(C^{n+1}_{i,j} - C^{n+1}_{i-1,j+1}\right)\right) + \delta g\left(C^{n+1}_{i,j}\right) = C^{n+1/2}_{i,j}
\end{aligned}
\tag{10}
$$

The resolution of equation (10) as a system of equation of the form: AC=B enables as to obtain the profile of concentration at time t+δt/2.Finally, solving biodegradation equations by a forth order Runge-Kutta method using several small time steps gives the concentrations *C, N*, and *B* at time t+δt.

4. Application

In this section, we consider a rectangular mesh in a two dimensions space (a simplified aquifer) and we simulate biorestoration of a single organic component $C=C_1$ and of dissolved oxygen $O=N_1$ by microbes $B=B_1$ in such porous media. We suppose that the domain is homogeneous and isotropic, the flow is one-dimensional and steady state.

The initial conditions: *C (x, y, t=0)=0* on the domain

Boundary conditions : $C(0, y , t >0) = C_0$ *if...* $/y/ < a ... a \in \Re$.

The domain is semi –finite. *C (x, y, t)* is only defined down stern the sources.

Initially, non dissolved oxygen is present in the aquifer and a constant microbes concentrations of 10^{-4}mg/l is assumed. The initial distribution of substrate concentration at time t=500 days is shown *in*(“*Figure* 3.”).

Figure 3: The initial distribution of substrate concentrations at time t=500 days

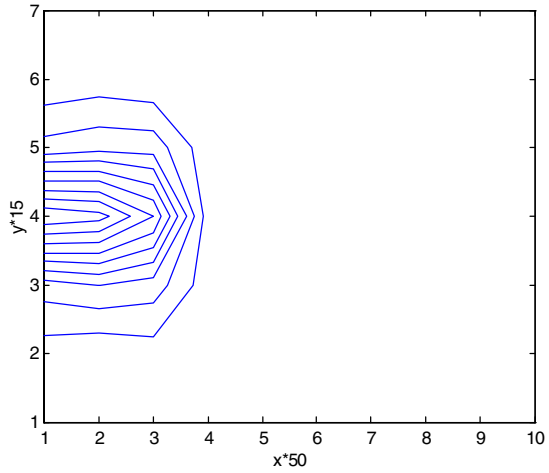

The biodegradation processes are then simulated by injecting 9 mg/l of dissolved oxygen at the inflow boundary. The biodegradation and transport parameters used in the simulation are [1]: $v=1.24m/d$, $R=1.5$, $D_l=50m^2/d$ $D_t=5m^2/d$, $K_c=0.07mg/l$, $K_0=2mg/l$, $\mu_0=0.6(d^{-1})$, $Y=0.2$, $F=1.5$, $K_d=0.1(d^{-1})$.

In "*Figure 4*" , we plot the substrate distribution after 500 days of biorestoration.

Figure 4: The distribution of substrate concentrations after 500 days of biorestoration

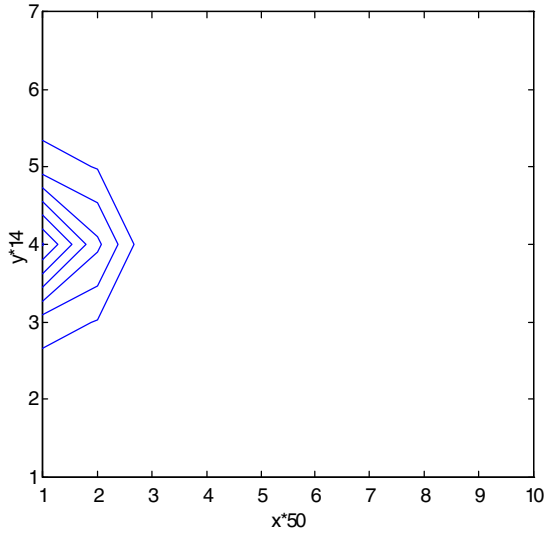

The second test consists on stimuling the microbial activities, so we inject in the domain from the inflow boundary 40 mg/l of oxygen. "*Figure 5*." Show the substrate concentrations after 500 days of pollution.

Figure 5: The distribution of substrate after 500 days of biorestoration with the injection of 40 mg of oxygen.

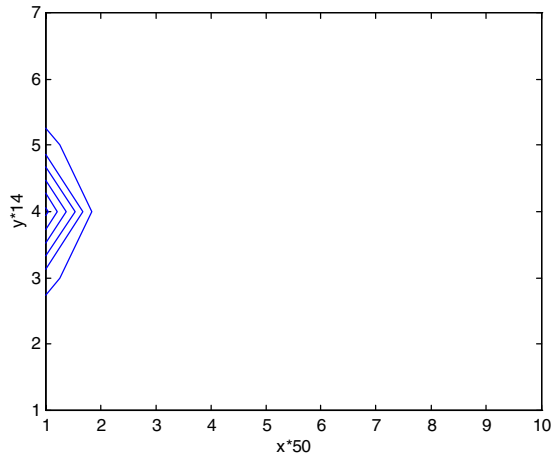

4. Conclusions

The whole numerical method using splitting technique enables us to treat separately the different physical and chemical processes. The discretization of the transport equation by a finite volume scheme is very efficient as it is shown on the various difficult tests presented. The biodegradation equations are treated as a system of ordinary differential equations using a forth order-Runge-Kutta method, which is too restrictive for time step. The biodegradation needs to be approximated on mush smaller time scale than the advection and the dispersion.

References

[1] M.A.Celia, J.S.Kinred, and I.. Herrera. (1989) Contaminant transport and biodégradation, 1. A numerical model for reactive transport in porous media, Water resour. Res.25, pp.1141-1148.

[2] C.H.Chiang, C.N.Dawwson, and M .F. Wheeler. (199 1) Modeling of in-situ biorestauration of organic compounds in Groundwater,Transport in porous media, 6, pp.667-702.

[3] C.N.Dawson, and M.F. Wheeler. (1991) Time-splitting methods for advection-diffusion-réaction équations arising in contaminant transport, ICIAM.

[4] B.D.Wood, C.N.Dawson, and G.P.Streile. (1994) Modeling contaminant transport and biodegradation in a layered porous media system, Water resources research, Vol. 30, NO.6, pp.1833-1845.

European Journal of Scientific Research
ISSN 1450-216X Vol.18 No.4 (2007), pp.680-688

http://www.eurojournals.com/ejsr.htm

Socio-Economics and Child-Bearing Characteristics of Young Adults in Jamaica

Tazhmoye Crawford
Department of Basic Medical Sciences, Faculty of Medical Sciences
University of the West Indies, Kingston 7, Jamaica
E-mail: crawfordtazhmoye@yahoo.co.uk
Tel: (876).362.3628

Donovan McGrowder
Department of Pathology, Faculty of Medical Sciences
University of the West Indies, Kingston 7, Jamaica

Michael Gardner
Department of Basic Medical Sciences, Faculty of Medical Sciences
University of the West Indies, Kingston 7, Jamaica

Lorenzo Gordon
Department of Medicine, Faculty of Medical Sciences
University of the West Indies, Kingston 7, Jamaica

Abstract

In Jamaica the family usually provides its members with support, livelihood and security. The traditional Jamaican family has been undergoing a profound transformation which includes higher educational achievement among women, fewer adults getting married, more children born out of wed-lock and an increase in single-parent households headed by women. This paper investigates the socio-demographic and economic variables of young adults (20 – 35 years old) in Jamaica. As part of a survey, data on the socio-demographic and child-bearing characteristics was assessed using a 56-item questionnaire of 213 randomly selected young adults (from the 14 parishes in Jamaica) attending two major public hospitals. Data on the level of educational attainment indicate that the majority of the respondents (75.0% women and 66.4% men) had achieved secondary education, followed by tertiary education (23.9% women and 8.8% men). The difference in educational achievement between women and men was statistically significant (χ^2 = 27.89, $p < 0.05$). The majority of women were permanently employed (39.8%) followed by those temporarily employed (29.5%) and seasonally employed (13.6%). This in contrast to the men where a greater proportion was temporarily employed (46.4%), followed by permanently employed (25.6%) and seasonally employed (16.0%). The majority of the respondents who had 4 to 6 children were permanently employed (47.6%), and those with 7 – 9 children were among the temporarily (44.7%) and permanently employed groups (50.0%). Most of the respondents with children were educated at the secondary level, and the number of children produced varied with the frequency of sexual activity, except for those who had 7 - 9 children. The number of children produced by Jamaican young adults

is high, although women are having fewer children than men. Individuals with more secured jobs, who had secondary and tertiary education, produced more children.

Keywords: Socio-economic, Childbearing, Young adults, Poverty, Jamaica

Introduction

The achievement of an acceptable level of education for children, young people and adults, is of one of the challenges facing developing countries in the 21st century. Education has proven to be an important key factor in the promotion of family well-being. It provides one of the surest paths to increasing an individual's chance of full participation in society including secured employment. Employment is an important link between increasing an individual's sense of citizenship, social inclusion, socio-economic mobility and the capacity to obtain food, shelter, clothing etcetera. Parents and other caregivers require certain economic resources to provide their children with proper nutrition, adequate housing, and sufficient health care. Numerous studies have shown that the education of women has a profound and positive effect upon family welfare (Hassan & Yasmeen, 1995).

Women and children are vulnerable to poverty and the majority of them live in rural and inner city areas with no education or skills. Poverty is a significant factor in the exchange of sexual favours for material gains and in many cases young women because of the situation of poverty tend to engage in illicit relationships with older men (Orubuloye et al., 1992). Poverty increases the vulnerability of women to sexually transmitted infections including HIV/AIDS through unsafe sexual practices, often due to lack of knowledge, lack of access to means of protection, and inability to negotiate condom use with sexual partners as a result of entrenched gender roles and power relations (Giles *et al.,* 1996).

Poverty is widespread in Jamaica, with 18.7% of the population living below the poverty line (World Bank, 2002). Lower socio-economic status and/or lower level of educational attainment is well recognized as generally associated with risky sexual behaviours (Figueroa et al., 1999). Early sexual activity, combined with a lack of relevant information, services, and skills to avoid risky situations, place Jamaican adults at risk of unintended pregnancies, sexually transmitted infections (STIs) including HIV, and other threats to their sexual and reproductive health (Ministry of Health, 2001).

This paper investigates socio-demographic and economic variables of young adults in Jamaica. The socio-medical variables include frequency of sexual activity, living conditions, the number of children produced, education, occupational and economic status and number of meals consumed per day. The study also investigated possible relationship between the number of children produced and education, occupational status, and frequency of sexual activity.

Materials and Methods

Data was collected as part of a survey about sexual activity and behaviour among young adults in Jamaica by the authors of this paper. The descriptive survey research method was employed for the study and field work was conducted between February and April, 2005. A standardized, structured questionnaire with close-ended questions captured socio-demographic and reproductive health information. The sample consisted of a total of two hundred and sixty five respondents from the 14 parishes in Jamaica who visited two public hospitals. Two hundred and sixty five questionnaires were distributed by medical professionals on duty. Two hundred and thirteen were satisfactorily completed and used in the analysis of this paper, representing a response rate of 80.4%. The respondents resided in various communities throughout the 14 parishes of the island, and represented a wide category of occupational and educational status. The authors were therefore able to capture a wider range of responses than if any one community was targeted. Adult males and females aged 20 – 35 were targeted. Pregnant women and persons of unsound minds were excluded from the study.

All questions were contained in the 4-page (56 questions) self-administered questionnaire. Respondents filled out the questionnaire themselves and placed it in a sealed envelope that was

collected by the medical professionals. The first part of the questionnaire contained questions on the socio-demographic data of the respondents, while the second contained questions which tested their sexual activities. Standard socio-demographic measures included age, sex, marital status, and educational level. In terms of sexual experience, respondents were asked whether they were sexually experienced, and whether they had sexual intercourse in the last 12 months. One questionnaire item asked respondents to indicate how often they had sexual intercourse in the last 12 months with primary and non-primary partners. For this item, three response category was given - daily, more than once per week and once per month. The paper examines the relationship between the number of children, occupational and educational status. In determining the non-financially viable group, this paper captured the respondents who were unemployed and not receiving monetary gifts on a regular basis. Also, in this category were those who were employed, but earned less than US$15.63 per week. The Statistical Package for Social Scientists (SPSS, Chicago, IL) was used to analyze the data. Both bivarate (chi square) and multivariate (logistic regression) analyses were used to examine the data.

Results

A total of 213 out of the 265 questionnaires distributed to the adults satisfactory completed and selected, having met the criteria for the study. Of the 213 respondents, 88 were women and 125 were men. Of the women in the sample, 4.5% was in the age group 20 – 24; 27.3% in the age group 25 – 29 and 68.2% in the age group 30 – 35. Of the men in the sample, 1.6% was in the age group 20 – 24; 17.6% in the age group 25 – 29 and 82.4% in the age group 30 – 35. Of the respondents, a similar proportion of women (75.0%) and men (76.8%) were married. Data on educational attainment indicate that the majority of the respondents (75.0% women and 66.4% men) had achieved secondary education; followed by tertiary education (23.9% women and 8.8% men); elementary education (19.2% men) and primary education (1.1% women and 5.6% men). The difference in educational attainment between men and women was statistically significant ($\chi^2 = 27.89$, $p < 0.05$). The majority of women were permanently employed (39.8%) followed by the temporarily employed (29.5%) and seasonally employed (13.6%). This in contrast to the men whereby a greater proportion was temporarily employed (46.4%), followed by those permanently employed (25.6%) and seasonally employed (16.0%). Based on the our assessment of the respondent's socio-economic status, 35.2% of women and 46.4% of men found to be of the lower economic class (< US $ 62.48/week), 48.9% women and 33.6% men of lower middle economic class (US 62.48 – US $109.36/week), and 15.9% of women 20.0% of men of the upper middle or upper economic class (> US $109.36/week).

Table 1: Socio-demographic characteristics of respondents

Variables	Men (n = 125)		Women (n = 88)	
	No.	%	No.	%
Age (years)				
20 – 24	2	1.6	4	4.5
25 – 29	22	17.6	24	27.3
30 – 35	103	82.4	60	68.2
Marital Status				
Legally Married	96	76.8	66	75.0
Unmarried	29	23.2	22	25.0
Educational Attainment				
Elementary	24	19.2	0	0.0
Primary	7	5.6	1	1.1
Secondary	83	66.4	66	75.0
Tertiary	11	8.8	21	23.9
Occupation				
Unemployed	8	6.4	7	8.0
Self employed	7	5.6	8	9.1
Seasonally employed	20	16.0	12	13.6
Temporary employed	58	46.4	26	29.5
Permanently employed	32	25.6	35	39.8
Number of children				
0	0	0.0	25	29.8
1 – 3	12	9.6	39	46.4
4 – 6	64	51.2	6	7.1
7 – 9	24	19.2	14	16.7
10+	25	20.0	0	0.0

The majority of women in the study lived in the inner-city areas (51.1%) in houses with 2 – 4 bedrooms (68.2%) and with 5 – 9 occupants (65.9%). They had 1 - 3 children (46.4%) and eat 1 meal per day (47.7%; Table 2). All of female respondents were sexually experienced, the majority had sex more than once per week (76.1%) followed by daily (23.0%) and once per month (21.6%). Similarly, majority of the men lived in inner-city areas (61.6%) in houses with 2 – 4 bedrooms (88.0%) and with 5 – 9 occupants (88.0%). They had 4 - 6 children (51.2%) and eat 1 meal per day (42.4%). None of the respondents who reside in a 1 bedroom house had 5 or more members. Similarly none of the respondents who had 2-4 bedrooms had 10 or more members per households. All of the men were sexually experienced, the majority had sex daily (49.6%) followed by once per week, and once per month (32.6 and 17.6% respectively).

Table 2: Socio-economic and frequency of sexual activity of respondents

Variables	Men (n = 125)		Women (n = 88)	
	No.	%	No.	%
Current Income				
< US$ 15.63/week	23	18.4	0	0.0
US 15.63 – US $ 62.48/week	35	28.0	31	35.2
62.48 – US $109.36/week	42	33.6	43	48.9
> US $109.36/week	25	20.0	14	15.9
Number of persons in households				
< 5	15	12.0	16	18.2
5 - 9	110	88.0	58	65.9
10 - 14	0	0.0	14	15.9
Number of bedrooms				
< 2	15	12.0	13	14.8
2 - 4	110	88.0	60	68.2
5+	0	0.0	15	17.0
Area of residence				
Inner-city	77	61.6	45	51.1
Rural	27	21.6	8	9.1
Residential	21	16.8	35	39.8
Number of meals per day				
Sometimes none	2	1.6	1	1.1
1	53	42.4	42	47.7
2	39	31.2	20	22.7
3 or more	31	24.8	25	28.4
Frequency of sexual intercourse				
Daily	62	49.6	2	23.0
Once per week	41	32.8	67	76.1
Once per month	22	17.6	19	21.6

Table 3 shows no relationship between an individual's occupational status and the number of children they produced. Majority of the respondents who had 4 to 6 children were permanently employed (47.6%). This bears no significant difference between those who had no children and were permanently (44.8%) and temporarily employed (41.4%). The majority of respondents with 7 – 9 children were among the temporarily (44.7%) and permanently employed groups (50.0%), whilst those with more than 10 children were also permanently employed (40.0%). Respondents with no children were among those who were unemployed (6.1%) and self employed (3.1%).

Table 3: The number of children and occupational status

Occupation status					
Number of children	**Unemployed**	**Self-employed**	**Seasonally employed**	**Temporary employed**	**Permanently employed**
0	2	1	1	12	13
	6.9%	3.4%	3.4%	41.4%	44.8%
1-3	11	7	5	14	8
	24.4%	15.6%	11.1%	31.1%	17.8%
4-6	0	1	19	24	40
	0.0%	1.2%	22.6%	28.6%	47.6%
7-9	2	0	0	17	19
	5.3%	0.0%	0.0%	44.7%	50.0%
10+	2	6	7	14	6
	5.7%	17.1%	20.0%	40.0%	17.1%

In Table 4, most of the respondents with children were educated at the secondary level. Respondents with secondary education had: none (58.6%), 1 – 3 (77.8%), 4 – 6 (72.6%) and more than

10 (88.6%) children. The majority of respondents having 7 – 9 children had tertiary level education. The number of children produced varied among the frequency of sexual activity, except in the case of those who had 7 - 9 children (Table 5). The majority of the respondents who had sex at least once per week none (88.0%), 1 – 3 (70.6%) and 4 – 6 (47.1%); compared to those who had sex daily with more than 10 children (52.0%), and once per month with 7 – 9 children (39.5%). There were no respondents who had sex once per month and had 10 or more children.

Table 4: Number of children for both men and women and their level of education

	Education status			
Number of children	**Elementary**	**Primary**	**Secondary**	**Tertiary**
0	0	0	17	12
0.0%	0.0%	58.6%	41.4%	
1-3	0	1	35	9
0.0%	2.5%	77.8%	20.0%	
4-6	13	7	61	1
15.5%	8.3%	72.6%	1.2%	
7-9	7	0	5	8
35.0%	0.0%	25.0%	40.0%	
10+	2	0	31	2
9.1%	0.0%	88.6%	5.7%	

Table 5: Number of children and frequency of sexual activity

	Frequency of sexual activity		
Number of children	**Daily**	**Once per week**	**Once per month**
0	2	22	1
8.0%	88.0%	4.0%	
1-3	11	36	4
21.6%	70.6%	7.8%	
4-6	5	33	32
7.1%	47.1%	45.8%	
7-9	9	14	15
23.7%	36.8%	39.5%	
10+	13	0	12
52.0%	0.0%	48.8%	

Discussion

These findings indicate that the number of children produced bears a relationship with educational status of the parents. Majority of the children produced were from individuals who were educated at the secondary followed by the tertiary level. With the exception of tertiary level of attainment, increased education is associated with increased number of children produced. The reasons for the number of children produced among the various literacy groups were expansion of generation; the fear that oral contraceptive could damage their health, security of relationship; the more 'baby-fathers' the more money for child support; ignorance, a show of manhood; not wanting to be referred to as being barren and specific religious reasons. In addition, factors that influence young adult child-bearing rates include public perceptions of the social and economic costs of childbearing, societal attitudes and openness regarding sexuality and the ease of access of information and services (Fu *et al.,* 1999).

There were more women in the study with secondary and tertiary education than men. In Caribbean countries such as Jamaica, there have been increasing proportions of women with secondary and tertiary education resulting in a greater likelihood that they will delay entry into first unions and the onset of pregnancy. However, increased education and the mass media can offer people new information and ideas, and greater opportunities, but the media can also present poor and young people with visions of commercialism and modern lifestyles that are way beyond their reach. In rural areas,

the desire to have a greater number of children among uneducated women is consistent with the notion that children are a source of wealth, thus adding value to the household economy as a result of their potential contribution in agricultural settings. In general, households below the poverty line tend to be larger, headed by females who are often single mothers with dependent children, or contain at least one elderly person living alone or in an extended family setting sometimes having responsibility for the entire household (St. Bernard, 2001). Therefore, although educational attainment is increasing in developing countries such as Jamaica, job prospects are not improving at the same pace, and large proportions of young adults cannot find full-time paying jobs.

The Jamaica Survey of Living Conditions, reported declines in mean household size from 3.9 in 1992 to 2.4 in 2002 in Jamaica (PIOJ and STATIN, 2003). Such findings are consistent with an inverse relationship between socioeconomic status and household size, with the richest quintile estimated to have a mean household size of 2.26 and the poorest quintile a mean household size of 5.23 persons. The average household size in 2001 was 3.4, with rural households continuing to be slightly larger with an average size of 3.7 persons. Households headed by females (3.6) and those in the poorest consumption group (5.23) were also larger than the national average, and findings also shows that women head 44.9 per cent of Jamaican households compared to 42.1 in 2000 (PIOJ and STATIN, 2003).

In this study, most of the young adults lived in houses with 2 – 4 bedrooms having 5 – 9 occupants. In Jamaica, men play important roles as heads of households, custodians of the interests of their lineage, protectors and providers of their families. They are the lead decision-makers on matters pertaining to the family life. More so, the social and economic dependence of wives gives men great influence in the household, a position that is strengthened by an organized family structure. However, there is the continued high incidence of female-headed households which has emerged as an accepted social fact in Jamaica. These households are more likely to be larger, possess more children and be in the lowest consumption quintile. Some 72.0 per cent of households headed by women have no spouse, as compared to those headed by men, which have spouses in 70.0 per cent of cases. This implies that the majority of women in these households are rearing children without the presence of a partner in the home (PIOJ and STATIN, 2001). There is evidence to suggest that children reared in households with two parents have greater advantages than children in other family formations (van Poppel, 2000). While some of this research is inconclusive, there is enough evidence to suggest a need for a programme of investigation, establishing the full impact of the high incidence of single parenting on child outcome and by extension national development. There is also a need for more policy research on the full implications of this for social and economic development.

Approximately 18 percent of the respondents who were all men were considered poor, and a large proportion of both men and women lived in inner-city areas. In Jamaica, the incidence of poverty decreased in 2005, moving to 14.8 per cent from 116.9 per cent in 2004 (PIOJ and STATIN, 2006). Rural Areas experienced a decline to 24.1 per cent from 25.1 per cent in 2000. For the Kingston metropolitan Area and Other Towns, the incidence of poverty was 7.6 per cent and 13.3 per cent, moving from 9.9 per cent and 16.6 per cent, respectively for 2000. The decline in 2001 comes after two consecutive years of increase in the incidence of poverty and continues a decreasing trend since 1991. The extent of poverty in the rural areas is reflected by the fact that despite an almost 17.0 per cent increase in per capita consumption for the region in 2001, the incidence of poverty declined by only 1.0 per cent. This could be the result of two main factors such as the depth of poverty (the poverty gap) i.e. the extent to which consumption of the poor actually falls below the poverty line, and the distribution of the increase in consumption. If the overall increase were pushed by increase in consumption in the higher consumption groups, its impact on poverty levels would be minimal (PIOJ and STATIN, 2002).

Poverty, deprivation, and unemployment work with gender relations to promote change of partner, con-currency, and unprotected sex (Blankenship et al., 2006). In this study, 6.4% of men and 8.0% of women were unemployed, and all the respondents were sexually active in the 12 months prior to answering the questionnaire. The rate of unemployment in Jamaica was recorded as 15.5% for men

in 2000, which is twice as high for women (Ministry of Health, 2005). Poverty and poor work prospects can undermine men's traditional roles as providers and can make them fatalistic about the consequences of risky behaviour. Urbanization can weaken the supports of traditional community life, especially when it separates poor men from their families, but it can also create the desire for smaller families. Economic adversity restricts the power of men and women to take control of their health, deprivation and unemployment might drive men and women to sell sex (Simon and Paxton, 2004). This risky sexual behaviour exposes men and women to contracting STIs including HIV/AIDS.

The majority of the respondents were married. Cultural, social, religious, economic and many other factors may influence and determine the patterns and prevalence of unprotected sex outside of mutually monogamous sex relationships. These different patterns, as well as, major differences in the proportion of the 15 – 49 year old population who regularly engage in such risky sexual behaviours are of paramount importance in determining the extent of HIV transmission that may occur in any specific heterosexual population. Poverty is known to increase people's vulnerability to STIs including HIV/AIDS because it reduces their access to information services, and commodities for HIV prevention, treatment, and cure. In order to finance their basic needs, poor persons may engage in specific high-risk behaviours such as having unprotected sex with individuals whose sero-status is unknown. In Jamaica, women might be disadvantaged in protecting their sexual health if their partner is older than they and of higher social status (Bajos and Marquet, 2000). Gender roles and inequalities such as female subservience in sexual decision-making influences behaviour choices and facilitate the spread of HIV (Bassett & Sherman, 1994).

In this study more men have 4 – 6 children while more women have 1 – 3 children. Jamaica's total fertility has been steadily declining since the 1970's. Many young adults 15 – 24 are in school or acquiring job-related training and work experience, and most still live with their family. Searching for sexual pleasure and intimacy to prove they are adults, men commonly begin their sexual lives during adolescence. Contraceptive use among young men at first intercourse rose from 21.6 percent in 1993 to 43% in 2002 (Population Reference Bureau, 2006). In spite of this progress, the adolescent fertility rate in Jamaica is the highest in the English-speaking Caribbean at 112 births per 1,000 women ages 15 - 19. More than 3 out of 4 pregnancies are still unplanned among women 15 - 25 years old. Approximately 40 percent of Jamaican women have given birth at least once before they each the age of twenty (Ministry of Education, Youth and Culture, 2003).

There are some limitations which may have impacted on the findings. The questionnaire had a few number sex-related, and a number of personal socio-demographic items. Surveys with sensitive issues are likely to contain some bias. Intentional misreporting, incomplete recall, and misunderstanding of survey questions could reduce both the reliability and the internal validity of the data.

In summary, the number of children produced by Jamaican young adults is high, although women are having fewer children than men. Persons who had frequent sexual encounters do not necessarily produce more children than those who were rarely or moderately active. Individuals with more secure jobs, who had secondary and tertiary education, produced more children.

References

[1] Bajos N, Marquet J (2000). Research on HIV sexual risk: social relations-based approach in a cross-cultural perspective. Soc Sci Med 50: 1533 – 1546.

[2] Bassett, M. and Sherman, J (1994). Female Sexual Behaviour and the Risk of HIV Infection: An Ethnographic Study in Harare, Zimbabwe. Women and AIDS Program Research Report Series, Washington DC: International Center for Research on Women.

[3] Blankenship KM, Friedman SR, Dworkin S, Mantell JE (2006). Structural interventions: concepts, challenges and opportunities for research. J Urban Health 83: 59–72.

[4] Figueroa JP, Fox K, Minor K (1999). A behaviour risk factor survey in Jamaica. West Indian Medical Journal 28: 9 – 15.

[5] Fu H, Darroch JE, Haas T and Ranjin (1999). Contraceptive failure rates: new estimates from the 1995 National Survey of Family Growth. Family Planning Perspectives.

[6] Giles PP, Tolley K, Wolstenholm J. Is AIDS a disease of poverty? (1996). AIDS Care 8: 351 – 363.

[7] Hassan, Yasmeen (1995). The Haven Becomes Hell Lahore, Pakistan: Shirkat Gah.

[8] Ministry of Health (2001). National HIV/STI Prevention & Control Programme,: Sexually Transmitted Infection (STI) Control Programme Annual Reports for 1993 to 2000.

[9] Ministry of Health (2005). Draft National HIV/AIDS Policy Jamaica, April 2005.

[10] Ministry of Education, Youth & Culture (2003). National Centre for Youth Development, National Youth Policy: Jamaican Youth Sharing the World. Kingston: NYCD.

[11] Orubuloye IO, Caldwell JC, Caldwell P (1992). Diffusion and focus in sexual networking: Identifying partners and partners. Health Transition Working Paper No. 11, National Centre for Epidemiology and Population Health, The Australian National University.

[12] PIOJ and STATIN (2001). Jamaica Survey of Living Conditions 2001. Planning Institute of Jamaica and Statistical Institute of Jamaica.

[13] PIOJ and STATIN (2002). Jamaica Survey of Living Conditions 2001. Planning Institute of Jamaica and Statistical Institute of Jamaica.

[14] PIOJ and STATIN (2003). Jamaica Survey of Living Conditions 2002. Planning Institute of Jamaica and Statistical Institute of Jamaica.

[15] PIOJ and STATIN (2006). Jamaica Survey of Living Conditions 2001. Planning Institute of Jamaica and Statistical Institute of Jamaica.

[16] Population Reference Bureau B (2006). The World's Youth 2006 Data Sheet. Washington, DC: PRB.

[17] Simon S, Paxton SJ (2004). Sexual risk attitudes and behaviours among young adult Indonesians. Cultural Health Sex 6: 393 – 409.

[18] St. Bernard, G (2001). Demographic characteristics and living arrangements in Commonwealth Caribbean in Caribbean Families in Britain and The Trans- Atlantic World, edited by Harry Goulbourne and Marry Chamberlain, Macmillan Education Limited: London and Oxford.

[19] van Poppel F (2000). Children in one-parent families: Survival as an indicator of the rule of the parents. Journal of Family History 25(3): 269 – 290.

[20] World Bank, Jamaica (2002). HIV/AIDS Prevention and Control Project (second phase of the multi-country HIV/AIDS prevention & control APL for the Caribbean), Washington DC: World Bank.

European Journal of Scientific Research
ISSN 1450-216X Vol.18 No.4 (2007), pp.689-699

http://www.eurojournals.com/ejsr.htm

Distribution of Mn in the Fruits and Wild Flora of Winder Area, Balochistan, Pakistan and its Impact on Human Health

Shahid Naseem
Department of Geology, University of Karachi, Karachi, Pakistan
E-mail: sngeo@yahoo.com
Tel: +92-300-2629759

Salma Hamza
Department of Geology, Federal Urdu University of Arts Science and Technology, Karachi, Pakistan

Erum Bashir
Department of Geology, University of Karachi, Karachi, Pakistan

Salman Ahmed
Center of Excellence in Marine Biology, University of Karachi, Karachi, Pakistan

Abstract

A number of fruit farms are present in the vicinity of Winder Town, Balochistan. Geologically, these farms are situated over the ophiolitic rocks of Cretaceous age in association with sedimentary rocks. The Quaternary sediments concealed the Bela Ophiolite. The soil derived from the weathering of these rocks provides good source of Mn in the area. Five fruits and 3 wild flora have been selected from different localities of Winder to estimate content of Mn in the twigs. The result reflects high Mn concentration in the fruits and wild flora, grown close to the ophiolite. The comparative study revealed high absorption of Mn in the twigs of *Salvadora oleoides*, a wild flora and in the guava fruit (*Psidium guajava*). The possible causes of variation in the Mn content from different localities have been demonstrated in the light of pillow basalt, soil chemistry, mobility of element and average abundance in the plants. The role of Mn in plants and its influence on human health have also been discussed.

Keywords: Balochistan, Bela Ophiolite, flora, human health, manganese, Pakistan, Winder

1. Introduction

Manganese is one of the minor elements of earth crust whose concentration is about 0.095 %. Manganese is the most abundant metal in soil, where it occurs as oxides and hydroxides (Albarede, 2003). It also acts as essential trace biophile element. It is required for the healthy growth of plants and the animals. The human consumption of Mn is mainly by food: such as fruits and vegetables. After absorption in the human body Mn will be transported through the blood to the liver, the kidneys, the

pancreas and the endocrine glands (Udayakumar and Begum, 2004). Deficiency and excess of Mn will affect on the health of human being, which ultimately cause mild to severe illness (Nergis et al., 2005).

Medical Geology started as a new discipline in 1998, since then medical geology has grown tremendously (Finkelman, et al., 2001). Initial work started in Scandinavian countries (Lag, 1983). Medical Geology deals with the effects of geological environment on human health and to explore preventative methods for improvement (Komatina, 2004). The present work is related to Medical Geology. The purpose of this study is to elaborate the distribution of Mn in rock-soil-water-vegetation and its impact on human health.

Present study carried out on the fruit farms and wild flora in the vicinity of Winder Town. The study area has a variety of native flora e.g. *Acacia nilotica, Tamarix aphylla, Salvadora oleoides* and *S. persica*. Among the fruit plants *Achras zapota* (Cheeko), *Mangifera indica* (Mango), *Syzygium cumini* (Jambolin), *Tamarindus indica* (Tamarind), *Psidium guajava* (Guava) and *Ziziphus jujuba* (Jujuba) are common. The study area lies on the southern tail of Bela Ophiolite. Pillow basalt in association with pelagic sediments is exposed in the area (Naseem et al., 2002). Sedimentary rocks ranging in age from Jurassic to Cretaceous are also exposed in the adjoining Mor and Pab ranges (Fig. 1). The Mn-bearing soil is derived from the weathering of these igneous and sedimentary rocks. Plants uptake Mn from soil and store it in the twigs of fruits and wild flora of the study area.

Illness due to elemental deficiency and excess of Mn are very common along with a number of infectious diseases (Nergis et al., 2000). Karachi is the neighbouring city of winder, having population more than 15 millions. The people of Karachi city are the main consumers of these fruits and are affected by the concentration of Mn. Present study discusses the availability of Mn in the soil, transmit and storage in the twigs of fruit and wild flora. The impacts of Mn on human body and possible health hazards are also discussed.

Figure 1: Satellite image of the study area showing exposure of rock types. Sampling sites are referred by numbers.

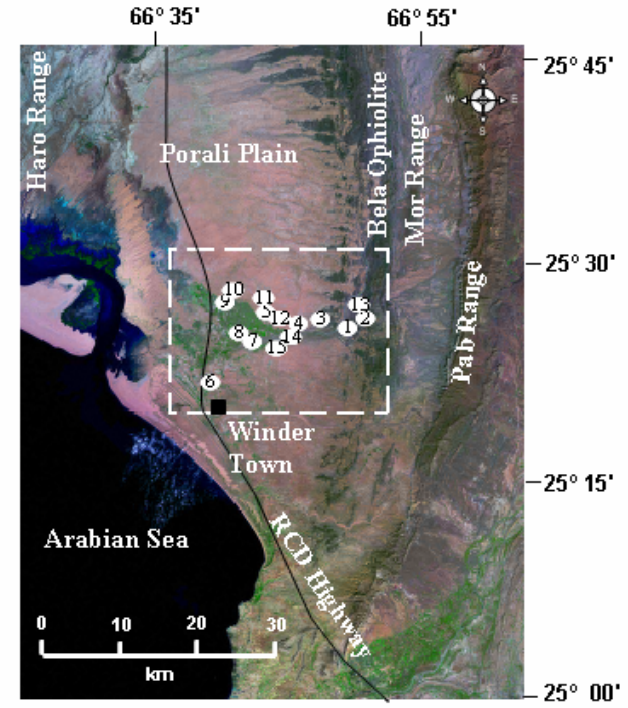

2. Sampling and Analytical Methods

Twigs of different fruit plants and wild flora were collected in the vicinity of Winder Town, Balochistan. Their locations are marked on the satellite image (Fig. 1) and other details are given in Table 1. Twigs are preferable for analysis because metal content of the mature twigs does not vary appreciably through the growing seasons, in contrast to the fruits, leaves, needles or other parts of plants. Furthermore, twigs samples are easier to collect and process than samples of barks or wood (Brooks, 1972). The samples were first washed with distilled water to remove external impurities such as dust, fungus and automobile exhaust. Then they were dried in a well-ventilated covered place for about 3 weeks. Twigs were ashed as recommended by Brooks (1972) and Martin et al. (1996). One gram of air-free ash was treated with concentrated perchloric and nitric acids at a ratio of 7:3. After heating to dryness the residue was leached with 6M nitric acid and diluted to 100 ml (Siegel et al., 1991). The solutions were analyzed for Mn using an Atomic Absorption Spectrophotometer.

3. Physiography

The study area lies in the Porali Plain, which is bounded by Pab and Mor ranges in the east and Haro Range in the west. The area is almost plain. The average height is 100 to 250 feet from mean sea level. The Winder River flowing from the Pab range in NE drains the area. The drainage pattern is sub-parallel to dentritic and flows towards southwest to south. Small streams are intermittent and seasonal, while the large one (Winder River) has limited perennial flow.

4. Climate

The climate of the area is semi-arid to arid, normally remains hot in summer and moderate in winter. The summer season starts from April and last till October whereas and June is the hottest month. The winter period is from November to March while January is the coldest month. Climate is moderate in February and March. The area has uncertain rainfall; mostly it is received during summer. However, precipitation mostly occurs in winter, during December to March. The annual mean maximum and minimum temperature remains around 17ºC and 3°C in January and above 38°C and 24°C in June respectively. The total annual mean precipitation is above 243 mm while the relative humidity about 35% (Chaudhry, 1999).

5. Geology of the Area

The study area lies in the southern extremity of Western Fold Belt. In the area, sedimentary and igneous rocks are well exposed in a series of mountainous ranges, namely, Pab and Mor ranges, including Bela Ophiolite (Fig. 1). The western part is mainly covered with Sub-Recent and Recent materials. The top 15 m material is sand dunes.

Rocks of Mor Range mainly belong to Ferozabad Group of Jurassic age and consists of Spingwar, Loralai and Angira formations (Ahsan and Bhutta, 1991; Ahsan and Mallick, 1996 and 1999). The Cretaceous sedimentary rocks are exposed in the eastern Pab Range. They include Sembar, Goru, Parh, Fort Munro, Moghal Kot and Pab (Naseem et al., 2005a, b). The tail of the Bela Ophiolite is intermittently exposed along the western contact of Mor Range (Ahsan et al., 1988). The Bela Ophiolite is well exposed in the northern part (Naseem et al., 2002; Ahmed, 1992 and 1993). From Winder, Bela Ophiolite is concealed under the Quaternary sediments (Zaigham and Mallick, 1994). However few isolated outcrops are exposed along the coast of Karachi (Naseem et al., 1996-1997).

6. Mn and Plant

Manganese is found in the soil from the weathering of Mn-bearing minerals and rocks (Manahan, 2000). Pillow basalt and associated Mn mineralization is widely found in the vicinity of the study area (Naseem et al., 1997). It generally occurs in soil as Mn^{++} ion, in the oxidizing condition it precipitates as MnO_2. Manganese in plants is found at low levels and it is considered as essential micronutrients. The function of Mn in the plant is closely associated with the function of Fe, Cu and Zn as coenzymes. Manganese is needed for photosynthesis, respiration and nitrate assimilation (Cresswell and James, 2004). Manganese is required for activity of some dehydrogenases, decarboxylases, kinases, oxidases and peroxidases. It is involved in other cation-activated enzymes and photosynthetic oxygen evolution (Thomas, 2003). High levels of Ca and P also increase the requirement for Mn in plants (Berger, 1995).

Manganese, like Fe, is not often deficient in soil but becomes insoluble under alkaline conditions. The deficiencies are more likely common in calcareous and alkaline soils (Cresswell and James, 2004). Manganese deficiency depresses oxygen production and phosphorylation.The deficiency of Mn leads to the accumulation of certain acids, such as citric acid, and is accompanied by a reduction in sugar and cellulose content of plants. Plants lacking Mn, accumulate considerable amounts of nitrate and nitrite, thus disrupting protein production. Manganese deficiency is associated with reduced flowering of plants, reduced resistance to cold and a higher susceptibility to viruses (Thomas, 2003). Plants grown over high Mn soil, sometime suffer from Mn toxicity due to the lack of chlorophyll (Dutcher et al., 2005). High concentration of Mn in plants can also cause swelling of cell walls, withering and brown spots on leaves.

7. Mn and Human Body

The role of Mn in humans is very important. It is classed as essential micro trace element (Manahan, 2000). Manganese in the body is mainly received through the daily diet. After absorption in the human body Mn will be transported through the blood to the liver, bones, kidneys, pancreas and the endocrine glands (William, 1990 and Whitney and Rolfes, 2002). Animal foods are poor sources (Williams, 1990), while vegetables provide good sources of Mn. Blueberries, pineapples, spinach, dried peas and green vegetables are among the better sources of Mn (Kirschmann, 1996).

The daily-recommended intake of Mn is about 2 to 5 mg per day (Wardlaw, 2000). Deficiency of Mn may lead to paralysis, convulsions, blindness and deafness in infants (Kirschmann, 1996), non-traumatic epilepsy, phenyketonuria (PKU), amyotrophic lateral sclerosis (ALS) and multiple sclerosis (Insel et al., 2004). From dietary intake, a high Ca and P intake will increase the need for Mn. Very high dosage of Mn results reduced storage and utilization of iron and may produce Fe-deficiency anemia. This condition is reversible with the addition of iron to the diet (Kirschmann, 1996). Symptoms of high Mn poisoning are hallucinations, forgetfulness and nerve damage (Table 2). Manganese can also cause lung embolism, bronchitis, low sex appeal, in-coordination and Parkinson syndrome (Zayad, 2002).

8. Results

Manganese in plants is considered as essential micronutrients. The concentration of Mn in the twigs of different plants is generally high. The average abundance of Mn in the ash of plant is 6,700 (Rose et al., 1979) and 4,800 mg/kg (Reedman, 1979). The Mn concentration of the twigs of different fruits plants of study area shows variations (Table 1). The higher concentration of Mn is found in the twigs of guava (*Pg*). Both the sampling sites (6 and 7) have 2,905 and 1,880 mg/kg of Mn respectively (Fig. 2A). Among the other fruits, Jambolin (*Sc*) contains higher amount of Mn (540 mg/kg) found in locality no. 12. It is also noticed that in the same locality, the samples of Jujuba (*Zj*) has also higher Mn

concentration than the others (Fig. 3). This locality provides more Mn ions because of the proximity of Winder River and the pillow basalt exposure (Fig. 4). The twigs of Cheeko plant (*Az*) show variable concentration of Mn from different localities (Fig. 2A). The level of Mn in *Az,* is relatively low (ranging between 235-355 mg/kg). Possibly the exclusion mechanism of *Az* is strong and restrict in the absorption of Mn. The enrichment level of Mn in the twigs of Mango (*Mi*) is nearly twice at the locality no. 15 (Fig. 3). Tamarind (*Ti*), collected from 7, 12, and 15 localities (Table 1), shows relatively low level of Mn concentration. The variability in the concentration levels in the same species of fruits indicates influence of soil composition, pH of soil, depth of root system, proximity of Winder River and pillow basalt.

Among the wild and native flora, the twigs of *Salvadora oleoides (So)* shows variable concentration of Mn in the study area (Table 1). It is important to note that *So* has absorbed relatively higher amount of Mn comparing to other wild flora of the study area (Fig. 2B). Maximum concentration of Mn is noted at locality 3, while lowest recorded at locality 10 (Fig. 2). The trend of distribution shows higher concentration near the ophiolite exposure, while Mn shows decrease in concentration away from the ophiolite. *Tamarix aphylla* (Ta) has intermediate Mn enrichment (165-260 mg/kg) among the wild flora, which is greatly influenced by the presence of pillow basalt (Fig. 1). The spread (SD) is low indicating that *Ta* has special mechanism to restrict the uptake of Mn. Similar species (*Ta*) shows high concentration of Mn (3,000, mg/kg) in the north of study area due to Mn mineralization (Naseem et al., 1995). *Acacia nilotica*, in spite of deep root system does not transfer much amount of Mn from soil. The values are nearly consistence (155-240 mg/kg). *Salvadora persica* was found in only one locality (9) and has very low Mn content (90 mg/kg).

Table 1: Concentration of Mn (mg/kg) in the fruits and wild flora of the study area. Number in subscript represents localities. Abbreviation of flora is given as superscript. Az = Achras zapota, Pg = Psidium guajava, Zj= Ziziphus jajuba, Sc = Syzgium cumini, Mi= Mangifera indica, Ti = Tamarindus

Fruits	Wild flora
$_{5}235^{Az}$	$_{1}155^{An}$
$_{6}2{,}905^{Pg}$	$_{1}365^{So}$
$_{7}215^{Mi}$	$_{2}240^{Ta}$
$_{7}260^{Ti}$	$_{3}735^{So}$
$_{8}310^{Az}$	$_{4}165^{Ta}$
$_{9}250^{Az}$	$_{9}240^{An}$
$_{10}355^{Az}$	$_{9}90^{Sp}$
$_{12}290^{Az}$	$_{10}100^{So}$
$_{12}495^{Zj}$	$_{10}195^{Ta}$
$_{12}540^{Sc}$	$_{11}210^{An}$
$_{12}235^{Mi}$	$_{11}190^{So}$
$_{12}275^{Ti}$	$_{13}495^{So}$
$_{14}260^{Az}$	$_{14}170^{An}$
$_{14}390^{Zj}$	$_{14}235^{So}$
$_{14}375^{Sc}$	$_{14}180^{Ta}$
$_{15}295^{Az}$	$_{15}430^{So}$
$_{15}465^{Mi}$	$_{15}180^{Ta}$
$_{15}220^{Ti}$	

Figure 2: Variations in concentration of Mn in the ash of a. fruits and b. wild flora, from different localities. Abbreviation of flora is given in Table 1.

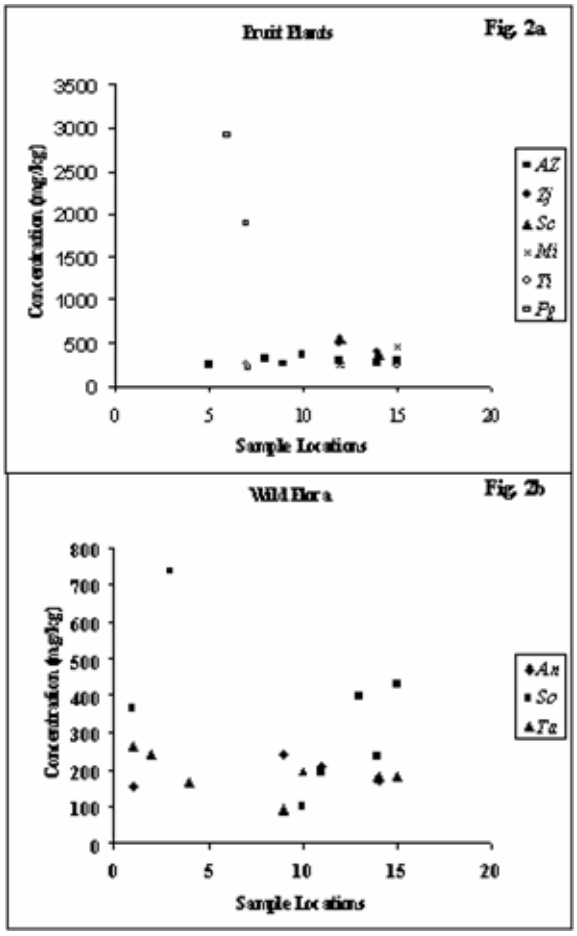

Figure 3. Concentration of Mn in different fruit plants of same locality.

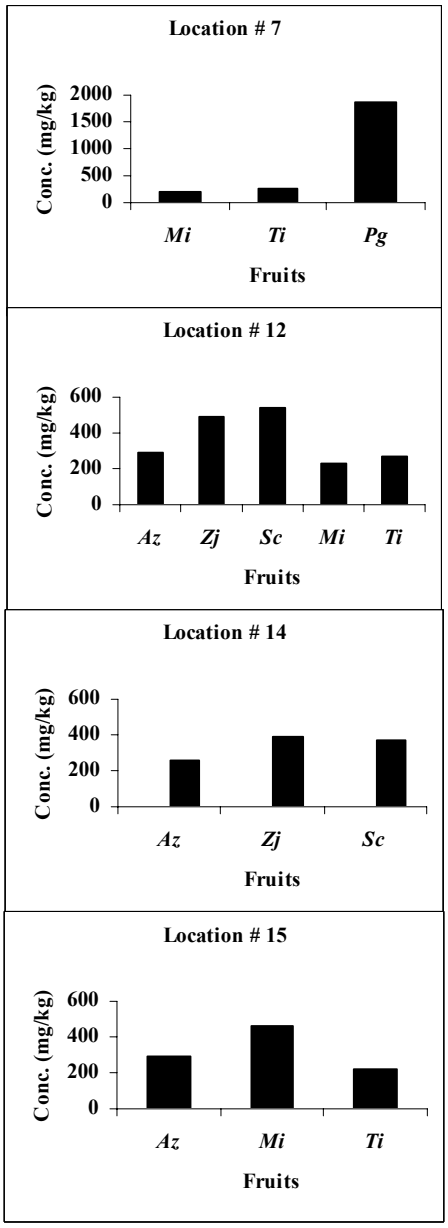

Figure 4: Exposure of pillow basalt in the eastern part of the study area, near locality # 2.

The pH and Eh of the soil plays important role in the bioavailability of Mn for the plants. The pH versus Eh plots of the soil of study area exhibits positive linear relationship (Fig. 5). The average concentration of Mn in the fruits and wild flora shows three distinct populations. The first cluster has lowest Mn (200, mg/kg) concentration at 7.8 pH and Eh -50 mv. The second group has moderate Mn (404 mg/kg) absorption at pH and Eh 8.05 and -60 mv, respectively. Maximum concentration of Mn (885 mg/kg) was observed as third population, grown in the soil having pH 8.3 and Eh -80 mv (Fig. 5). The present study revealed high bioavailability of Mn in the soil is favored by reduce alkaline environment. This kind of environment brought Mn to higher oxidation state that mobilizes Mn in the form of complex oxy-anion (Rose et al., 1979). The cationic Mn is readily soluble in acid soil (Michopoulos and Cresser, 2002).

Figure 5: Average concentration of Mn in fruits and wild flora and relationship with pH and Eh of the soils of study area.

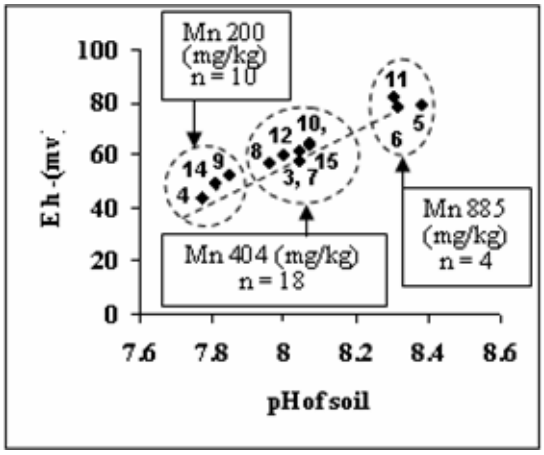

9. Discussion and Conclusions

The area in the vicinity of Winder Town has exposures of Bela Ophiolite in association with sedimentary rocks of Jurassic to Cretaceous age. These rocks are rich in Mn bearing minerals (Naseem et al., 1997). The soil derived from the weathering of these rocks has high Mn concentration. Many fruit farms are present in the Valley. The Winder River passes across the sedimentary and ophiolitic rocks, which provides good sources of Mn. The comparative study showed that the twigs of *Salvadora oleoides*, a wild flora and in the guava fruit (*Psidium guajava*) have higher concentration of Mn. The twigs of other fruits also have relatively high amount of Mn.

The chemistry of pillow basalt, distance from the pillow basalt, composition of water, mobility of elements, dispersion mechanism, pH, Eh, nature of weathering and exclusion mechanism of the species has played an important role in the concentration of Mn in different plant species. The reduced alkaline environment favours high bioavailability of Mn in the soil. This kind of environment brought Mn to higher oxidation state that mobilizes Mn in the form of complex oxy-anion. Plants grown close to the pillow basalt and close to Winder River have absorbed high Mn in contrast to plants cultivated on thick wind-blown soil cover and away from basalt exposures.

Manganese is essential micronutrient, required for healthy growth of human beings. The daily-recommended intake of Mn is about 2 to 5 mg per day (Wardlaw, 2000). Deficiency or excess of Mn may lead to many diseases (Table 2). The people of Karachi are the main consumer of these fruits. Possibly these fruits may provide high Mn, beside the other sources. This condition may leads to high level of Mn in the human body, causing a number of diseases. On the other hand, tea and coffee are the best source of Mn. Tea is one of the common and favorite drinks of Karachiites. Some estimates suggest that tea supplies as much as 20 to 30 percent of our daily Mn intake (Insel; et al, 2004). Probably in this situation fruits from Winder area may further aggravate the balance of Mn. In the recent past, diseases due to Mn are very common in Karachi because of the high Mn intake. Proper survey is needed to verify the action of Mn in the citizens of Karachi. Hopefully, the physicians, food scientists and pharmacists can apply the present knowledge in evaluating the budget of Mn in the human body to overcome many Mn related disease.

Table 2: Role of Mn in human body (complied from various sources).

Daily Requirement	Chief Functions in the body	Deficiency Symptoms	Toxicity Symptoms	Significant Sources
Men: 2-5 mg/day **Women** 1.8mg/day	Cofactor for several enzymes, associated with the formation of connective and skeletal tissues, growth and reproduction and carbohydrate and lipid metabolism	Fatness, glucose intolerance, blood clotting, skin problems, lowered cholesterol levels, skeleton disorders, birth defects, changes of hair colour, blindness and deafness in infant, reproductive abnormalities, neurological symptoms	Nervous system disorders, hyperirritability, violent acts, hallucinations, low sex interest, incoordination, Parkinson syndrome	Nuts, beans, whole grains, beet green, leafy vegetables, fruits, tea and coffee

Acknowledgement

The authors are grateful to Mr. Shabbir Ahmed Baloch, proprietor, Industrial Mineral Syndicate, Karachi for providing logistic support during fieldwork and sampling. We extend our appreciation to Dr. Surayya Khatoon, Professor, Department of Botany, for her critical examination of the species.

References

[1] Ahmed, Z. (1992). Composition of chromite from the northern part of Bela ophiolite, Khuzdar district, Pakistan. *Acta Mineralogica Pakistanica*, 6, 4-20

[2] Ahmed, Z. (1993). Leucocratic rocks from the Bela ophiolite, Khuzdar District, Pakistan. In Treloar, P.J. and Searle, M.P. (eds.), Himalayan Tectonics Geological Society Special Pubulication, No. 74, UK, pp. 89-100.

[3] Ahsan, S. N. & Bhutta, A, M. (1991). Geology and Mineralogy of the Zinc-Lead-Barite Prospects, Lasbela District, Balochistan, Pakistan. Rec. vol. LXXXVII, Geological Survey of Pakistan.62pp.

[4] Ahsan, S. N. & Mallick, K. A. (1996). A Genetic Modle for Zinc-Lead Mineral Deposits, Lasbela and Khuzdar District, Balochistan, Pakistan. *Geologica*, 2, 1-22. Geoscience Laboratory Project, Islamabad, Pakistan.

[5] Ahsan, S. N. & Mallick, K. A. (1999). Geology and Genesis of Barite Deposits of Lasbela and Khuzdar District, Balochistan, Pakistan. *Resource Geology*, 49(2), 105-111.

[6] Ahsan, S. N., Akhtar, T. & Khan, Z. A. (1988). Petrology of Bela-Khuzdar Ophiolites, Balochistan, Pakistan. I.R. no. 307, Geological Survey of Pakistan.32pp.

[7] Albarede, F. (2003). *Geochemistry An Introduction*. (United Kingdom: Cambridge University Press)

[8] Berger, L. L. (1995). Factors Affecting the Trace Mineral Composition of Feedstuffs. Salt Institute Report, University of Illinois. Retrieved from http://www.saltinstitute.org/publications/stm/STM-6.html

[9] Brooks, R. R. (1972). *Geobotany and Biogeochemistry in mineral exploration*. (New York: Harper & Row Pub.)

[10] Chaudhary, K. L. (1999). District census report of Lasbela, Population census org. Stat. Div. Govt. Pakistan, Islamabad.

[11] Cresswell, G. & James, L. (2004). Nutrient Disorders of Greenhouse Lebanese Cucumbers. Agfact H 8.3.3(1st ed), Department of Primary Industries, South Wales. Retrieved from http://www.ricecrc.org/reader/horticulture-greenhouse/h833.htm

[12] Dutcher, R. A., Jensn, C. O. & Althouse, P. M. (2005). *Introduction to Agricultural Biochemistry.* (India: Biotech Books)

[13] Finkelman, R. B., Skinner, C. W., Plumlee, G. S. & Bunnell, J. E. (2001, November). Medical Geology. *Geotimes*,. Retrieved from www.agiweb.org/geotimes/nov01/feature_medgeo.html#author

[14] Insel, P., Turner, R. E. & Ross, D. (2004). *Nutrition*. (USA: Jones and Bartlett Publishers)

[15] Kirschmann, G. J. (1996). *Nutrition Almanac*. (New York: McGraw-Hill)

[16] Komatina, M. (2004). Medical Geology- Effects of Geological Environments on Human Health. (USA: Elsevier Science)

[17] Lag, J. (1983). Geomedicine in Scandinavia. (In I. Thornton (Ed.), *Applied Environmental* Geochemistry (pp. 335-353). London: Academic Press Inc.)

[18] Manahan, S. E. (2000). *Fundamentals of Environmental Chemistry*. (USA: Lewis Publishers)

[19] Martin, H. W., Young, T. R., Kaplan, D. I., Simon, L. & Adriano, D. C. (1996). Evaluation of three herbaceous index plant species for bioavailability of soil cadmium, chromium, nickel and vanadium. *Plant Soil*, 182, 199-207

[20] Michopoulos, P. & Cresser, M. S. (2002). Effects of simulated acid precipitation on the cycles of manganese under Sitka spruce *Picea sitchensis. Biogeochemistry*, 61, 323-335

[21] Naseem, S., Sheikh, S. A. & Qadeeruddin, M. (1995). Biogeochemical Study of *Tamarix aphylla* from Lasbela Area and its Application in Prospecting of Ore Deposits. *Chinese Journal of Geochemistry*, 14(4), 303-312

[22] Naseem, S., Sheikh, S. A. & Mallick, K. A. (1997). Lithiophorite and Associated Manganese Mineralization in Lasbela Area, Balochistan, Pakistan. *Geoscience Journal*, 1(1), 10-15

[23] Naseem, S., Sheikh, S. A. & Qadeeruddin, M. (1996-1997). Geochemistry and Tectonic Setting of Gadani-Phuari Segment of Bela Ophiolites, Balochistan, Pakistan. *Journal of King AbdulAziz University, Earth Sciences*, 9, 127-144

[24] Naseem, S., Sheikh, S. A. & Qadeeruddin, M. (2002). Petrography and Geochemistry of Wadh Plagiogranites and associated Gabbros from Bela Ophiolite, Pakistan. *Journal of Geological Society of the Philippines*, 57, 1-18

[25] Naseem, S., Naseem, S. & Sheikh, S. A. (2005a, November). *Geochemical Evaluation of Depositional Environment of Parh Limestone, Southern Pab Range, Balochistan, Pakistan*. (Paper presented at the SPE/PAPG Annual Technical Conference, Islamabad, Pakistan)

[26] Naseem, S., Sheikh, S. A., Bashir, E. & Shirin, K. (2005b). Geochemistry and Depositional Setting of Fort Munro Formation, Middle and Lower Indus Basin, Pakistan. Journal of China, 16(2), 160-169

[27] Nergis, Y., Naseem, S. & Mallick, K. A. (2000). Geological Sources of Heavy Metal Distribution in the Blood of Cancer Patients: A Geomedicinal Study in the inhabitants of Karachi. *Hamdard Medicus*, XLIII, (1), 61-70

[28] Nergis, Y., Ahmed, S. I. and Shareef, M. (2005). Effect of Pollution on Human Health by Contaminated Vegetables. *Hamdard Medicus*, XLVIII (1), 10-26

[29] Reedman, J. H. (1979). *Techniques in mineral exploration.* (London: Applied Sci. Pub.) 4th Ed.

[30] Rose, A. W., Hawkes, H. E. & Webb, J. S. (1979). *Geochemistry in mineral exploration.* (London: Academic press) 2nd Ed.

[31] Siegel, F. R., Barrows, J. A. N. & Barrows, E. M. (1991). Biogeochemical prospecting for gold-bearing quartz veins of the piedmont, Great Falls, Maryland. *J. Geochem. Explor.*, 41, 275-289

[32] Thomas, B., Murphy, D. J. & Murray, B. G, (eds) (2003). Encyclopedia of Applied Plant Sciences. vol. 2, Elsevier Academic Press, Canada. pp. 647- 648

[33] Udayakumar, R. & Begum, V. H. (2004). Elemental Analysis of Medicinal Plants Used in Controlling Infectious Diseases. *Hamdard Medicus*, XLVII(4), 35-39

[34] Wardlaw, G. M. (2000). *Contemporary Nutrition*. (USA: McGraw-Hill Companies)

[35] Whitney, E. N. & Rolfes, S. R. (2002). *Understanding Nutrition.* (USA: Wadsworth/ Thomson Learning)

[36] William, S. R. (1990). *Essentials of Nutrition and Diet Theraphy.* (USA: Time Mirror/Mosby College Publishing)

[37] Zaigham, N. A. & Mallick, K. A. (1994). Sub surface continuation of the ophiolites in the Bela Plain of Balochistan, Pakistan. *Ofioliti*, 19, 269-278

[38] Zayad, J. (2002). Assessment of Toxicological Risks of Environmental Contamination by Manganese. Retrieved from http://www.hc-sc.gc.ca/sr-sr/finance/tsri-irst/proj/metals-metaux/tsri-109_e.html

European Journal of Scientific Research
ISSN 1450-216X Vol.18 No.4 (2007), pp.700-706

http://www.eurojournals.com/ejsr.htm

On the Estimation and Performance of Subset Autoregressive Moving Average Models

Ojo J.F
Department of Statistics, University of Ibadan, Ibadan, Nigeria
E-mail: jfunminiyiojo@yahoo.co.uk

Abstract

Full autoregressive moving average model are always characterize by many parameters and this is a problem. Some of these parameters are always close to zero and there is the need to eliminate these parameters and this can be done through subsetting. In this paper subset autoregressive moving average models is considered using the proposed algorithm and as well compare with subset autoregressive models. The autoregressive models of order p and autoregressive moving average models of order p and q from which we can have various subsets is represented respectively thus:

$$X_t = \phi_1 X_{t-1} + \phi_2 X_{t-2} + \phi_p X_{t-p} + \varepsilon_t \quad (1)$$

$$(1 - a_1 \beta - a_2 \beta^2 - \ldots - a_p \beta^p)\, Y_t = (1 + b_1 \beta + b_2 \beta^2 + \ldots + b_p \beta^p)\, \varepsilon_t \quad (2)$$

The best model among the subsets autoregressive models and subsets autoregressive moving average models is selected using the Akaike Information Criteria. The best models in the subsets autoregressive models and the subsets autoregressive moving average models are compared using residual variance.

Results revealed that the residual variance attached to the subset autoregressive moving average model is smaller than the residual variance attached to the subset autoregressive model. We conclude that the subset autoregressive moving average model perform better than subset autoregressive model.

Keywords: Full Autoregressive moving average model, Subsets Autoregressive models. Subset selection, Order Determination Criterion, Model Estimation.

Introduction

It may be said that the era of linear time series models began with such linear models as Yule's autoregressive (AR) models (1). In the past five decades or so, we have seen remarkable successes in the application of linear time series models in diverse fields for example Box and Jenkins (2); Hannan (3) (4); Chatfield (5); Anderson T. W.(6) (7). Nottingham International Time Series Conference in March 1979. These successes are perhaps rather natural in view of the significant contributions of linear differential equation in all branches of science.

In time series modeling, subset models are often desirable, especially when the data exhibits some form of periodic behaviour. In such cases, fiitting full order models often results in the fitted coefficients of some lags being close to zero. Before considering subset modeling, consider the problem of fitting a full order autoregressive model of order k, AR(k) as well as the fitting of a full order autoregressive moving average model of order kq ARMA(kq) This we consider in the next section.

Materials and Methods

Autoregressive Model

A time series [X_t] is said to follow an autoregressive process of order p if satisfied the difference equation.

$$X_t - \mu = \phi_1(X_{t-1} - \mu) + \phi_2(X_{t-2} - \mu) + \text{----------} \phi_p(X_{t-p} - \mu) + \varepsilon_t \quad (2.1)$$

A finite stationary stochastic process [X_t] is defined as;

$$X_t = \phi_1 X_{t-1} + \phi_2 X_{t-2} + \phi_p X_{t-p} + \varepsilon_t \quad (2.2)$$

Where,

1. ε_t is a gaussian process
2. $\phi_1 - -\phi_2 - - - - - \phi_p$ is a finite set of weight parameter
3. $E(X_t) = m = 0$

In backward shift operation rotation presentation this model can be written as;

$$(1 - \phi_1 B - \phi_2 B^2 \text{----------} \phi_p B^p) X_t = \varepsilon_t \quad (2.3)$$

i.e $$\phi(B) X_t = \varepsilon_t$$

where

$$\phi(B) = 1 - \phi_1 B - \phi_2 B^2 \text{----------} \phi_p B^p \quad (2.4)$$

and the equation $\phi(B) = 0$ is called the characteristics equation. For stationary the roots of the characteristic equation $\phi(B) = 0$ must be outside the unit circle. The estimate of the parameter Φi, i = 1, 2, …, p can be obtained by Yule Walker method as follows.

Model Estimation

The autoregressive model (2.2) is a useful model, since it usually explains much of the variation and often has some physical foundation. Furthermore, its test theory is typical of a much more general case. The basic problem is actually the estimation of the parameters ϕ_i and σ_2.

If the error $_t$ and x_t have means 0 and μ_x, respectively, then we modify (2.2) as

$$\sum_{I=0}^{P} \phi_i (x_t - \mu) = \epsilon_t \quad (2.5)$$

Although we usually assume that the ϵ_t are normally distributed. This is not a restrictive assumption as it appears but to a first approximation the means and variances of autocorrelations are unaffected by non normality and estimates of parameters such as the autoregressive coefficients, ϕ_i, should be similarly robust.

Now, for normal processes the log-likelihood of the sample $x_1, x_2, \ldots, x_n$ is, for large n,

$$L = const - \frac{n}{2}\log\sigma^2 - \frac{1}{2\sigma^2}\sum_{i=1}^{n}\left[\sum \phi_i (X_{t-i} - \mu)\right]^2 \quad (2.6)$$

Maximising this expression with respect to μ, one obtains the estimator

$$\mu = \frac{\sum\sum \phi X_{t-ii}}{n\sum \phi_i} = \frac{1}{n}\sum X_t \quad (2.7)$$

Inserting (7) in (6), one finds

$$L \approx const - \frac{n}{2}\left[\log\sigma^2 + \frac{1}{\sigma^2}\sum_j\sum_k \phi_j \phi C_{i-ki}\right]$$

where C_{J-i} is the estimate of the autocovariance of lag J – i.

So that the maximum likelihood estimators of the remaining parameters are determined approximately by the relations

$$\Sigma \phi_i C_{J-i} = 0, \; j = 1, 2, \ldots, p \quad (2.8)$$

$$\sigma^2 = {}^1/n \, \Sigma \Sigma \phi_j \phi_i \, C_{J-i}$$

$$= {}^1/n \sum_{i=0}^{p} \Sigma \phi_i \, C_i \qquad (2.9)$$

The analogus form of (2.8) and (2.9) is the Yule-Walker relations is given as:

$X_t = \phi_{p1} X_{t-1} + \phi_{p2} X_{t-2} + \ldots + \phi_{pp} X_{t-p} + \epsilon_t$

Multiply through by X_{t-k} and take expectations we have

$\gamma_k = \phi_{p1} \gamma_{k-1} + \phi_{p2} \gamma_{k-2} + \ldots + \phi_{pp} \gamma_{k-p} \ldots k > 0$

set k = 1, 2, …, p

$$\begin{aligned} \gamma_1 &= \phi_{p1} \gamma_0 + \phi_{p2} \gamma_1 + \ldots + \phi_{pp} \gamma_{p-1} \\ \gamma_2 &= \phi_{p1} \gamma_1 + \phi_{p2} \gamma_0 + \ldots + \phi_{pp} \gamma_{p-2} \\ &\vdots \\ \gamma_p &= \phi_{p1} \gamma_{p-1} + \phi_{p2} \gamma_{p-2} + \ldots + \phi_{pp} \gamma_0 \end{aligned} \qquad (2.10)$$

Expression (2.10) is termed Yule-Walker equations. Divide (2.10) by γ_0 and write in matrix form as

$$\begin{pmatrix} \rho_1 \\ \rho_2 \\ \vdots \\ \rho_p \end{pmatrix} = \begin{pmatrix} 1 & \rho_1 & \rho_2 & \ldots & \rho_{p-1} \\ \rho_1 & 1 & \rho_1 & \ldots & \rho_{p-2} \\ \vdots & \vdots & \vdots & & \vdots \\ \rho_{p-1} & \rho_{p-2} & \rho_{p-3} & \ldots & 1 \end{pmatrix} \begin{pmatrix} \phi\rho_1 \\ \phi\rho_1 \\ \vdots \\ \phi\rho_1 \end{pmatrix}$$

$\underline{\rho}_p = \underline{P}_p \, \phi_\rho$, $\underline{P}_p$ is positive definite and hence P_p^{-1}exists, therefore,

$$\phi_{\underline{\rho}} = \underline{R}_p^{-1} \underline{S}_p \qquad (2.11)$$

where R and S are sample estimates of P and ρ respectively.

Autoregressive Moving Average Model

A useful class of model is that formed from a combination of MA and AR processes. The autoregressive moving average process ARMA(p, q) satisfies the equation

$$(1 - a_1 \beta - a_2 \beta^2 - \ldots - a_p \beta^p) \, Y_t = (1 + b_1 \beta + b_2 \beta^2 + \ldots + b_p \beta^p) \, \varepsilon_t \qquad (2.12)$$

The estimation procedure requires initial estimates of the coefficients $a_1, a_2, \ldots, a_p, b_1, \ldots, b_q$.

Given a series of observations $y_1, y_2, \ldots, yn$ on the process Y_t of (2.12) with sample autocovariances denoted by

$$C_\tau = \frac{1}{n} \sum_{t=\tau+1}^{n} (y_t - \bar{y})(y_{t-\tau} - \bar{y}), \tau = 0,1,2,.... \qquad (2.13)$$

and $C_{-\tau} = C_\tau$, it follows that the autoregressive coefficicents $a_1, a_2, \ldots, b_p$ can be estimated by solving the set of equations.

Assuming, now that one can write

$(1 - \hat{a}_1 \beta - \hat{a}_2 \beta_2 - \ldots - \hat{a}_p \beta^p) \, Y_t = \tilde{Y}_t \approx (1 + b_1 \beta + b_2 \beta^2 + \ldots + b_q \beta^q) \, \varepsilon_t$

the coefficients $b_1, b_2, \ldots b_q$ can be estimated using the autocovariance properties of the moving average process Y_t. Denote the sample autocovariances of this process as $\tilde{C}_\tau$. It can then be shown that

$$\widetilde{C}_\tau = \sum_{j=0}^{p} a_j^2 c_\tau + \sum_{j=1}^{p} (a_0 a_j + a_1 a_{j+1} + ... + a_{p-1} + ... + a_{p-j} a_p)(c_{\tau+j} + c_{\tau-j}) \quad (2.14)$$

where $a_0 = -1$. A Newton-Ralphson algorithm, can then be employed to generate estimates of the moving average coefficients by an iterative procedure.

Model Identification and Order Determination

The traditional tools used in the identification of the model of a time series are the partial autocorrelation function (PACF) and the autocorrelation function (ACF). They help to determine the model that is best and gives a precise representation of the time series.

A stationary series is modeled as an AR(p) if the sample autocorrelation function (ACF) decays exponentially to zero and the partial autocorrelation function (PACF) cut off after lag P.

On the other hand, a series is modeled as an MA(q) if the partial autocorrelation function (PACF) decays exponentially to zero and the autocorrelation function (ACF) cut off after lag q.

If however, neither the autocorrelation function nor the partial autocorrelation cuts off, the series is modeled as an autoregressive moving average ARMA (pq).

The lag at which the partial autocorrelation function (PACF) or autocorrelation function (ACF) cuts off determines the order of the model. It is important to note that in practice, neither ACF nor PACF cuts off at lag p or q exactly, rather their value drops to zero at these points.

Akaike Information Criterion (AIC) can also be used in the determination of the order Akaike, (8). Also Final Prediction Error (F.P.E.), Parzen (9), Criteria for Autoregressive Transfer Function (CAT).

For the kth autoregressive model, the FPE criterion is given by

$FPE_{(k)} = \sigma_k^2$ [1 - k/N]

where σ_k^2 is the unbiased estimator of σ^2 using the kth order model, that is

$\sigma_k^2 = RSS_k / (N-k)$

Similarly for a pth order model

$AIC_{(p)} = N\ln \sigma_p^2 + 2p$ where

$$\sigma_p^2 = \frac{1}{N}\sum_{i=1}^{N}\left(x_t - \sum_{t=1}^{p}\phi_i x_{t-i}\right)^2$$

is the maximum likelihood estimate of the residual variance after fitting the AR(p).

In practice, we specify a maximum lag L and fit successively

AIC(1), AIC(2), ….

The minimum FPE or AIC is the best model for the data. AIC is known to perform better than FPE.

Algorithm for 2^k-1 Possible Subsets in Time Series Models

Hocking, R. R. and R. N. Leslie (10) and Furnival G. M (11) considered 2^k-1 subsets of a regression model while Hagan V. and Oyetunji O. B. (12) considered the selection of possible subsets for Autoregressive models. This algorithm takes care of selection of 2^k-1 subsets in Autoregressive moving average models and it goes thus: The 2^k-1 subsets of time series models make use of the properties of permutation and combinatorial analysis and the algorithm goes thus: The k value, which is an integer and a maximum lag, is identified in our model. The first sets of numbers are one digit number 1, 2, 3, up to k. The second sets of numbers are 2-digit numbers arranged in such a way that the first digit 1 is taking and combine with the next number until k is reached; the next digit 2 is picked and combines with the next number until k is reached, the next digit with the next number until k is reached. This is continuing until (k-1) and k is reached.

The third sets of numbers are three digits and the second digit is operated on to produce third digit. Our guide is that the 2-digit must have the next forward number until k is reached and the next two digits must have the next forward digit until k is reached. This is continuing until we have (k-2)(k-1) and k. This is continuing until we have the maximum digit, which is the digit k that is (k-n)(k-s)(k-u)(k-z)(k-m)(k-y)……k. where n<k by 1, s<k by 2, u<k by 3……..k. Suppose we have our k to be 4, (the best bilinear) there are $2^4 - 1$ possible subsets that is 15 subsets. Following our algorithm we shall have the following:

1, 2, 3, 4, 12, 13, 14, 23, 24, 34, 123, 124, 134, 234, 1234.

The equations for the following are

$X_t = b_1 x_{t-1} - + e_t$

$X_t = b_2 x_{t-2} - + e_t$

$X_t = b_3 x_{t-3} - + e_t$ (2.15)

$X_t = b_1 x_{t-1} + b_2 x_{t-2} + b_3 X_{t-3} + b_4 x_{t-4} - + e_t$ (2.16)

Where $1=b_1$, $2=b_2$, $3=b_3$, $4=b_4$. If the minimum AIC occurred in (2.15) that model is the Subset Time Series model.

Results and Discussion

The data used in this study is the record of sunspot numbers between 1734 and 1883. An efficient computer package was used to fit various full AR(p), Subset AR(p), ARMA(p,q), Subset ARMA (p,q) models to the data.

Fitting of Full and Subset Autoregressive Models

Autoregressive model of orders 1 to 10 was fitted using the real series. The choice of the best order is made on the basis of AIC and the minimum AIC is the best model and this was found when p=7. The fitted model is

$$X_t = 0.373901X_{t-1} - 0.277742X_{t-2} - 0.228855X_{t-3} - 0.128061X_{t-4} - 0.238603X_{t-5} - 0.105105\ X_{t-6} - 0.280308\ X_{t-7} + e_t$$

R-Squared	=0.518146
S. E. of Regression	=15.62754
Sum Squared Residual	=32969.70
Akaike Information Criterion	=8.383986
F-Statistic	=24.19461
Prob(F-Statistic)	=0.0000

There are 2^7-1=127 possible subsets. The choice of the order is made on the basis of minimum AIC and having considered the 127 possible subsets, it was found that AIC is minimum in the following model

$$X_t = 0.412820X_{t-1} - 0..271125X_{t-2} - 0.270908X_{t-3} - 0.339150X_{t-5} - 0.293320X_{t-7} + e_t$$

R-Squared	=0.506373
S. E. of Regression	=15.70142
Sum Squared Residual	=33775.22
Akaike Information Criterion	=8.379955
F-Statistic	=35.13437
Prob(F-Statistic)	=0.00000

Fitting of Full and Subset Autoregressive moving average models

Autoregressive moving average model of orders 1 to 10 was fitted using the real series. The choice of the best order is made on the basis of AIC and the minimum AIC is the best model and this was found when p=7 and q=1. The fitted model is

$$X_t = 0.900946X_{t-1} - 0.506534X_{t-2} + 0.109560X_{t-3} - 0.010835X_{t-4} - 0.205652X_{t-5} - 0.014015X_{t-6} - 0.146900\ X_{t-7} - 0.585412\ e_{t-1} + e_t$$

R-Squared	=0.531015
S. E. of Regression	=15.47486
Sum Squared Residual	=32089.14
Akaike Information Criterion	=8.370999
F-Statistic	=21.67479
Prob(F-Statistic)	**=0.00000**

There are 2^7-1=127 possible subsets. The choice of the order is made on the basis of minimum AIC and having fitted the 127 possible subsets, it was found that AIC is minimum in the following model

$$X_t = 0.905337X_{t-1} - 0.509454X_{t-2} - 0.107803X_{t-3} - 0.007407X_{t-4} - 0.215636X_{t-5} - 0.152380X_{t-7} - 0.588895e_{t-1} + e_t$$

R-Squared	=0.530962
S. E. of Regression	=15.41830
Sum Squared Residual	=32092.76
Akaike Information Criterion	=8.357027
F-Statistic	=25.47056
Prob(F-Statistic)	=0.00000

Table 1: Values of σ_e^2 And AIC

Model & Parameter	**Subset (AR)**	**Subset (ARMA)**
σ_e^2	237.8208	225.9679
AIC	8.379955	8.357027

The result of the analysis is presented in the table above. We could see from the table the value for the residual variances and Akaike Information Criterion of the subset autoregressive model and subset autoregressive moving average model. This result has shown that subset autoregressive moving average model outperformed subset autoregressive model.

Conclusions

We have described an algorithm for estimating subset stationary linear time series autoregressive and autoregressive moving average models, and the estimation procedure is illustrated with a real time series. The residual variance attached to the subset autoregressive moving average model is smaller than the residual variance attached to the subset autoregressive model suggesting that subset autoregressive moving average model perform better than subset autoregressive model.

References

[1] Yule, G. U. (1927) On the Method of Investigating Periodicities in Disturbed Series with Special Reference to Wolfer's Sunspot Numbers. Phil. Trans. Roy. Soc. London (A) 226-267.
[2] Box, G. E. P. and G.M. Jenkins (1970) Time Series, Forecasting and Control. Holden-Day: San Francisco.
[3] Hannan, E. J. (1962) Time Series Analysis. Methuen Monographs.
[4] Hannan, E. J. (1970) Multiple Time Series. John Wiley: New York
[5] Chatfield, C. (1980) The Analysis of Time Series: An Introduction. Chapman and Hall.
[6] Anderson, T. W. (1971) The Statistical Analysis of Time Series, New York and London Wiley.
[7] Anderson T. W. (1977) Estimation for Autoregressive Moving Average Models in the Time and Frequency Domains. The Ann. of Stat. Vol 5 No. 5, 842-865 .
[8] Akaike, H. (1977) On the Entropy Maximasation Principle. *Proc. Symp. on Application of Statistics*, Dayton, Ohio, June 1977 (P. R. Krishnaiah, ed.) .
[9] Parzen, E. (1974) Some Recent Advances in Time Series Modelling. IEEE Trans Automatic Control AC-19, 723-730.
[10] Hocking, R. R. and R. N. Leslie (1967) Selection of the Best Subset in Regression Analysis. Technometrics 9, 531-540 .
[11] Furnival, G. M. (1971) All possible Regressions with Less Computation. Technometrics 13, 403-408.
[12] Haggan , V. and O. B. Oyetunji, (1980) On the Selection of Subset Autoregressive Time Series Models. UMIST Technical Report No. 124 (Dept. of Mathematics).

European Journal of Scientific Research
ISSN 1450-216X Vol.18 No.4 (2007), pp.707-729

http://www.eurojournals.com/ejsr.htm

A Semiparametric Joint Model for Longitudinal and Time-to-Event Univariate Data in Presence of Cure Fraction

Mohd. Rizam Abu Bakar
Department of Mathematics, University Putra Malaysia, Malaysia

Khalid A. Salah
Institute for Mathematical Research, University Putra Malaysia, Malaysia

Noor Akma Ibrahim
Institute for Mathematical Research, University Putra Malaysia, Malaysia

Kassim B Haron
Department of Mathematics, University Putra Malaysia, Malaysia

Abstract

Many medical investigations generate both repeatedly-measured (longitudinal) biomarker and survival data. One of complex issue arises when investigating the association between longitudinal and time-to-event data when there are cured patients in the population, which leads to a plateau in the survival function $S(t)$ after sufficient follow-up. Thus, usual Cox proportional hazard model Cox (1972) is not applicable since the proportional hazard assumption is violated. An alternative is to consider survival models incorporating a cure fraction. In this paper we present a new class of joint model for univariate longitudinal and survival data in presence of cure fraction. For the longitudinal model, a stochastic Integrated Ornstein-Uhlenbeck process will present, and for the survival model a semiparametric survival function will be considered which accommodate both zero and non-zero cure fractions of the dynamic disease progression. Moreover, we consider a Bayesian approach which is motivated by the complexity of the model. Posterior and prior specification needs to accommodate parameter constraints due to the nonnegativity of the survival function. A simulation study is presented to evaluate the performance of this joint model.

Keywords: Survival model, Longitudinal model, Cure rate model, fixed effects, Random effects, Bayesian approach, Integrated Ornstein-Uhlenbeck.
Mathematics *Subject classifications (2000)*: 62F15, 62G99, 62M05, 62N01

1. Introduction

Joint models for longitudinal and survival data have recently become quite popular in cancer, AIDS, and environmental health studies where a longitudinal biologic marker of the health-related outcome such as CD4 counts (A type of T cell involved in protecting against viral, fungal, and protozoal infections), immune response to vaccine, or quality of life in clinical trial can be an important predictor of survival or some other time-to-event. Often the observed longitudinal data are incomplete or may

be subject to error. Since such longitudinal markers (covariates) are measured with error, the analyses become more complex than one that treats these as fixed covariates in a survival model.

A joint model is comprised of two linked submodels, one for the true longitudinal process and one for the failure time, along with additional specifications and assumptions that allow ultimately a full representation of the joint distribution of the observed data. All joint models developed so far in the statistical literature have focused on time-to-event data models with no survival fraction. However, in many applications the time-to-event data may have joint or marginal survival curves that plateau beyond a certain period of follow-up, Empirical evidence to confirm this feature of the population is a long and stable plateau with heavy censoring at the tail of the Kaplan-Meire survival curve. With long term survivors, the usual Cox proportional hazard model Cox (1972) is not applicable since the proportional hazard assumption is violated, therefore, it is important to develop a survival model capable of accommodating a possible cure fraction for each marginal survival function as well as linking relevant longitudinal markers to such a model.

In many cancer treatment trials, the prognosis for the patients under study might be quite good and such patients may by cured after treatment and sufficient follow up. In these situations, a plateau typically occurs in the survival curve and a survival model with $S(\infty) = 0$ is no longer appropriate. An alternative is to consider survival models incorporating a cure fraction. Which, often referred to as a cure rate models, which are becoming increasingly popular in analyzing data from cancer clinical trials. Perhaps the most popular type of cure rate model is the mixture model discussed by Berkson and Gage (1952). In this model, they assume a certain fraction θ of the population is "cured" and the remaining $(1-\theta)$ are not cured. the standard mixture cure model $S(t)$ is defined as

$$S(t) = \theta + (1-\theta)S_1(t), \tag{1}$$

where $S_1(t)$ denotes the survivor function for the non-cured group in the population. Clearly (1) is improper since $S(\infty) = \theta,$ and when covariates are included we have a different θ_i for each subject $i = 1,...n.$ A logistic regression structure for θ_i is usually given by

$$\theta_i = \frac{\exp\left(\delta^T Z_i\right)}{1+\exp\left(\delta^T Z_i\right)}, \tag{2}$$

as assumed by Kuk and Chen (1992), where θ_i is a probability and cannot be zero and Z_i is a vector of covariates. The standard mixture cure model has been extensively studied in the literature Gray and Tsiatis (1989); Taylor (1995); Maller and Zhou (1996); Peng and Dear (2000); Sy and Taylor (2000); Betensky and Schoenfeld (2001); Yin (2005) ; Yin and Ibrahim (2005); among others. An alternative cure rate model, with a proportional hazards structure for the population, sometimes called the promotion time cure rate model Yakovolev et al. (1993); Chen et al. (2000) is given by

$$S(t) = \exp\{-\theta F(t)\} \tag{3}$$

where $F(t)$ is a proper cumulative distribution function and represents the promotion time, that is, time to development of a detectable tumor mass. Common parametric choices for $F(t)$ are exponential Goldman (1984) and Ghitany et al. (1994) and weibull distribution Farwell (1977), Farwell (1982), Kimber Crowder (1984) and Chi et al (2006). Nonparametric choices have also been considered Kuk and Chen (1992), Taylor (1995), Sy and Taylor (2001), Ibrahim et al. (2004). There are also formulations of non-mixture cure models to incorporate long-term survivors Yakovlev and Tsodikov (1996), Tsodikov (1998), Chen et al. (2000), Chen and Ibrahim (2001), Chen et al. (2004) and Brown and Ibrahim (2003a, 2003b).

The basic idea of the joint modeling of longitudinal and survival data in presence of cure fraction is to model these data through the cure fraction $\theta,$ that is

$$\theta_i = \exp(\gamma Y_i^*(t) + \delta^T Z_i(t)), \tag{4}$$

Where γ and δ are vectors of regression coefficient, $Y_i^*(t)$ is the longitudinal measurements. There has been relatively little publications about jointly modeling longitudinal and survival data with surviving fraction, Law, Taylor and Sandler (2002) proposed a joint longitudinal and survival cure mixture model, they obtained maximum likelihood estimations of the parameters using Monte Carlo Expectation Maximization (MCEM) algorithm. While Ibrahim et al. (2001), Brown and Ibrahim (2003a), Chen et al. (2004), Chi and Ibrahim (2006) and Cowling et al. (2006) obtained the parameter estimation using the Bayesian approach.

The presentation of our proposed joint model in this article proceeds as follows. In subsection 2.1, we begin by presenting a longitudinal model, in which the longitudinal response measurements are consisting of a combination of fixed effect, random effect, An Integrated Ornstein-Uhlenbeck (IOU) stochastic process and measurement error. In subsection 2.2 we present a cure rate model that allows for a zero as well as a nonzero cure fraction, So that, in addition to some carcinogenic cells remaining active after initial treatment, new carcinogenic cells are assumed to occur over time after this treatment with promotion times are assumed to be independent and identically distributed with a common *semiparametric* distribution function. We then combine these two models to obtain a joint longitudinal and cure rate model. In section 3 we will derive the likelihood function by introducing the *semiparametric* distribution function. Two methods will used to assess the joint model fit will present in section 4. To evaluate the performance of this joint model, simulation study will be present in section 5. And then we conclude with discussion.

2. A New Class of longitudinal and survival joint model

In this section we will propose and setup for our new class of joint model. For subject *I,* $i = 1,...,n,$ let T_i and C_i denote the event time and censoring time respectively; let Z_i be a q-dimensional vector of baseline covariates and let $Y_i(t)$ be the longitudinal process at time $t \geq 0$. Components of Z_i might also be time dependent covariates whose values are known exactly and that are "external" in the sense described by Klabfleisch and Prentice (2002). Rather than observe V_i for all *i,* we observe only $V_i = \min(T_i, C_i)$ and the censored indicator $\Delta_i = I(T_i \leq C_i),$ which equals one for time-to-event and zero otherwise. Values of $Y_i(t)$ are measured intermittently at times $t_{ij} \leq V_i,\ \ j = 1,...,n_i,$ for subject *i,* which may be different for each *i,* often; target values for the observations times are specified by a study protocol, although deviations from protocol are common. The observed longitudinal data on subject *i* may be subject to "error", thus we observed only $Y_i^* = \{Y_i^*(t_{i1}),...,Y_i^*(t_{in_i})\}^T,$ whose elements may not exactly equal the corresponding $Y_i(t_{ij})$. A joint model is comprised of two linked submodels, one for the true longitudinal process $Y_i^*(t_{i1})$ and one for the failure time T_i, along with additional specifications and assumptions that allow ultimately a full representation of the joint distribution of the observed data $D_i = \{V_i, \Delta_i, Y_i^*, t_i\}$, where $t_i = (t_{i1},...t_{in_i})^T$. The D_i are taken to be independent across *i,* reflecting the belief that the disease process evolves independently for each subject. In the framework of joint modeling, we specifically assume that the time-to-event T and vector of repeated measurements $Y,$ are conditionally independent given Y^*

2.1. The longitudinal process

In this article, for the longitudinal process, we focus on a model consisting of a combination of fixed effect, random effect, An Integrated Ornstein-Uhlenbeck (IOU) stochastic process and measurement error, Taylor et al. (1994). In general we assume that

$$\begin{cases} Y_i(t_{ij}) = Y_i^*(t_{ij}) + \varepsilon_i(t_{ij}) \\ Y_i^*(t_{ij}) = \varpi_1 U_1(t_{ij}) + \varpi_2 U_2(t_{ij}) + W_i(t_{ij}), \end{cases} \tag{5}$$

where ϖ_1 are fixed effects coefficients, ϖ_2 are random effects coefficients, $W_i(t_{ij})$ is an IOU stochastic process, and $\varepsilon_i(t_{ij})$ is measurement error. To be more specific, we will consider the situation where the only coefficients in U_1 and U_2 are the intercept, *t*, then, as a special case, with some change in notation, (5) can be written as

$$\begin{cases} Y_i(t_{ij}) = Y_i^*(t_{ij}) + \varepsilon_i(t_{ij}) \\ Y_i^*(t_{ij}) = a_i + b_i t_{ij} + \beta X_i(t_{ij}) + W_i(t_{ij}), \end{cases} \tag{6}$$

where $Y_i(t_{ij})$ denotes the observed value of a continuous time-dependent covariates (or disease marker) for subject i $(i = 1,..,n)$ at t_{ij} $(j = i,..,n_i)$; n number of the subjects in the study n_i; number of repeated measurements for subject *i* and may be different for each subject, $Y_i^*(t_{ij})$ is the true value of the marker at time t_{ij}, $a_i \sim N(\mu_a, \sigma_a^2)$ are independent random intercept of subject *i,* b_i is the random slope, $X_i(t_{ij})$ is a $(p \times 1)$ vector of the values of *p* variables for subject *i* at time t_{ij}. The $1 \times p$ vector of unknown regression parameter β represents the effect of the *p* variables on the marker, $W_i(t_{ij}) \sim N(0, \Sigma)$ are independent IOU stochastic process with covariance structure given by

$$Cov(W_i(t), W_i(s)) = \frac{\sigma^2}{2\alpha^3}\left(2\alpha \min(s,t) + e^{-\alpha s} + e^{-\alpha t} - 1 - e^{-\alpha|t-s|}\right); \tag{7}$$

where α and σ^2 are parameters, and $\varepsilon_i(t_{ij}) \sim N(0, \sigma_\varepsilon^2)$ represents deviations due to measurement error. An appealing feature of model (6) is that it corresponds to a random effects model as α approaches zero and $\sigma^2 / 2\alpha$ maintains a constant. This can be seen directly from the observation under this circumstance, the IOU process is no more than a random effects model. Also, it is interesting to note that scaled Brownian motion is a special case of $W(t)$ in which α is infinitely large and $\sigma^2 / 2\alpha$ is constant. In general, this model is more flexible and plausible than a random effects model since it allows the marker to vary a round a straight line and allows the data to determine the degree of this variation.

Note that $Cov(W_i(t), W_i(s))$ in (7) depends on *s* and *t* and not just on their difference, which can be described as a disadvantage of the IOU process, that is not a stationary, and hence it is necessary to have a natural time zero for each subject. In some applications it may be that there is no natural time zero or that time zero is not exactly known. Thus, following Taylor et al. (1994), we can overcoming this problem by analyzing the differences.

Let Y_{iF_i} be the first measurements on subject i at time F_i, and let $D_{it} = Y_{it} - Y_{iF_i}$; for $t > F_i$. Then

$$D_{it} = b(t - F_i) + \beta(X_{it} - X_{iF_i}) + W_{it} - W_{iF_i} + \varepsilon_{it} - \varepsilon_{iF_i}, \tag{8}$$

and

$$Cov(D_{it_1}, D_{it_2}) = A + B + C, \tag{9}$$

where

$$A = (t_1 - F_i)(t_2 - F_i)\,\mathrm{var}(b) - (X_{it_1} - X_{iF_i})(X_{it_2} - X_{iF_i})\,\mathrm{var}(\beta)$$

$$B = Cov(W_{it_1} - W_{iF_i}, W_{it_2} - W_{iF_i})$$

$$= \frac{\sigma^2}{2\alpha^3}\left(2\alpha(t_1 - F_i) - 1 - e^{-\alpha(t_2 - t_1)} + e^{-\alpha(t_2 - F_i)} + e^{-\alpha(t_1 - F_i)}\right)$$

$$C = \sigma_e^2\left(1 + I(t_1 = t_2)\right) = \begin{cases} 2\sigma_e^2 & \text{if} \quad t_1 = t_2 \\ \sigma_e^2 & \text{if} \quad t_1 \neq t_2 \end{cases},$$

For $t_1 \le t_2$. By this assumption, we see that $Cov(D_{it_1}, D_{it_2})$ and hence $Cov(W_i(t), W_i(s))$, depends only on the difference in times, so it avoids the need to define natural time zero.

2.2. The Time-to-Event Model

Motivated by the promotion time model, discussed by Yakovlev and Tsodikov (1996).we present a model which allows for a zero as well as a nonzero cure fraction Chi and Ibrahim (2006). We propose such model by specifying an alternative mechanism for the characteristics of tumor growth. Instead of assuming the carcinogenic cells turn active only at the beginning of the study, we allow the possibility that active carcinogenic cells may occur at anytime after the start of the study. So that, in addition to some carcinogenic cells remaining active after initial treatment, new carcinogenic cells are assumed to occur over time after this treatment. Thus the number of carcinogenic cells changes over time, and the risk of developing a cancer relapse becomes dynamic over time. the development of any active carcinogenic cells to become a detectable tumor then leads to relapse. In terms of the statistical modeling, the promotion times for carcinogenic cells to become detectable tumor are assumed to be independent and identically distributed with a common *semiparametric* distribution function. A stochastic nonhomogeneous Poisson process is also introduced to model the variation of the number of carcinogenic cells over time.

For an individual in the population let $N(t)$ denote the number of carcinogenic cells occurring at time t and $C_l, (l = 1,..., N^*)$ denote the random time for the lth carcinogenic cell to produce a detectable cancer mass, C_l are independent and identically distributed with a common semiparametric distribution function

$$F(y) = 1 - S(y) \tag{10}$$

where $N^* = \int_0^y N(t)dt$, represents the total number of active carcinogenic cells that have occurred before relapse at $T = y$.

Definition 1: *A Poisson process with a non-constant rate $\lambda = \lambda(t)$ is called a non- homogeneous Poisson process. In this case we have*

- *Non-overlapping increments are independent ,*
- $P(N(t + \Delta t) - N(t) = 1) = \lambda(t)\Delta t + o(\Delta t)$
- $P(N(t + \Delta t) - N(t) \ge 2) = o(\Delta t)$,

where $g(y) = o(y), \; y \to 0$ is the usual symbolic way of writing the relation $\lim_{y \to 0} \frac{g(y)}{y} = 0.$

In the promotion time model, N is assumed to be independent of t and has a Poisson distribution at the beginning of the study, in our model we propose to have $N(t)$ changed over time so that, according to definition (1), $N(t)$ will follow the non-homogeneous Poisson process with mean $\lambda(t)$.

Theorem 1: *If* $N(t), t > 0$ *is a Poisson process with mean* $\lambda(t)$, *then* $N^* = \int_0^y N(t)dt$ *is a Poisson random variable with parameter* $\Lambda(y) = \int_0^y \lambda(t)dt$. i.e. $P(N^* = k) = \frac{[\Lambda(y)]^k e^{-\Lambda(y)}}{k!}$.

Proof: Recall that the moment generating function of a continuous random variable is defined through Laplace transform

$$G_x(z) = E(z^x) = \sum_{i=0}^{\infty} z^i p_i \tag{11}$$

Where $p_i = P(x = i)$. Assume that N^* is a Poisson random variable with parameter $\Lambda(y)$ then $P(N^* = i) = \frac{[\Lambda(y)]^i e^{-\Lambda(y)}}{i!}$, $i = 0,1,2,...$ and

$$G_{N(t)}(z) = \exp[N(t)(z-1)]. \tag{12}$$

Define the generating function as G_t [illegible] then we can write

$$\begin{aligned} G_{t+\Delta t}(z) &= E[z^{N(t+\Delta t)}] = E[z^{N(t)+N(t+\Delta t)-N(t)}] \\ &= E[z^{N(t)}]E[z^{N(t+\Delta t)-N(t)}] \\ &= G_t(z)\left[1 - \lambda(t)\Delta t + o(\Delta t)z^0 + (\lambda(t)\Delta t + o(\Delta t)z^1) + o(\Delta t)(z^2 + z^3 + \cdots)\right] \end{aligned}$$

Furthermore

$$\frac{G_{t+\Delta t} - G_t(z)}{\Delta t} = G_t(z)\left[-\lambda(t) + \frac{o(\Delta t)}{\Delta t} + (\lambda(t) + \frac{o(\Delta t)}{\Delta t})z + \cdots\right]$$

that implies $\lim_{\Delta t \to o} \frac{G_{t+\Delta t} - G_t(z)}{\Delta t} = G_t(z)[-\lambda(t) + \lambda(t)z]$, $\frac{d}{dt}G_t(z) = G_z(t)\lambda(t)[z-1]$, and $\log G_t(z) - \log G_0(z) = \int_0^t \lambda(\xi)d\xi[z-1]$. Thus

$$G_t(z) = e^{\int_0^t \lambda(\xi)d\xi[z-1]}. \tag{13}$$

Comparing the result in (13) to that in (9) we conclude that N^* is a Poisson random variable with parameter $\Lambda(y) = \int_0^y \lambda(t)dt$ ■

Moreover, for $t \in (0, y)$, the conditional distribution of the exact time of the occur of an active carcinogenic cells given $N^*(> 0)$ are independent and identically with probability density function

$$g(t) = \frac{\lambda(t)}{\int_0^y \lambda(t)dt} = \frac{\lambda(t)}{\Lambda(t)}, \qquad t \in (0, y) \tag{14}$$

Upon the random variable C_l with distribution function $F(y)$, the conditional population survival function given N^* can then be derived as

$$S(y) = P(T > y \mid N^*) = P(\text{no carcinogenic cells by time } y \text{ given } N^*)$$
$$= \prod_{i=1}^{N^*} \left\{ \int_0^y \frac{\lambda_i(t)(1-F(y-t))}{\int_0^y \lambda_i(\xi)d\xi} dt \right\} \tag{15}$$
$$= \left\{ \int_0^y g(t)S(y-t)dt \right\}^{N^*}$$

and hence, the survival function for the population is given by

$$S_P(y) = P(\text{no cancer cells by time } y)$$
$$= P(N^* = 0) + P(C_1 > y,\ C_2 > y, ..., C_{N^*} > y,\ N^* \geq 1)$$
$$= \exp(-\Lambda(y)) + \sum_{k=1}^{\infty} \left\{ \left[\int_0^y g(t)S(y-t)dt \right]^k \times \frac{(\Lambda(y))^k \exp(-\Lambda(y))}{k!} \right\} \tag{16}$$
$$= \exp\left[\int_0^y -\lambda(t)F(y-t)dt \right]$$

the cure fraction is thus given by

$$S_P(\infty) = \exp\left\{ -\lim_{y\to\infty} \int_0^y \lambda(t)F(y-t)dt \right\}, \tag{17}$$

if the integral in (17) is bounded then the survival function has a non-zero cure fraction, otherwise the survival function in (16) leads to a proper survival function, that is $S_P(\infty) = 0$.

Using the properties of a distribution function $F(t)$ and the fact that $\lambda(t)$ is non-negative, as $y \to \infty$ the population survival function in (17) reduces to

$$S_P(\infty) = \exp\left\{ -\lim_{y\to\infty} \Lambda(t) \right\}, \tag{18}$$

that's to say, a cure rate model is characterized by a bounded cumulative mean for the number of carcinogenic cells, while a proper survival model is characterized by an unbounded cumulative risk. And hence, this development of the stochastic disease process allows models for both zero and non-zero cure fractions.

The density function corresponding to (16) is given by

$$f_P(y) = \frac{d}{dy} F_P(y)$$
$$= \int_0^y \lambda(t)f(y-t)dt \exp\left[-\int_0^y \lambda(t)F(y-t)dt \right] \tag{19}$$

where $f(y) = \frac{d}{dy}F(y)$. The hazard function is then given by

$$h_P(y) = \frac{f_P(y)}{S_P(y)} = \int_0^y \lambda(t)f(y-t)dt. \tag{20}$$

Since $S_P(y)$ is not a proper survival function when the integral $\int_0^y \lambda(t)F(y-t)dt$ is unbounded, and hence $f_P(y)$ is not a proper probability density function and $h_P(y)$ is not a hazard function corresponding to a probability distribution. However, $f(y)$ is a proper probability density function and $h_P(y)$ is compound of θ, $F(y)$, and $f(y)$. Thus, it has the proportional hazard structure when the covariates modelled through $\lambda(t)$. This structure is more appealing than the one from the standard cure rate model (1) and is computationally attractive.

The survival function for the non-cured population is given by

$$\begin{aligned} S_1(y) &= P(T > y \mid N^* \geq 1) \\ &= P(N^* \geq 1,\, T > y)/P(N^* \geq 1) \\ &= \frac{\exp\left[-\int_0^y \lambda(t)F(y-t)dt\right] - \exp[-\Lambda(y)]}{1-\exp[-\Lambda(y)]}. \end{aligned} \tag{21}$$

Note that $S_1(0) = \lim_{y\to 0} S_1(y) = 1$, and $S_1(\infty) = \lim_{y\to\infty} S_1(y) = 0$, that is, $S_1(y)$ is a proper survival function. The probability density function for the non-cured population is given by

$$\begin{aligned} f_1(y) &= -\frac{d}{dy} S_1(y) \\ &= \frac{\exp\left[-\int_0^y \lambda(t)F(y-t)dt\right]}{1-\exp[-\Lambda(y)]} \int_0^y \lambda(t) f(y-t)dt, \end{aligned} \tag{22}$$

and the hazard function for the non-cured population is then given by

$$\begin{aligned} h_1(y) &= \frac{f_1(y)}{S_1(y)} \\ &= \frac{\exp\left[-\int_0^y \lambda(t)F(y-t)dt\right]}{\exp\left[-\int_0^y \lambda(t)F(y-t)dt\right] - \exp[-\Lambda(y)]} \int_0^y \lambda(t) f(y-t)dt. \end{aligned} \tag{23}$$

The hazard function in (23) depends on y, then, we can say that $h_1(y)$ does not have a proportional hazard structure. To write $S_P(y)$ in term of the cure fraction θ, one can use the mathematical relationship between the models in (1) and (16), and then the model can be written as

$$\begin{aligned} S_P(y) &= \exp\left[-\int_0^y \lambda(t)F(y-t)dt\right] \\ &= \exp[-\Lambda(y)] + \{1-\exp[-\Lambda(y)]\} S_1(y), \end{aligned} \tag{24}$$

thus, $S_P(y)$ is a standard cure rate model with cure fraction $\theta = \exp[-\Lambda(y)]$.

To incorporate information from both the longitudinal trajectories $Y^*(t)$ and the other potential covariates (time dependent or time fixed) for survival model, then they can be joint through the rate $\lambda(t)$ by the relation

$$\begin{aligned} \lambda(t) &= \exp\{\gamma Y^*(t) + \delta Z(t)\} \\ &= \exp\{\gamma[a + bt + \beta X(t) + W(t)] + \delta Z(t)\}, \end{aligned} \tag{25}$$

where γ is a $p\times 1$ vector of regression coefficient represents the effects of the marker on the disease risk, and δ is $q\times 1$ vector of regression coefficient corresponding to the other covariates $Z(t)$. Thus $\lambda(t)$ is the conditional mean of $N(t)$ given $Y^*(t)$. The case $\gamma = 0$ implies that the subject-specific marker response is not associated with the number of carcinogenic cells in the body, i.e. we got separate model.

3. Joint Likelihood and Priors

In our joint model the unknown parameters are $\Omega = \{\mu_a,\, \sigma_a^2,\, b,\, \beta,\, \gamma,\, \delta,\, \sigma_e^2,\, \alpha,\, \sigma^2\}$. There are two methods that may be used to obtain the estimates of these parameters, the first method is the standard maximum likelihood approach, while the second method is the Bayesian approach. The Bayesian

approach avoids the troubles in maximizing the likelihood function, making inferences based on the posterior density of the parameters. We will use this approach in our modeling, focusing on the estimation of the joint posterior density of all unknown model parameters Ω.

The joint posterior density of the parameters depends on their prior density and likelihood assumptions, we will specify these assumptions as follows:

We use the notation $[\cdot]$ and $[\cdot|\cdot]$ to denote marginal and conditional densities respectively . For the priors density in Ω, we assume that all the parameters have independent prior densities and given $(\mu_a,\ \sigma_a^2)$, $a_i \overset{ind}{\sim} N(\mu_a,\ \sigma_a^2)$, and $(W_i,\ i=1,...,n)$ are independent IOU process with parameters $(\alpha,\ \sigma^2)$. The contribution of subject *i* to the conditional likelihood is

$$
\begin{aligned}
[Y_i(t_{ij}),\ (y_i,\Delta_i)|\Omega,\ X_i,\ Z_i] &= [Y_i(t_{ij})|\Omega,\ X_i,\ Z_i][y_i,\Delta_i|\Omega,\ X_i,\ Z_i] \\
&= \prod_{j=1}^{n_i} \frac{1}{\sqrt{2\pi\sigma_e^2}} \\
&\quad \times \exp\left\{ -\frac{\left(Y_i(t_{ij}) - (a+bt+\beta X(t)+W(t))\right)^2}{2\sigma_e^2} \right\} \\
&\quad \times \{P(y_i,\Delta_i|a_i,\ b,\ W_i(t),\ \beta,\ X_i,\ Z_i,\ N_i^*) \\
&\quad \times P(N_i^*|\gamma,\ \delta)\}.
\end{aligned} \tag{26}
$$

The likelihood function for the joint model involves two components. The first component involves the longitudinal process and denoted by L_1. The second component involves the likelihood function of the time-to-event variable T, denoted by L_2. Then the likelihood function for the joint model will be the product of L_1 and L_2.

For the likelihood function L_2, we will describe a semiparametric version of the parametric cure rate model in (24). In the literature most of the authors consider $F(y)$ as parametric exponential or Weibull distribution. In the promotion time model with *N* assumed to be independent of t, Ibrahim et. al. (2001) consider a piecewise exponential model for $F(y)$ which is a flexible and widely used modeling scheme for survival data.

Towards this goal, and for C_l, $(l=1,...,N^*)$ the random time for the *l*th carcinogenic cell to produce a detectable cancer mass, we will derive and construct a new distribution function $\widetilde{F}(y)$. Let y_i, be the observed time for the subject *i,* $i=1,...,n$, and we partition the time scale into *J* intervals, i.e. $0<s_1<\cdots<s_J$, $s_J > y_i$ for all *i.* Thus we have *J* intervals $(0,s_1],...,(s_{J-1},s_J]$ we thus assume that the hazard for $F(y)$ is constant and equal to π_j for the *j*th interval, $j=1,...,J$. By increasing J, the piecewise constant hazard model can essentially model any shape of the underlying hazard. A larger *J* allows more flexibility but it also introduce more unknown parameters, namely π_j 's. Thus, there is a trade-off in determining the optional *J* The best *J* usually lies between 5 and 10.

Under the piecewise exponential assumption the promotion time distribution in the *j*th interval will derived by the hazard function as:

$$
h_i(y) = \frac{f_i(y)}{S_i(y)} = \pi_j \quad \Rightarrow \quad \frac{f_i(y)}{1-F_i(y)} = \pi_j \quad \Rightarrow \quad \frac{dF_i(y)}{dy} = \pi_j\left(1-F_i(y)\right)
$$

by solving the above ordinary differential equation, we will got

$$F(y) = 1 - \exp\left\{ - \pi_j (y - s_{j-1}) - \sum_{q=1}^{j-1} \pi_q (s_q - s_{q-1}) \right\}. \tag{27}$$

Then given N^*, the conditional survival function of an active carcinogenic cell to become detectable tumor at time y_i is given by

$$\begin{aligned} \widetilde{S}(y_i) &= \int_0^{y_i} g_i(t) S(y_i - t) dt \\ &= \frac{1}{\Lambda_i(y_i)} \int_0^{y_i} \exp\{\gamma [a_i + bt + \beta X_i(t) + W_i(t)] + \delta Z_i(t)\} \\ &\quad \times \exp\left\{ - \pi_j \left(y_i - t - s_{j-1} \right) - \sum_{q=1}^{j-1} \pi_q \left(s_q - s_{q-1} \right) \right\} dt \\ &= \frac{\exp(\gamma a_i)}{\Lambda_i(y_i)} \left(\sum_{k=1}^{j} \exp\left\{ - \pi_k \left(r - s_{k-1} \right) - \sum_{q=1}^{k-1} \pi_q \left(s_q - s_{q-1} \right) \right\} \right. \\ &\quad \left. \times I(y_i > s_{k-1}) \xi(\varsigma) \right), \end{aligned} \tag{28}$$

where *j* is the interval index such that $y_i \in (s_{j-1},\ s_j]$, and $r = \min(y_i, s_k)$

$$\xi(\varsigma) = \int_{s_{k-1}}^{r} \exp\{\gamma [a_i + bt + \beta X_i(t) + W_i(t)] + \delta Z_i(t) + \pi_k t\} dt.$$

Information about the continuous stochastic process $W_i(t)$ is needed to calculate $\xi(\varsigma)$. We approximate the continuous function $W_i(t)$ by its value at a finite set of i_w grid points $(t_{i1}^w, t_{i2}^w, ..., t_{ii_w}^w)$ in order to facilitate the estimation of all parameters in the joint model. The i_w grid points are chosen to contain all the time points where marker measurements is taken for subject *i,* since the value of $W_i(t)$ at these points are used in the longitudinal model and needed to be estimated. also we choose the grid points so that the maximum of $\{t_{ij}^w - t_{ij-1}^w,\ \ j = 1, ..., i_w\}$ (assuming $t_{i0}^w = 0$) is very small and $W_i(t)$ can be considered as constant over the interval $(t_{ij-1}^w,\ t_{ij}^w]$. Further, we assume also that the time dependent covariates (if there any) are constant over the same interval.

Since we already partition the scalar time y_i into *J* intervals then the i_w grid points will be considered only in one interval of *J*, so that in each grid i_w interval we will assume $t_{i0}^w = s_{k-1},\ k = 1, ..., J.$

Thus $\xi(\varsigma)$ can be evaluated as

$$\xi(\varsigma) = \sum_{l=1}^{l_i} \int_{t_{l-1}'}^{l} \exp\{\gamma(bt + \beta X_i(t) + W_i(t)) + \delta Z_i(t) + \pi_k t\} dt$$
$$- \int_{t_{l_i}'}^{r} \exp\{\gamma(bt + \beta X_i(t) + W_i(t)) + \delta Z_i(t) + \pi_k t\} dt$$
$$= \sum_{l=1}^{l_i} \sum_{m=1}^{M_i(l)} \exp\left\{\gamma\left(\beta X_i(t_{lm}'') + W_i(t_{lm}'')\right) + \delta Z_i(t_{lm}'')\right\}$$
$$\times \frac{\exp(\gamma b + \pi_k) t_{lm}'' - \exp(\gamma b + \pi_k) t_{l(m-1)}''}{(\gamma b + \pi_k)}$$
$$- \sum_{m=1}^{M_i(r)} \exp\left\{\gamma\left(\beta X_i(t_{rm}'') + W_i(t_{rm}'')\right) + \delta Z_i(t_{rm}'')\right\}$$
$$\times \frac{\exp(\gamma b + \pi_k) t_{rm}'' - \exp(\gamma b + \pi_k) t_{r(m-1)}''}{(\gamma b + \pi_k)},$$

where $r = \min(y_i, s_k)$, $l_i = \max\{l : t_l' \le r\}$, for $l = 1,..., l_i$, $t_{l0}'' = t_{l-1}'$, $t_{lM_i(l)}'' = t_l'$ and $(t_{l1}'', t_{l2}'',..., t_{l(M(l)-1)}'')$ all are grid points ordered in interval (t_{l-1}', t_l'), for subject *i;* $(t_{r1}'', t_{r2}'', \ldots, t_{r(M_i(r)-1)}'')$ all are grid points ordered in interval (t_{li}', r) for subject *i*, $t_{r0}'' \blacksquare t_{li}'$, $t_{l_i M_i(r)}'' = r$, and $t_0' = s_{k-1}$.

Given N_i^* the conditional distribution function $F_i(y_i)$ for an active carcinogenic cells to become a detectable tumor cells at time y_i is given by

$$\widetilde{F}(y) = 1 - \widetilde{S}(y_i) \tag{29}$$

also the conditional density function is given by

$$\widetilde{f}(y_i) = \frac{d}{dy_i}\widetilde{F}(y) = \frac{d}{dy_i}(1 - \widetilde{S}_i(y_i)) = \pi_j \widetilde{S}_i(y_i) \tag{30}$$

where $f(y) = \frac{d}{dy}F(y) = \pi_j \exp\left\{-\pi_j\left(y - s_{j-1}\right) - \sum_{q=1}^{j-1} \pi_q\left(s_q - s_{q-1}\right)\right\}$.

For the cumulative rate $\Lambda_i(y_i)$, again we will use the same techniques that we used in derivation of $\widetilde{S}(y_i)$, since the IOU stochastic process $W_i(t)$ appear in the integral, so that, we have

$$\Lambda_i(y_i) = \int_0^{y_i} \lambda_i(t) dt$$
$$= \sum_{k=1}^{k_i} \sum_{j=1}^{J_i(k)} \exp\left\{\gamma\left(a_i + bt_{kj}^i + \beta X_i(t_{kj}^i) + W_i(t_{kj}^i)\right) + \delta Z_i(t_{kj}^i)\right\}$$
$$\times \left\{\exp\left(\gamma b t_{kj}^i\right) - \exp\left(\gamma b t_{k(j-1)}^i\right)\right\} / \gamma b \tag{31}$$
$$- \sum_{j=1}^{J_i(y_i)} \exp\left\{\gamma\left(a_i + bt_{y_{ii}j}^i + \beta X_i(t_{y_{ii}j}^i) + W_i(t_{y_{ii}j}^i)\right) + \delta Z_i(t_{y_{ii}j}^i)\right\}$$
$$\times \left\{\frac{\exp\left(\gamma b t_{y_i j}^i\right) - \exp\left(\gamma b t_{y_i(j-1)}^i\right)}{\gamma b}\right\}.$$

Given the parameters $\phi_1 = \{b, \mu_a, \sigma_a^2, \beta, \alpha, \sigma^2, \sigma_e^2\}$, then for the longitudinal data, the likelihood can be defined as:

$$L_1(\phi_1) = \prod_{i=1}^{n} \left\{ \prod_{j=1}^{n_i} \left[Y_i(t_{ij}) \mid a_i,\, b,\, W_i(t),\, \beta,\, \sigma_e^2\ X_i \right] \right\} \times \left[W_i(t) \mid \alpha,\, \sigma^2 \right] \left[a_i \mid \mu_a,\, \sigma_a^2 \right] \tag{32}$$

where the full conditional distribution $[W_i(t) \mid \alpha,\, \sigma^2]$ for the discrete IOU process $W_i = (W_i(t_{i1}^w),\ W_i(t_{i2}^w),\ \ldots,\ W_i(t_{ii_w}^w))$ can be defines as follows: let Σ_i be the variance covariance matrix of $(W_i(t_{i1}^w),\ W_i(t_{i2}^w),\ldots,\ W_i(t_{ii_w}^w))$. Then we have

$$\left[W_i \mid \alpha,\, \sigma^2 \right] = \frac{\Sigma_i^{-\frac{1}{2}}}{2\pi} \exp\left(-\frac{W_i^T \Sigma_i^{-1} W_i}{2} \right),$$

and the full conditional distribution $[a_i \mid \mu_a,\, \sigma_a^2]$ given by

$$\left[a_i \mid \mu_a,\, \sigma_a^2 \right] = \frac{1}{\sqrt{2\pi\sigma_a^2}} \exp\left(-\frac{(a_i - \mu_a)^2}{2\sigma_a^2} \right).$$

Given the parameters $\phi_2 = \{\gamma, \delta, \pi_j\}$, then the second component of the likelihood function $P(Y \mid Y^*, Z, N^*)$ can be derived as

$$\begin{aligned} L_2(\phi_2) &= P(y_i;\, \Delta_i \mid a_i,\, b,\, W_i(t),\, \beta,\, X_i,\, Z_i,\, N_i^*)\, P(N_i^* \mid \gamma,\, \delta) \\ &= \prod_{i=1}^{n} \prod_{j=1}^{J} (\widetilde{S}_i(y_i))^{(N_i^* - \Delta_i)\Delta_{ij}}\, (N_i^* \widetilde{f}(y_i))^{\Delta_i \Delta_{ij}} \\ &\quad \times \exp\left\{ \sum_{i=1}^{n} N_i^* \log(\Lambda_i(y_i)) - \log(N_i^*!) - \Lambda_i(y_i) \right\} \end{aligned} \tag{33}$$

where $\widetilde{S}_i(y_i)$, $\widetilde{f}(y_i)$ and $\Lambda_i(y_i)$ are given in (29) , (30) and (31) respectively, Δ_{ij} censored indicator equal one if the *i*h subject fails in the *j*h interval and zero otherwise.

Now, let $\phi = \phi_1 \cup \phi_2 = \{b, \mu_a, \sigma_a^2, \beta, \alpha, \sigma^2, \sigma_e^2, \gamma, \delta, \pi_j\}$, the prior specification for ϕ are given jointly as

$$[\phi] = [b][\mu_a][\sigma_a^2][\beta][\alpha][\sigma^2][\sigma_e^2][\gamma][\delta][\pi_j], \tag{34}$$

and hence, the joint likelihood of the complete data is given by

$$L(\phi) = L_1(\phi_1) L_2(\phi_2)[\phi] \tag{35}$$

4. Bayesian Model Assessment

To assess the model fit and compare different models, we calculate the Conditional Predictive Ordinate (CPO), Gelfand et all (1992), and the Deviance Information Criterion (DIC) recently proposed by Spielhalter et al. (2002). where there formulas given by

$$CPO_i = \left(\int \frac{1}{f\left(Y_i^*, T_i, \Delta_i \mid \phi, X_i, Z_i\right)} \left[\phi \mid D \right] d\phi \right)^{-1} \tag{36}$$

where $\left[\phi \mid D \right]$ is the posterior density of ϕ based on the data including all subjects. Using (36) a Monte Carlo method presented in Chen (2000) is readily used for computing CPO_i if $f(Y_i^*, T_i, \Delta_i \mid \phi, X_i, Z_i)$ can be evaluated for each ϕ. However, due to the complexity of the joint model, an analytical

evaluation of $f(Y_i^*, T_i, \Delta_i \mid \phi, X_i, Z_i)$ does not appear possible. Therefore, an alternative Monte Carlo CPO_i approximate of will be used, which given by

$$\widehat{CPO_i} \approx \left(\frac{1}{M} \sum_{m=1}^{M} \frac{1}{L_i(\theta_m)} \right)^{-1} \tag{37}$$

models with greater $\sum_{i=1}^{n} \log(CPO_i)$ indicate a better fit, and

$$DIC = -\frac{4}{M} \sum_{m=1}^{M} \log L(\phi_{[m]}) + 2\log(\overline{\phi_{[m]}}), \tag{38}$$

the smallest the DIC , the better the fit of the model.

5. Sampling Methods and Simulation Study

In the previous sections, we have proposed a new class of joint semiparametric cure rate model to analyze a univariate longitudinal and survival data in the presence of cure fraction. In this section, we will evaluate the performance of this joint model by conducting a simulation study. We investigate how will the population parameters can be estimated in terms of bias and converge rate, and compare these results to that of the separate modeling approach by applying methods of MCMC sampler. Also we study how the following factor affects the performance of the joint model: censoring rate and prior information for the parameters.

5.1. Simulation Design

To illustrate our joint semiparametric model, we setup our simulation study represent a randomize clinical trial, in which $n = 100$ subjects are randomized. Each longitudinal marker $Y_i(t_{ij})$, $i = 1,...,n$; $j = 1,...,n_i$, was simulated as the sum of the trajectory function $Y_i^*(t_{ij})$ and the error terms $\varepsilon_i(t_{ij})$, each subject has his observed longitudinal measured $n_i = 10$ at time points $t_1 = 0.1,...,t_{10} = 1,$ until the relapse or the end or the study. For the survival data, we consider a model in the presence of cure; that is we took the mean of the Poisson process at time *t* as in (25) to be

$$\lambda_i(t) = \exp\{\gamma[a_i + bt + \beta X_i(t) + W_i(t)] + \delta Z_i\},$$

for $i = 1,...,100$, where Z_i is a binary baseline covariates with half of the subjects having one and the other half having zero, and the promotion time was considered as in (29) with $J = 5,10$ which gives a semiparametric cure rate model. This setup leads to a cure rate structure for the survival time. we will modeled the longitudinal data and survival data separately i.e. for longitudinal data we will use model (6) and for survival data we will use model (25) with $\gamma = 0,$ and use the maximum likelihood estimation to get an initial estimate of the population parameters $\phi = \{b, \mu_a, \sigma_a^2, \beta, \alpha, \sigma^2, \sigma_e^2, \gamma, \delta\}$ say $\phi^{(0)} = \{b^{(0)}, \mu_a^{(0)}, (\sigma_a^2)^{(0)}, \beta^{(0)}, \alpha^{(0)}, (\sigma^2)^{(0)}, (\sigma_e^2)^{(0)}, \gamma^{(0)}, \delta^{(0)}\}$ and use them as initial values in MCMC sampler.

For data generating and parameter estimations , we sample from the following conditional posterior distributions:

1) $\left[\sigma_a^2 \mid \cdot\right] \propto IG\left(\left(\frac{n}{2} - 1\right), \frac{\sum_{i=1}^{n}(a_i - \mu_a)^2}{2}\right)\left[\sigma_a^2\right]$

2) $\left[\mu_a \mid \cdot\right] \propto N\left(\frac{\sum_{i=1}^{n} a_i}{n}, \frac{\sigma_a^2}{n}\right)$

3) $\left[\sigma_e^2 \mid \cdot\right] \propto IG\left(\frac{\sum_{i=1}^{n} n_i}{2},\ \frac{\sum_{i=1}^{n}\sum_{j=1}^{n_i}\left(Y_i(t_{ij})-\left(a_i+bt_{ij}+\beta X_i(t_{ij})+W_i(t_{ij})\right)\right)^2}{2}\right)\left[\sigma_e^2\right]$

4) $\left[\sigma^2 \mid \cdot\right] \propto IG\left(\frac{\sum_{i=1}^{n} i_w}{2}-1,\ \frac{\sum_{i=1}^{n} W_i^T \frac{\Sigma_i^{-1}}{\sigma^2} W_i}{2}\right)\left[\sigma^2\right]$

5) $\left[\beta_l \mid \cdot\right] \propto N(m_{\beta_l}, v_{\beta_l})\left[\beta_l\right]\exp\sum_{i=1}^{n}\left\{\Delta_i \log\left(\tilde{f}_i(y_i)\right)+\Delta_i \log\left(\Lambda_i(y_i)\right)-\Lambda_i(y_i)\left(1-S_i(y_i)\right)\right\}$,

where $m_{\beta_l} = \frac{\sum_{i=1}^{n}\sum_{j=1}^{n_i} X_{il}(t_{ij})\left(Y_i(t_{ij})-\left(a_i+bt_{ij}+\beta(-l)X_i(-l)(t_{ij})+W_i(t_{ij})\right)\right)}{\sum_{i=1}^{n}\sum_{j=1}^{n_i} X_{il}^2(t_{ij})}$, and

$v_{\beta_l} = \frac{\sigma_e^2}{\sum_{i=1}^{n}\sum_{j=1}^{n_i} X_{il}^2(t_{ij})}$.

6) $\left[a_i \mid \cdot\right] \propto N(m_a, v_a)\exp\left\{\Delta_i \log\left(\tilde{f}_i(y_i)\right)+\Delta_i \log\left(\Lambda_i(y_i)\right)-\Lambda_i(y_i)\left(1-S_i(y_i)\right)\right\}$,

where $m_a = \frac{\frac{\mu_a}{\sigma_a^2}+\sum_{j=1}^{n_i}\left(Y_i(t_{ij})-bt_{ij}-\beta X_i(t_{ij})-W_i(t_{ij})\right)}{\frac{n_i}{\sigma_e^2}+\frac{1}{\sigma_a^2}}$, and $v_a = \left(\frac{n_i}{\sigma_e^2}+\frac{1}{\sigma_a^2}\right)^{-1}$

7) $\left[b \mid \cdot\right] \propto N(\mu_b, \sigma_b^2)\exp\sum_{i=1}^{n}\left\{\Delta_i \log\left(\tilde{f}_i(y_i)\right)+\Delta_i \log\left(\Lambda_i(y_i)\right)-\Lambda_i(y_i)\left(1-S_i(y_i)\right)\right\}\left[b\right]$,

where, $\mu_b = \sum_{i=1}^{n}\sum_{j=1}^{n_i} t_{ij}\left(Y_i(t_{ij})-a_i-\beta X_i(t_{ij})-W_i(t_{ij})\right)$ and $\sigma_b^2 = \frac{\sigma_e^2}{\sum_{i=1}^{n}\sum_{j=1}^{n_i} t_{ij}^2}$

8) $\left[N_i^* \mid \cdot\right] \propto Pois(S_i(y_i)\Lambda_i(y_i))+\Delta_i$

9) $\left[\alpha \mid \cdot\right] \propto \frac{\exp\left(-0.5\sigma^2\sum_{i=1}^{n} W_i^T \frac{\Sigma_i^{-1}}{\sigma^2} W_i\right)}{\prod_{i=1}^{n}\left|\frac{\Sigma_i}{\sigma^2}\right|^{\frac{1}{2}}}\left[\alpha\right]$

10) $\left[\gamma \mid \cdot\right] \propto \exp\sum_{i=1}^{n}\left(\Delta_i \log\left(\Lambda_i(y_i)\tilde{f}_i(y_i)\right)-\Lambda_i(y_i)\left(1-S_i(y_i)\right)\right)\left[\gamma\right]$

11) $\left[\delta \mid \cdot\right] \propto \exp\sum_{i=1}^{n}\left(\Delta_i \log\left(\Lambda_i(y_i)\right)-\Lambda_i(y_i)\left(1-S_i(y_i)\right)\right)\left[\delta\right]$

12) $\left[\pi_j \mid \cdot\right] \propto G\left(\alpha_\pi, \beta_\pi\right)$,

where

$\alpha_\pi = \sum_{i=1}^{n}\Delta_i I\left(s_{k-1} < y_i \le s_k\right)$

and

$\beta_\pi = \sum_{i=1}^{n} I\left(y_i > s_{k-1}\right)\int_{s_{k-1}}^{r}\exp\left\{\gamma\left[a_i+bt+\beta X_i(t)+W_i(t)\right]+\delta Z_i(t)\right\}$

The full conditional distributions of the parameters σ_e^2, μ_a σ_a^2 and σ^2 that appearing only in the longitudinal model are a product of its prior density and some standard distribution which are conjugate priors for these parameters. While the conditional distribution of the parameters b, $(\beta_1,...,\beta_p)$, if the contributions from the survival data are ignored, then the normal distribution are conjugate priors, if the contributions from the survival data are not ignored, then we will use it as a proposed density in ARMS sampler. The main difficulty which we will meet in the prior distributions is that when no standard form appears in the posterior distribution. In general, we do not have performance in choosing priors for the parameters α, γ, δ since their full conditional densities have no

conjugate priors. One may use normal priors for γ, δ since they take values belong to the real line For the IOU stochastic process parameter α, gamma and inverse gamma distributions are potential choices as priors since it takes only positive values.

We examined our joint model at $J = 5,10$ (a semiparametric exponential model) with $b = -3.5$, $\beta = 1$, $\mu_a = 4.0$, $\sigma_a^2 = 0.02$, $\alpha = 0.138$, $\sigma^2 = 0.12$, $\sigma_e^2 = 0.05$, $\gamma = -1$, $\delta = 2.4$, and $\pi_k = 0.05$ for $k = 1,...,J$. All the parameters were assumed independent a proiori and assigned non-informative priors, so we choose $b \sim N(-4.00,1.00)$; $\beta \sim N(1.5,0.50)$; $\mu_a \sim N(4.00,1.00)$; $\sigma_a^2 \sim IG(2.00,0.01)$; $\alpha \sim F(1.5,1.5)$; $\sigma^2 \sim IG(1.00,0.02)$; $\sigma_e^2 \sim IG(2.00,0.01)$; $\gamma \sim N(-1.5,1.0)$; $\delta \sim N(3.0,1.0)$ and $\pi_k \sim G(0.02,1.0)$.

For the parameters $\{\mu_a, \sigma_a^2, \sigma^2, \sigma_e^2, \pi_k\}$ drawing random variates from their full conditional distribution is straight forward, therefore, we will use the full conditional density as a proposal density in Gibbs sampler algorithm, and in sampling process each updating step for these parameters, a new draw from the full conditional density is always accepted. We perform this algorithm for each parameter 2,000 Gibbs samples after 1000 burn-in. The histogram, the time series plots of one sequence of Gibbs samples for different number of iterations and the average number of these iterations for the parameter μ_a are presented in Figure (1).

Figure 1: Histogram, time series and average values plots respectively for the parameter values μ_a at 500, 1000, and 2000 iterations respectively, using Gibbs sampler.

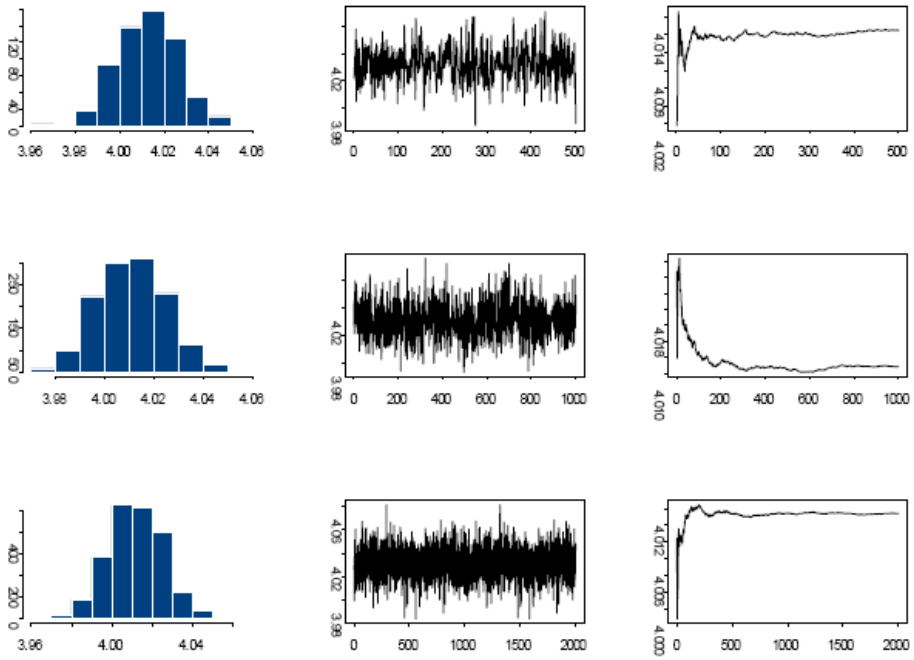

Figure 2: Posterior histogram, time series and average value plots respectively for the parameter values β at 500, 1000, and 2000 iterations respectively, using MH sampler.

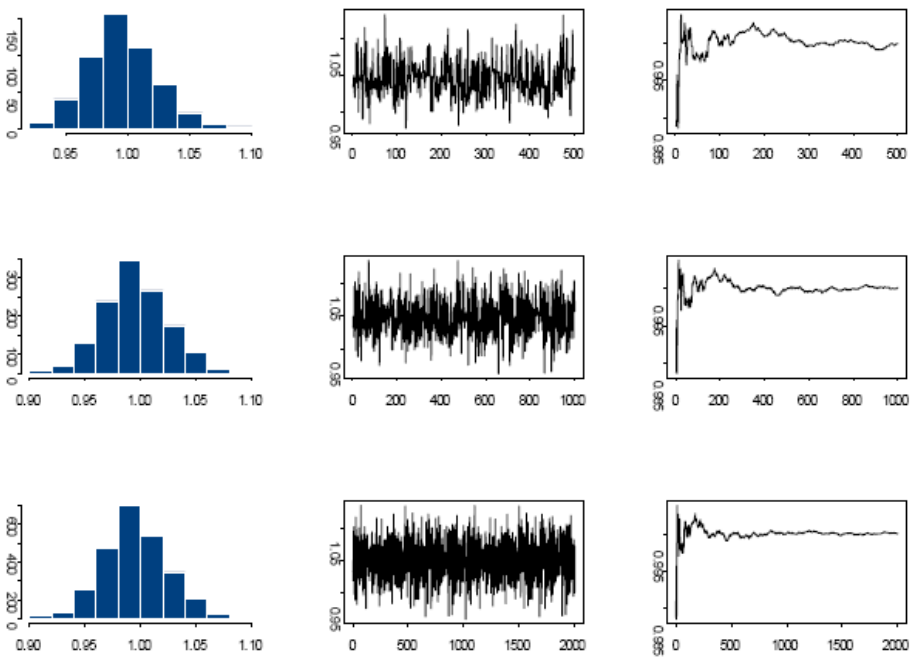

For the parameters $\{b, \beta\}$ one can not draw a random variate from these densities directly due to the terms from the time-to-event data. For each one of these parameters, we use the Metropolis Sampling (MS) algorithm to obtain the update in the Gibbs sampling sequence. With the Gibbs algorithm, a proposal density is required to draw a random variates and to be compared with the full conditional density at this random variate and at the current value of the parameter. so that we will use the standard density, which we got from the contribution of the longitudinal data and priors as a proposal density. The histogram, the time series plots of one sequence of Gibbs samples for different number of iterations and the average number of these iterations for the parameter ϕ_a are presented in Figure (2). For the parameters $\{\alpha, \gamma, \delta_1 ..., \delta_p\}$ is not follow any standard distribution, it is just an algebraic expression which come from the contribution the longitudinal and time-to-event data, so that, for such parameters, one can not draw random variates from their full conditional densities. For each of these parameters we propose using a normal density as a proposal density, and then the Adaptive Rejection Metropolis Sampling (ARMS) within Gibbs sampling will be used by considering $f(x) = q(\theta \mid D)$, and then constructing a sampling distribution function g for which samples can be readily drawn. The histogram, the time series plots of one sequence of Gibbs samples for different number of iterations and the average number of these iterations for the parameter μ_a are presented in Figure (3).

Figure 3: Posterior histogram, time series and average values plots respectively for the parameter values δ at 500, 1000, and 2000 iterations respectively, using ARMS sampler.

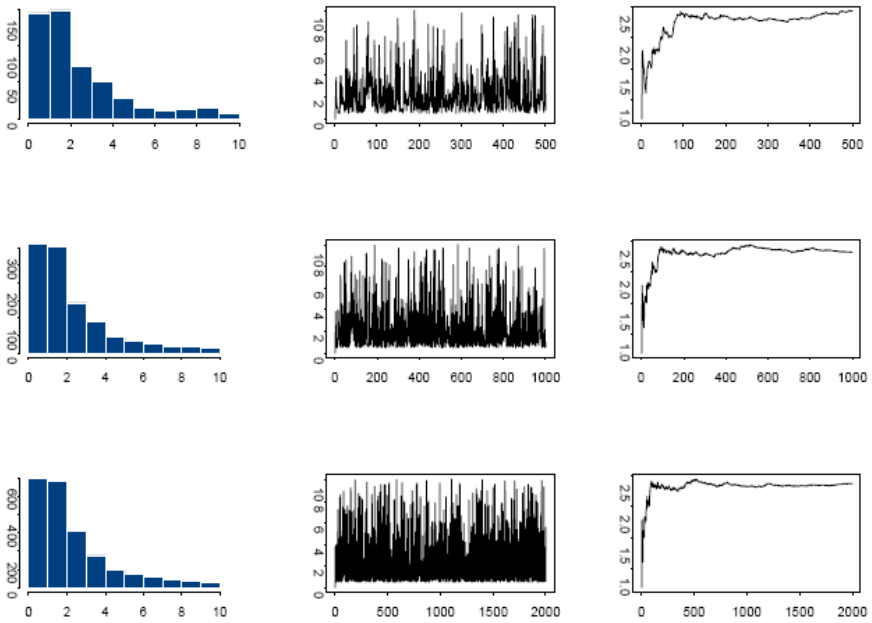

5.2. Numerical Results

With the initial values of the parameters for which the data are generated considered as the truth values of the parameters, estimate Monte Carlo Summary statistics, Monte Carlo Standard Deviation (MCSD), Mean Squared Error (MSE), 95% Confidence Converge Rate (CCR), and Bias in Percentage Terms (BPT) are presented in Table (1), where, MCE stand for Monte Carlo Error and it can be evaluated as follows : In our simulate study we used 100 data replications, thus the resulting estimates are subject to sampling variation (Monte Carlo Error), this variation for the point estimate can be calculated as $\hat{p} = MCSD/\sqrt{100}$, the MCE then can be found by $MCE = \sqrt{\frac{\hat{p}(1-\hat{p})}{100}}$.

Table 2: Estimate Monte Carlo Summary statistics

Para- meter	True Value	Estimated Value	MCSD	MSE	95% CCR	BP	MCE
b	-3.500	-3.498	0.031	8.236×10^{-4}	95%	-0.057%	6×10^{-3}
μ_a	4.000	4.001	0.019	3.450×10^{-4}	98%	0.025%	4×10^{-3}
σ_a^2	0.020	0.020	0.005	2.471×10^{-5}	99%	-0.001%	2×10^{-3}
α	0.138	1.400	0.967	0.928	93%	1.450%	3×10^{-2}
σ^2	0.120	0.119	0.0823	6.622×10^{-3}	96%	-0.833%	9×10^{-3}
β	1.000	0.997	0.041	1.688×10^{-3}	95%	-.274%	6×10^{-3}
σ_e^2	0.050	0.050	0.008	6.855×10^{-5}	94%	0.140%	3×10^{-3}
γ	-1.000	-1.003	0.117	1.469×10^{-4}	97%	0.291%	1×10^{-2}
δ	2.400	2.401	0.259	0.0701	94%	0.042%	2×10^{-2}

The results in table (1) assert the convergence of the Markov Chain and the samplers reached the convergence after 2,000 iterations after 1,000 iterations are burn-in. With less nonparametricity $(J = 5)$, posterior means, posterior standard deviations, and 95% highest posterior density intervals for each parameter in the joint and separate models, are represented in Tables(2). With high

nonparametricity ($J = 10$), posterior means, posterior standard deviations, and 95% highest posterior density intervals for each parameter in the joint and separate models, are represented in Tables(3)

Table 2: Posterior Estimate, SD, and 95% C.I. for Separate and Joint Models at J=5

Para- meter	Joint Model mean	Separate Models SD	95% C.I.	mean	SD	95% C.I.
b	-3.492	0.074	(-3.63, -3.34)	-3.489	0.110	(-3.71, -3.27)
μ_a	4.001	0.013	(3.975, 4.026)	4.001	0.013	(3.975, 4.026)
σ_a^2	0.019	0.011	(0, 0.041)	0.019	0.011	(0, 0.041)
α	1.405	0.283	(0.850, 1.960)	1.414	0.352	(0.724, 2.104)
σ^2	0.119	0.016	(0.088, 0.150)	0.119	0.016	(0.088, 0.150)
β	0.997	0.028	(0.942, 1.052)	0.991	0.090	(0.815, 1.167)
σ_e^2	0.051	0.011	(0.294, 0.073)	0.051	0.011	(0.294, 0.073)
γ	-1.008	0.080	(-1.16, -0.85)	-1.013	0.127	(-1.26, -0.76)
δ	2.405	0.051	(2.305, 2.505)	2.391	0.088	(2.219, 2.563)
π_1	0.061	0.014	(0.033, 0.088)	0.064	0.016	(0.033, 0.095)
π_2	0.055	0.008	(0.039, 0.071)	0.053	0.008	(0.037, 0.069)
π_3	0.068	0.022	(0.025, 0.111)	0.065	0.018	(0.030, 0.100)
π_4	0.037	0.030	(0.0, 0.096)	0.042	0.025	(0.0, 0.091)
π_5	0.052	0.003	(0.046, 0.058)	0.055	0.008	(0.039, 0.071)

Table 3: Posterior Estimate, SD, and 95% C.I. for Separate and Joint Models at J=10

Para- meter	Joint Model mean	Separate Models SD	95% C.I.	mean	SD	95% C.I.
b	-3.498	0.031	(-3.559, -3.437)	-3.493	0.082	(-3.654, -3.332)
μ_a	4.001	0.013	(3.975, 4.026)	4.001	0.013	(3.975, 4.026)
σ_a^2	0.020	0.011	(0, 0.041)	0.019	0.011	(0, 0.041)
α	1.400	0.210	(0.988, 1.812)	1.404	0.263	(0.889, 1.920)
σ^2	0.119	0.016	(0.088, 0.150)	0.119	0.016	(0.088, 0.150)
β	0.999	0.004	(0.991, 1.007)	0.996	0.057	(0.884, 1.108)
σ_e^2	0.050	0.011	(0.294, 0.073)	0.051	0.011	(0.294, 0.073)
γ	-1.003	0.037	(-1.076, -0.930)	-1.004	0.048	(-1.098, -0.910)
δ	2.401	0.021	(2.360, 2.442)	2.395	0.066	(2.266, 2.524)
π_1	0.058	0.013	(0.033, 0.083)	0.059	0.015	(0.033, 0.090)
π_2	0.042	0.025	(0.0, 0.091)	0.037	0.030	(0.0, 0.096)
π_3	0.070	0.036	(0.0, 0.140)	0.073	0.038	(0.0, 0.147)
π_4	0.056	0.009	(0.039, 0.072)	0.055	0.008	(0.039, 0.071)
π_5	0.047	0.003	(0.041, 0.053)	0.043	0.025	(0.0, 0.091)
π_6	0.059	0.015	(0.031, 0.085)	0.061	0.012	(0.037, 0.088)
π_7	0.055	0.008	(0.039, 0.071)	0.050	0.002	(0.046, 0.054)
π_8	0.044	0.026	(0.0, 0.092)	0.041	0.028	(0.0, 0.095)
π_9	0.027	0.087	(0.0, 0.198)	0.025	0.088	(0.0, 0.20)
π_{10}	0.032	0.030	(0.0, 0.097)	0.040	0.028	(0.0, 0.096)

By using $M = 1000$ for model assessment by measuring the $LPML$ statistic, also to assert our assessment, DIC were calculated for different models and the results are described in Table(4).

Table 4: The *LPML* and *DIC* for separate and joint models

		J=5		J=10	
Model		***LPML***	***DIC***	***LPML***	***DIC***
Joint Model IOU included		-726.47	1385.71	-718.66	1376.13
Joint Model IOU excluded		-739.38	1402.35	-730.81	1394.65
Joint Model with B.M.		-7235.94	1388.85	-722.64	1387.17
Separate Models :	Survival	-290.07	639.15	-282.33	618.55
	Longitudinal	-555.11	836.95	-539.94	788.97
	Total	-845.18	1476.10	-822.27	1407.52

We observe that the joint model that include the IOU stochastic process and the Joint Model corresponds to Brownian Motion give a better fit to the data than the one excluding the IOU term and separately. In other words, the longitudinal model with the IOU stochastic process or Brownian motion (α is finite or infinitely large) yields a superior fit than the model with the random effects, also comparing the values of $LPML$ and DIC statistics for joint model and the separate models, the results indicate that the joint cure rate model appear to provide a more adequate fit to the simulated data than the separate models. Moreover, with heavy expensive computational process by increasing the value of J (more nonparametricity), we got more adequate fit to the simulated data and more precise estimate for the most important parameter.

Conclusion and Future Study

We have proposed a new model for jointly modeling longitudinal and time-to-event data in presence of cure fraction, our joint model allows for a zero as well as a nonzero cure fraction. With the ready availability of power desktop computers to fitting these complicated joint models by incorporating the IOU stochastic process in the longitudinal model and considering a semiparametric distribution function for the promotion times progression with $N(t)$ the number of carcinogenic cells changed over time *t*, we have attractive, a flexible and robust approach to fitting the longitudinal measures in the joint model.

For the purpose of checking the nonparametricity in the simulation study and more computational process, we choose *J*=5, and *J*=10. Bayesian inferences implemented via modern MCMC methods is used to fit our joint model and the *LMP* and *DIC* are used as formal iteration for model selection. The convergence of each MCMC were checked by monitored estimating the scale factor $\sqrt{\hat{R}}$, and the convergence of the Markov Chain and the samplers reached the convergence after 2,000 iterations after 1,000 iterations are burn-in.

The numerical results in this simulation study show that by incorporating the IOU stochastic process in the longitudinal trajectory and considering a semiparametric exponential function for the time progression distribution give amazing fit for the simulated data. Moreover, when there is an association between the longitudinal and the survival data (joint model), ignoring this association (separate models) would lead to biased estimates for the most important parameters, and thus results in a lack of fit for the data.

For future, this work will be extended for multivariate longitudinal and time-to-event data, however, to induce correlation between failure times, shared frailty will be introduced. and then real data will be used.

References

[1] Betensky, R. A. and Schoenfeld, D. A. (2001), Nonparametric Estimation in A cure Model with Random Cure times, Biometrics 57, 282-286.

[2] Brown, E.R. and Ibrahim, J.G. (2003a). A Bayesian semiparametric joint hierarchical model for longitudinal and survival data. Biometrics 59, 221-228.

[3] Brown, E.R. and Ibrahim, J.G. (2003b). Bayesian approaches to joint cure rate and longitudinal models with applications to cancer vaccine trials. Biometrics 59, 686 ≤ 693.

[4] Bycott, P. and Taylor, J. (1998). A comparison of smoothing techniques for CD4 data measured with error in a time-dependent Cox proportional hazards model. Statistics in Medicine 17, 2061-2077.

[5] Carlin, B. P. and Louis, T. A. (2000), Bayes and Empirical Bayes Methods for Data Analysis, Chapman and Hall.

[6] Chen, M. H., Ibrahim, J. G., Sinha, D. (2004). A new Joint Model for Longitudinal and Survival Data with a Cure Fraction, Journal of Multivariate Analysis. 91, 18-34.

[7] Chen, M. H., Shao, Q. M., Ibrahim, J. G. (2000), Monte Carlo Methods in Bayesian Computation, Springer, New York.

[8] Chi, Y. and Ibrahim, J. G. (2006), Joint Models for Multivariate Longitudinal and Multivariate Survival Data, Biometrics 62, 432--445.

[9] Cowling, B. J., Hutton, J. L., and Shaw, J. E. H. (2006), Joint modelling of Event Counts and Survival Times, Journal of Applied, Statistics 55, part 1, 31-39.

[10] Cowles, M. K. and Carlin B. P. (1996) , Markove Chain Monte Carlo Convergence Diagnostics: A comparative Review, Journal of the American Statistical Association 91, 883-904

[11] Cox, D.R. (1972). Regression models and life tables (with Discussion). Journal of the Royal Statistical Society, Series B 34, 187-200.

[12] Dafni, U.G. and Tsiatis, A.A. (1998). Evaluating surrogate markers of clinical outcome measured with error. Biometrics 54, 1445-1462.

[13] Davidian, M. and Gallant, A.R. (1993). The nonlinear mixed effects model with a smooth random effects density. Biometrika 80, 475-488.

[14] DeGruttola, V. and Tu, X.M. (1994). Modeling progression of CD-4 lymphocyte count and its relationship to survival time. Biometrics 50, 1003-1014.

[15] Demidenko E. (2004), Mixed Models Theory and Applications, John Wiley and Sons .

[16] Dey, D. K., Chen, M. H., Chang H. (1997), Bayesian Approach For Nonlinear Random Effects Models, Biometrics 53, 1239-1252.

[17] Farewell, V. T. (1986), Mixture Models in Survival Analysis: Are They Worth the Risk?, The Canadian Jpurnal of Statistics 14, 257-262.

[18] Faucett, C.J. and Thomas, D.C. (1996). Simultaneously modeling censored survival data and repeatedly measured covariates: A Gibbs sampling approach. Statistics in Medicine 15, 1663-1685.

[19] Faucett, C.L., Schenker, N., and Taylor, J.M.G. (2002). Survival analysis using auxiliary variables via multiple imputation, with application to AIDS clinical trials data. Biometrics 58, 37-47.

[20] Geisser, S., and Eddy, W. (1979), Apredictive Approach to Model Selection, Journal of the American Statistical Association 74, 153-160.

[21] Gelfand, A. E., and Mallick, B. (1995), Bayesian of Proportional Hazards Model Built From Monotone Function, Biometrics 51, 843-852

[22] Gilks, W. R., Best, N. G., and Tan, K. K. C. (1995), Adaptive Rejection Metropolis Sampling within Gibbs Sampling. Journal of Applied Statistics 44, No. 4, 455-472.

[23] Goldman, A. I. (1984), Survivorship Analysis when Cure is A Possibility: A Monte Carlo Study, Statistics in Medicine 3, 153-163.

[24] Gray, R. J. and Tsiatis, A.A. (1989), A linear Rank Test for Use when the Main Interest is in Differences in Cure Rates, Biometrics 45, 899-904.
[25] Henderson, R., Diggle, P., and Dobson, A. (2000). Joint modeling of longitudinal measurements and event time data. Biostatistics 4, 465-480.
[26] Hogan, J.W. and Laird, N.M. (1997). Mixture models for the joint distributions of repeated measures and event times. Statistics in Medicine 16, 239-257.
[27] Ibrahim, J.G., Chen, M.H., and Sinha, D. (2001). Bayesian Survival Analysis. Springer, New York.
[28] Ibrahim, J. G., and Laud, P. (1994), A predictive Approach to the Analysis of Designed Experiments, Journal of the American Statistical Association. 89, 309-319.
[29] Ibrahim, J. G., Chen, M. H., Sinha, D. (2004), Bayesian Methods for Joint Modeling of Longitudinal and Survival Data with Applications to Cancer Vaccine Trials, Statistica Sinica 14, 863-883.
[30] Kalbfeisch, J.D. and Prentice, R. L. (2002). The Statistical Analysis of Failure Time Data, Second Edition. John Wiley, New York.
[31] KUK , A. Y. C. and CHEN, C. H.(1992), A mixture Model Combining Logistic Regression with Proportional Hazards Regression, Biometrika 79, 531-541.
[32] Laird, N.M. andWare, J.H. (1982). Random effects models for longitudinal data. Biometrics 38, 963-974.
[33] Lavalley, M.P. and DeGruttola, V. (1996). Model for empirical Bayes estimators of longitudinal CD4 counts. Statistics in Medicine 15, 2289-2305.
[34] Law, N.J., Taylor, J.M.G., and Sander, H. (2002). The joint modeling of a longitudinal disease progression marker and the failure time process in the presence of cure. Biostatistics 3, 547-563.
[35] Lin, H., Turnbull, B.W., McCulloch, C.E., and Slate, E.H. (2002). Latent class models for joint analysis of longitudinal biomarker and event process data: Application to longitudinal prostate-specific antigen readings and prostate cancer. Journal of the American Statistical Association 97, 53-65.
[36] Maller, R. and Zhou, X. (1996), Survival analysis with Long-Term Survivors. New York, Wiley.
[37] Pawitan, Y. and Self, S. (1993). Modeling disease marker processes in AIDS. Journal of the American Statistical Association 83, 719-26.
[38] Peng, Y. and Dear, K. B. G. (2000), A nonparametric Mixture Model for Cure Rate Estimation, Biometrics 56, 237-243.
[39] Prentice, R. (1989). Surrogate endpoints in clinical trials: Definition and operation criteria. Statistics in Medicine 8, 431-440.
[40] Raboud, J., Reid, N., Coates, R.A., and Farewell, V.T. (1993). Estimating risks of progressing to AIDS when covariates are measured with error. Journal of the Royal Statistical Society, Series A 156, 396-406.
[41] Self, S. and Pawitan, Y. (1992). Modeling a marker of disease progression and onset of disease. In AIDS Epidemiology: Methodological Issues (N.P. Jewell, K. Dietz, and V.T. Farewell, eds.). BirkhÄ auser, Boston.
[42] Sinha, D., Dey, D. K. (1997), Semiparametric Bayesian Analysis of Survival Data, Journal of the American Statistical Association. 92, 1195-1212.
[43] Song, X., Davidian, M., and Tsiatis, A.A. (2002) A semiparametric likelihood approach to joint modeling of longitudinal and time-to-event data. Biometrics 58, 742-753.
[44] Spielhalter, D. J., Best, N. G., Carlin, B. P., and van der Linde, A., Bayesian measures of model complexity and fit. Journal of Royal Statistical Society, Series B 64, (2002) 583-616.
[45] Sy, J. P. and Taylor, J. M. G. (2000), Estimation in A Cox Proportional Hazard Cure Model. Biometrics 56, 227-236.

[46] Taylor, J. M. G. (1995), Semi-Parametric Estimation in Failure Time Mixture Model, Biometrics 51, 899-907.

[47] Taylor, J. M. G., Cumberland, W.G., and Sy, J.P. (1994). A stochastic model for analysis of longitudinal data. Journal of the American Statistical Association 89, 727-76.

[48] Tsiatis, A.A., DeGruttola, V. and Wulfsohn, M.S. (1995). Modeling the relationship of survival to longitudinal data measured with error: Applications to survival and CD4 counts in patients with AIDS. Journal of the American Statistical Association 90, 27-37.

[49] Tsiatis, A.A. and Davidian, M. (2001). A semiparametric estimator for the proportional hazards model with longitudinal covariates measured with error. Biometrika, 88, 447-458.

[50] Tsiatis, A.A. and Davidian, M. (2004). Joint Modeling of Longitudinal and Time-To-Event Data: An Overview. Statistica Sinica, 14, 809-834.

[51] Tsodikov, A. D., Ibrahim, J.G., Yakovlev, A. Y. (2003), Estimating Cure Rate from Survival Data: An Alternative to Two-Component Mixture Models, Journal of the American Statistical Association 98,1063-1078.

[52] Wang, Y. and Taylor, J.M.G. (2001). Jointly modeling longitudinal and event time data with application to acquired immunode¯ ciency syndrome. Journal of the American Statistical Association 96, 895-905.

[53] Wulfsohn, M.S. and Tsiatis, A.A. (1997). A joint model for survival and longitudinal data measured with error. Biometrics 53, 330-339.

[54] Xu, J. and Zeger, S.L. (2001). Joint analysis of longitudinal data comprising repeated measures and times to events. Applied Statistics 50, 375-387.

[55] Yakovlev, A. Y. and Tsodikov, A. D. (1996), Stochastic Models of Tumor Latency and Their Biostatstical Applications, Hackensack, New Jersey: World Scientific.

[56] Yin, G. (2005), Bayesian Cure Rate Frailty Models with Application to Root Canal Therapy Study, Biometrics 61, 552-558.

[57] Yin, G., Ibrahim, J. G. (2005), A General Class of Bayesian Survival Models with Zero and Nonzero Cure Fractions, Biometrics. 61, 403-412.

[58] Zhang, D. and Davidian, M. (2001). Linear mixed models with flexible distributions of random effects for longitudinal data. Biometrics 57, 795-802.

European Journal of Scientific Research
ISSN 1450-216X Vol.18 No.4 (2007), pp.730-736

http://www.eurojournals.com/ejsr.htm

Radiographic Heart Sizes of Adult Nigerian Population

Anyanwu G.E
Department of Anatomy, College of Medicine, University of Nigeria, Enugu, Nigeria
E-mail: anyanwugemeks@yahoo.com

Agwuna K.K
Department of Radiation Medicine, University of Nigeria Teaching Hospital, Enugu, Nigeria

Abstract

A radiological study of the various heart size parameters was carried out within an adult population of Nigerians. A total of 1,300 Nigerians of age range 20 to 90 years were physically examined and enrolled for this study, but only 459 male and 452 female posterior anterior radiographs of the chest were accepted for this study. Heart size parameters studied in this research were the heart diameters, chest diameters and cardiothoracic ratio. The entire distribution was broken into two groups; the normal population called the normotensive group and the hypertensive group. Age correlated significantly with all the heart size parameters in the normal group. The research determined normograms of the heart and chest diameters and cardiothoracic ratios for all the various age and sexes in the normal distribution of the Nigerian population. Upper and lower limits of such normal values were also determined and comparisons of these values with other values established for Caucasians, Asians, Americans and the rest Africans were done.

Keywords: Nigerian population, Heart size, heart diameter, chest diameter, cardiothoracic ratio, Cardiac size parameters.

Introduction

As far back as 1919, Danza was able to establish a relationship between the transverse heart diameter and the transverse thoracic diameters, which he called the cardiothoracic ratio (Danza, 1919). Subsequently various formula based on determination of heart size have been established (Hodges and Eyester 1926, Bainton 1932, Ungerleider and Clarke 1938). And as early as 1931, clinical extrapolations and interpretations based on such formula were accepted and endorsed by many organizations such as the New York heart Association, American Heart Association (Nemet and Geza 1931) and life insurance associations (Turner et al 1933). More recently, such measurements have been useful in computer aided diagnosis of cardiomegally (Nakamori et al 1991), in automated analysis of heart and lung in chest images (Nakamori et al 1990), estimation of lung volume and area obscured by the heart (Chotas and Ravin 1994), in image feature analysis and computer aided determination of rib cage boundary (Xu and Doi 1995) and as a guide in ultra filtration therapy in dialyzed patients (Poggi and Maggiore 1980).

Despite the presence of new invasive and non-invasive radiological technologies for faster and more precise evaluations, the chest x-ray still remains the primary and most common way of determination of heart size (Tatsuji et al 1991). This is most especially as a result of easy availability

and affordability particularly in third world nations. (Obikili and Okoye 2004). Literatures abound on variations of anatomical and physiological parameters as a result of race, ethnic and geographic factors. Presently, various authors have established racial variation on heart size (kerwin 1944, Nickol and Wade 1987). And this work has been designed to establish the normal transverse heart and chest diameters and cardiothoracic ratio in a Nigerian population, determine the role of gender and age on this parameters and also determine the roles of these parameters in the estimation of heart size. As a result of the established racial and ethnic variations of some these parameters, it also is the aim of this study to compare the observed values with other documented American, Asian, Caucasian values.

Subject and Method

This study was carried out in the in the department of radiation medicine, university of Nigeria teaching hospital (UNTH) Enugu Nigeria. The study sample included male and female Nigerians from the ages 20 to 90 years. A total of 1300 samples were physically examined and enrolled for this study, but based on technical details of the radiographs such as thoracic wall deformity, inadequate inspiration, over expanded chest, inability to determine one or both heart borders with confidence, incompletely erect radiograph, mediastinal deviation and significant rotation, only 911 radiographs of the subjects were used for interpretation and analysis of this study. The study sample was divided into two groups; A and B. Group A, was made up of healthy normotensive subjects without signs of any cardiovascular disease symptoms. The samples in this group were selected from candidates that came for chest X-ray examination as a result of requirements such as pre-employment, pre-admission, visa application and volunteer candidates without any cardiovascular disease symptoms. The subjects in group B included patients with clinically diagnosed cases of hypertension. Blood pressures of the candidates from the two groups were obtained. For group A, only candidates that had systolic blood pressure of between 110 and 145mmHg and diastolic pressure of 60 and 100mHg were included for this work. The posterior anterior (PA) chest radiographs of all the candidates were taken in the erect position with a film focus distance of 1.8m. The exposures were made at normal quiet inspiration. Subject's sex, age, and medical history were noted.

Measurements of the thoracic and cardiac diameters were made. The transverse cardiac diameter was measured as the sum of the greatest cardiac distance to the right and to the left of the midline, while the transverse thoracic diameter was measured as the widest horizontal distance inside the rib cage at the level of the dome of the right diaphragm. The cardiac and thoracic diameters were all measured in centimeters. Age was in years.

Results

A total of four hundred and four (404) and four hundred and nine (409) radiographs of females and males respectively were admitted and analyzed for members of group A, while a total number of forty eight (48) and fifty (50) radiographs of females and males from group B, respectively were used. Ages of individuals in group A, ranged from 20 to 80 with a mean of 37.4$\pm$15.14 years. The range in group B was from 30 to 90 with a mean of 50.4$\pm$15.16 years. Age was broken into 10-year intervals in both groups.

Cardiothoracic Ratio (CTR) is the ratio of the heart diameter (HD) with the thoracic diameter (TD), expressed in percentage. This ratio is calculated from the

Formula:

$$CTR = \frac{\text{heart Diameter X100}}{\text{Diameter.}}$$

Table 1 gives the summary of the relationship of age with all the heart size parameters. The table also gives the mean values of the thoracic and heart diameters, and cardiothoracic ratios for the various age groups of the male and female populations of both the normotensive and hypertensive groups. Heart and chest diameters were noted to be larger in the males than in the female population of

the normotensive group while the CTR values were larger in the female population. A significant difference was noted between the heart size parameters of the two populations of groups A and B ($p \leq 0.05$). Unlike in the normotensive group of the sample, none of the heart size parameters showed significant relationship with age, as has been clearly shown in table 2.

Table 1: Relationship of age with heart parameters.

		Normotensive group				Hypertensive group			
Sex	**Age**	**N**	**T.D**	**H.D**	**CTR**	**N**	**T.D**	**H.D**	**CTR**
Males	21-30	146	29.1±4.8	13.2±1.2	45.4±3.6	-	-	-	-
	31-40	100	29.4±5.0	13.4±1.5	45.6±5.0	05	27.3±1.4	14.4±1.4	52.6±5.1
	41-50	70	28.9±5.0	13.6±1.2	47.4±4.2	11	30.3±1.3	15.5±0.7	51.1±3.0
	51-60	62	28.5±5.1	13.5±1.0	47.3±3.6	11	28.9±1.5	15.1±1.0	52.2±3.1
	61-70	20	27.8±5.5	13.6±1.5	49.0±4.4	11	28.6±2.0	15.0±1.0	52.7±4.0
	71-80	11	28.1±5.1	13.2±1.2	46.9±4.2	05	27.9±2.4	14.6±1.8	52.4±3.4
	81-90	-	-		-	10	28.1±1.6	15.3±1.5	54.5±3.9
	Mean		**28.3±4.9**	**13.0±1.5**	**46.2±4.1**	**-**	**28.7±2.0**	**15.1±1.1**	**52.3±3.6**
Females	21-30	186	26.3±4.5	12.0±1.1	45.9±3.8	-	-	-	-
	31-40	100	26.9±4.6	12.8±1.1	47.9±3.9	06	26.8±1.3	14.4±1.2	54.0±5.0
	41-50	69	26.5±4.8	13.1±1.3	49.6±6.1	08	26.6±1.7	14.7±2.0	55.4±6.2
	51-60	33	26.4±4.9	12.7±1.0	48.2±2.9	10	26.2±1.1	14.4±0.7	54.9±3.0
	61-70	14	26.3±4.8	12.9±1.4	49.0±3.8	15	26.0±1.4	13.7±1.1	52.7±4.0
	71-80	2	25.0±5.1	12.1±1.4	48.7±4.2	09	26.0±1.9	14.6±1.2	56.6±6.5
	Mean	**-**	**26.0±4.5**	**12.3±1.3**	**47.2±4.4**	**-**	**26.2±1.5**	**14.3±1.3**	**54.5±5.0**
Both	21-30	332	27.52±4.6	12.6±1.3	45.7±3.7	-	-	-	-
	31-40	200	28.12±4.8	13.1±1.4	46.7±4.6	11	27.0±1.3	14.4±1.2	53.4±4.8
	41-50	139	27.71±5.0	13.3±1.2	48.5±5.3	19	28.7±2.4	14.4±1.2	53.0±5.0
	51-60	95	27.74±5.0	13.2±1.0	47.6±3.4	21	27.6±1.9	14.4±1.2	53.5±3.3
	61-70	34	27.13±5.4	13.3±1.5	49.0±4.1	26	27.1±2.1	14.4±1.2	52.7±4.0
	71-80	13	27.62±5.1	13.0±1.1	47.1±4.0	14	26.6±2.2	14.4±1.2	55.3±6.0
	81-90	-	-	-	-	10	28.1±1.6	14.4±1.2	54.5±3.9
	Mean		**27.15±4.6**	**12.6±1.5**	**46.7±4.3**		**27.5±2.1**	**14.4±1.2**	**53.5±4.3**

Table 2: Summary of the correlation coefficients (r) of Age with various heart parameters in both groups.

Heart parameters	**Chest diameter**	**Heart diameter**	**CTR**
Normotensive	*-0.315	*0.414	* 0.181
Hypertensive	-0.018	0.064	0.081

*Correlation significant at P≤ 0.01 level (2-tailed)

To establish a range of normal values of both heart diameter and CTR in the studied population of normotensive group, upper and lower limits were set using the 90th and the 10th percentiles respectively as the upper and lower limits. The two limits have been designed to cut off those extreme but normal values noted in the distribution which occurrences are relatively infrequent. These values have been shown in Table 3 with corresponding values of the hypertensive groups also noted. Table 4 gives the records of differences in the CTR, heart and chest diameter values between the male and female populations of the normotensive group. While table 5 shows a record of differences in the CTR, heart and chest diameter values between each of the age groups.

Table 3: The values of the 80% central tendency in the CTR and heart diameter Values of the sampled population.

Sex	**Normotensive group**		**Hypertensive group**	
	CTR (%)	Heart D (cm)	CTR (%)	Heart D (cm)
Male	40 – 49	11.4 – 14.7	48 – 58	13.5 – 16.2
Female	41 – 51	10.8 – 13.7	50 – 59	13.0 – 15.6
Both	40 – 50	11.0 – 14.4	48 – 58	13.0 – 16.0

Table 4: Differences in the chest and heart diameters and CTR values between Both sexes in the normotensive group.

Age	Heart diameter		Chest diameter		CTR	
	Change	Change in %	Change	Change in %	Change	Change in%
21 – 30	1.2	10	2.8	10.7	0.4	0.9
31 – 40	0.6	4.6	2.5	9.2	2.3	5.0
41 – 50	0.5	3.8	2.4	8.9	2.2	4.6
51 – 60	0.8	6.3	2.1	8.1	0.9	1.9
61 – 70	0.7	5.4	1.4	5.3	-	-
71 – 80	1.1	9.1	3.1	12.4	1.8	3.8
Mean	**0.82**	**6.5%**	**2.4**	**9.1%**	**1.5**	**3.2%**

Table 5: Differences in the chest and heart diameters and CTR values between age groups in the normotensive group.

Age	Heart diameter (HD)		Chest diameter (CD)		CTR	
	ΔHD	ΔHD%	ΔCD	ΔHD%	ΔCTR	ΔCTR%
21 – 30 to 31 – 40	0.5	4.0	-0.6*	2.2*	1.0	0.02
31 – 40 to 41 – 50	0.2	1.5	0.7	2.5	1.8	3.7
41 – 50 to 51 – 60	-0.1*	0.8*	0.03	0.1	-0.9*	1.9*
51 – 60 to 61 – 70	0.1	0.8	0.6	2.2	1.4	2.9
61 – 70 to 71 – 80	-0.3*	2.3*	-0.5*	1.8*	-1.9*	4.0*
Mean	**0.27**	**2.1**	**0.4**	**1.6**	**1.4**	**2.2**

Δ = Symbol Used For "change IN".
* = Points That Showed Reverse Trends. These Points Have Not Been Included In The Computation Of The Mean Values.

Discussion

The first suggestion that racial difference might affect the interpretation of chest radiograph of the heart size was provided by Kerwin (1944). Danzer (1919), in his pioneer study gave the normal range of CTR in adults to be between 39 – 50% with a mean of 45%, against the range of 40 – 50% and the mean of 46.7±4.3% obtained for this study. Danzer went ahead and recommended that ratios of up to 52% be allowed in the assessment of the normal sized heart. Nichol and Wade (1982) in their study; "Radiological heart size and Cardiothoracic Ratio in Three Ethnic Groups," found a significant relationship between cardiac measurements with age and ethnicity. Other authors (Cowan 1964, Ashcroft and Miall 1969, Dysart et al 1994, Patrick and Boyd) in their studies in different backgrounds and ethnicities have come with similar results. This platform, which informed the bases of this study in Nigeria, was noted to be true considering the observed differences noted in the result of this study with other documented studies in other races.

From the results between the normotensive and the hypertensive populations in this study, CTR, chest and heart diameters have been noted as reliable indices for estimation of heart sizes. Also normal values of heart and chest diameters and CTR have been established for the males and females of various age groups of the Nigerian population. Comparing these values with some of the reported values for Caucasians and Asians, (Cowan 1964, Kerwin 1943, Nickol and Wade 1982), Americans (Oberman 1967, Ashcroft and Miall 1969) and the values submitted by Nickol and Wade (1982) for the combined population of Africans and West Indians, the reported values for this research were noted to be slightly larger than these reported values. The result of this research is in complete agreement with the submission of Munro-Faure (1979) who in a comparison of the CTR values of black and white individuals opined that mean CTR values are about 4% greater in blacks than whites.

For the normal population sample, age as in some of the previous studies mentioned, showed very strong significant correlations with CTR, heart and chest diameters. Edge et al (1959), found a significant reduction in the chest diameter of women only, while this result shows a significant reduction in chest diameters of both sexes but with greater reduction in women, which is in agreement

with the findings of Milne and Lauder (1974) and potter et al (1982). This result shows a slight diminution in the magnitude of the mean heart diameter in the 5th decade of men and women, an observation also noted by Tirman and Hamilton (1952) and Cowan (1964). This work noted a mean change of 3mm (2.1%) in heart diameter, 4mm (1.6%) in chest diameter 1.4 (2.2%) CTR, from one age decade to another, against a mean change of 1mm in heart diameter predicted by Hodges and Eyester (1926).

Brainton (1932) in an orthographic study of transverse heart diameters reduced the transverse heart diameters of men by 0.8cm to obtain the standard for women. The findings of this study reveal a consistent sex difference in the heart diameter of 0.5cm to 1.2cm with a mean of 0.83cm, against the 0.5 to 1.0cm observed by Oberman (1965).

This research offers a central 80 percent range of the distribution of the studied population within which the ranges are certainly normal. A range of 40 – 50% of CTR values noted for the normal population of Nigerians when compared with the range of 48 – 58% of the CTR value noted in the hypertensive group leaves us with reasons to reconsider some of the upheld limits for considering normal size of the heart. Before now, ranges of CTR values within the mean of 50% have been very much regarded as normal values (Hemingway 1997, Nickol and Wade 1999, Poutanem et al 2003, Danzer 1919, Clarke and Coates 2000) and some authors have even suggested for the extensions of such normal CTR values to a mean of 52% (Danzer 1919) and these views have not been reviewed . As a result of the overlap of the ranges of the upper limits of CTR values of the normal population (group A) with the lower limits of the hypertensive population (group B) within the ranges of 48 to 50%, it shows that CTR values within this range could belong to either of the two groups of the population. it is our view that caution be expressed in interpretations of CTR values within this overlapping range, and whatever results gotten be confirmed by other methods of determining normal heart function and size. We also suggest a reconsideration and review of the views of the inclusion of CTR values of within ranges of 50 –53% within the range of normal considering that the population and race in this study was noted with slightly higher CTR values than documented values noted for other races, and if values of 50-53% should be considered high for this population, then it should also be considered high for other races with noted lower CTR values.

References

[1] Ashcroft MT, Miall WE, (1969) Cardiothoracic ratio in two Jamaican communities Am J Epidemiol. **89**, 166-167

[2] Bainton J.H (1932) The transverse diameter of the heart. Am Heart J **7**:331 – 333

[3] Chotas HG, and Ravin CE (1994) Chest radiography; estimated lung volume and projected area obscured by the heart, mediastinum, and diaphragm. Radiology. **193**, 403-404.

[4] Clark AL, Coat AJ. (2000) Unreliability of cardiothoracic ratio as a marker of left ventricular and echocardiography. Br Med J **895**, 289-91

[5] Cowan N.R, (1964) The heart lying Coefficient and the transverse diameter of the heart Br heart J **26**, 116 - 120

[6] Danzer CS (1919) The cardiothoracic ratio: an index of cardiac enlargement Am J Med Sci. **157**, 513 – 516.

[7] Dysart JM, Treiber FA, Pflieger K. Davis H, Strong WB, (1994) Ethnic differences in the myocardial girls. Am J Hypertens **7**, 15-22

[8] Edge JR, Millard FJ, Reid I, and Simon G (1941) The radiographic appearances of the chest in persons of advanced age Br Heart J. **37**, 769 - 372

[9] Hemingway H, Shipley M, Christie D, Marmolt M (1996) Cardiothoracic ratio and relative heart volume as predictors of coronary heart disease mortality? Whitehall study, 25 year follow up. BMJ **317**, 1321 –2.

[10] Hodges FJ and Eyster JAE (1926) Estimation of transverse Cardiac diameter in man. Arch Int. Med. **37**, 707 – 711.

[11] Kerwin AJ (1943) Observations on the heart size of Natives Living At High Altitudes. Am Heart J **28** 69-80.

[12] Milne JS Lauder IJ (1974) Heart size in older people. Br Heart J. **36** 352 –356.

[13] Munro-Faure A.O, Beilin L,J , Bulpittt C.J, et al (1979) Comparison of black and white patients. Attending hypertension clinics in England. Br Med J I, 1044-1047

[14] Nakamori N. Doi K, Mac Mahon H, sagacity Montner S. (1991) Effects of heart size Parameters computed from digital chest radiographs on detection of cardiomegally. Potential usefulness for computer aided diagnosis. Invest Radiol **26**, 546-50.

[15] Nemet and Geza (1931) Guide to Radiological Diagnosis in Heart Disease, Heart Committee of the New York. Tuberculosis and Health Association, Inc.

[16] Nickol K & Wade AJ. (1982) Radiographic heart size and cardiothoracic ratio in three ethnic groups; a basis for a simple screening test for cardiac enlargement in men. BJR **654**, 399 - 403.

[17] Oberman A, Allen R, Thomas K. Fredrick E (1967) Heart size of adults in a National Population Tecumseh, Michigan. Circulation: xxxv, 724 –733.

[18] Obikili EN, Okoye I.J (2004) Aortic Arch diameter in frontal chest radiographs of a normal Nigerian population Nig J med; **13** 171-174.

[19] Patrick AL, Boy –Patrick HA (1986) Blood pressure level and cardiothoracic ratio of a mixed African West Indian community. West Indian Med J. **35**, 76-83

[20] Poggi A, Maggiore Q (1980) Cardiothoracic ratio as a guide to ultra filtration therapy in dialyzed patients. Int J Artif Organs. **6**, 332 – 337.

[21] Potter JF, Elahi D, Tobin JD, and Andrews R. (1982) Effects of Aging on the cardiothoracic ratio of men. J Am Geriatric Sc. **30** 404 – 409.

[22] Poutanem T, Tikanoja T, sairanem H, Jokinem (2003) Normal Aortic dimensions and flow in 168 children and young adults. Clin Physiology Funct Imaging. **23**, 224-9

[23] Tatsuji K, Michihiro S, Hisashi H, Yuzo H, Keishiro K (1992) Clinical significance of normal cardiac silhouette in dilated cardiomyopathy. Japanese circulation J **56** 359-365.

[24] Tirman WS and Hamilton J.B (1952) Aging in apparently normal men. The roentgen logic appearance of the thorax and thoracic organs. J Geront; **7**:384 –389.

[25] Turner H.B, Nicholas C.F, and Ungerleider H.E (1933) A recommended Standard for the determination of Cardiac Enlargement: Transactions of the Association of Life Insurance Medical Directors. 184 –187.

[26] Ungerlaider H.E & Gubner R. (1942) Evaluation of heart size measurements. Am Heart J. **24**, 494-510.

[27] XU XW, Doi K. (1995) Image feature analysis for computer aided diagnosis: accurate determination of rib cage boundary in chest radiographs. Med Phys. **22**, 617 – 626.